Development and Evolution of the Flamborough Head Disturbance

Richard McKeen

Submitted for the degree of Master of Science by Research

Applied Geoscience

Heriot-Watt University

School of Energy, Geoscience, Infrastructure and Society

Institute of Petroleum Engineering

January 2019

ABSTRACT

Previous models on the formation of the Flamborough Head Disturbance have been hindered by a lack of data integration, especially between onshore and offshore subsurface datasets. This project resolves the problem and long-standing controversies through the interpretation of an extensive, seismic and borehole dataset that spans the coastline and delivers a unified geological model for the Flamborough Head Disturbance. The model consists of a W-E striking array of planar basement faults, throwing to the north and controlled by the presence of the granite cored Market Weighton Block to the south, marking an onshore extension of the Dowsing Fault Zone. Above this and striking in the same orientation is a Late Triassic-Early Jurassic to Lower Cretaceous aged listric fault controlled Mesozoic graben system that is decoupled from the basement by thick Permian evaporites. Migration of Permian salt in the Lower Cretaceous has resulted in the syn-halokinetic but post-rift deposition of the Cromer Knoll Group marine strata. The model recognises two episodes of major basin reconfiguration during the Cenozoic: regional tilting to the south-east and basin inversion through the reactivation of basement faults. Basement fault reactivation was focussed in the hanging wall of the fault system due to buttressing against the Market Weighton Block buried granite during compression. Fault reactivation did not propagate through the Zechstein salt, with shortening being taken up by buckling of the post-salt section in the hanging wall of the fault system. This preserved the extensional geometries of the detached listric faults of the detached graben system and resulted in the deformation structures observed in outcrop. Cenozoic tilt and structural inversion has resulted in hydrocarbon trap breaching in the hanging wall of the Flamborough Head fault system and the depressurisation of Carboniferous source rocks. This study complements existing research on Cenozoic uplift and intraplate deformation in the UK and emphasises the importance that buried Caledonian granites and mobile salt have on the creation and inversion of Mesozoic sedimentary basins in the UK.

ACKNOWLEDGMENTS

The work presented in this thesis is the product of a Heriot-Watt scholarship funded by the UK Onshore Geophysical Library (UKOGL) and I sincerely thank UKOGL and its Chairman, Dr Malcolm Butler, for their generous financial contribution and provision of seismic data that has enabled this research.

Special thanks must be given to my two supervisors, Prof. John Underhill and Dr. Rachel Jamieson who both have offered invaluable and enthusiastic support and guidance throughout the course of this study.

The work for this project was undertaken in the Shell Centre for Exploration Geoscience, the underpinning financial and computer support for which is gratefully acknowledged. This project includes content supplied by IHS Markit; Copyright © IHS Markit, Ltd. [2017]. All rights reserved, who are appreciatively acknowledged in providing seismic and well data and allowing permission to publish examples in this project. I thankfully acknowledge the UKOilandGasData.com website owned by Common Data Access Ltd. (CDA) and administered by Schlumberger for access to their seismic data volumes and released UK well database. I am grateful to Schlumberger and Zetaware for providing academic licenses for their Petrel E&P Software Platform and Genesis 1D basin modelling software, respectively. Thanks also go to Shell who provided the financial and logistical assistance that enabled me to visit key outcrop localities in the study area.

I also wish to sincerely thank all my fellow students and staff at the Shell Centre for Exploration Geoscience for their amazing friendship and support over the past year. Special thanks are extended to my fellow Southern North Sea researchers Ross Grant and Matthew Booth for putting me right on the Zechstein and the Carboniferous, respectively and my office mates, Sam Head and Stavros Vrachliotis for their feedback on my seismic interpretations and invaluable Petrel support.

Finally, I wish to say heartfelt thanks to my wife. None of this would have been possible without her.

DECLARATION STATEMENT

Research Thesis Submission Form should be placed here.

TABLE OF CONTENTS

LIST OF FIGURES AND TABLES

CHAPTER 1. INTRODUCTION

1.1 Introduction to Flamborough Head

Flamborough Head is a major promontory lying on the North Yorkshire coast in the east of the UK (Figure 1.1). It is formed of unusually resistant Cretaceous aged chalk and is the site of an enigmatic, W-E striking, complex area of structural deformation, the Flamborough Head Fault Zone or Flamborough Head Disturbance (Figure 1.1 and Figure 1.2). To the north of Flamborough Head lies the inverted, Mesozoic-aged Cleveland Basin and, to the south, the Caledonian granite cored Market Weighton Block. The general stratigraphy of Flamborough Head and the surrounding regions is documented in Figure 1.3, and shows a sedimentary fill from the Carboniferous to the Upper Cretaceous that comprises of siliciclastic, carbonate and evaporitic rock types. The regional bedrock geology is displayed in Figure 1.5, which highlights the W-E trend of the Upper Cretaceous Chalk outcrop seen at Flamborough Head, and the now exposed older Mesozoic strata of the inverted Cleveland Basin. The regional structural elements, in conjunction with the W-E trending Flamborough Head Fault Zone, are: the generally NW-SE striking Dowsing Fault Zone in the offshore Southern North Sea; the inverted, Mesozoic-aged Sole Pit Basin situated to the east of the Dowsing Fault Zone and the NNW-SSE trending Peak Trough fault system (Figure 1.1, Figure 1.2 and Figure 1.5).

The Flamborough Head Fault Zone has been of particular interest to geological research for over a century (Philips 1835; Davis 1885; Lamplugh 1895), due to the spectacular onshore outcrops. These are characterised by local areas of intensive folding and thrusting, in otherwise relatively un-deformed strata, in the Upper Cretaceous Chalk Group sea cliffs around Flamborough Head at Selwicks Bay and Staple Newk (Figure 1.2). Building on the geological importance of the area, Flamborough Head contains the type section of the Lower Cretaceous Speeton Clay Formation of the Cromer Knoll Group (Lamplugh 1889) and represents the most complete and representative section of marine Lower Cretaceous strata encountered onshore in the UK (Lott, *et al*. 1986), (Figure 1.2, Figure 1.3 and Figure 1.4). More recently, the deformation structures of the Upper Cretaceous Chalk Group at Flamborough Head have been documented through detailed field mapping in the area (Starmer 1995; 2008; 2013).

The acquisition and interpretation of the first seismic reflection data across Flamborough Head revealed a far more structurally and stratigraphically complex subsurface than is suggested from the relatively simple Upper Cretaceous Chalk cover, revealing a Mesozoic aged graben – the Flamborough Head Graben System - and the listric nature of the faulting recognised at surface (Figure 1.5). The combination of offshore and onshore seismic reflection data appeared to suggest that the Flamborough Head Fault Zone extends offshore, potentially joining with the Dowsing Fault Zone seaward of Flamborough Head (Kent 1980).

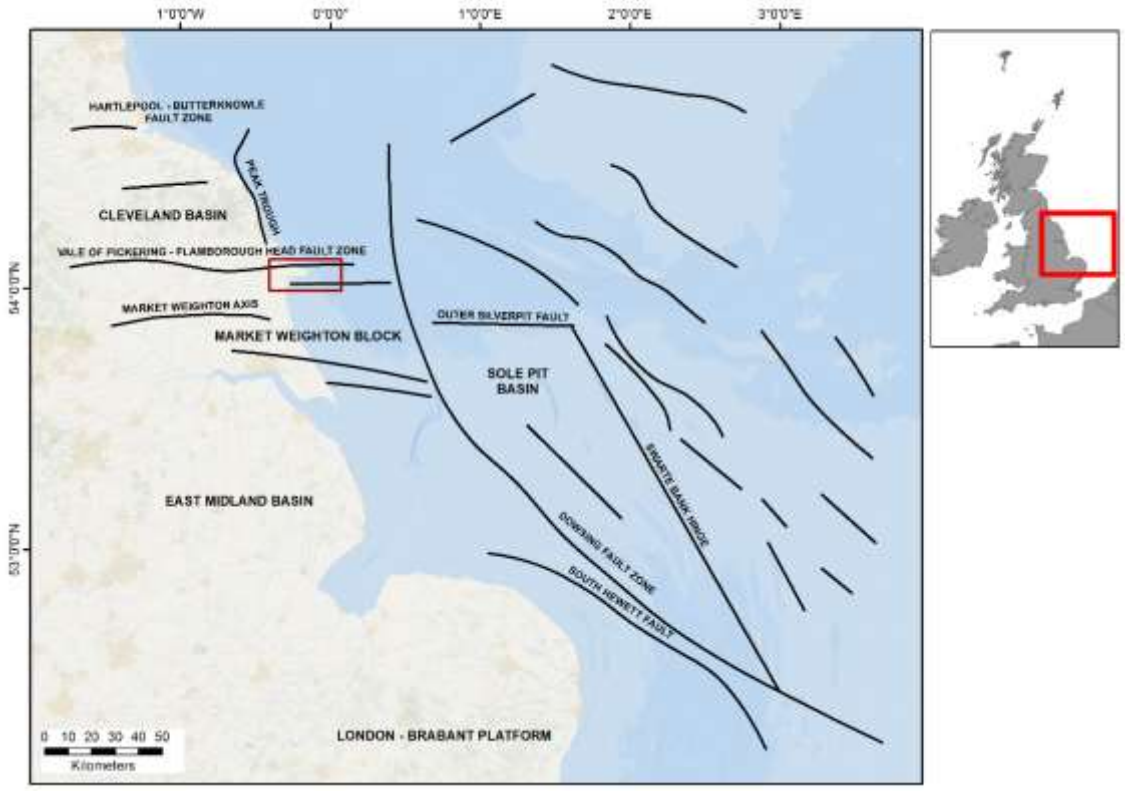

Figure 1.1 Major structural features of the UK Southern North Sea and surrounding areas. Flamborough Head promontory and research area of interest outlined by red box. Modified after Glennie & Boegner (1981); Dixon (1990) and Kent (1980).

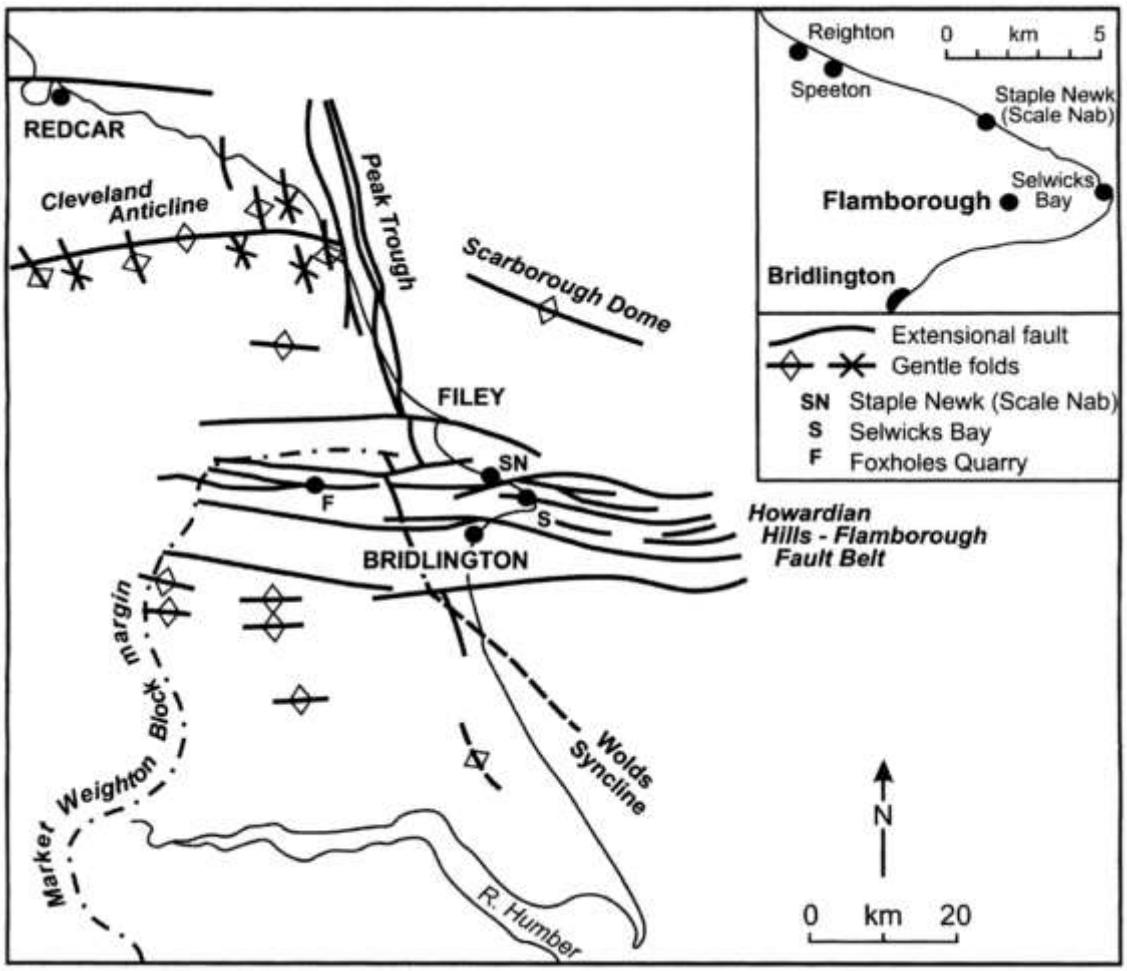

Figure 1.2 Detailed structural map of Flamborough Head Fault zone with key outcrop localities of deformed Cretaceous chalk at Staple Newk and Selwicks Bay (Starmer 2008).

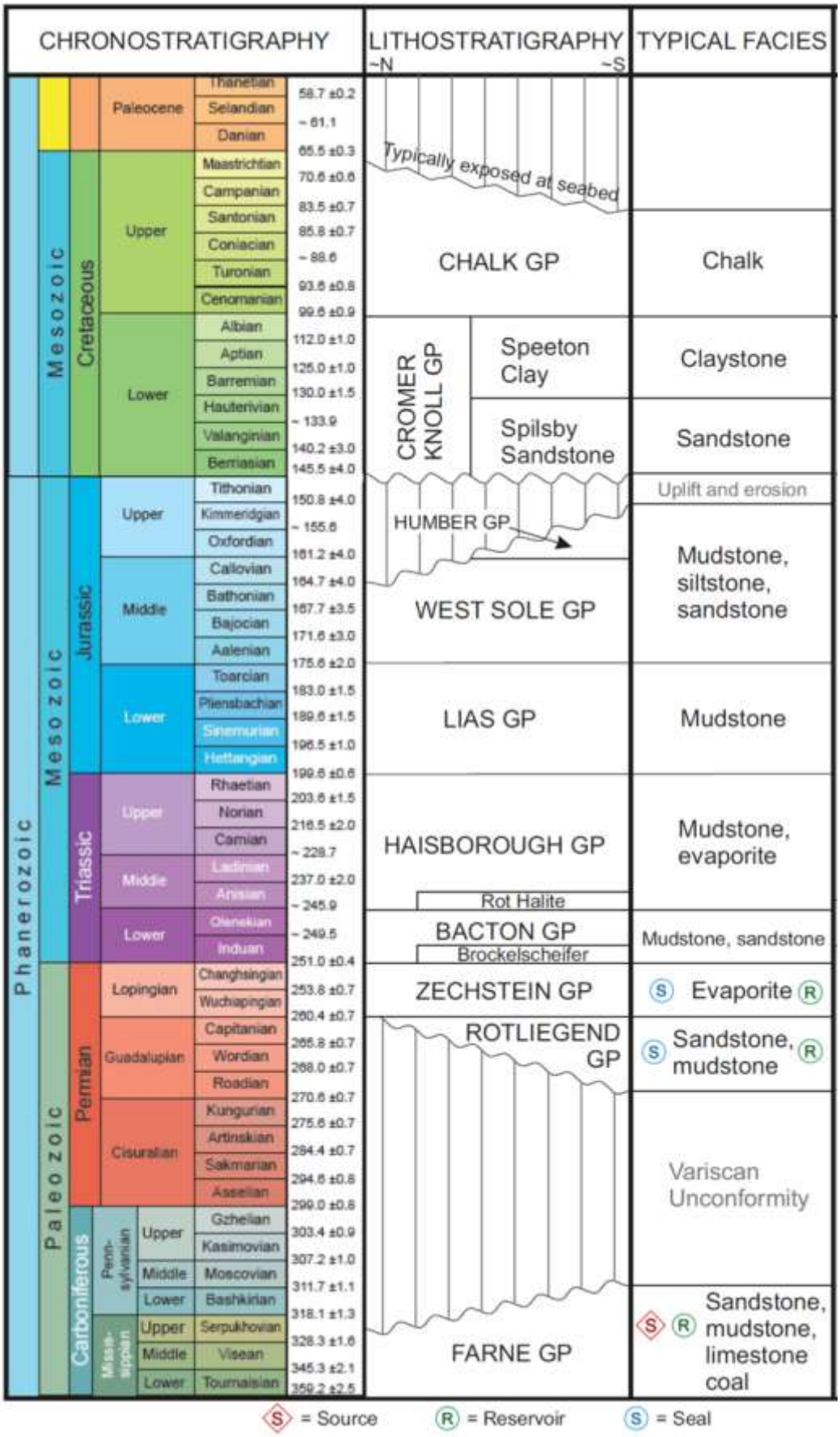

Figure 1.3 Generalised stratigraphic chart and petroleum play elements for Flamborough Head, the Cleveland Basin and surrounding Southern North Sea. Modified after Cohen, et al. (2018)

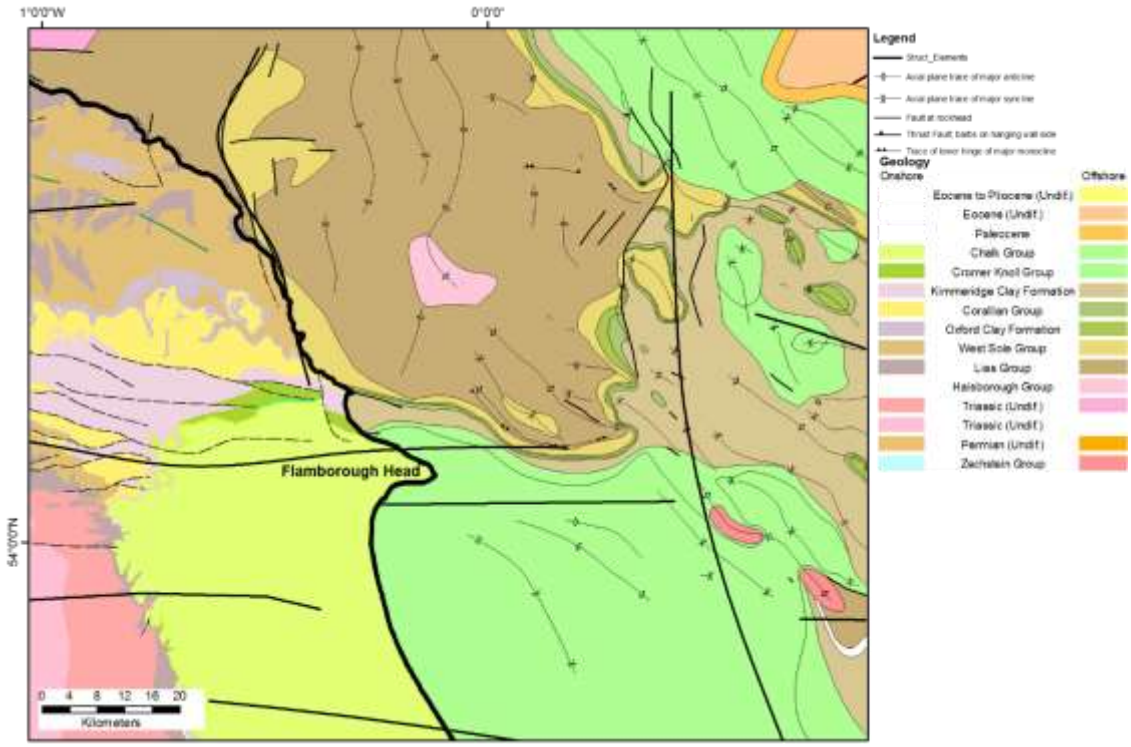

Figure 1.4 Bedrock geology of Flamborough Head and neighbouring areas. Data courtesy of British Geological Survey.

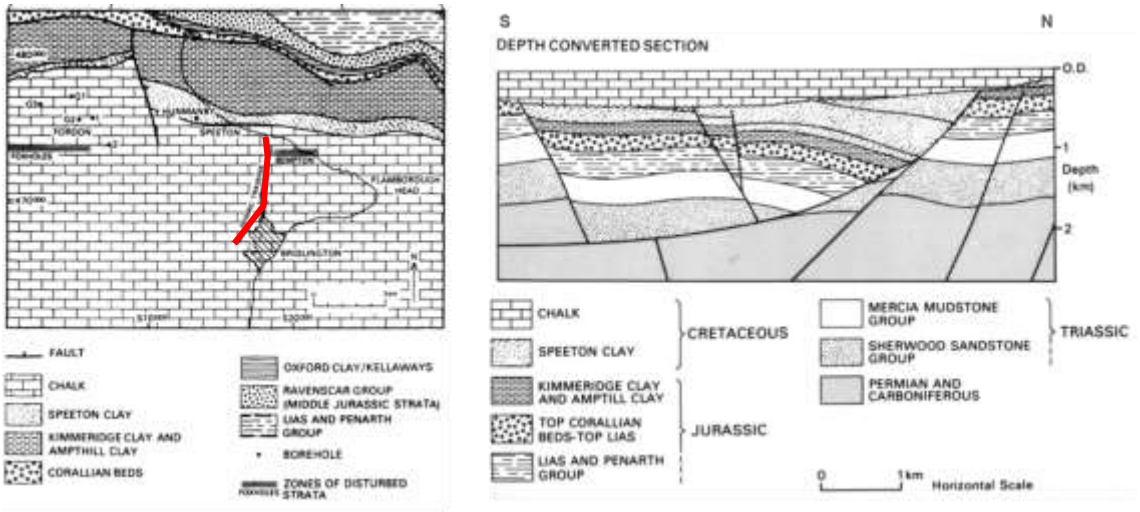

Figure 1.5 Simplified surface geology of the Flamborough Head region (L) and an interpreted composite seismic reflection line (R). Line of section shown in (L) as red line. Modified after Kirby & Swallow (1987).

1.2 Rationale and Scientific Importance

The geological development and evolution of Flamborough Head remains poorly understood for three main reasons:

1. The surface exposures of Upper Cretaceous Chalk, and younger sediments of the inverted Cleveland Basin to the north, do not provide enough information to fully assess the structuration, and mask a far more structurally and stratigraphically complex subsurface of Late Paleozoic to Mesozoic evaporite, siliciclastic and carbonate units (Figure 1.4, Figure 1.5).

2. Subsurface data provide a better opportunity to understand the genesis of the complex fault systems but onshore data are often poorly resolved and consist of short 2D seismic lines, often with a crooked-line geometry (see Chapter 2.2 below for an explanation of seismic data).

3. Subsurface data in the offshore provide a higher quality of imaging of the fault systems that underlie the Flamborough Head Disturbance but have historically been considered separately from any onshore information and no link has been made that would allow a fully comprehensive model to be constructed.

These difficulties have led to the development, over the years, of multiple different hypotheses for the formation of the Flamborough Head Disturbance, each derived from the different datasets available to the study in question. There is, therefore, no fully unified model and the establishment of are the overall aim of this study. Therefore, it is vital to understand what features must be explained by any proposed model and compare these with the findings of previous work undertaken on the area. This will determine if any areas require further study and will help to ascertain where controversy exists. The aim of the following section is to achieve this and to set out where the current study could aid in the understanding of this geologically complex area.

1.3 Overview of Previous Work

1.3.1 Introduction

The unique and anomalous geological features observed at Flamborough Head that require investigation in the unifying model of this study are as follows:

1. A geologically complex subsurface and pre-Chalk subcrop that belies the simple bedding geometries of the Upper Cretaceous Chalk surface exposures (Figure 1.5).

2. Building upon point 1, above, the presence of two distinctive structural styles within the subsurface at Flamborough Head are recognised: an array of W-E striking planar faults, termed the Flamborough Head Fault Zone, which offset Permo-Carboniferous and older strata; a Mesozoic graben structure, termed the Flamborough Head Graben System[1], that is controlled by W-E striking listric faults that detach into Permian and Triassic salts. The Permian salts separate the two structural features.

3. The recognition that the Flamborough Head Fault Zone marks a hinge zone that acts as the boundary between the buoyant, granite-cored Market Weighton Block in the south of the study area and the inverted, Mesozoic-aged Cleveland Basin in the north, accommodating the differential subsidence that originally led to the development of the Cleveland Basin (Bott, *et al*. 1978; Kent 1980).

4. Regional tilting and the structural inversion of the Cleveland Basin has not resulted in any observable, at seismic scale, reactivation of the listric faults of the Mesozoic Flamborough Head Graben System, which appears to remain in net extension at present day (Figure 1.5).

[1] These terms are used throughout this thesis and to clarify and distinguish: the Flamborough Head Fault Zone refers to the planar faults that offset the pre-salt Permo-Carboniferous and older strata; The Flamborough Head Graben System refers to the post-salt Mesozoic graben and its controlling listric faults that detach into Permian and Triassic salts. The Flamborough Head Disturbance is a general, historical term that refers to the zone of deformation at Flamborough Head.

5. The proposal that the Flamborough Head area uniquely displays evidence of a "double inversion" event, one at the end-Carboniferous and a second, analogous inversion occurring in the Late Mesozoic (Kent 1980).

6. The propagation of the Flamborough Head Fault Zone offshore and the probability of it representing an extension to the offshore Dowsing Fault Zone (Figure 1.1), (Kent 1980).

7. The development of intense contractional deformation structures within the Upper Cretaceous Chalk exposures.

8. The absence of any hydrocarbon fields with significant reserves to the north of the Flamborough Head Fault Zone, within the inverted Cleveland Basin and the coincident location of the Flamborough Head Fault Zone with the Permian Rotliegend Leman Sandstone Formation (the primary hydrocarbon reservoir in the Southern North Sea) facies boundary to the non-reservoir Silverpit Claystone Formation (Underhill 2003).

Several theories have been suggested in an attempt to elucidate all of the geological features noted and the key models have been explored to identify their strengths and weaknesses and how adequately they describe the features seen in and around the Flamborough Head Disturbance.

1.3.2 Key Models

1.3.2.1 Subsurface Evolution Resulting in a Complex Pre-Chalk Subcrop and the Importance of Salt[2]

As detailed previously, the development and evolution of Flamborough Head remains poorly understood and the relatively simple surface exposure of Cretaceous Chalk, passing into the younger sediments of the inverted Cleveland Basin to the north, mask a far more structurally and stratigraphically complex subsurface of Late Paleozoic to Mesozoic evaporite, siliciclastic and carbonate units (Figure 1.5 and Figure 1.4).

[2] Throughout this thesis the term "salt" is used to refer to mobile evaporites in the subsurface

Movement along the Flamborough Head Fault Zone faults and associated erosion of upthrown blocks has resulted in the complex subcrop configuration seen in the pre-chalk sequences (Kirby & Swallow 1987).

The importance of the presence of ductile and mobile Triassic and Permian salts in the Flamborough Head area and surrounding Southern North Sea, and the effects that they have had on basin evolution, has been previously investigated and is summarised in the following paragraph. Experimental work has shown that, where a ductile salt layer is present, the propagation of basement faults into post-salt cover sequences can be repressed if the salt is of sufficient thickness, with vertical displacement being distributed laterally through the salt layer (Richard 1991; Stewart, *et al*. 1996). The role of a mobile salt substrate on development of the Flamborough Head Disturbance, in particular the influence that salt has had on basement – cover fault relationships during compression, has also been investigated previously (Stewart & Coward 1995 and Stewart, *et al*. 1996) where these authors recognise a decoupled pre-salt and post-salt cover with little evidence of reactivation of listric fault systems within the post-salt.

1.3.2.2 Stresses Resulting in Regional Uplift, Cleveland Basin Inversion and the Deformation in Chalk Exposures

The deformation features of the Flamborough Head Disturbance have been inferred as resulting from oblique – slip reactivation of the cover faults of the Flamborough Head Fault Zone with a speculative underlying basement fault control (Kent 1980; Kirby & Swallow 1987; Starmer 1995; 2008 and 2013). Weak reactivation of major extensional basin faults due to horizontal, north to south orientated compressive stress, perpendicular to Flamborough Head Fault Zone, has also been proposed (Dixon 1990).

These structural processes have been linked to regional uplift and local fault reactivation episodes in the latest Cretaceous to early Tertiary and the mid Tertiary (Glennie & Boegner 1981; Green 1989; Starmer 1995; Stewart & Bailey 1996; Starmer 2008 and Green, *et al*. 2017). Late Cretaceous to early Tertiary basin reconfiguration episodes have been attributed to mantle plume driven regional uplift, either in the North Atlantic or the Irish Sea, and south-easterly tilting of the UK (Cope 1994; Stewart & Bailey 1996; Underhill 2003; Hillis, *et al*. 2008; Green, *et al*. 2017; Gale & Lovell 2017) and basement fault reactivation through dextral shear (Glennie & Boegner 1981; Kirby & Swallow 1987) resulting in the inversion of the Cleveland Basin (Starmer 1995) and nearby Sole

Pit Basin (Figure 1.1), (Glennie & Boegner 1981). It has been proposed that basement fault reactivation and consequent basin inversion occurred under north to south intra-plate compression and north-west to south-east transpression and has been attributed to far field stresses related to Alpine collision (Glennie & Boegner 1981; Ziegler 1989; Starmer 1995; Stewart & Bailey 1996; Starmer 2008 and 2013).

1.3.2.3 Strengths and Limitations of Previous Research

Some of the previously published research in this region, particularly regarding the onshore, has been constrained by the limited subsurface data available to the authors at the time or have inhibited their interpretations to physical boundaries, such as the shoreline, to create an artificial, geographical partition of a laterally complex and extensive subsurface geology. For instance, key observations have been limited to borehole and surface geology only (Kent 1980; Starmer 1995 and 2008), single or composite line 2D sections restricted to the onshore (Kirby & Swallow 1987; Starmer 1995; 2008 and 2013) with limited offshore seismic integration (Dixon 1990).

Offshore research has benefitted from more detailed and comprehensive subsurface datasets obtained through hydrocarbon exploration in the prolific Southern North Sea gas basin. The models of structural inversion of the Sole Pit Basin and the impact that mobile salt has had on the geological evolution of the region have been derived from detailed subsurface interpretation of these datasets (Glennie & Boegner 1981; Stewart & Coward 1995; Stewart, *et al*. 1996; Stewart & Bailey 1996). They have also benefitted from commissioning analogue models to support their hypotheses (Richard 1991).

1.4 Aims and Objectives

This research project builds on the previous work described above and aims to test the proposed models. However, this author is unaware of any published research to date on the formation of the Flamborough Head Disturbance that has attempted to incorporate a comprehensive onshore and offshore subsurface dataset into one unified model. Thus, the overall objective of this research project is to generate a new and holistic geological model that extends from the onshore, across Flamborough Head, and offshore into the neighbouring waters of the UK Southern North Sea. This will be achieved by utilising the current and up to date UK Onshore Geophysical Library's (UKOGL) onshore 3D seismic surveys and well datasets and Oil & Gas UK's Common Data Access (CDA) offshore 3D seismic surveys and well datasets, both supplemented by 2D seismic from

each authority. A full description of the dataset utilised in this study is included in Chapter 2.3 below.

This new and updated geological model will be used as a benchmark to critically evaluate the observations and hypotheses on the geological evolution of the study area and on the formation of the Flamborough Head Disturbance from the previous research. The pertinent points that this study will address are to:

1. Detail the tectono-stratigraphic history of the study area and the relative timing of basin formation and sedimentary deposition, relating to regional geological trends.

2. Determine the structural regime present at Flamborough Head, in terms of differentiating between dip-slip or strike-slip tectonics and documenting the supporting evidence.

3. Investigate any evidence that supports or refutes the proposal that the Flamborough Head Fault Zone is a continuation of the Dowsing Fault Zone (Kent 1980).

4. Evaluate the role that the Market Weighton Block buried Caledonian granite has had on the geological evolution of the region.

5. Assess the impact that mobile salt has had on the structural and stratigraphic evolution of the study area. Investigate if there is evidence of a decoupled basement – cover at Flamborough Head, as described in the offshore Dowsing Fault Zone (Stewart, *et al*. 1996) and what role, if any, the spatial distribution of Permian Zechstein salt and its shelf edge has had on the geological history of the area.

6. Document any evidence for regional uplift, tilt and structural inversion at Flamborough Head and their relative timings to assess if regional tilt and inversion of the Cleveland Basin are coeval. Relate this to regional stress trends to explain any basin reconfiguration events recognised in the study area.

7. Provide a robust model that describes the preservation of extensional geometries in the post-salt cover at Flamborough Head despite the structural inversion of the Cleveland Basin.

8. Propose a model that describes the formation of the compressive deformation documented in the Chalk outcrops at Flamborough Head.

9. Utilise analogues of inverted Mesozoic basins from around the UK, to aid in developing the Flamborough Head geological model and document any similarities or differences between the study area and the analogues.

10. Investigate any geological controls on the distribution of the prolific Permian Rotliegend Sandstone reservoir within the study area and the present-day hydrocarbon distribution of this and other plays in the wider area.

1.5 Generalised Regional Geology

In order to address the formation of the Flamborough Head Disturbance, it is important to understand the feature in its geological context. The Flamborough Head Disturbance currently straddles the UK coastline, extending from onshore to offshore, but the geology is continuous, with the Flamborough Head Fault Zone continuing offshore. Additionally, an onshore and offshore expression of the inverted Cleveland Basin is recognised to the north of the Flamborough Head Fault Zone (Figure 1.4).

The current configuration was developed during successive periods of deformation that spanned from the pre-Carboniferous to Recent. Although pre-Carboniferous strata have not been penetrated by boreholes in the study area, previous periods of deformation can influence later episodes through control on structural styles or by acting as a locus of deformation through inherited zones of weakness. Therefore, it is important to document the geological history of the area.

1.5.1 Pre-Carboniferous

The Paleozoic geological history of the study area and surrounding UK was marked by two tectonic megasequences: the Late Cambrian to Late Silurian Caledonian Plate Cycle and the Devonian to Late Carboniferous Variscan Plate Cycle. The Caledonian Plate

Cycle represents a cycle of SW-NE Iapetus Ocean opening, closing and terminal collision of both the Iapetus Ocean and the NW-SE trending Tornquist Sea (Underhill 2003), (Figure 1.6).

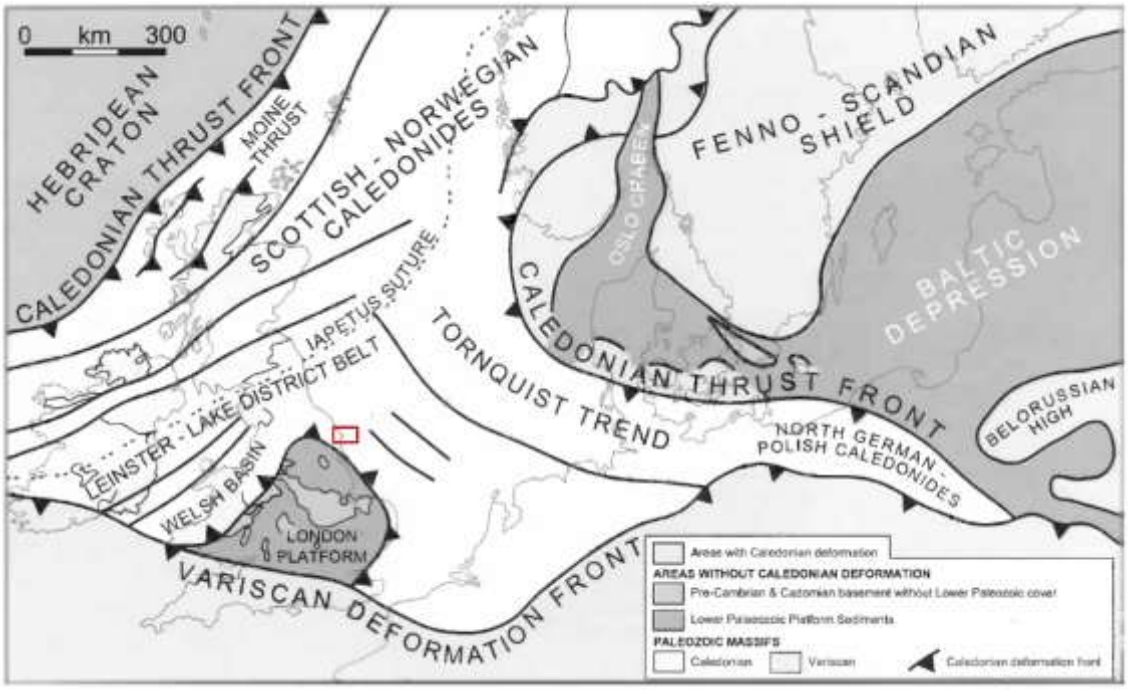

Figure 1.6 Structural framework for NW Europe showing areas affected by Variscan and Caledonian orogenic deformation. Research area shown in red. Modified after Underhill (2003).

Closure of the Iapetus resulted in the formation of the super-continent Laurussia and building of the Appalachian – Caledonide mountain chain. The latest episodes of collision were supplemented by the intrusion of Early Devonian granites (Underhill 2003), such as the one emplaced beneath the Market Weighton Block. These Caledonian granites formed the cores of tectonic "blocks", which remained shelfal areas throughout the later Phanerozoic and control the distribution of basinal areas between them (Underhill 2003).

The Variscan Plate Cycle represents an episode comprising the creation and destruction of the Rheic Ocean. The Rheic Ocean was created during a period of rifting due to intramontane collapse of the Caledonides during the Devonian to Carboniferous, creating an E-W trending passive continental margin across the southern UK (Underhill 2003). The closure of the Rheic Ocean occurred as a consequence of the Late Carboniferous, broadly E-W trending Variscan Orogeny and the creation of the supercontinent Pangaea (Underhill 2003).

The SW-NE Iapetus and NW-SE Tornquist trends of the Caledonian Plate Cycle and the E-W Variscan trend of the Variscan Plate Cycle mark the dominant Paleozoic basement fault trends of the UK and the North Sea (Figure 1.6) and these fault patterns played an important role in controlling basin formation and sedimentation throughout the Carboniferous (Underhill 2003).

1.5.2 Carboniferous

During Early Carboniferous extension, a mixed clastic – carbonate syn-rift depositional system was present. Subsidence at this time exceeded the sediment supply rate so that clastic deltas were restricted to northern parts of the UK. In the southern parts of the UK, carbonate reefs formed along basin margins and as progradational wedges on depositional slopes (Figure 1.3), (Underhill 2003). Extension was replaced by post rift thermal subsidence in the Namurian (Serpukhovian to Bashkirian) and Westphalian (Bashkirian to end Kasimovian) and fluvio-deltaic clastics were widely deposited over the eastern UK and Southern North Sea through progradation to the south from a sedimentary feeder system derived from erosion of the Fenno – Scandian Shield to the north (Figure 1.6). This led to the deposition of the Westphalian Coal Measures group (Figure 1.7), both an important source and reservoir rock contributor to the Southern North Sea gas basin and onshore UK basins (Underhill 2003).

Loading of the Variscan Front during the Late Carboniferous resulted in the formation of an asymmetrical foredeep basin to the north of the emerging Variscan mountain belt covering much of the southern UK. Material sourced from the Variscan Mountains and deposited to the north resulted in the formation of the Stephanian (Gzhelian) aged Barren Red Measures unit, (Underhill 2003).

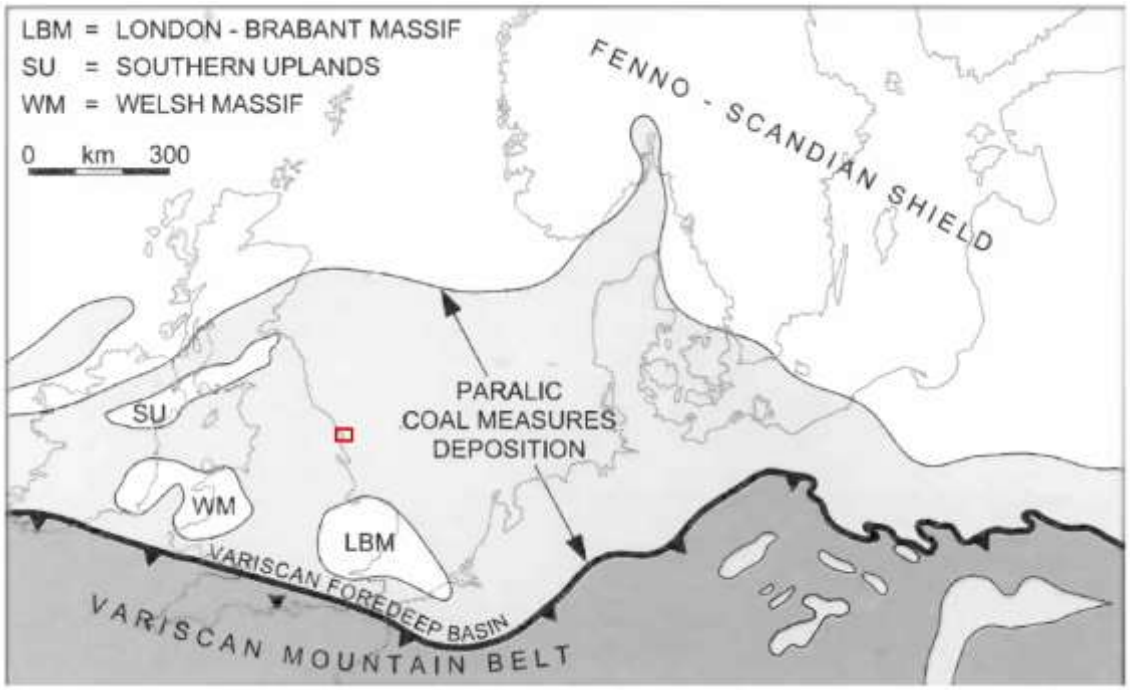

Figure 1.7 Late Carboniferous Variscan Foreland Paleogeography. Study area shown as red box. Modified after Underhill (2003).

1.5.3 Permian

Variscan regional uplift in the Late Carboniferous let to the virtual peneplenation of the existing topography. This was followed by Early Permian subsidence through intramontane collapse of the Variscan Orogen and led to the development of two E-W trending sedimentary basins: the Northern and Southern Permian Basins (Figure 1.8) and widespread deposition of the Rotliegend Group, characterised by arid desert sedimentary facies (Kent 1980; Underhill 2003). The aeolian dune to fluvial gravel beds and sandstones form the Leman Sandstone Formation of the Rotliegend Group, the primary reservoir of the Southern North Sea gas basin. To the north of the Southern North Sea gas basin, the Leman Sandstone Formation is replaced by the non-reservoir Silverpit Claystone Formation. This mudstone-dominated unit represents deposition in a desert lake sabkha environment and provides the top seal for the underlying prospective Carboniferous reservoirs (Underhill 2003).

Figure 1.8 Permian Rotliegend Group paleogeography showing main Northern and Southern Permian Basins. Study area outlined in red. Modified after Underhill (2003)

A major marine transgression led to the deposition of the Zechstein Group over the Rotliegend Group (Figure 1.3). This was a cyclic system of marine incursion; regression and evaporation, leading to the deposition of carbonates and evaporates, with six recognised cycles in the Southern Permian Basin (Underhill 2003; Taylor 2009). Zechstein Group evaporites form the regional super seal for the Rotliegend Group reservoirs in the basin. Zechstein Group carbonates also form a proven hydrocarbon reservoir in the onshore part of the study are and wider Cleveland Basin.

1.5.4 Triassic

In the Early Triassic, the North Sea region was subjected to tensional stresses, resulting in differential subsidence and the creation of a network of grabens and troughs through the UK (Ziegler & van Hoorn 1989). Continental conditions dominated in the Triassic, with the deposition of the fluvial red bed Bunter Sandstone Formation of the Bacton Group across the entire study area. These sandstones are proven hydrocarbon reservoirs in the Southern North Sea and are sealed by the overlying lacustrine shales and evaporates of the Haisborough Group, in particular the Röt Halite unit (Figure 1.3), (Underhill 2003).

1.5.5 Jurassic

Permian and Triassic extension was followed by thermal subsidence in the Early Jurassic. In the post rift sag basins that formed due to this thermal relaxation, marine conditions

dominated, which resulted in the deposition of the marine mudstones of the Lias Group (Figure 1.3). The formation of the Cleveland Basin was initiated during this time, as a result of differential movement between the rigid and buoyant Market Weighton Block to the south and the rapidly subsiding Cleveland Basin to the North, creating a structurally complex hinge zone separating the two structural regions. This hinge zone is the Flamborough Head Fault Zone (Figure 1.1), (Kent 1980).

Uplift followed in the Middle Jurassic as a result of plume-driven thermal doming in the Central North Sea: the "Mid-Cimmerian Event" (Figure 1.9). Subsequent deflation and erosion of the dome led to the development of fluvio-deltaic sandstones which prograded off the collapsing flanks of the dome, including the volumetrically significant Brent Group in the Northern North Sea (Underhill 2003). These units are represented by the time equivalent estuarine sandstone and mudstone facies of the West Sole Group within the study area (Figure 1.3), (Underhill 2003).

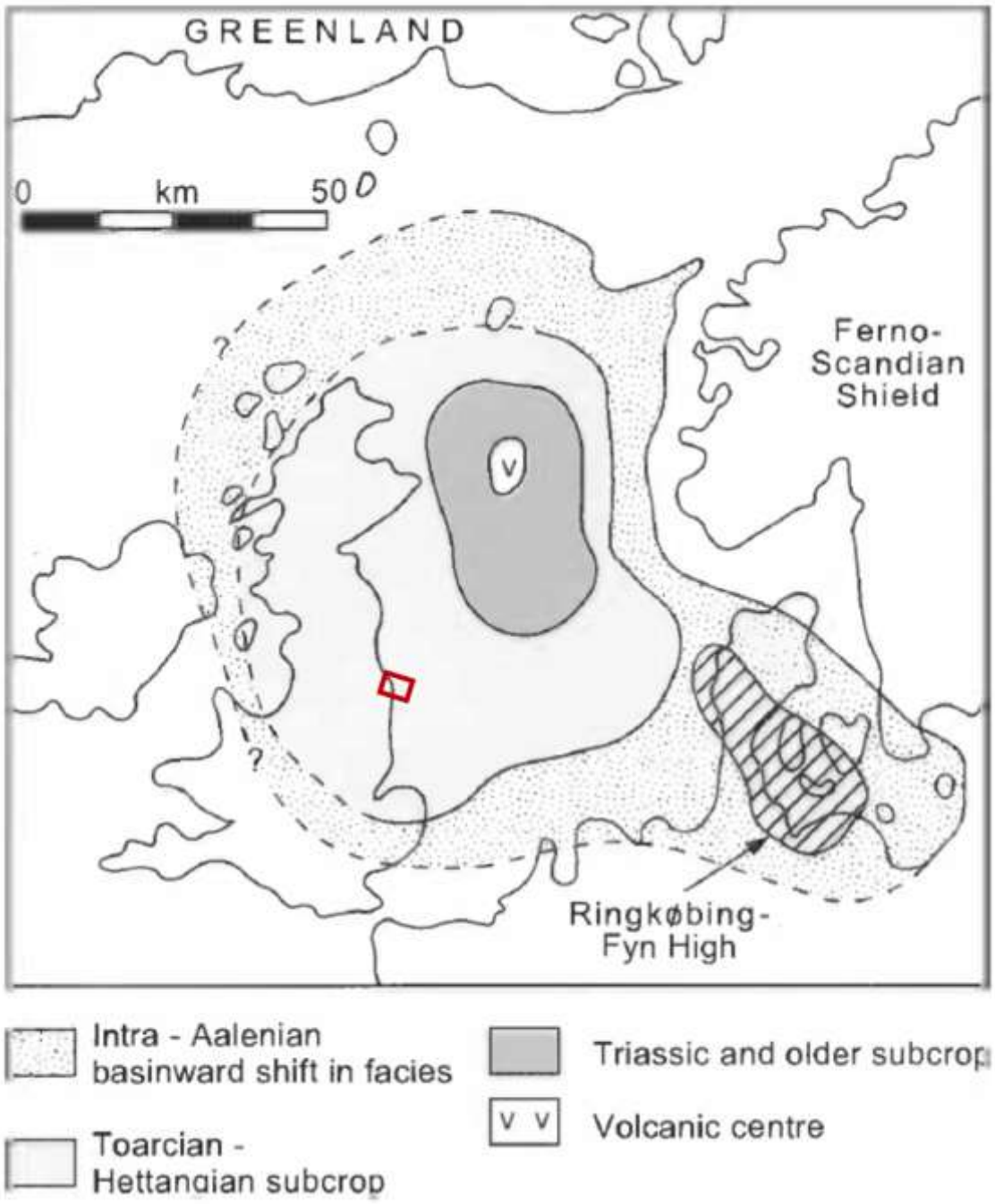

Figure 1.9 Extent of Middle Jurassic Central North Sea Dome. Study area shown as red box. Modified after Underhill, (2003)

Collapse of the thermal dome marked a return to extensional tectonics in the Late Jurassic to Early Cretaceous. To the north of the study area, this led to the development of the Viking Graben, Central Graben and Moray Firth trilete system to the north of the study area (Figure 1.10), (Underhill 2003).

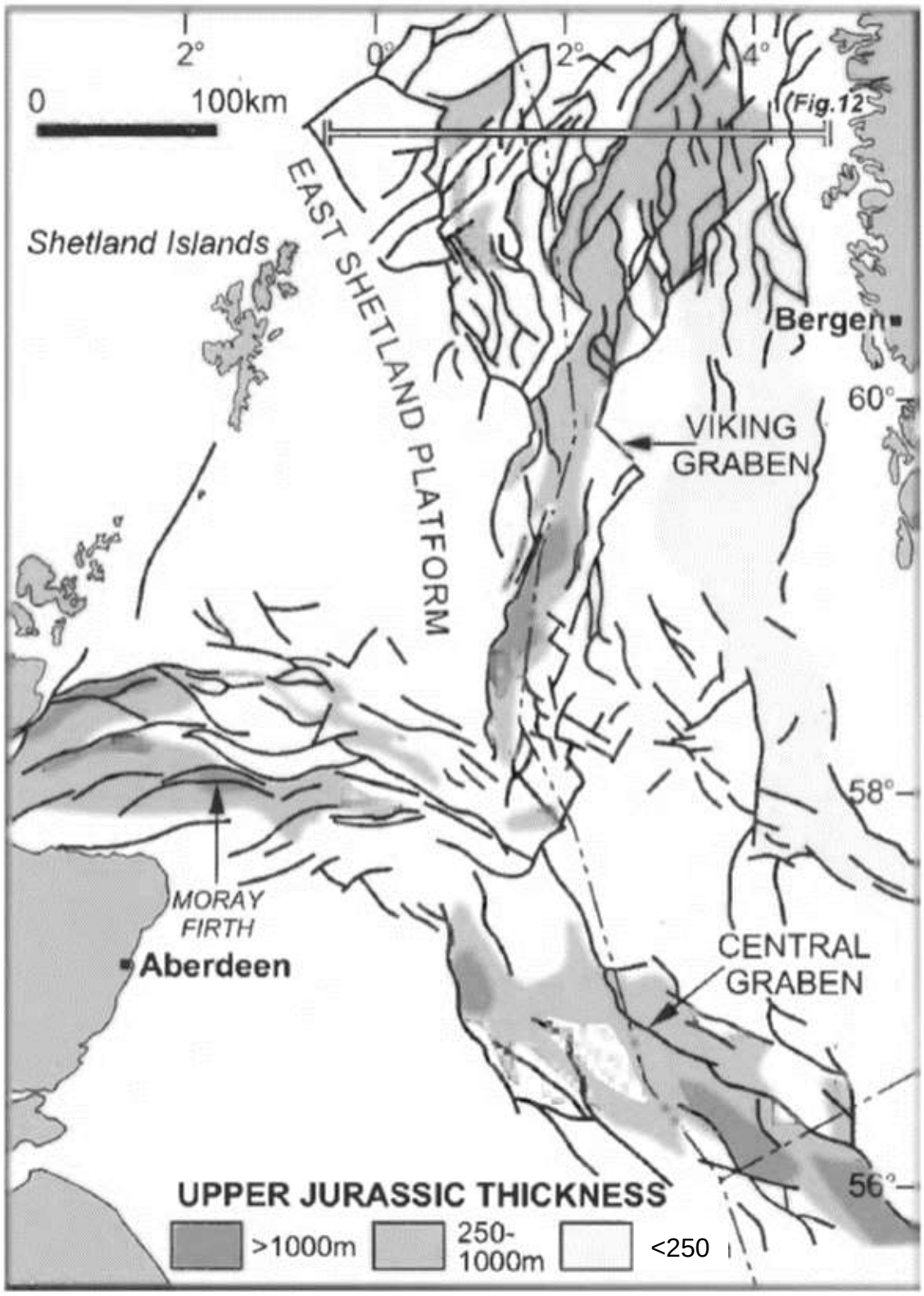

Figure 1.10 North Sea trilete rift system and gross Upper Jurassic syn-rift fill thickness. Modified after Underhill, (2003).

Marine flooding of Late Jurassic extensional basins led to the widespread deposition of the Kimmeridge Clay Formation of the Humber Group, the major source rock of the North Sea Basin (Figure 1.3).

1.5.6 Cretaceous

Any far-field stresses derived from North Sea rifting ceased by the Late Jurassic. An erosive event, the "Late-Cimmerian Event", is noted at approximately the end of the Jurassic, which may relate to this or a postulated southwards migration of the thermal anomaly that created the doming during the Jurassic. In the Lower Cretaceous, deposition of marine claystones of the Cromer Knoll Group occurred within the study area (Figure 1.3), (Underhill 2003). In the Upper Cretaceous, global hothouse conditions and high eustatic sea levels, coupled with low terrigenous sediment input to UK basins due to a mostly flooded topography, resulted in the widespread deposition of Chalk Group carbonates. The Chalk Group deposition marks an end to differential subsidence between the Cleveland Basin and the Market Weighton Block and the beginning of regional subsidence (Figure 1.3), (Dixon 1990; Underhill 2003).

1.5.7 Cenozoic

The opening of the North Atlantic from the Late Cretaceous to the Tertiary initiated intraplate compression through ridge push and the development of the Iceland hot-spot and the Tertiary Igneous Province causing a regional uplift and tilt of the UK to the south east (Guariguata-Rojas & Underhill 2017; Gale & Lovell 2017). This in conjunction with far-field compressional consequences from Alpine collision (Ziegler 1989), resulted in the inversion of UK sedimentary basins, including the Cleveland Basin (Underhill 2003).

1.6 Hydrocarbon Exploration History

The hydrocarbon exploration history for the study area that follows has been divided into an onshore and an offshore component, due to the UK government's policy of licensing these areas separately.

Figure 1.11 displays the distribution of discovered hydrocarbon fields and drilled wells in the study area and surrounding area. Table 1.1 lists a summary of selected hydrocarbon fields from the area and Table 1.2 lists the eighty-one exploration wells that have been drilled to date in the region.

1.6.1 Onshore

Onshore drilling in the Cleveland Basin started in the late 19th century but focussed hydrocarbon exploration did not begin until the 1930's, when D'Arcy Exploration (a

precursory company of BP) discovered gas in Permian Zechstein Group carbonates at Eskdale in 1939. The Eskdale gas field was put on stream in 1960 and produced 860 million cubic feet of gas over seven years until the field was shut in in 1967 (Figure 1.11 and Table 1.1), (Egdon Resources (UK) Ltd. 2000).

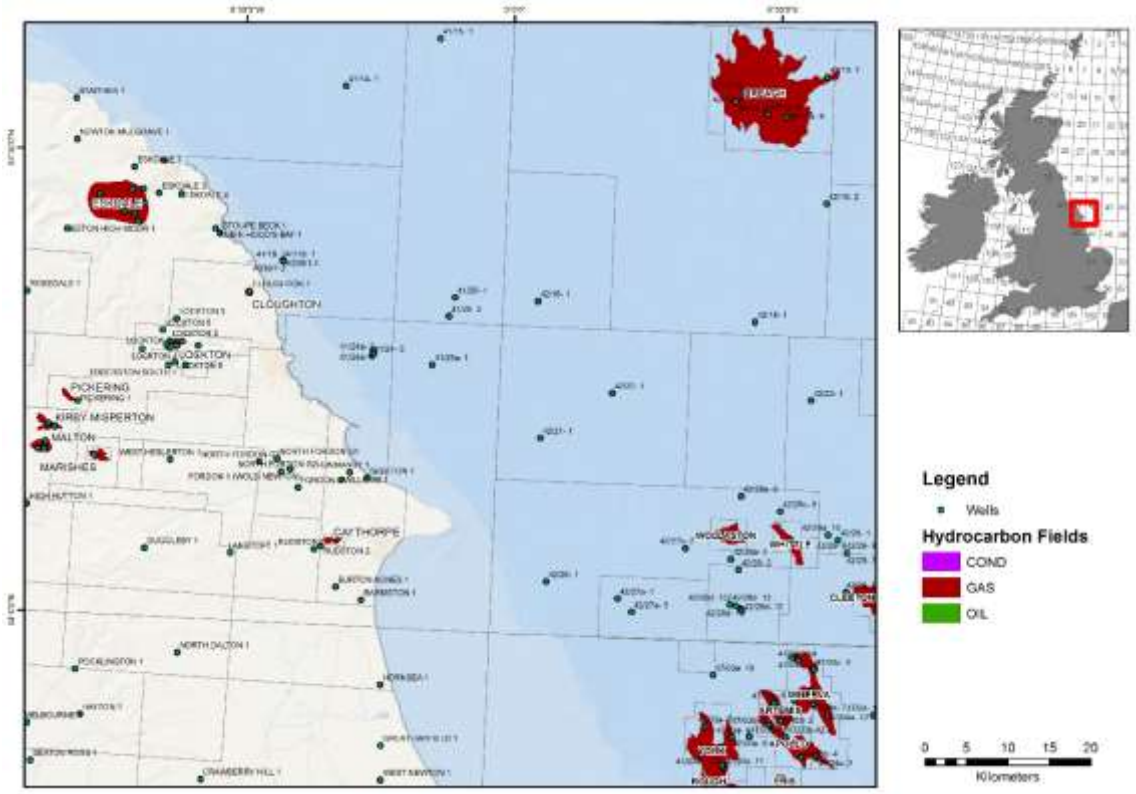

Figure 1.11 Discovered hydrocarbon fields and drilled wells in the study area and surrounding areas of the Cleveland Basin and Southern North Sea. Data courtesy of the Oil & Gas Authority.

*Table 1.1 Summary of selected fields from the study area and surrounding areas. * Roc Oil (UK) Ltd. (2002); ‡ Offshore Technology.com (2017a); † (Offshore Technology.com (2017b)*

Field Name	Shore Status	Discovery Year	Original Operator	Current Operator	Reservoir	Reserves (bcf)	Status
Eskdale	Onshore	1939	D'Arcy Exploration	-	Zechstein Carbonates	0.86*	Abandoned (1967)
Lockton	Onshore	1966	Home Oil of Canada	Third Energy	Zechstein Carbonates	11.3*	Abandoned (1975)
Malton	Onshore	1970	Home Oil of Canada	Third Energy	Zechstein Carbonates	9.8*	Producing
Cleeton	Offshore	1983	BP	Perenco	Rotliegend Leman Sandstone	-	Producing
Kirby Misperton	Onshore	1985	Taylor Woodrow	Third Energy	Zechstein Carbonates & Namurian Sandstones	17.4*	Producing
Cloughton	Onshore	1986	Bow Valley	Third Energy	-	-	-
Caythorpe	Onshore	1987	Taylor Woodrow	Centrica	Zechstein Carbonates & Rotliegend Leman Sandstone	7.5*	Shut in
Marishes	Onshore	1988	Kelt	Third Energy	Zechstein Carbonates	8.1*	Producing
Wollaston	Offshore	1989	BP	Perenco	Rotliegend Leman Sandstone	-	Producing
Whittle	Offshore	1990	BP	Perenco	Rotliegend Leman Sandstone	-	Producing
Pickering	Onshore	1991	Kelt	Third Energy	Zechstein Carbonates	10*	Producing
Breagh	Offshore	1997	Mobil	Ineos	Lower Carboniferous Sandstones	600†	Producing
Tolmount	Offshore	2011	E.ON E&P	Premier Oil	Rotliegend Leman Sandstone	1000 (in place)‡	Pre-development

Table 1.2 Exploration wells drilled within the study area and surrounding region.

Well Name / Number	Shore Status	Spud Year	Operator	Status
ESKDALE 1	Onshore	1937	D'ARCY	P&A Dry
ESKDALE 2	Onshore	1938	D'ARCY	Gas
LOCKTON 1	Onshore	1945	D'ARCY	P&A Oil Shows
HAYTON 1	Onshore	1946	D'ARCY	P&A Dry
ROBIN HOOD'S BAY 1	Onshore	1949	BP	P&A Gas Shows
NORTH FORDON G1	Onshore	1955	D'ARCY	P&A Dry
NORTH FORDON G2	Onshore	1955	D'ARCY	P&A Dry
NORTH FORDON G3	Onshore	1955	D'ARCY	P&A Dry
FORDON 1 (WOLD NEWTON)	Onshore	1956	BP	P&A Oil & Gas Shows
WEST HESLERTON 1	Onshore	1960	SHELL	P&A
SPEETON 1	Onshore	1960	SHELL	P&A
NEWTON MULGRAVE 1	Onshore	1965	HOME	P&A
STAITHES 1	Onshore	1965	HOME	P&A
41/20- 1	Offshore	1965	-	P&A Dry
A339/1-1	Onshore	1966	TOTAL	P&A
ROSEDALE 1	Onshore	1966	HOME	P&A
A339/1-2	Onshore	1966	TOTAL	P&A
42/23- 1	Offshore	1966	-	P&A Gas Shows
41/18- 1	Offshore	1966	-	P&A Dry
41/18- 2	Offshore	1966	-	Unknown
EGTON HIGH MOOR 1	Onshore	1968	BP	P&A
42/13- 1	Offshore	1968	-	P&A Dry
42/29- 1	Offshore	1968	-	P&A Dry
41/24a- 1	Offshore	1969	-	Gas
41/25a- 1	Offshore	1969	-	Gas
41/20- 2	Offshore	1969	-	Gas
42/28- 1	Offshore	1969	-	Gas
HORNSEA 1	Onshore	1970	TEXACO	P&A
MALTON 1	Onshore	1970	HOME	Gas
LANGTOFT 1	Onshore	1970	HOME	P&A
GREAT HATFIELD 1	Onshore	1971	BP	P&A
WYKEHAM 1	Onshore	1971	HOME	P&A Gas
BARMSTON 1	Onshore	1971	BURMAH	P&A
NORTH DALTON 1	Onshore	1972	CANDECCA	P&A
POCKLINGTON 1	Onshore	1973	CANDECCA	P&A
SEATON ROSS 1	Onshore	1973	CANDECCA	P&A
HUNMANBY 1	Onshore	1973	BURMAH	P&A
42/28- 2	Offshore	1973	-	P&A Gas Shows
FORDON 2	Onshore	1974	BP	P&A Gas
42/26- 1	Offshore	1974	-	P&A Dry
LOCKTON EAST 1	Onshore	1980	TAYLOR WOODROW	P&A
RUDSTON 1	Onshore	1984	TAYLOR WOODROW	P&A
KIRBY MISPERTON 1	Onshore	1985	TAYLOR WOODROW	Gas
CLOUGHTON 1	Onshore	1986	BOW VALLEY	P&A Gas Shows
42/29- 5	Offshore	1986	-	P&A Dry
CAYTHORPE 1	Onshore	1987	TAYLOR WOODROW	Gas
HIGH HUTTON 1	Onshore	1987	ENTERPRISE	P&A Oil & Gas
42/22- 1	Offshore	1987	-	P&A Gas Shows
MARISHES 1	Onshore	1988	KELT	Gas
42/29- 6	Offshore	1989	BP EXPLORATION OPERATING COMPANY LIMITED	Gas
DUGGLEBY 1	Onshore	1990	AMOCO	P&A
41/14- 1	Offshore	1990	-	P&A Gas Shows
42/28b- 5	Offshore	1990	-	Gas
42/29- 7	Offshore	1990	BP EXPLORATION OPERATING COMPANY LIMITED	Gas
42/29- 8	Offshore	1990	BP EXPLORATION OPERATING COMPANY LIMITED	Gas
42/27a- 1	Offshore	1990	-	P&A Gas Shows
PICKERING 1	Onshore	1991	KELT	Gas
42/18- 1	Offshore	1991	-	P&A Dry
41/15- 1	Offshore	1991	-	P&A Dry
42/28a- 6	Offshore	1992	-	Gas
41/24- 3	Offshore	1992	-	Gas
42/18- 2	Offshore	1993	-	P&A Dry
42/16- 1	Offshore	1993	-	P&A Dry
42/27b- 2	Offshore	1994	-	P&A Gas Shows
RUDSTON 2	Onshore	1996	PERENCO	P&A Gas Shows
STOUPE BECK 1	Onshore	1997	CANDECCA	P&A
42/13- 2	Offshore	1997	-	Gas
ESKDALE 13	Onshore	2000	STAR	P&A Gas
42/21- 1	Offshore	2005	CENTRICA RESOURCES LIMITED	P&A Gas Shows
WILLOWS 1	Onshore	2006	ROC	P&A
42/28c- 9	Offshore	2006	CENTRICA RESOURCES LIMITED	P&A Dry
EBBERSTON MOOR 1	Onshore	2007	VIKING	P&A
BURTON AGNES 1	Onshore	2007	EGDON	P&A Gas Shows
42/27a- 3	Offshore	2007	RWE DEA UK LIMITED	P&A Gas Shows
EBBERSTON SOUTH 1	Onshore	2008	MOORLAND	P&A
42/28d- 10	Offshore	2008	DANA PETROLEUM (E&P) LIMITED	Junked
42/28d- 11	Offshore	2010	E.ON E&P UK LIMITED	Junked
42/28d- 11Z	Offshore	2010	E.ON E&P UK LIMITED	Junked
42/28d- 12	Offshore	2011	E.ON E&P UK LIMITED	Gas
CRAWBERRY HILL 1	Onshore	2013	RATHLIN ENERGY (UK) LIMITED	P&A
WEST NEWTON 1	Onshore	2013	RATHLIN ENERGY (UK) LIMITED	P&A

The next intensive phase of exploration occurred in the 1960's and 1970's when Home Oil of Canada acquired the first 2D reflection seismic in the area. Gas was discovered in Permian Zechstein Group carbonates at Lockton in 1966 and Malton in 1970 (Figure 1.11 and Table 1.1). Lockton produced 11.3 billion cubic feet of gas while on production from 1971-1974 prior to being abandoned due to excessive formation water production (Egdon Resources (UK) Ltd. 2000). Burmah Oil Exploration, Candecca and Taylor Woodrow began exploring the area in the 1970's and 1980's, leading to the discovery of gas in Permian Zechstein Group carbonates at Malton in 1970 and the first commercially significant Carboniferous gas discovery in Namurian aged sandstones at Kirby Misperton in 1985 by Taylor Woodrow (Figure 1.11 and Table 1.1). Gas produced at Kirby Misperton is used for local power generation (Egdon Resources (UK) Ltd. 2000). Burmah had little success in the local area, drilling the Barmston-1 and Hunmanby-1 dry holes in 1971 and 1973 respectively. From the 1980's to the 1990's, Kelt entered the basin and discovered gas in Permian Zechstein Group carbonates at Marishes in 1981 and Pickering in 1991. The discovery of the Caythorpe gas field by Taylor Woodrow in 1987 led to the first significant Permian Rotliegend Group Leman Sandstone Formation gas discovery in the Cleveland Basin. Additional gas was found at this field in shallower Permian Zechstein Group carbonates. The site was converted to power generation in 1997 and production ceased in 2008 with a cumulative 5.8 billion cubic feet gas produced from in place volumes on 9.8 billion cubic feet (Warwick Energy 2006). The most recent exploration well drilled in the Flamborough Head area was Burton Agnes-1 dry hole, drilled by Egdon Resources in 2007. The Permian Rotliegend Group Leman Sandstone Formation was the main objective in this well. Current exploration activity is focussing on unconventional prospectivity of the Carboniferous Bowland Shale Formation.

1.6.2 Offshore

Offshore, exploration in Quad 41 to the north of Flamborough Head was dominated by Total in the 1960's and 1970's where they discovered three non-commercial discoveries at 41/20-2, 41/24a-1 and 41/25a-1 (Figure 1.11). All of these wells tested gas from Permian aged Zechstein Group fractured dolomites (Roc Oil (UK) Ltd. 2002). In addition to these proven hydrocarbon discoveries a small, untested gas cap (identified through electric log interpretation) was encountered at the top of the Triassic Bunter Sandstone Formation in the 41/20-1 well.

In Quad 42, seaward of Flamborough Head, Amoco (and subsequently BP) was the dominant operator from the late 1960's through to the early 2000's and found success through the discovery of the Cleeton, Wollaston and Whittle gas fields. All three fields had gas accumulations within the Permian Rotliegend Group Leman Sandstone Formation and were discovered in 1983, 1989 and 1990, respectively. From the 2000's Centrica, RWE Dea, Dana Petroleum and E.ON drilled in the local area. The only success of this campaign was the Permian Rotliegend Group Leman Sandstone Formation Tolmount gas discovery by the 42/28d-12 well by an E.ON / Dana Petroleum consortium in 2011 (Figure 1.11). The Tolmount discovery is currently in the front-end engineering design phase, and is expected to be brought on-stream in 2020 with potential in place gas volumes of up to one trillion cubic feet (Offshore Technology.com 2017a).

The Breagh field to the north – east of the study area represents a volumetrically significant Lower Carboniferous (Scremerston Formation sandstones) gas discovery in the surrounding region (Figure 1.11). The field was discovered in 1997 when Mobil drilled the 42/13-2 well. The field was brought on-stream in 2013 and is estimated to contain 600 billion cubic feet recoverable gas reserves (Offshore Technology.com 2017b)

The current licencing situation for the study area is displayed in Figure 1.12. Ineos, Cuadrilla and Third Energy dominate the onshore licencing around Flamborough Head. Offshore shows a more diverse licencing situation, with the presence of UK independents, IOC's, NOC's and supermajors.

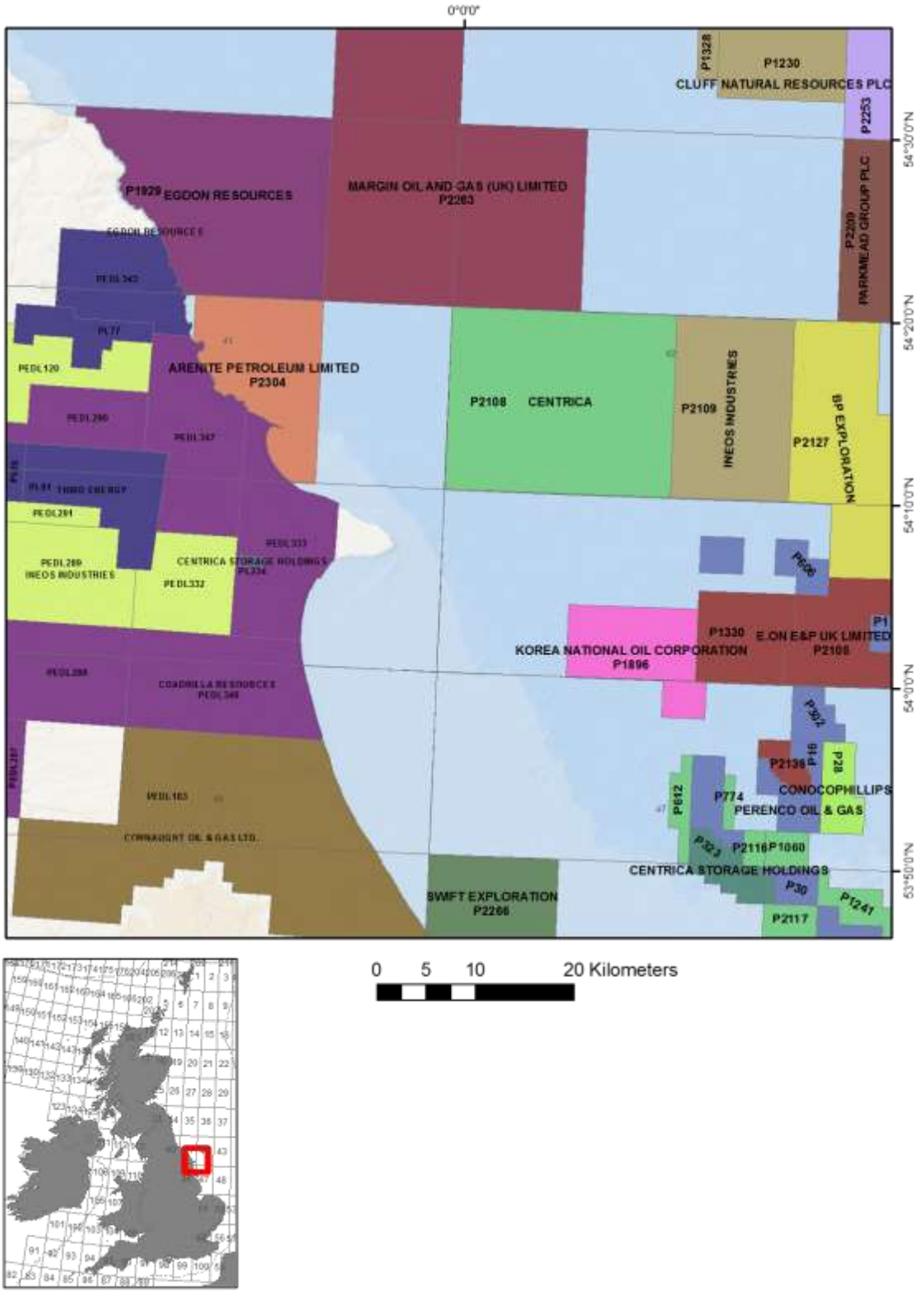

Figure 1.12 Present day licence status of the study area with UKCS quadrant map shown as context. Data courtesy of the Oil & Gas Authority

CHAPTER 2. DATA AND METHODOLOGY

2.1 Introduction

The data interpreted for this study consist of a surface and a subsurface geological element. Available surface geological data are primarily in the form of published maps by the British Geological Survey and published research on geological outcrops in and around the study area. In addition, outcrop localities on the Yorkshire coast were visited to aid in developing the geological model of this study, encompassing Lower and Middle Jurassic coastal exposures of the Cleveland Basin and Upper Cretaceous Chalk cliffs at Flamborough Head. However, as documented in Chapter 1 above, the geological complexities of Flamborough Head are best resolved through observations made in the subsurface. Therefore, this chapter describes and documents the subsurface dataset that has been interpreted and which forms the basis of the evaluations in this research project. It also provides an overview of the theory and applications used in acquiring such data and the best practice methods employed in the oil and gas industry to interpret it. The primary form of subsurface data used for investigating the shallow subsurface is seismic reflection data.

2.2 Seismic Reflection Basics

Seismic reflection data is a fundamental interpretational tool that is used by geoscientists to understand the development of the depositional and tectonic history of a basin (Bertram 2012). For the purpose of this study, the seismic data were provided in their final processed, form which consists of either 2D lines or 3D volumes. 2D seismic lines consist of a representation of the subsurface along a single vertical transect. A 3D seismic volume is comprised of multiple 2D lines gathered in two perpendicular orientations that are closely enough spaced that they essentially form a three-dimensional representation of the subsurface within a specific area. Both are measured in the time domain because the process of acquisition uses the travel time of sound waves propagating through the subsurface. Seismic data recorded in time can be equated to depth through mathematical equations. However, although the data utilised in this study were not specifically acquired and processed for it, it is still important to understand the fundamentals of acquiring and processing the data as the methods used can have implications for interpretation.

2.2.1 Seismic Acquisition and the Seismic Pulse

The basic concept of seismic reflection surveying is to use sound waves to investigate the subsurface. Sound waves are generated from an artificial seismic source and their transmission paths and propagation velocities through the subsurface are mapped to deliver information on the distribution of subsurface boundaries at depth (Kearey, *et al*. 2002). In the case of a typical conventional marine seismic reflection survey, a towed air gun and receiver cable arrangement is used to acquire seismic data (Figure 2.1).

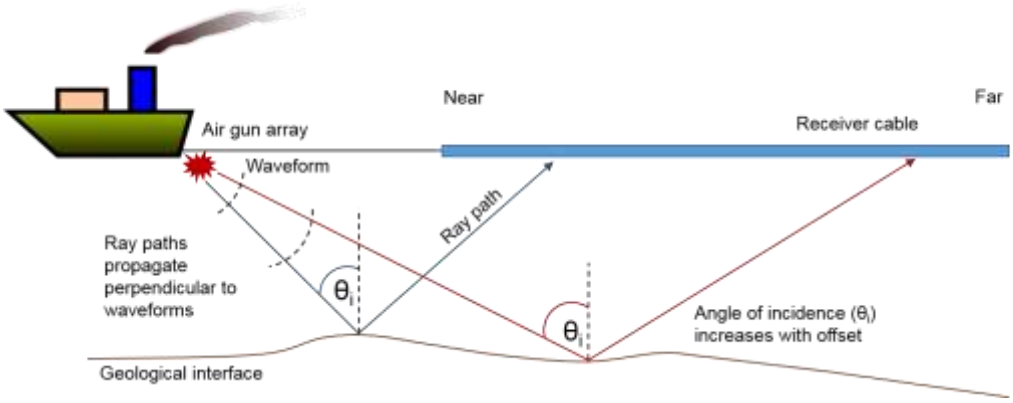

Figure 2.1 Geometry of a typical marine seismic acquisition arrangement. Modified after Chamberlain & Rock Physics Associates (2013)

The principles for a conventional land seismic reflection survey are similar but the receiver cables remain static on the ground and the source (usually explosives or a seismic vibrator) location is moved. In a marine seismic acquisition survey, an air gun produces an artificial seismic source through the rapid release of a highly pressurised air bubble that sends a wave of sound energy into the subsurface. As the wave-path propagates through the subsurface, it reflects at geological surfaces. Acoustic impedance (AI) is the rock property that governs reflections, specifically its difference between two geological layers (Chamberlain & Rock Physics Associates 2013). Acoustic impedance is a function of the density and seismic velocity of a rock unit and is represented as:

$$AI = \rho_B \times V_P$$

Equation 2.1 Acoustic impedance (AI) formula where ρ_B = bulk density of rock unit and V_P = P-wave interval velocity of rock unit

Reflection strength is governed by the contrast in acoustic impedance between geological units so that a greater acoustic impedance contrast generates a stronger reflection. The size of this change is represented by the reflection coefficient (RC). Where acoustic

impedance increases then the reflection coefficient is positive and where it decreases the reflection coefficient is negative. The seismic response from an acoustic impedance change is a wave consisting of troughs and peaks (Figure 2.2), (Badley 1990).

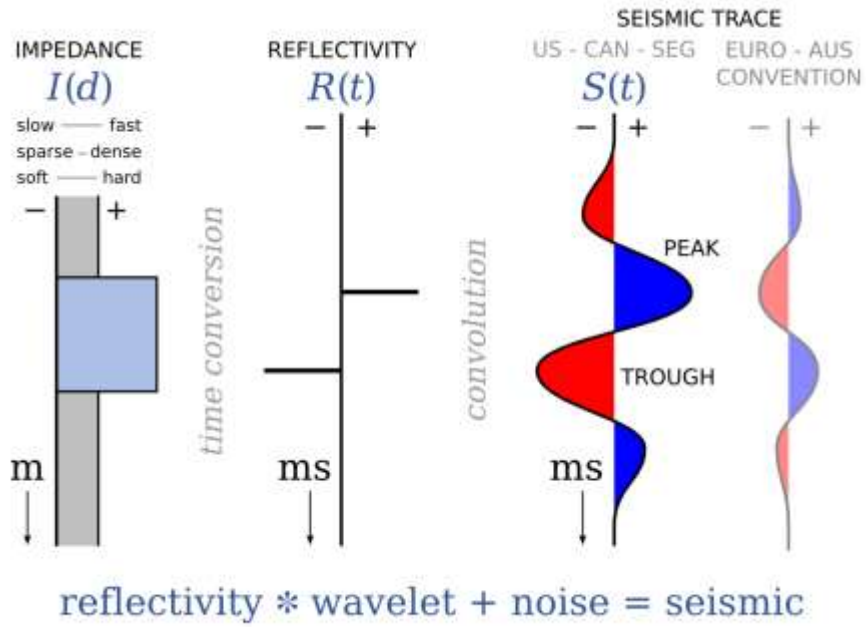

Figure 2.2 Model of seismic reflection – the convolution model (Agile Geoscience 2016).

The seismic response to an acoustic impedance contrast is recorded on a seismic display as a pulse with either a minimum phase or zero phase shape (Figure 2.3). A minimum phase pulse is where the energy is concentrated at the start of the pulse i.e. the wavelet starts at the acoustic impedance boundary and the maximum amplitude is located in the first peak or trough of the signal (Badley 1990). Most percussive seismic sources generate a minimum phase signal. In a zero phase wavelet, the wavelet starts at the acoustic impedance boundary and this is where the maximum amplitude is recorded. Seismic data are typically converted to a zero phase wavelet during processing as this improves signal to noise ratio and benefits interpretation as the maximum amplitude recorded represents the exact location of the acoustic impedance contrast (Badley 1990).

Figure 2.3 also demonstrates the two polarity types used in the recording and displaying of seismic data. The Society of Exploration Geophysicists (SEG) has defined the polarity standard as such that compressional waves from a seismic source or a positive reflection coefficient boundary (i.e. minimum phase) are recorded as a negative number and displayed as a trough, usually plotted in white. In the case of a zero phase wavelet, a

positive reflection coefficient is displayed as a central peak, usually plotted in black (Badley 1990). This standard is often referred to as normal polarity. In Europe and Australia, this convention is reversed and is termed reverse polarity.

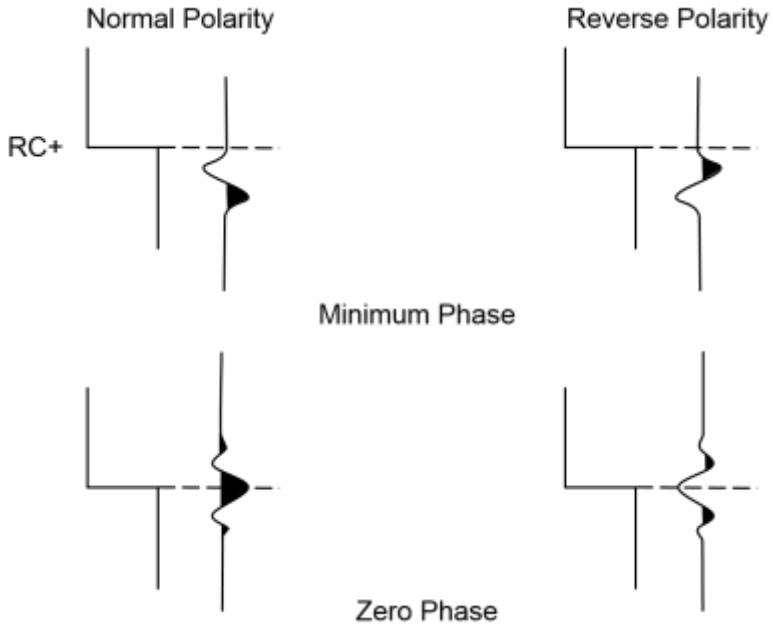

Figure 2.3 Illustration of normal and reverse polarity for minimum and zero phase wavelets at an acoustic impedance boundary with a positive reflection coefficient (RC). Modified after Badley (1990).

As shown in Figure 2.1 the path of sound energy from source to receiver is described by rays that are perpendicular to the seismic wave front and it these paths that are recorded by multiple hydrophone receivers on each receiver line of the towed gun – tow line assembly (Chamberlain & Rock Physics Associates 2013). It is the travel time of a sound energy wave from the source down to a reflection surface and back to an array of receivers at surface that is measured and is known as two-way travel time (TWTT).

Seismic acquisition is made of many shot and receiver recordings. Every receiver records every shot and each receiver records reflections from different subsurface locations for every shot (Figure 2.4). The product of this is the shot gather, which is a combination of energy from multiple subsurface locations. To compensate for this and to relate the reflection energy to the same subsurface point, the reflection energy is rearranged in terms of line location or common mid-point (Chamberlain & Rock Physics Associates 2013). To achieve a common reflection point, the shots and receivers are positioned equal distances either side of the desired reflection point so that they have a common mid-point (CMP) gather (Figure 2.4), (Chamberlain 2013).

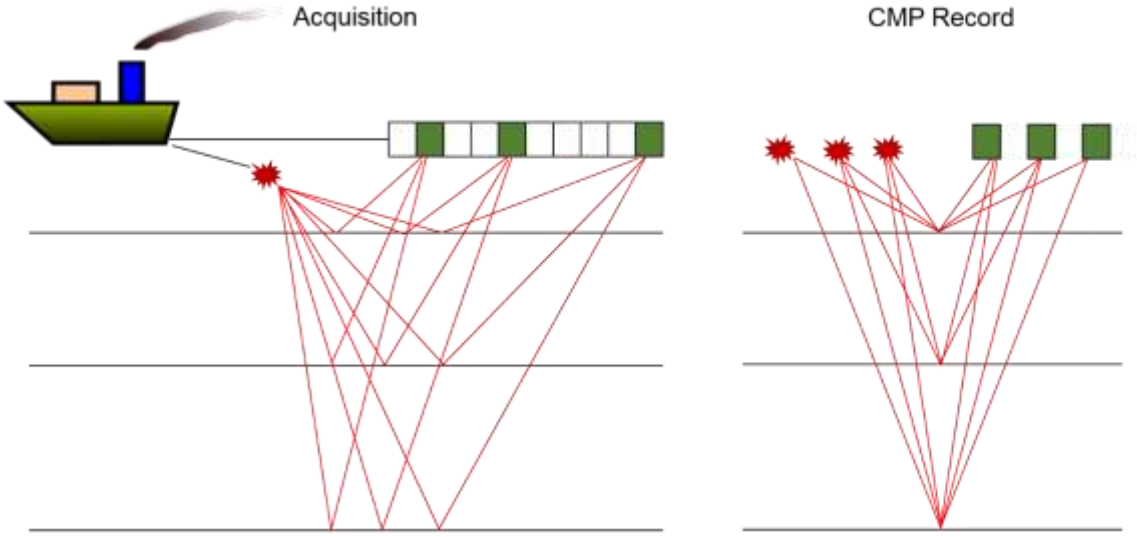

Figure 2.4 Marine seismic acquisition geometry and re-arranging to common mid-point (CMP). Modified after Chamberlain & Rock Physics Associates (2013)

2.2.2 Seismic Processing

In order to generate a seismic profile that can be interpreted the gathers need to be processed. A detailed description of the steps used in seismic processing is beyond the scope of this thesis (for more information see Kearey, *et al*. 2002). Three important processing steps in visualising seismic sections and which are relevant to the seismic dateset interprteted in this project are time migration, stacking and static corrections.

The common mid point record shown in Figure 2.4, where the reflection point is located directly beneath the mid-point is only true where reflectors are perfectly horizontal. Time migration is a geometric correction which rearranges seismic data so that reflection events are displayed nearer their true subsurface positions (Chamberlain 2013). In the case of inclined reflectors, the reflector will be displayed downdip and the reflection will be longer than the reflector. Where reflectors are inclined in a plane which dips across the survey line then the reflection is displaced out of plane of the survey section line (Kearey, *et al*. 2002). Migration moves reflection events laterally to their true locations which results in the steepening of reflector dips and reflectors being moved up dip (Chamberlain 2013).

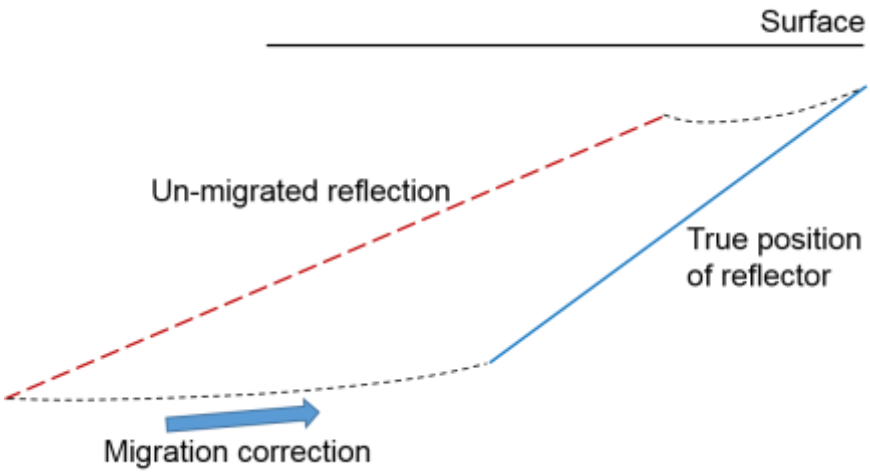

Figure 2.5 Migration correction for displaying reflections at their true position. Modified after Badley (1990)

Stacking is the summing and normalising procedure used to combine properly processed (and usually migrated) seismic gathers that are reflected from the same subsurface point but which have different source-reciever pairs, in order to remove the increasing delay in transit time that is seen with increasing source-receiver offset. To achieve this, the data are alligned to correct for the varying delay with offset and then summed (stacked). Post stacking, the data are then normalised by dividing the value at each sample by the number of active traces (Figure 2.6), (Chamberlain 2013).

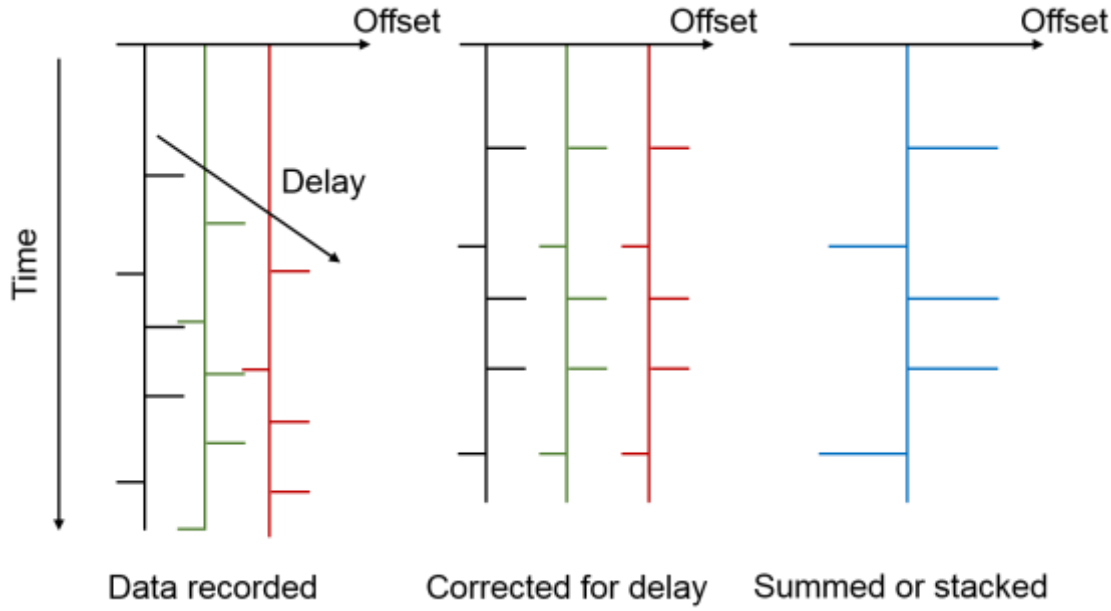

Figure 2.6 Stacking seismic gathers to correct for travel time delay with increasing source-receiver offset. Modified after Chamberlain (2013).

Static corrections are a fundamental stage in the processing of seismic data that has been acquired on land. These are corrections made to the timing of the data to remove the effects due to varying elevation or short-wavelength near-surface velocity variations caused by the weathering layer (Figure 2.7). If these effects are not accounted for, then data will not stack together properly and false structures may be introduced (Chamberlain 2013).

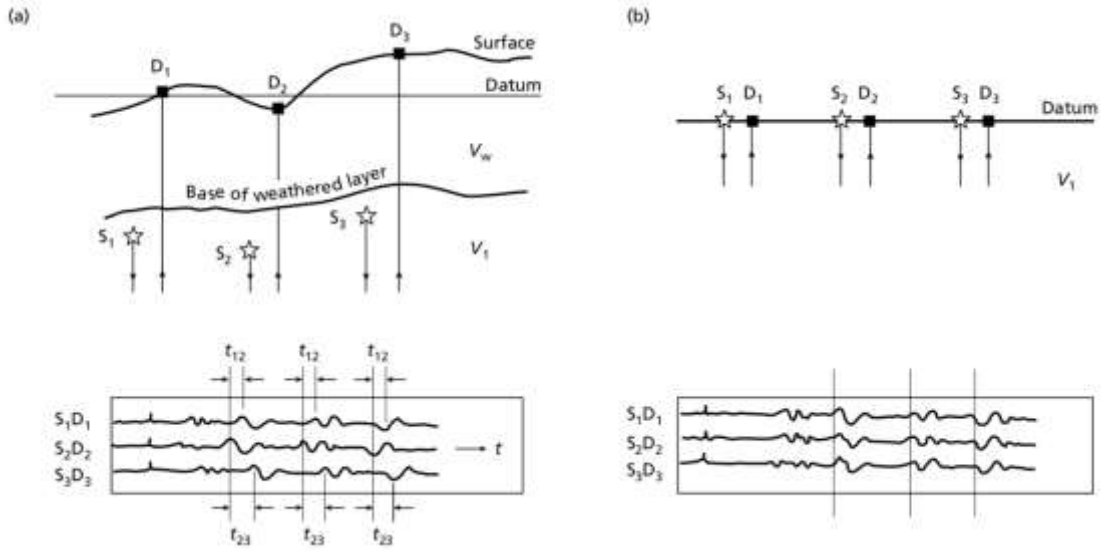

Figure 2.7 Static corrections. (a) Seismograms displaying time differences between reflection events on adjacent seismograms due to variations in shot-receiver point elevations and the presence of a weathering layer. (b) The same seismograms after elevation and weathering static corrections have been applied, showing good alignment of reflection events (Kearey, et al. 2002).

2.2.3 Resolution, Noise and Distortions

Even with well processed seismic data, there are a number of limitations and artificial responses that the seismic interpreter should be aware of. A key factor is the effect of depth on the seismic signal. For a normal pressure gradient, acoustic impedance will increase with depth as rocks compact. Where a lithology is highly compactable, such as in a shale, the acoustic impedance of this lithology will increase with burial depth at a greater rate than a lithology which is less compactable, such as a sandstone or a limestone. The result of this is that even though the acoustic impedance of rock layers increases with depth, the contrast in acoustic impedance between rock layers decreases and therefore the reflections become weaker with depth for a given lithology pair (Badley 1990). In addition to a decrease in acoustic impedance contrast, the seismic signal becomes weaker with depth due to transmission losses. The third factor that affects seismic resolution with depth is the result of the earth naturally filtering out the high frequencies of the

propagating wavelet than the lower frequencies so that a progressively lower frequency wavelet will be reflected with depth resulting in poorer seismic resolution (Badley 1990).

As well as seismic resolution issues, there are also noise and distortions that can affect the seismic signal, resulting in the recording of reflections that are not primary reflections. An example of this is the recording of multiples. Multiples occur when upcoming reflectors are bounced back into the subsurface by a strongly contrasting acoustic impedance interface (Figure 2.8). A common example of this is the sea water – seabed interface encountered in marine seismic environments. Figure 2.8 illustrates that multiple reflections have a time delay that is equivalent to the thickness of the strongly contrasting acoustic impedance layer in which the extra reflection has occurred. Because of this effect, multiples that are reflected from inclined reflectors will be recorded as having twice the dip of the primary reflection. Multiple reflections will also have an opposite seismic polarity to the primary reflection (Badley 1990).

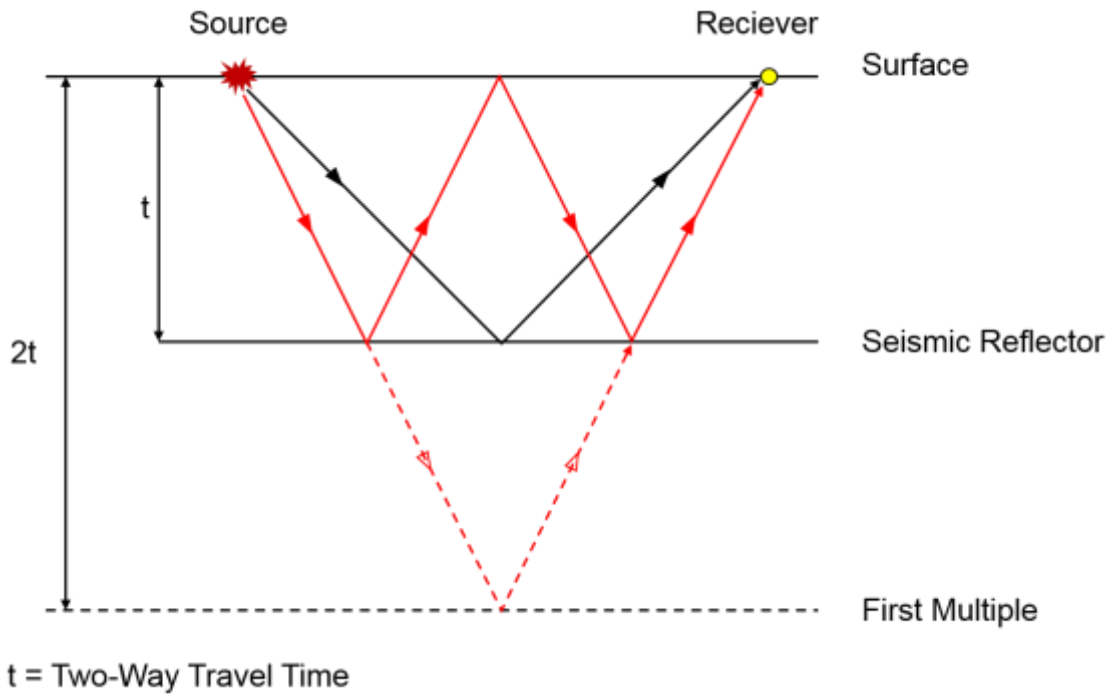

Figure 2.8 Diagram illustrating the ray path geometry of a simple multiple. The black line shows the primary. Solid red line represents the bounced wave. Dashed red line shows the multiple as recorded on the receiver. Modified after Badley (1990).

Sound waves are scattered by features such as faults, which have a sharp acoustic impedance interface, creating diffractions. Diffractions are commonly encountered on un-migrated seismic where they appear as hyperbolic reflections or "smiles" (Figure 2.9).

Diffractions are usually removed by migration but can still occur as remnant refractions from out of plane objects on migrated seismic sections (Badley 1990).

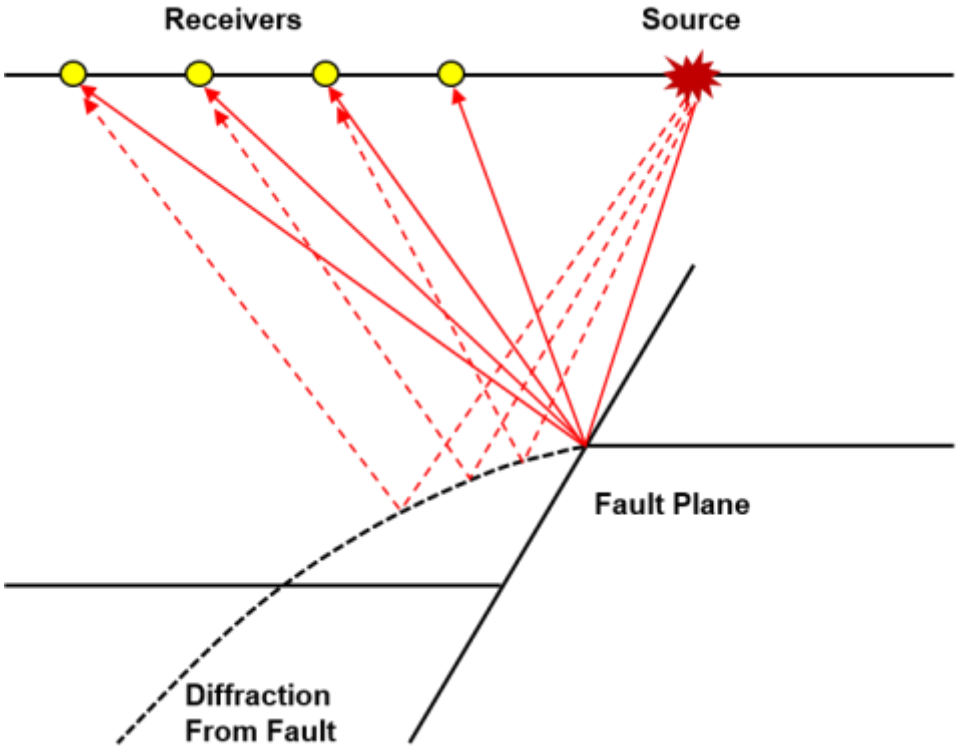

Figure 2.9 Diagram illustrating the development of a diffraction from a fault plane. The hyperbolic shape results from the assumption made by the common mid-point method that reflections occur at the mid-point between the source and the receiver. Modified after Badley (1990)

2.2.4 Resolution, Noise and Distortions Specific to the Study Area

The previous section detailed the main common factors that can impact upon the seismic signal and data quality. The study area and greater Southern North Sea contain unique lithological characteristics that have been shown to adversely affect seismic data quality and introduce anomalies, and these are detailed below.

As documented in Section 1.5 above, the study area and surrounding Southern Permian Basin contains a succession of Permian aged Zechstein Group evaporites which contain halite, anhydrite, gypsum and carbonates such as limestone and dolomite. In the subsurface, salt, such as halite, is unstable as it is almost incompressible and its density is significantly less than other sedimentary rocks (2.160 g/cc compared to around 2.5 g/cc for a sandstone), (Fossen 2010). This makes salt buoyant and it has a tendency to become ductile and flow when it is physically loaded (Badley 1990). Once salt has started to flow, it can form either linear features, such as salt rollers, salt walls and anticlines, or

vertical structures, such as salt pillows, salt domes or, where the salt pierces its overburden, a salt diapir (Figure 2.10), (Fossen 2010).

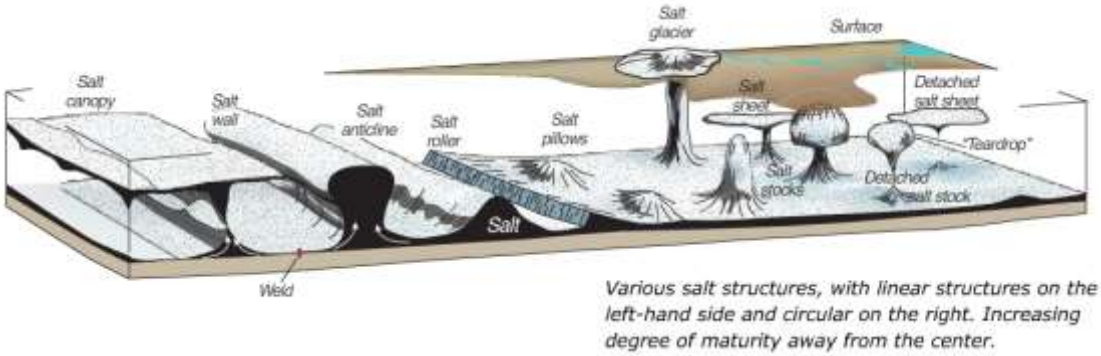

Figure 2.10 Examples of the geometries of salt structures formed by once salt has started to flow (Fossen 2010).

As Figure 2.10 illustrates, the subsurface structures generated by the movement of salt result in significant thickness changes of the salt layer. Even though the density of salt is low, it has a relatively high interval velocity when compared to sedimentary rocks (around 4,500m/s compared to around 3,000m/s for a sandstone), (Badley 1990). Because of this, where salt is thick (such as at a salt diapir) sound waves will travel through the salt more quickly than through the surrounding sediments. This results in reflectors below the salt being recorded sooner than laterally adjacent areas where salt is thin or absent (Badley 1990). This phenomenon is known as velocity pull up (Figure 2.11). Salt structures are often steep sided. Therefore, this steeply inclined acoustic impedance contrast at the edge of a salt body introduces noise and diffractions into the seismic data which obscures the exact geometry of the structure (Fossen 2010).

Lithology effects are also recognised to cause a degradation in seismic quality in parts of the North Sea, particularly the presence of a Chalk subcrop at sea bed (Figure 2.12). This reduction in seismic quality results from energy dispersal and attenuation in the Chalk as well as the generation of multiples due to reverberation within the water column where the Chalk subcrops at sea bed (Argent, *et al*. 2000).

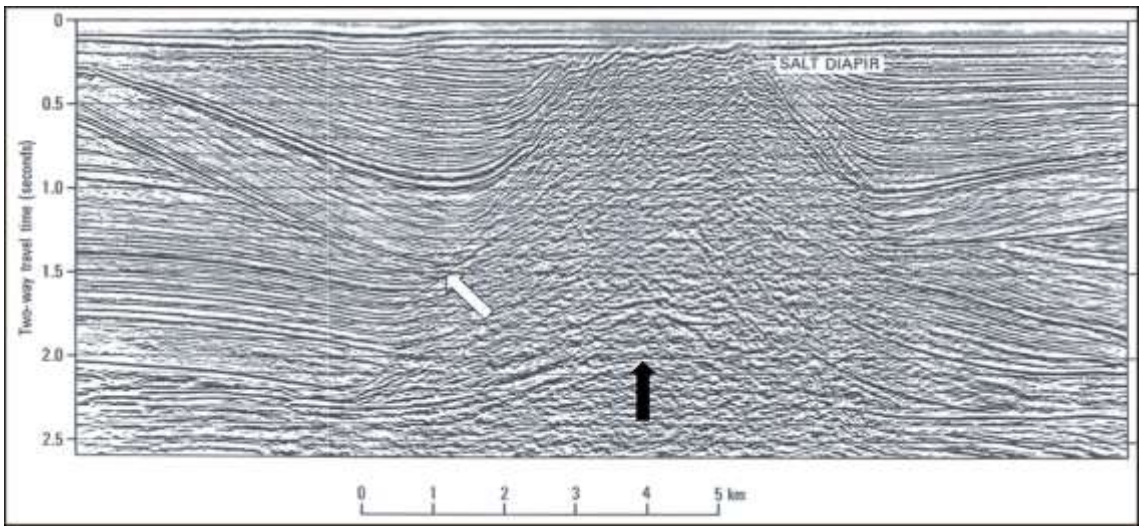

Figure 2.11 Velocity pull up of reflectors beneath a salt diapir (black arrow) and diffractions at the edge of the diapir (white arrow). Modified after Stewart (2008)

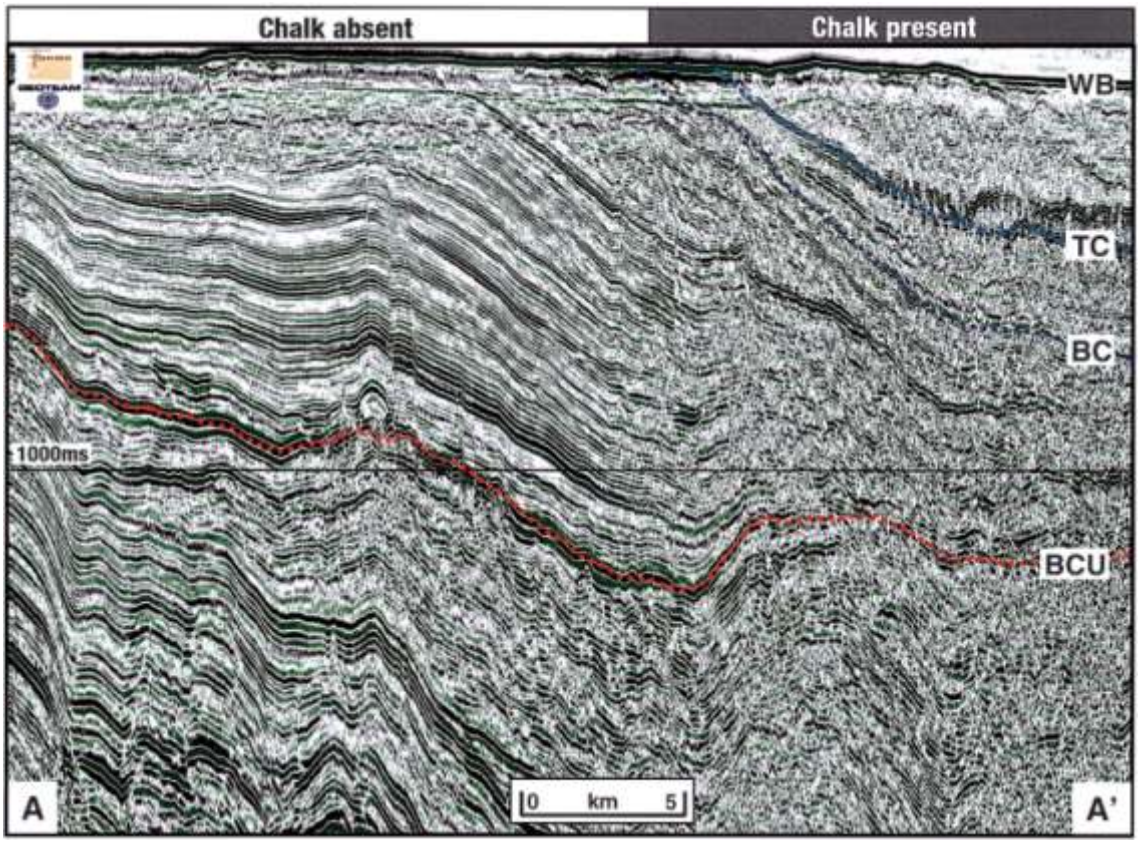

Figure 2.12 Seismic profile from the Inner Moray Firth highlighting the reduction in seismic data quality where Upper Cretaceous Chalk is present. WB=Water Bottom; TC=Top Chalk; BC=Base Chalk; BCU=Top Jurassic (Argent, et al. 2000)

2.3 Project Dataset

The seismic and well data subsets used in this study are displayed in Figure 2.13. The seismic and well data was loaded into the Schlumberger Petrel E&P Software Platform 2015 for workstation interpretation.

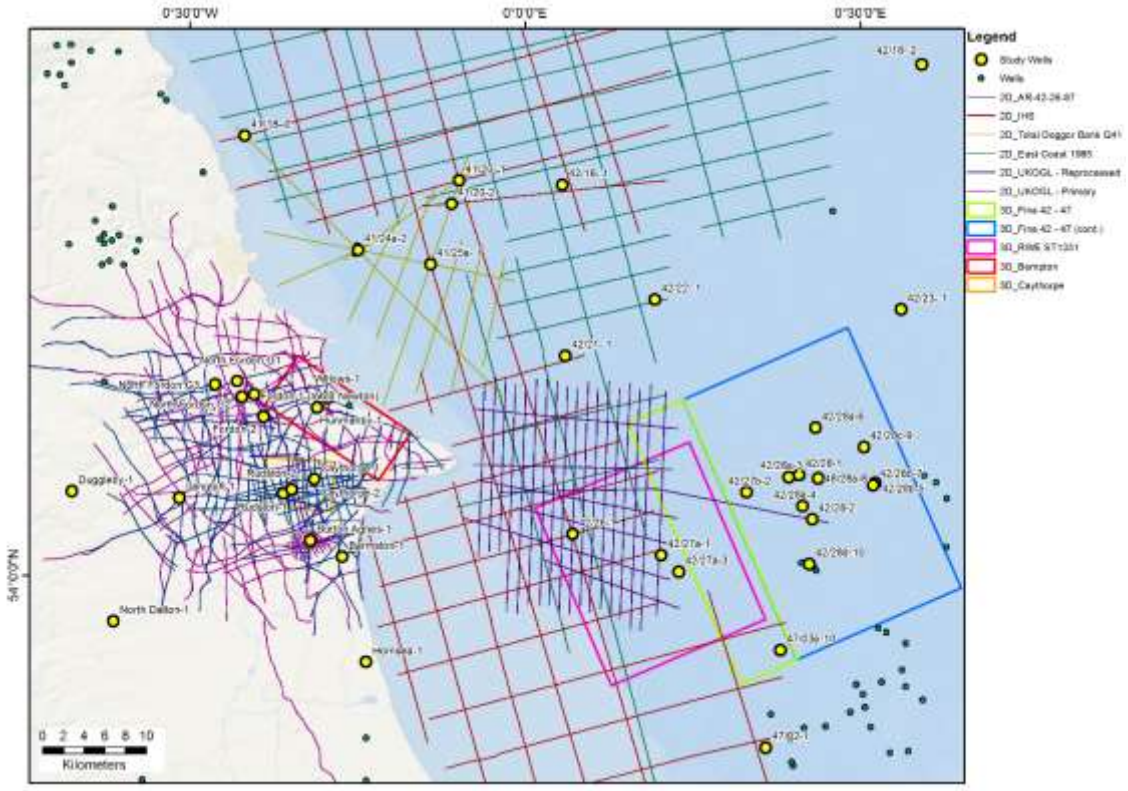

Figure 2.13 Well and seismic dataset used in this study.

2.3.1 Seismic Data

Five stacked, time migrated 3D seismic surveys have been utilised in this study with a total area of 1,028km^2. Acquisition and processing vintage years range from 1992 to 2009 (Table 2.1). Offshore 3D data were obtained from the Oil and Gas UK Common Data Access (CDA) data store. Onshore 3D data was provided by the UK Onshore Geophysical Library (UKOGL).

Table 2.1 Summary of 3D seismic database

Survey Name	Acquisition Year	Acqusition Contractor	Processing Year	Processing Contractor	Inline Range	Crossline Range	Area / km2
Fina 42 - 47	1992	Simon Horizon	1992	Digital Exploration Ltd.	150 - 7100	120 - 2320	163
Fina 42 - 47 (cont.)	1992	Simon Horizon	1992	Digital Exploration Ltd.	150 - 2520	120 - 2320	478
Bempton	2002	IMC	2002	-	4994 - 5434	1014 - 1202	51
RWE ST1331	2003	Fugro Geoteam AS	2003	-	990 - 1639	431 - 1927	303
Caythorpe	2009	IMC	2009	-	6 - 336	6 - 241	33
						Total	**1,028**

Six 2D survey campaigns were available for this project, consisting of 470 lines and approximately 8,156 line km of 2D seismic data. These 2D surveys were acquired from 1967 to 2005 and were available as migrated and/or stacked data (Table 2.2).

Table 2.2 Summary of 2D seismic database

2D Survey Group Name	Acquisition Year(s)	Acqusition Contractor(s)	Processing Year(s)	Processing Contractor	Available Formats	Number of Lines	Total Line Length / km
Dogger Bank Q41	1986	Digicon Geophysical Inc.	1986	Digicon Geophysical Inc.	Digital Segy	12	220
East Coast 1985	1985	WesternGeco	1985	-	Digital Segy	73	3,539
AR-42-26-87	1987	Digicon Geophysical Inc.	1987	-	Digital Segy	25	524
IHS	1986	Digicon Geophysical Inc.	1992	Jebco Seismic Ltd.	Digital Segy & scanned sections	36	1,450
UKOGL Primary	1967 - 2005	Horizon Exploration Ltd. / Geco UK / Rees Geophysical Ltd. / SSI / Spectrum / Prakla / Peak Geophysical	1967 - 2005	Simon Horizon / GSI / SSI / Geco UK / Tesla IMC Geophysics / Horizon	Digital Segy & scanned sections	218	1,632
UKOGL Reprocessed	1969 - 1995	Horizon Exploration Ltd. / Geco UK / Rees Geophysical Ltd. / SSI / Prakla / Peak Geophysical	1984 - 2003	Simon Horizon / Robertson / Horizon /	Digital Segy & scanned sections	106	791
					Total	**470**	**8,156**

Dogger Bank Q41, East Coast 1985 and AR-42-26-87 survey vintages were obtained from the Oil and Gas UK CDA portal as digital Segy only. The IHS and UKOGL datasets were provided by IHS Global Ltd. and UKOGL respectively, and contained both digital Segy and scanned paper sections. The CDA derived offshore 2D seismic processing vintages appear to be original. The IHS offshore 2D survey lines were acquired by Digicon Geophysical Inc. in 1986 and reprocessed by Jebco Seismic Ltd. in 1992. Two

datasets were provided by UKOGL, a greater set of 218 lines of original acquisition and processing vintages and a smaller subset of 106 lines of reprocessed data dating from 1984 to 2003. The UKOGL 2D datasets were acquired and processed by a variety of contractors and are documented in Table 2.2. As shown in Figure 2.13 most of the onshore UKOGL 2D lines have a crooked line geometry due to preferential acquisition along pre-existing tracks and roads.

Seismic is all European reverse polarity convention, where an increase in acoustic impedance corresponds to a negative recorded value and a trough (see Section 2.2.1 above). All data are assumed to have been zero phased during processing, based on the processing report for the Fina 42-47 3D survey, the only seismic processing report available for this study (Digital Exploration Ltd 1993).

For all seismic data obtained from the CDA data store, the current owner of the data has been referenced, where known.

2.3.1.1 Seismic Data Quality

The quality of the seismic data utilized in this project is highly variable, qualitatively ranging from good to very poor. A qualitative seismic data quality base-map is shown in Figure 2.14.

In general, data quality is primarily a function of the vintage of the acquisition and processing i.e. the most recent surveys are typically the best quality due to recording bandwidth improvements and processing advancements over time. Because of this, where reprocessed surveys are available, they display a significant improvement in seismic quality compared to original processed vintages. Seismic quality also varies spatially throughout the study area. In regions of intense structural deformation, there is a very pronounced reduction in seismic fidelity due to complex faulting, which severely distorts the seismic ray paths passing through this section. A similar trend in data quality reduction is also noticed where salt has flowed to form diapirs, which introduces velocity issues and ray path distortions in and around the anomaly. Seismic quality, in addition to subsurface structure and stratigraphy, has been the main factor in constraining the areal extents of the seismic interpretation across the study area. A map of interpreted seismic compared to that available is shown in Figure 2.15. In general, structural trends can be

extrapolated on to the poorest quality seismic sections even if picking a continuous seismic reflector proved difficult.

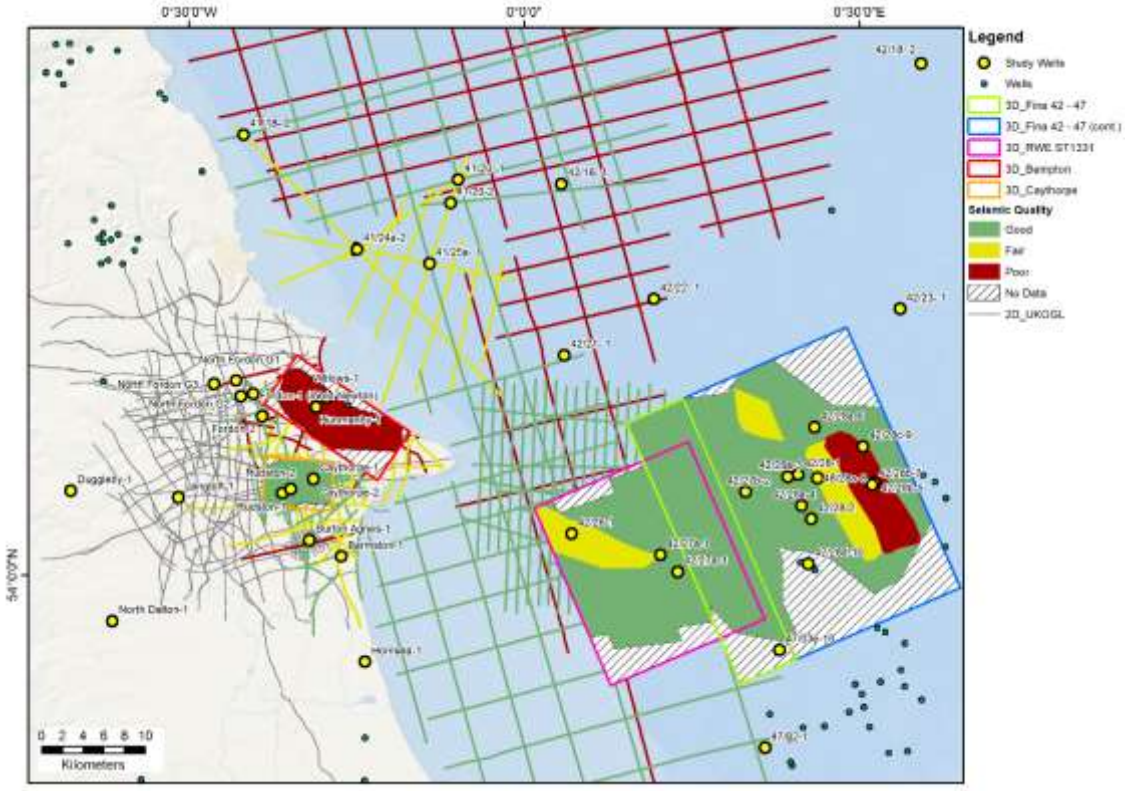

Figure 2.14 Base map showing seismic data quality. Coloured polygons represent 3D seismic quality. Coloured lines represent 2D seismic quality.

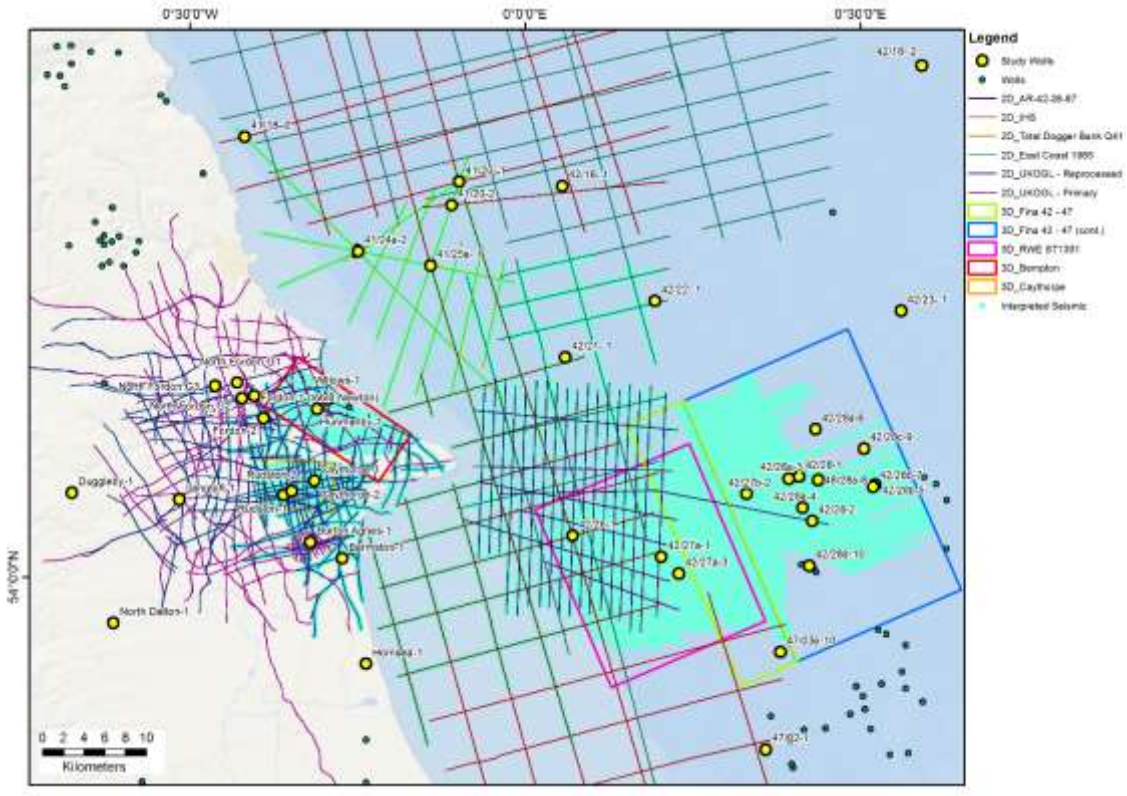

Figure 2.15 Base map showing seismic lines that have been interpreted for this study, in green, in relation to the available data.

All of the offshore seismic surveys are greatly affected by the presence of seabed multiples which overprints genuine reflectors from around 300ms TWTT to the seabed and poses a challenge to offshore shallow section interpretation (Figure 2.16). There is no noticeable reduction in seismic data quality in regions where Upper Cretaceous chalk is present at outcrop or subcrop, as seen elsewhere in the North Sea (see Section 2.2.4 above).

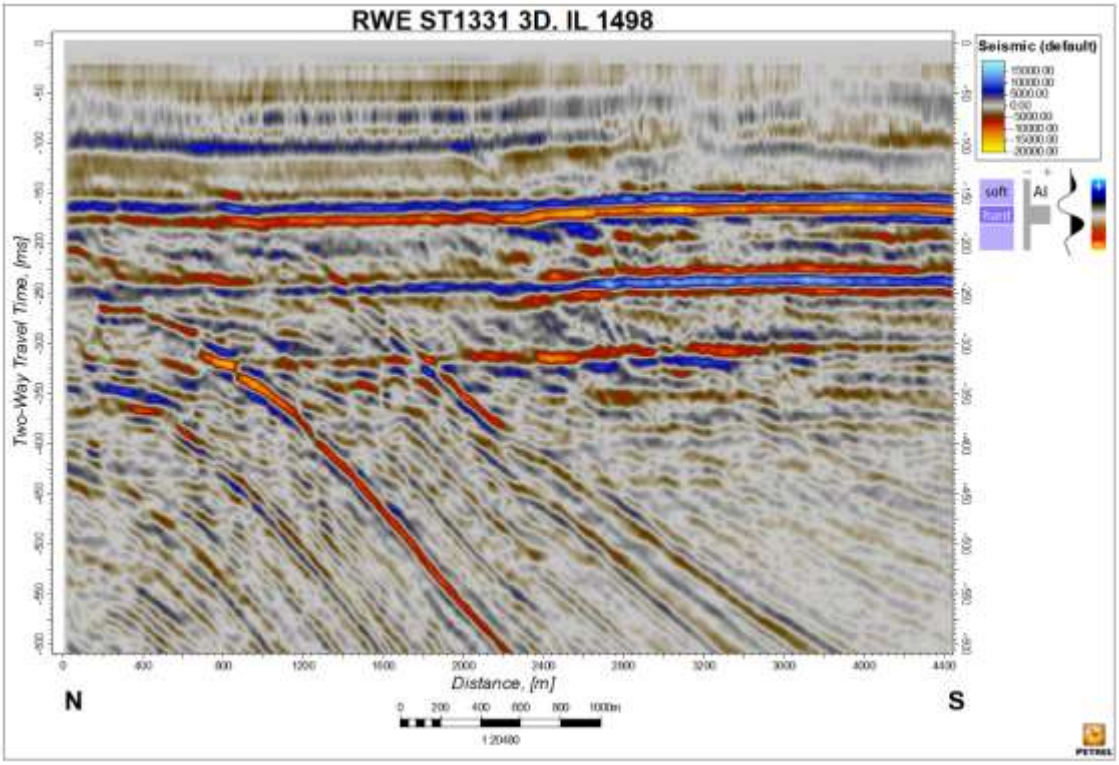

Figure 2.16 Example of horizontal seabed multiples at approximately 170ms, 250ms and 325ms overprinting inclined reflectors from 0 - 2000m horizontal distance. Seabed is at approximately 25ms. Notice polarity reversal of first multiple reflection. Five times vertical exaggeration. See Figure 2.20 for line location. Data currently owned by Ineos Industries.

The northern and southern bounds of the interpreted data are geographically controlled. The eastern extent of interpreted seismic corresponds with a significant degradation in quality of the Fina 42-47 cont. 3D survey. This poor-quality zone is attributed to the development of a significant Permian Zechstein Group salt diapir, which introduces significant seismic noise and velocity, pull up of underlying reflectors (Figure 2.17).

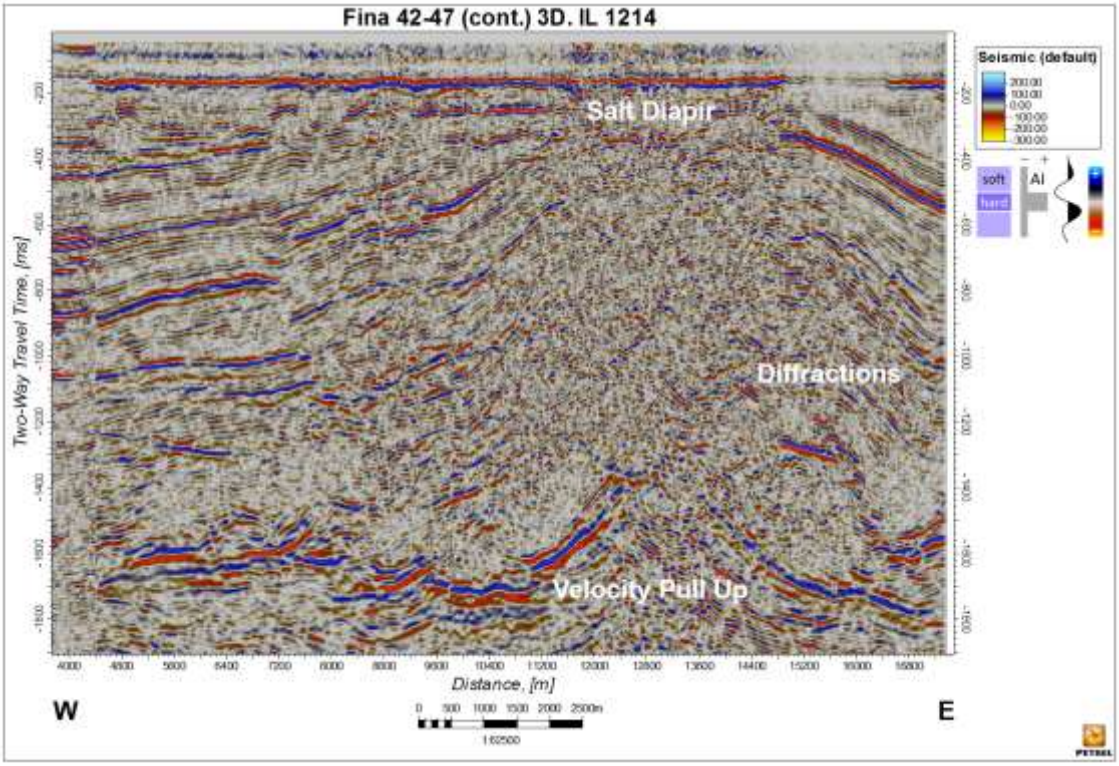

Figure 2.17 Velocity pull up and degradation of seismic character at salt diapir at the eastern edge of the dataset. Five times vertical exaggeration. See Figure 2.20 for line location. Data currently owned by Total.

Moving westwards towards the shoreline, there are no significant data quality issues. The RWE ST1331 3D, AR-42-26-87 and IHS 2D surveys are all good quality although the distortion of ray paths and out of plane reflectors on 2D surveys due to the structurally complex subsurface are present. This is particularly pronounced on the AR-42-26-87 2D dataset and results in reflector miss ties between structural dip and strike lines (Figure 2.18). Because of this dip lines have been preferentially interpreted for this survey.

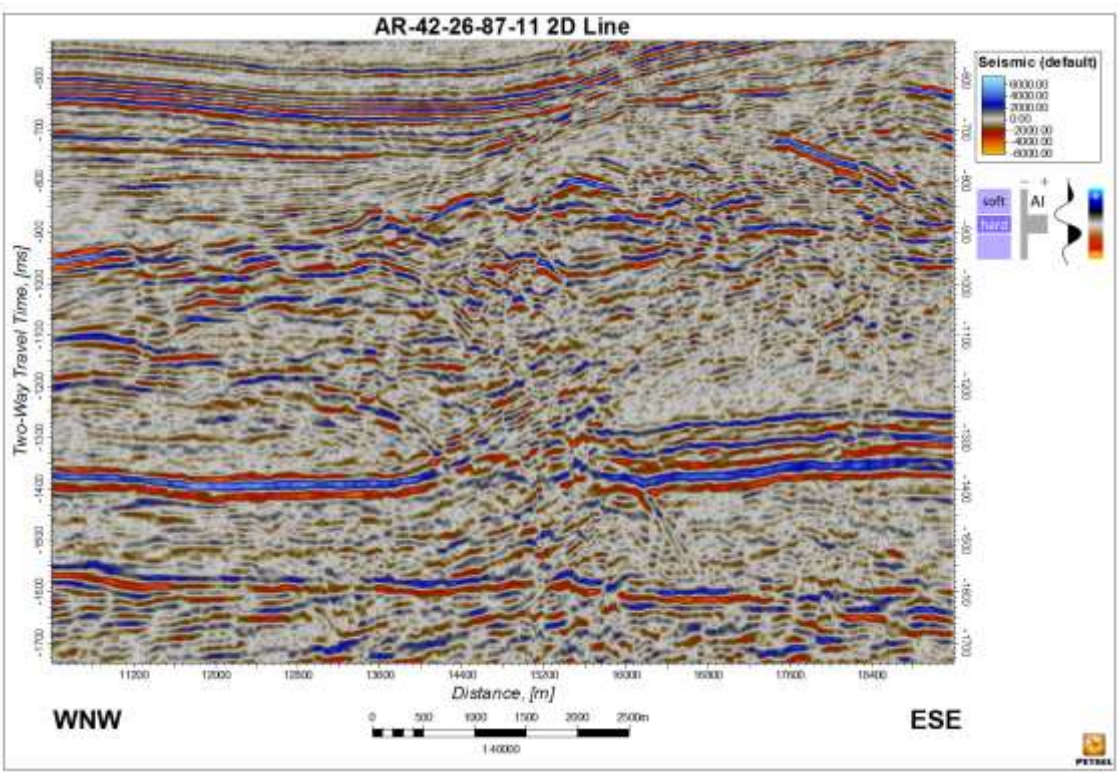

Figure 2.18 Poor seismic quality on a 2D strike line due to ray path distortions and out of plane diffractions through a zone of intense faulting. Five times vertical exaggaration. See Figure 2.20 for line location. Data currently owned by BP.

The East Coast 1985 and Total Dogger Bank Q41 2D surveys are poor to fair quality, respectively, but adequate enough to pick the major structural and stratigraphic features. Of the two onshore 3D surveys available, the Caythorpe 3D is good quality whereas the Bempton 3D is very poor quality with confident seismic interpretation only achievable in the vicinity of boreholes (Figure 2.19). The reprocessed UKOGL 2D lines are of significantly higher quality than the original processed vintages, which are also occasionally un-migrated, and were therefore preferentially interpreted over the original vintage lines. The western edge of the Caythorpe 3D survey marks the geographical boundary for the western limit of the interpreted seismic data.

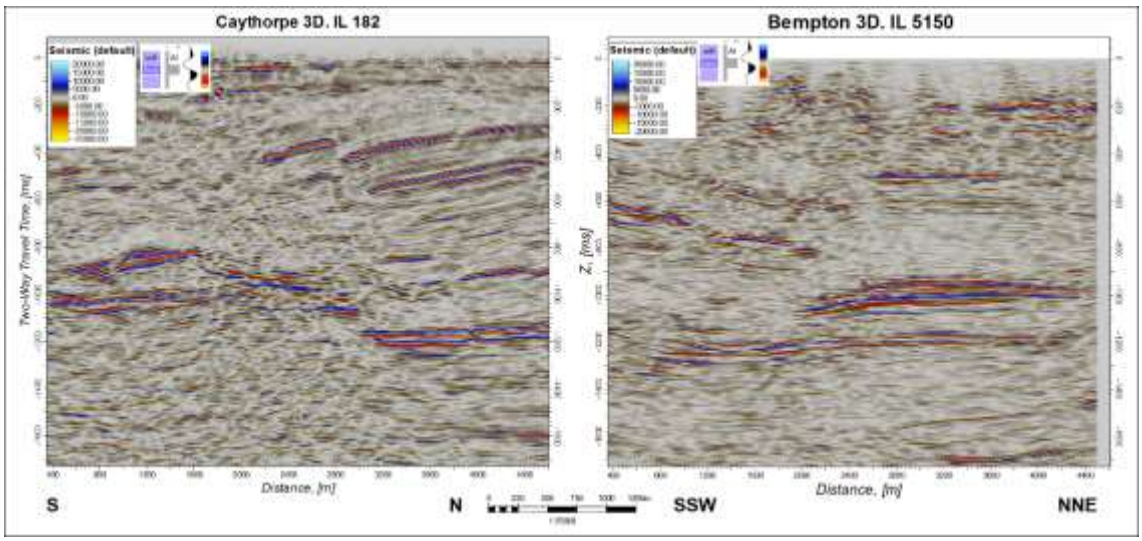

Figure 2.19 Data quality comparison between good quality Caythorpe 3D (left) and poor quality Bempton 3D (right). Two times vertical exaggeration. See Figure 2.20 for line location. Data courtesy of UKOGL.

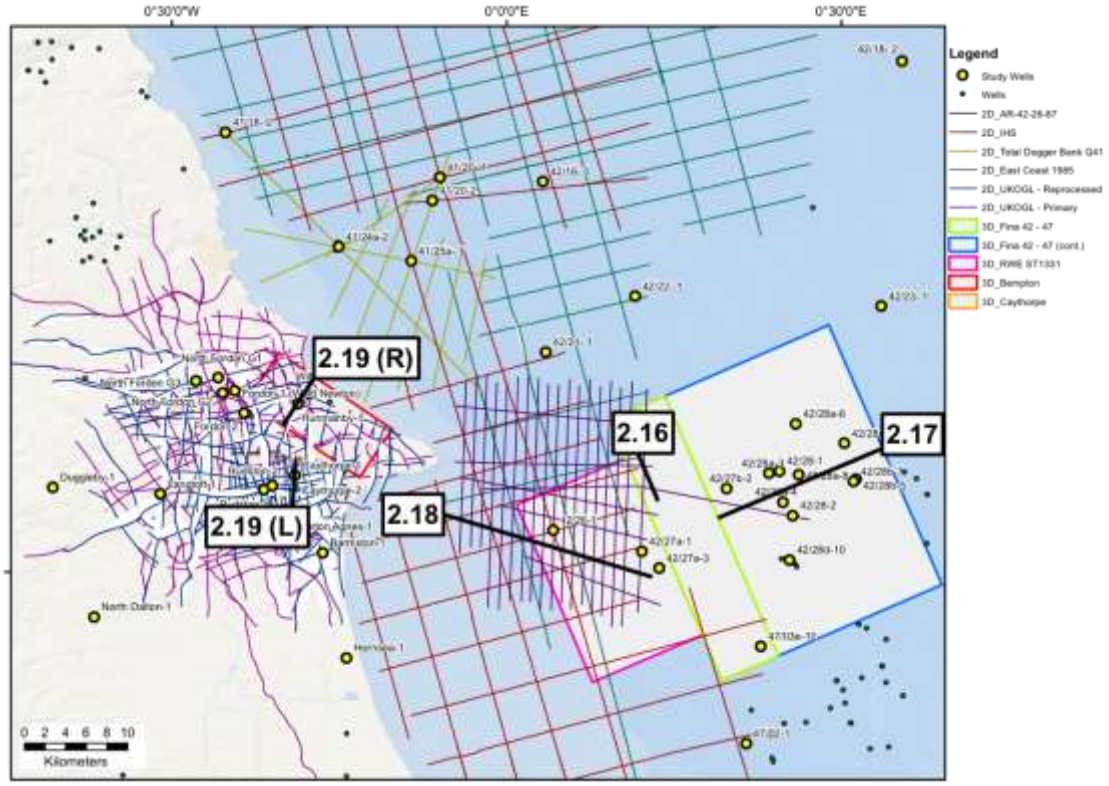

Figure 2.20 Location of seismic line examples used in this section. Line numbers correspond to figure numbers.

2.3.2 Well Data

Forty-three wells and their associated data were used in this study and are shown in Table 2.3. Data available includes a combination of open access metadata such as well header information (including location coordinates, date well was drilled, total depth reached and encountered formation tops) and commercially restricted electronic log data. Open access data were accessed from the Oil & Gas Authority's Open Data portal and from UKOGL for offshore and onshore wells, respectively. Electronic log data for offshore wells was obtained from Oil and Gas UK's CDA portal. Electronic log data for a subset of the onshore study wells (shown in Table 2.3) were purchased from IHS Markit, the data resale vendor.

Table 2.3 Table of wells and associated data used in this study

Well Name / Number	Well Status	Shore Status	Spud Year	Formation Tops	Composite Log	EOW Report	Borehole Geometry	e-logs	Sonic	Density	Velocity Data - Checkshots /	TD (MD) m	TD (TVDSS) m
North Fordon G1	P&A Dry	Onshore	1955	Yes	-	-	Vertical	-	-	-	-	302.7	211.3
North Fordon G2	P&A Dry	Onshore	1955	Yes	-	-	Vertical	-	-	-	-	275.8	201.1
North Fordon G3	P&A Dry	Onshore	1955	Yes	-	-	Vertical	-	-	-	-	275.8	112.1
Fordon-1 (Wold Newton)	P&A Dry	Onshore	1956	Yes	-	-	Vertical	-	-	-	Yes	2303.9	2173.1
41/20- 1	P&A Dry	Offshore	1965	Yes	Yes	Yes	Vertical	-	-	-	Yes	3453.1	3422.9
41/18- 2	P&A Dry	Offshore	1966	Yes	Yes	Yes	Deviated	-	-	-	-	2067.8	2036.4
42/18- 2	P&A Dry	Offshore	1966	Yes	Yes	Yes	Vertical	Yes	Yes	Yes	-	3292.5	3252.5
42/23- 1	P &A Gas Shows	Offshore	1966	Yes	Yes	-	Deviated	Yes	Yes	Yes	-	2961.2	2921.4
41/20-2	P&A Dry	Offshore	1969	Yes	Yes	Yes	Vertical	-	-	-	-	1872.7	1838.2
41/25a- 1	Gas	Offshore	1969	Yes	Yes	Yes	Vertical	-	-	-	Yes	1792.8	1758.4
42/28-1	Gas	Offshore	1969	Yes	Yes	-	Deviated	Yes	Yes	-	Yes	2824	2790.2
Hornsea-1	P&A Dry	Onshore	1970	Yes	-	-	Vertical	-	-	-	-	2059.7	2043.9
Langtoft-1	P&A Dry	Onshore	1970	Yes	Yes	-	Vertical	Yes	Yes	Yes	Yes	1993.3	1852.5
Barmston-1	P&A Dry	Onshore	1971	Yes	-	-	Vertical	-	-	-	Yes	1973.5	-
North Dalton-1	P&A Dry	Onshore	1972	Yes	-	-	Vertical	-	-	-	-	1580	1513.9
42/28-2	P &A Gas Shows	Offshore	1973	Yes	Yes	-	Vertical	Yes	Yes	Yes	Yes	3093.7	3060.8
Hunmanby-1	P&A Dry	Onshore	1973	Yes	Yes	-	Vertical	Yes	Yes	Yes	Yes	2252.4	2171.6
42/26-1	P&A Dry	Offshore	1974	Yes	Yes	Yes	Vertical	-	-	-	Yes	2799.9	2780.4
Fordon-2	P&A Dry	Onshore	1974	Yes	-	-	Vertical	-	-	-	Yes	2444.4	2376.7
41/24a-2	Gas	Offshore	1981	Yes	Yes	Yes	Vertical	Yes	Yes	Yes	Yes	3169.2	3134.2
Rudston-1	P&A Dry	Onshore	1984	Yes	Yes	-	Vertical	Yes	Yes	Yes	Yes	2514.6	2461
42/22- 1	P &A Gas Shows	Offshore	1987	Yes	Yes	Yes	Deviated	Yes	Yes	Yes	-	2639.6	2580.8
Caythorpe-1	Gas	Onshore	1987	Yes	Yes	-	Deviated	Yes	Yes	Yes	Yes	2066.4	2039.9
42/28a-3	Gas	Offshore	1989	Yes	Yes	Yes	Vertical	Yes	Yes	Yes	Yes	2958.1	2915.4
Caythorpe-2	Gas	Onshore	1989	Yes	-	-	Deviated	-	-	-	-	2316.5	1929.9
42/27a-1	P&A Dry	Offshore	1990	Yes	Yes	Yes	Deviated	Yes	Yes	Yes	Yes	3221.6	3184.4
42/28a-4	P&A Dry	Offshore	1990	Yes	Yes	-	Vertical	Yes	Yes	Yes	Yes	2958.1	2915.4
42/28b-5	Gas	Offshore	1990	Yes	Yes	-	Deviated	-	-	-	Yes	2828.5	2792.6
Duggleby-1	P&A Dry	Onshore	1990	Yes	-	-	Vertical	-	-	-	Yes	3055.5	2850.4
42/28a-6	Suspended	Offshore	1992	Yes	Yes	-	Deviated	Yes	Yes	Yes	Yes	2561.8	2512.8
42/16- 1	P&A Dry	Offshore	1993	Yes	Yes	-	Vertical	-	-	-	-	3292.5	3252.5
47/02-1	Gas	Offshore	1993	Yes	-	-	Vertical	-	-	-	-	3104.1	3066
42/27b-2	P&A Dry	Offshore	1994	Yes	Yes	Yes	Deviated	Yes	Yes	Yes	Yes	3180.6	3134.4
47/03e-10	P&A Dry	Offshore	1996	Yes	Yes	Yes	Vertical	-	-	-	-	1459	1419.7
Rudston-2	P&A Dry	Onshore	1996	Yes	Yes	-	Deviated	Yes	Yes	Yes	Yes	2459.3	1912.8
42/28b-7	Gas	Offshore	2002	Yes	Yes	-	Deviated	-	-	-	-	2770.9	2725.3
48/28a-8	Gas	Offshore	2002	Yes	Yes	-	Deviated	-	-	-	-	3755.1	2745.7
42/21- 1	P &A Gas Shows	Offshore	2005	Yes	Yes	Yes	Deviated	Yes	Yes	Yes	-	2628.9	2578.2
42/28c-9	P&A Dry	Offshore	2006	Yes	Yes	-	Deviated	-	-	-	-	2719.4	2680.5
Willows-1	P&A Dry	Onshore	2006	Yes	-	-	Deviated	Yes	Yes	Yes	-	2405	2252
42/27a-3	P&A Dry	Offshore	2007	Yes	Yes	Yes	Deviated	Yes	Yes	Yes	-	3238	3087
Burton Agnes-1	P&A Dry	Onshore	2007	Yes	Yes	-	Deviated	-	-	-	Yes	2268	1971.5
42/28d-10	P&A Dry	Offshore	2008	Yes	Yes	-	Vertical	-	-	-	-	830.6	789.1

2.4 Methodology

The following section addresses the theory and methods commonly employed to accurately interpret the well and seismic data used in this research study. This includes a brief description of the theory and application of seismic stratigraphy and the workflows used for assessing the structural domain represented on seismic.

2.4.1 Seismic Stratigraphy

2.4.1.1 Introduction

Although drilled borehole data provide an exact representation of the subsurface, this is restricted to the immediate vicinity of the borehole. In order to extrapolate beyond the borehole, seismic data can be used to identify the acoustic impedance contrasts between the interfaces of two lithological units that correspond to stratigraphic horizons in wells. Tracing these reflections laterally provides a representation of their extent, surface geometry and thickness which can deliver information on the structural configuration of the subsurface. There are techniques used for the interpretation of seismic reflection data that complement existing borehole data and that can also be used in areas where there is an absence of borehole data, and are discussed below.

Seismic stratigraphy is a methodology that promotes the interpretation of seismic data for use as a stratigraphic, rather than solely a structural tool. The key principle of seismic stratigraphy is that seismic reflectors are parallel to contemporaneous bedding surfaces and they represent correlatable time surfaces rather than lithological boundaries representing a lateral facies change (Bertram 2012).

There are exceptions to this general rule. Seismic noise and distortions such as those described in Section 2.2.3 above are artefacts and where they occur on seismic data, are not representative of the physical characteristics of the subsurface layers. Seismic reflectors can be generated where there is an extreme change in acoustic impedance contrast, such as a flat spot, where the density contrast across a hydrocarbon – fluid contact creates a reflector that cuts across bedding and does not represent a time line (Figure 2.21). Bottom-simulating reflectors due to the presence of gas hydrates (Figure 2.22) and the Opal A to Opal C/T transition diagenetic reflector are other examples of primary seismic reflectors that do not approximate to time surfaces (Bertram 2012).

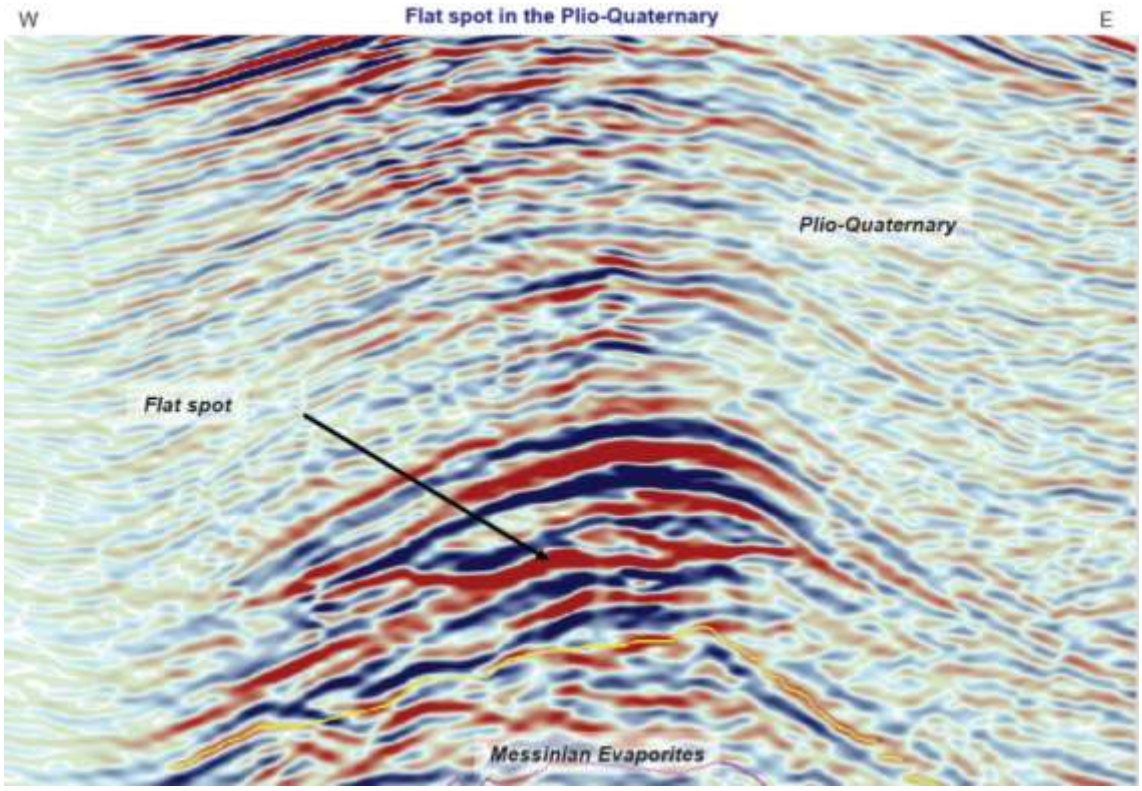

Figure 2.21 Example from a 2D line of a horizontal flat spot seismic reflector cutting across inclined depositional bedding reflectors (Wikipedia 2016)

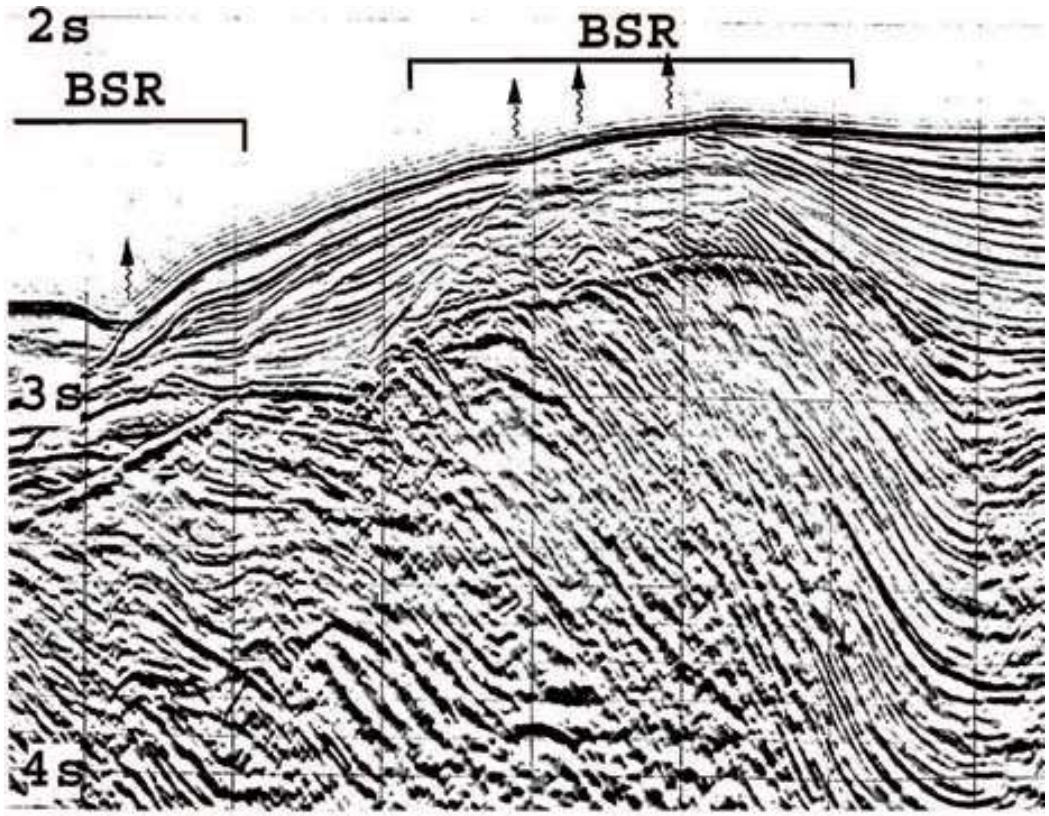

Figure 2.22 Bottom-simulating reflectors (BSR) as a result of the presence of gas hydrates (Smith 2009).

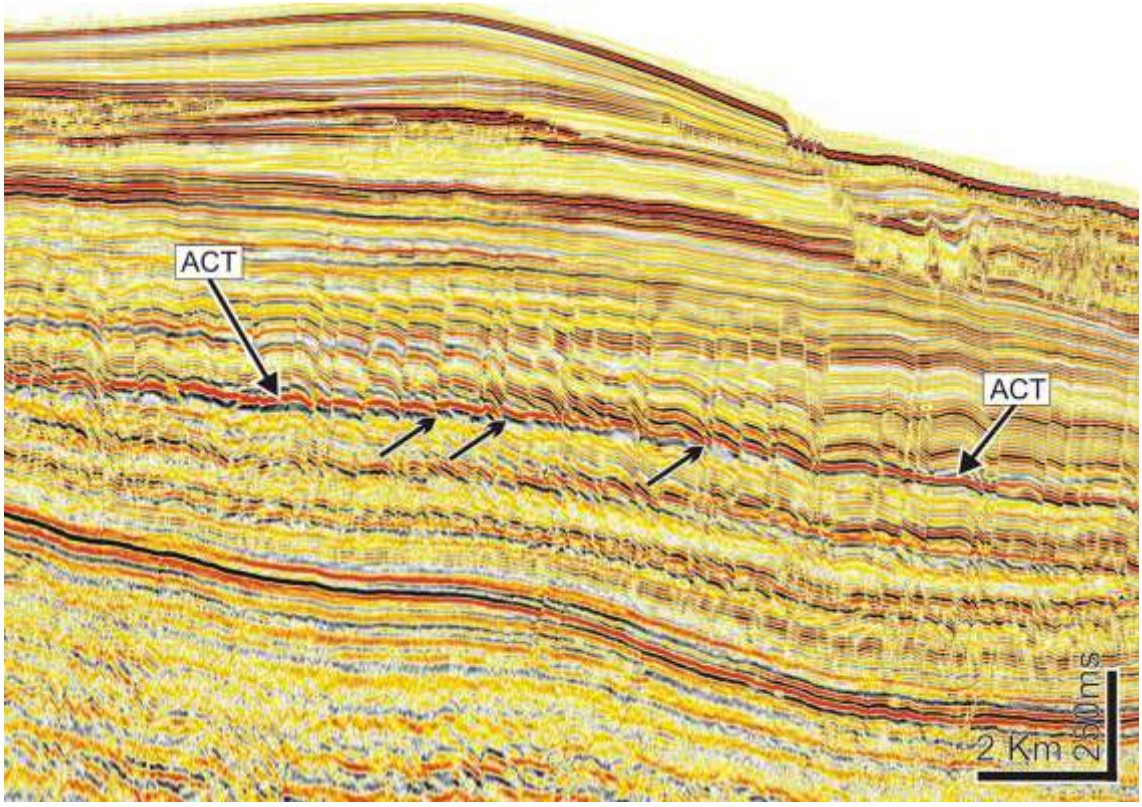

Figure 2.23 3D seismic reflection profile showing the Opal A to Opal C/T) diagenetic reflection (ACT). In this example, the reflection is offset through faulting, shown by small arrows (Cartwright 2009).

2.4.1.2 Interpretation Methods

The basis of seismic interpretation is to trace laterally continuous seismic reflectors. However, as evident from all seismic datasets, individual seismic reflectors are not continuous but rather are recognised to terminate in a consistent manner. The manner in which seismic reflectors terminate defines a line on a seismic section, which can be mapped out as a surface across a complete data set. This surface is known as a "seismic surface" (Figure 2.24), (Bertram 2012).

The termination of seismic reflectors can either represent the termination of a bedding surface or the point at which beds thin to a level beyond seismic resolution. The termination of seismic reflectors marks the position of depositional hiatuses or potential unconformities within the seismic data, subdividing the stratigraphy into depositional packages showing conformable reflection geometries (Bertram 2012). Types of seismic reflection terminations are shown in Figure 2.24.

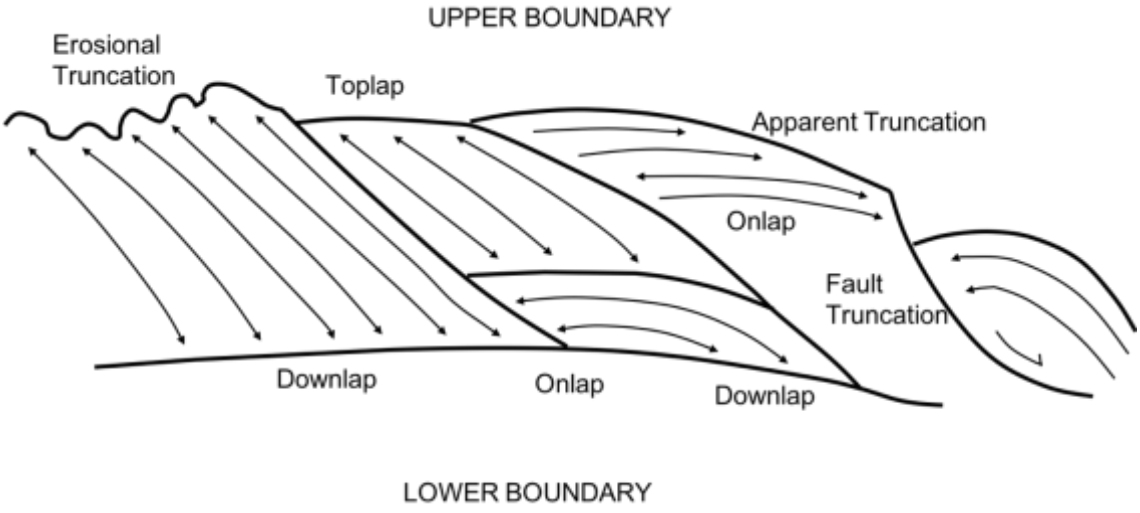

Figure 2.24 Types of reflection terminations. Solid black lines represent idealised seismic surfaces. Modified after Bertram & Milton (1996)

The terminology and description of reflector termination geometries detailed in Figure 2.24 were originally proposed by (Mitchum 1977). These reflection terminations can be summarised as:

Onlap[3] – where initially horizontal or low angle reflectors terminate against an inclined surface that is steeper relative to the reflectors (Mitchum 1977), (Bertram 2012).

Toplap – the termination of inclined reflectors (known as clinoforms) against an overlying surface that is lower angle than the terminating reflectors. The inclined reflectors commonly relate to sets of prograding clinoforms. This termination commonly represents a period of non-deposition and sedimentary bypass (Mitchum 1977), (Bertram 2012).

Downlap – where inclined seismic reflectors terminate against a horizontal or lower angle reflector (relative to the terminating reflectors). Downlap is commonly associated to the progradation of a shelf or slope system into deeper water and is therefore seen at the base of prograding clinoforms. Downlap documents the transition from either marine or lacustrine slope deposition to marine or lacustrine condensation with the downlap surface

[3] In this thesis, onlap refers to seismic onlap

representing a marine condensed unit (Mitchum 1977; (Bertram & Milton 1996; Bertram 2012).

Erosional Truncation – the termination of seismic reflectors along an unconformity surface due to erosion. Erosional processes may be tectonic in nature such as regional uplift or depositional such as the basal erosion of a channel complex system (Mitchum, 1977; (Bertram, 2012).

Apparent Truncation – where low angle reflectors terminate beneath a dipping seismic reflector. The dipping reflector represents a period of marine non-deposition (condensation) and the terminations relate to either bed thinning below seismic resolution or the distal depositional limit of the unit (Bertram & Milton 1996).

Fault Truncation – where seismic reflectors terminate against a fault (syn or post depositional), slump, guide or intrusion plane (Bertram & Milton 1996).

The methods outlined previously make up a powerful interpretative tool for analysing subsurface data. The application of these principles have provided a robust framework for, and aided in, the interpretation of seismic reflector packages in the dataset available for this study.

2.4.2 Identifying Structural Styles on Seismic Reflection Data

As detailed in Chapter 1, several different tectonic mechanisms have been proposed that resulted in the formation of the Flamborough Head Disturbance, including oblique-slip and dip-slip compression. As a primary aim of this study is to use an interpreted seismic dataset to document the structural processes responsible for the geological evolution of the area and the development of the Flamborough Head Disturbance, it is essential to attempt to identify the structural styles responsible for creation of the features observed in the seismic dataset. Therefore, of particular importance for this study is the differentiation of compressional and extensional strike-slip (wrench) and dip-slip deformation.

The criteria for differentiating structural styles can be obtained through the recognition of key structural elements, critical differences in local trend arrangements and gross

regional patterns of structures (Harding & Lowell 1979). This definitive classification scheme of structural styles composed by Harding and Lowell (1979) is outlined in Table 2.4. This scheme is primarily based on the involvement or non-involvement (detached) of basement features in the observed structures, with additional criteria in the inferred deformational force and mode of tectonic transport inferred from the strain features of the structures (Harding & Lowell, Structural styles, their plate tectonic habitats and hydrocarbon traps in petroleum provinces., 1979).

Table 2.4 Structural styles and habitats. Modified after Harding & Lowell (1979)

Structural Style	Dominant Deformational Force	Typical Transport Mode	Plate-Tectonic Habitats	
			Primary	Secondary
BASEMENT INVOLVED				
Wrench-fault assemblages	Couple	Strike-slip of subregional to regional plates	Transform boundaries	Convergent boundaries: 1. Foreland basins 2. Orogenic belts 3. Arc massif Divergent boundaries: 1. Offset spreading centres
Compressive fault blocks and basement thrusts	Compression	High to low-angle convergent dip-slip of blocks, slabs and sheets	Convergent boundaries: 1. Foreland basins 2. Orogenic belt cores 3. Trench inner slopes and outer highs	Transform boundaries (with component of convergence)
Extensional fault blocks	Extension	High to low-angle divergent dip-slip of blocks and slabs	Divergent boundaries: 1. Completed rifts 2. Aborted rifts, aulacogens Intraplate rifts	Convergent boundaries: 1. Trench outer slope 2. Arc massif 3. Stable flank of foreland and fore-arc basins 4. Back-arc marginal seas (with spreading) Transform boundaries: 1. With component

				of divergence 2. Stable flank of wrench basins
Basement warps: arches, domes, sags	Multiple deep-seated processes (thermal events, flowage, isostacy, etc)	Subvertical uplift and subsidence of solitary undulations	Plate interiors	Divergent, convergent, and transform boundaries Passive boundaries
DETACHED				
Decollement thrust-fold assemblages	Compression	Subhorizontal to high-angle convergent dip-slip of sedimentary cover in sheets and slabs	Convergent boundaries: 1. Mobile flank (orogenic belt) of forelands 2. Trench inner slopes and outer highs	Transform boundaries (with component of convergence)
Detached normal-fault assemblages ("growth faults" and others)	Extension	Subhorizontal to high-angle divergent dip-slip of sedimentary cover in sheets, wedges and lobes	Passive boundaries (deltas)	
Salt structures	Density contrast Differential loading	Vertical and horizontal flow of mobile evaporites with arching and/or piercement of sedimentary cover	Divergent boundaries: 1. Completed rifts and their passive margin sags 2. Aborted rifts; aulacogens	Regions of intense deformation containing mobile evaporite sequence
Shale structures	Density contrast Differential loading	Dominantly vertical flow of mobile shales with arching and/or piercement of sedimentary cover	Passive boundaries (deltas)	Regions of intense deformation containing mobile shale sequence

As shown in Table 2.4, basement involved structural styles include wrench-fault assemblages, compressive fault blocks and basement thrusts, extensional fault blocks and basement warps, such as arches, domes and sags. Detached styles include decollement thrust-fold assemblages, detached normal faults, salt structures and shale structures.

Table 2.4 also highlights the plate tectonic environment in which these structural styles are typically encountered. Figure 2.25 illustrates the example hydrocarbon trap types associated with the structural styles documented in Table 2.4.

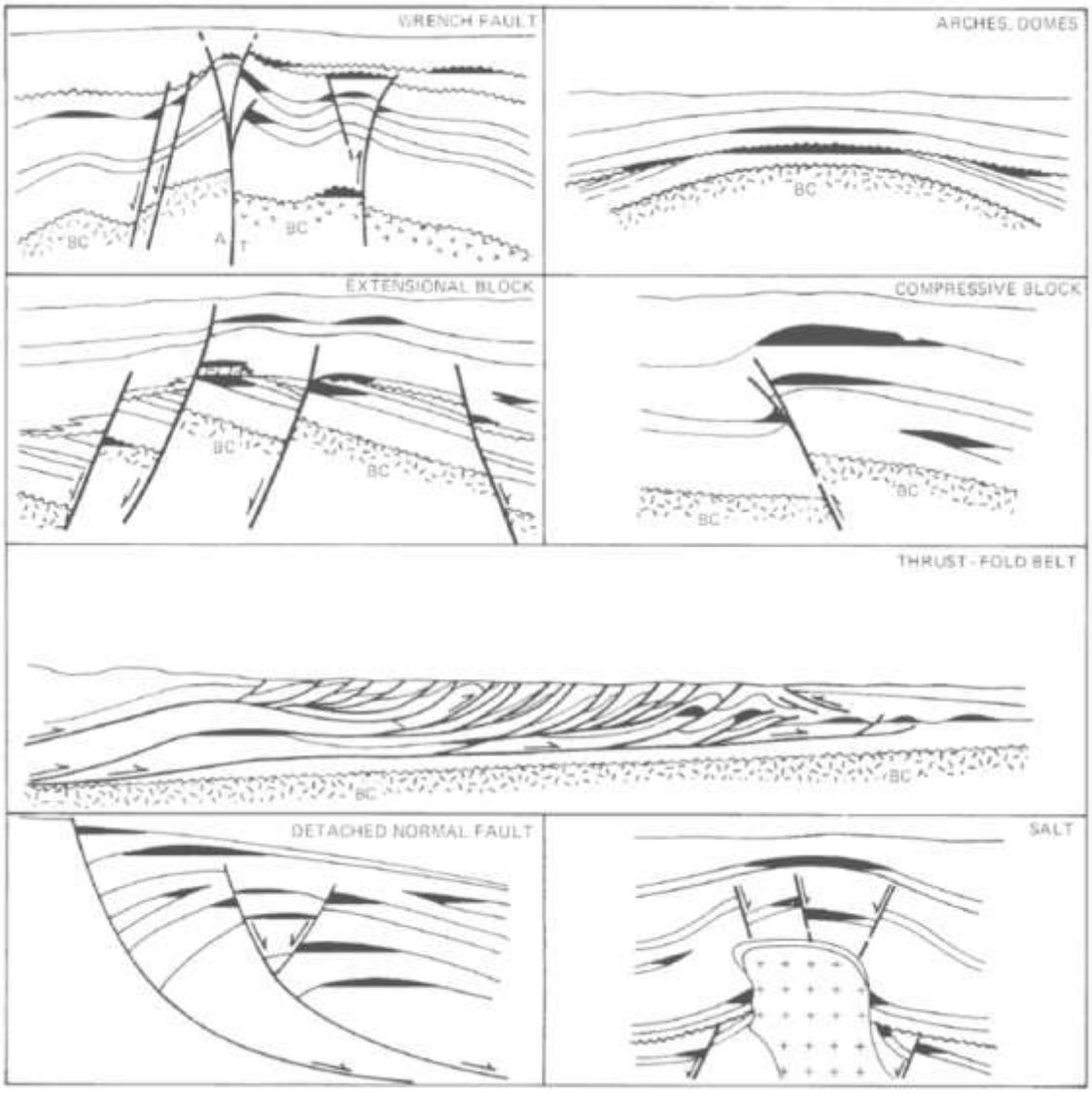

Figure 2.25 Example hydrocarbon traps (shaded black) associated with structural styles outlined in Table 2.4 (Harding & Lowell 1979).

Refining the criteria described above, Harding (1990) proposed identification criteria to differentiate wrench or strike-slip tectonic structures from dip-slip structures by combining seismic section and base map observations. This work by Harding (1990) states that strike-slip structures are identifiable by:

- A narrow, long, straight, central, solitary master fault at depth or at all structural levels or a linear, solitary zone of deformation with coeval extensional or

contractional en-echelon trending deformation structures. The throughgoing linear trend does not move laterally along strike (parallel) seismic reflection profiles. This is in comparison to dip-slip deformation structures, which will move laterally along strike (parallel) seismic reflection profiles and may abruptly terminate (Figure 2.26 and Figure 2.27).

- A steep to moderate dip of the master fault that exhibits displacement at the contact between basement and sedimentary cover. This differs from some listric normal or thrust faults that can detach in sediments overlying the basement (Figure 2.26, Figure 2.28 and Figure 2.29).

- Variations in relative up-thrown side (in terms of displacement) and/or fault dip direction at depth along the strike of the master fault (Figure 2.26 and Figure 2.27).

- A zone of narrow, elongate fault slices that steepen and join at depth (defined as either positive (Figure 2.28) or negative (Figure 2.29) flower structures depending on vertical displacement sense). The identification of flower structures on vertical seismic reflection profiles is one of the most reliable indicators of the presence of a strike-slip fault system (Harding 1990).

- Different fault displacement sense and orientation of the relative up-thrown side of these flower structure fault segments along strike seismic reflection profiles (Figure 2.26).

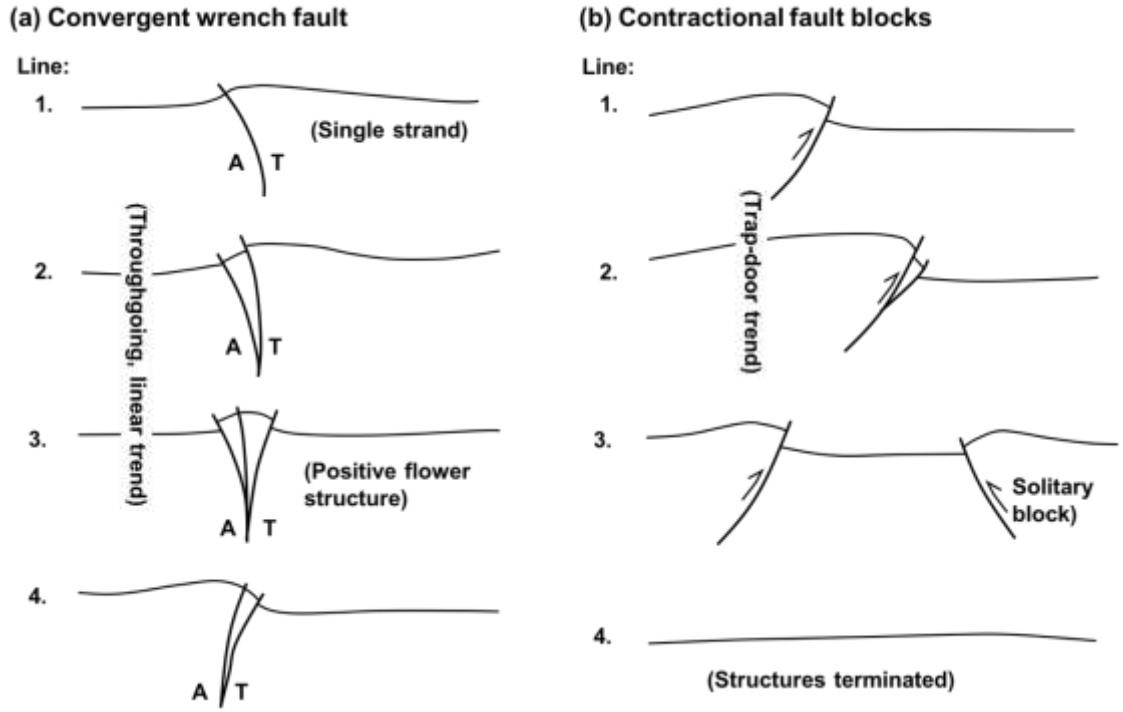

Figure 2.26 Cross sections composed from hypothetical sequential seismic reflection profiles (1 to 4) across: (a) an idealised strike-slip zone and (b) contractional fault blocks. A = displacement sense away from viewer. B= displacement sense towards viewer. Note that strike-slip fault in (a) is straight and throughgoing. Block faults in (b) shift position on successive profiles or terminate abruptly, as shown in profile (b) 4. Modified after Harding (1990).

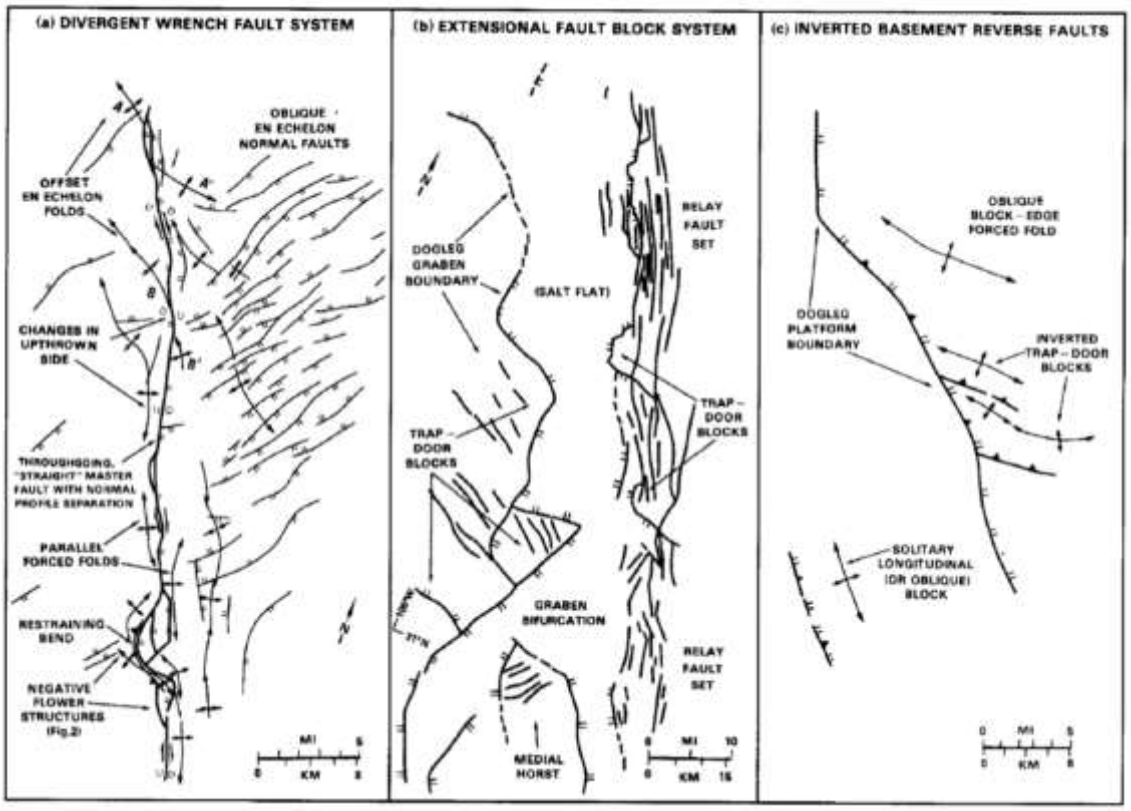

Figure 2.27 Differences in map patterns of extensional structural styles that can have similar profiles. Note the presence of a master central fault in the wrench setting and coeval en-echelon structures (Harding 1990).

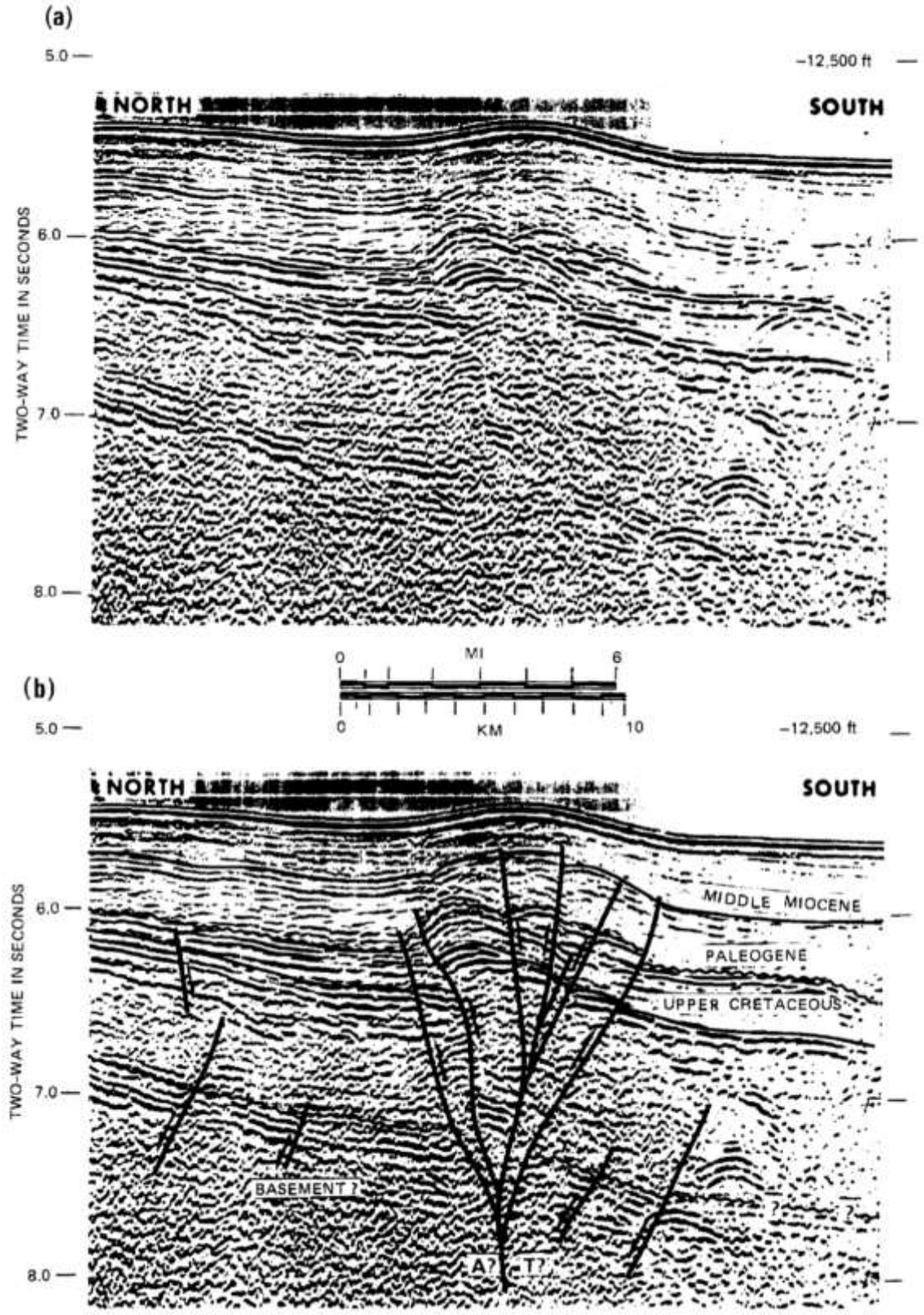

Figure 2.28 (a) un-interpreted and (b) interpreted seismic reflection profile across a convergent wrench fault showing a positive flower structure. A? = displacement sense away from viewer. T? = displacement sense towards viewer (Harding 1990).

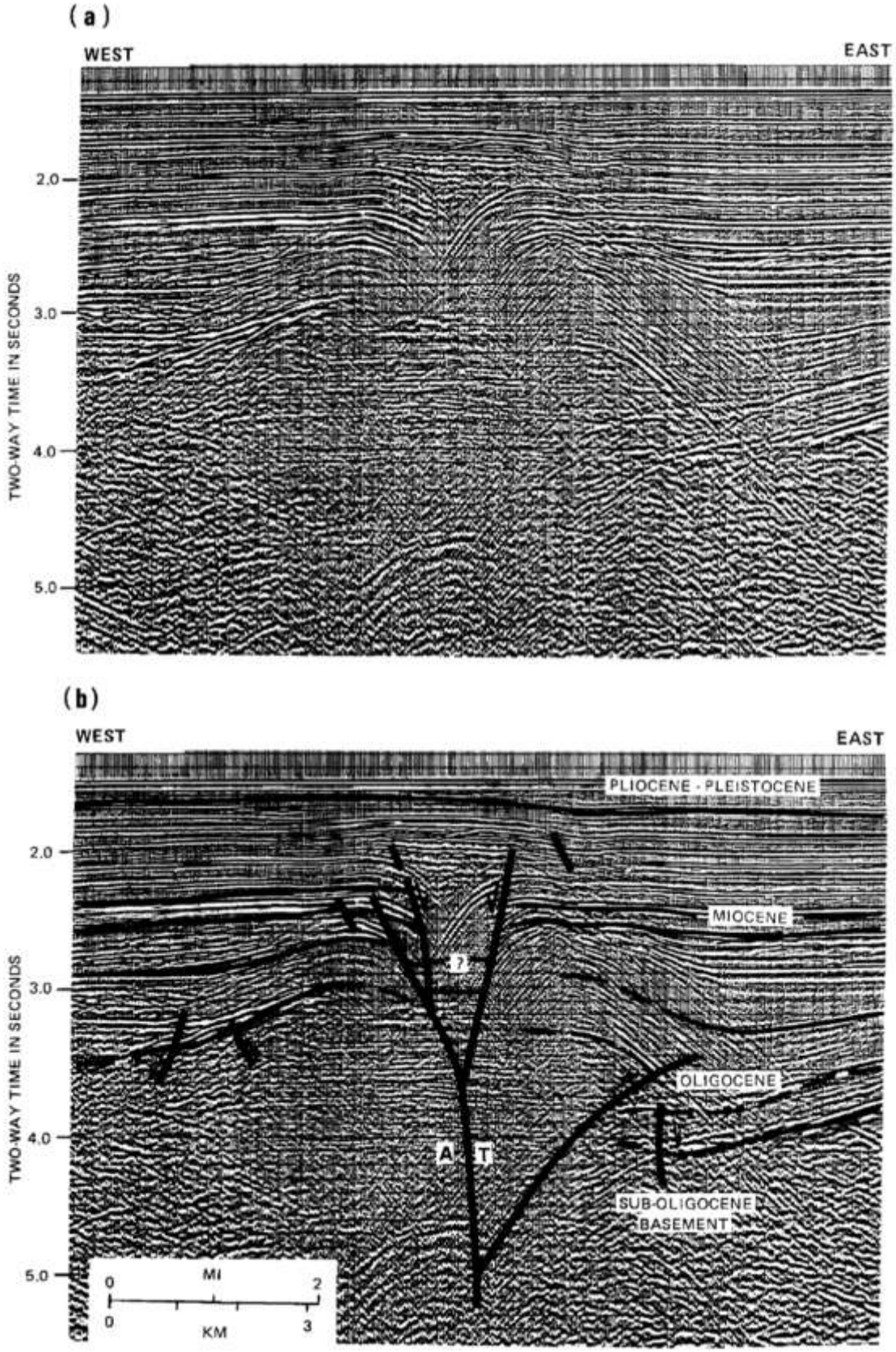

Figure 2.29 (a) un-interpreted and (b) interpreted seismic reflection profile across a divergent wrench fault showing a negative flower structure geometry. A= displacement sense away from viewer. B=displacement sense towards viewer (Harding 1990).

When identifying strike-slip structures with the criteria described, it is important to confirm the identification by refuting any possible alternative interpretations such as an extensional or contractional dip-slip environment (Harding 1990).

Following these wrench fault identification criteria, and considering alternative interpretations, has aided in identifying the structural styles of the subsurface features observed on vertical seismic profiles and base maps for the dataset of this project, in particular, evidence for presence or absence of strike-slip fault systems.

CHAPTER 3. SEISMIC INTERPRETATION

3.1 Introduction

This chapter documents the results of the interpretation of the seismic reflection data available for this project, describing the well to seismic tie process and the time to depth conversion workflow.

3.2 Well to Seismic Tie

The fundamental starting point of any seismic interpretation project is to calibrate the seismic data, which in this project is in time, to well data that is in depth, so that the acoustic impedance contrasts that generate seismic reflections can be related to well bore stratigraphy. This allows the interpreter to identify the origin of seismic reflectors and what they represent in terms of subsurface geology and to correctly identify the seismic reflectors to pick.

The seismic to well tie is achieved by creating a synthetic seismic response from calibrated well log data that are matched to a real seismic trace and thus, features from the well are correlated to the seismic data (White & Simm 2003). As detailed in Section 2.2, the recorded seismic signal is the product of the convolution model where reflection spikes at acoustic impedance contrast boundaries are represented by reflection pulses with different amplitudes and polarity (Figure 2.2). The shape of the pulse is the wavelet, which is the waveform returned by an isolated reflector at target depth (White & Simm 2003). The synthetic seismogram is generated by imitating the convolution process in seismic interpretation software, where the wavelet is either expressed as an ideal deterministic wavelet or extracted from the source seismic dataset and the reflectivity series is calculated from well sonic and density log curves (Chamberlain 2013).

The well to seismic tie workflow procedure used in this project can be summarised as:

1. Editing and calibrating sonic and density well logs

2. Construct synthetic seismogram from calibrated well logs

3. Perform the synthetic to real seismic match, determining the best match location and estimating the wavelet that gives an accurate tie.

Sonic and density well logs are very sensitive to changes in borehole geometry. Therefore, it is necessary to quality check these logs against a calliper log, which records the shape and diameter of the borehole, and edit to remove values associated with borehole washout. These anomalous readings are not representative of the physical properties of the subsurface and would result in the generation of artificial events in the synthetic seismogram. For this study, sonic and density well logs were edited manually.

As electrical logs typically have a decimetre scale resolution whereas reflection seismic typically has a decametre resolution, velocity logs need to be up scaled prior to their use in generating the synthetic seismogram. Backus averaging of well logs is a widely used method in the oil and gas industry to achieve this up scaling and has been utilised in this study. The Backus average departs from an arithmetic average where there are strong contrasts of velocity (Simm 2014).

Once the sonic log has been edited to remove anomalous values and up scaled (smoothed), sonic log calibration is required to reconcile the differences between the timing of a sonic log and the seismic times from a checkshot survey or a vertical seismic profile (VSP) (White & Simm 2003).

The variances between the sonic log times and checkshot times define a drift curve, which is plotted as a function of depth and is defined as: drift = checkshot time – integrated sonic time (Figure 3.1). In this study, the drift curve was fitted to the difference between the integrated sonic log times and corrected checkshot times using a linear fit between knee points (Figure 3.1) (White & Simm 2003).

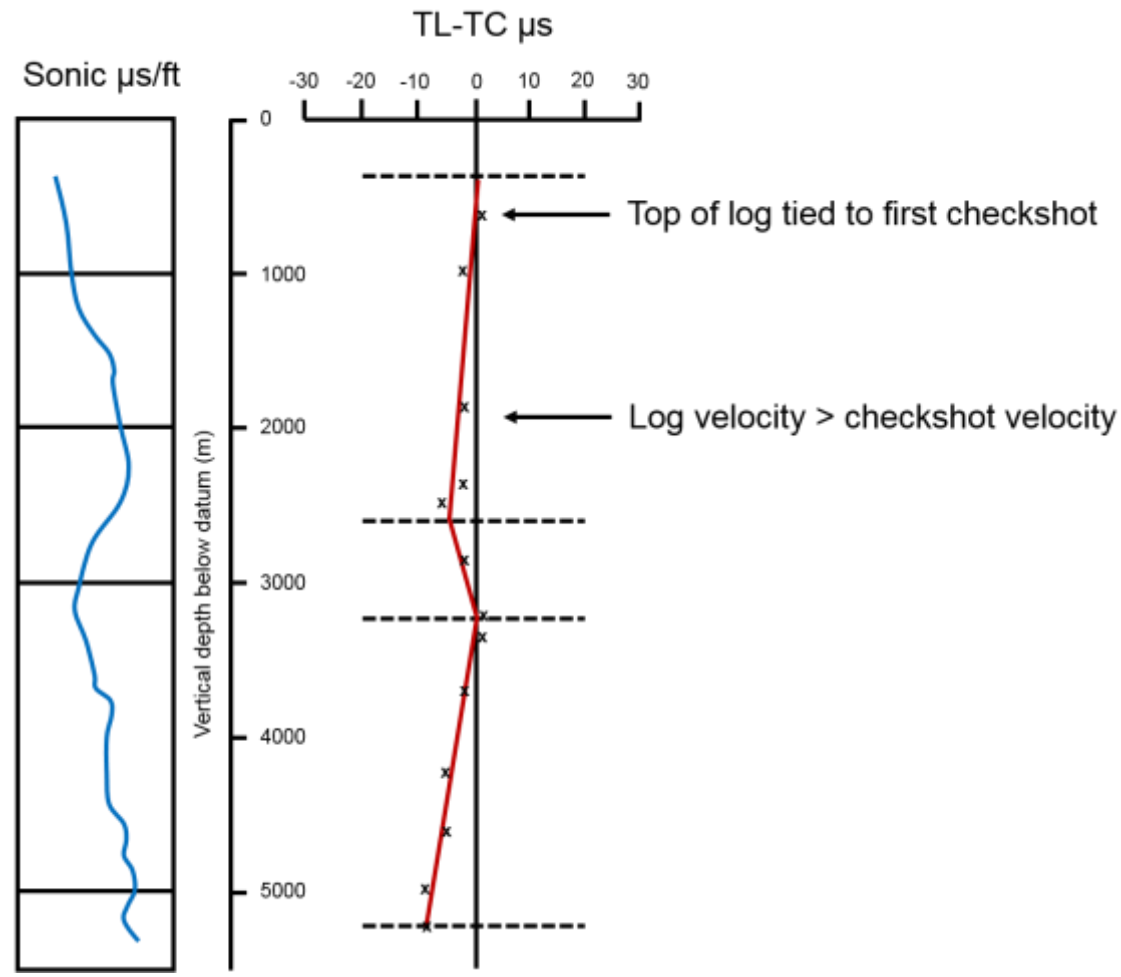

Figure 3.1 Linear fit of sonic drift curve to knee points. Knee points defined at each checkshot point. Modified after Simm (2014).

The synthetic seismogram can now be created by using the edited, up scaled and calibrated log data to create a reflection series in time, which is convolved with a wavelet to create the synthetic trace (White & Simm 2003). In this project, the wavelet was estimated through extraction from the investigated seismic volume in Petrel, at the investigated well location (Figure 3.2).

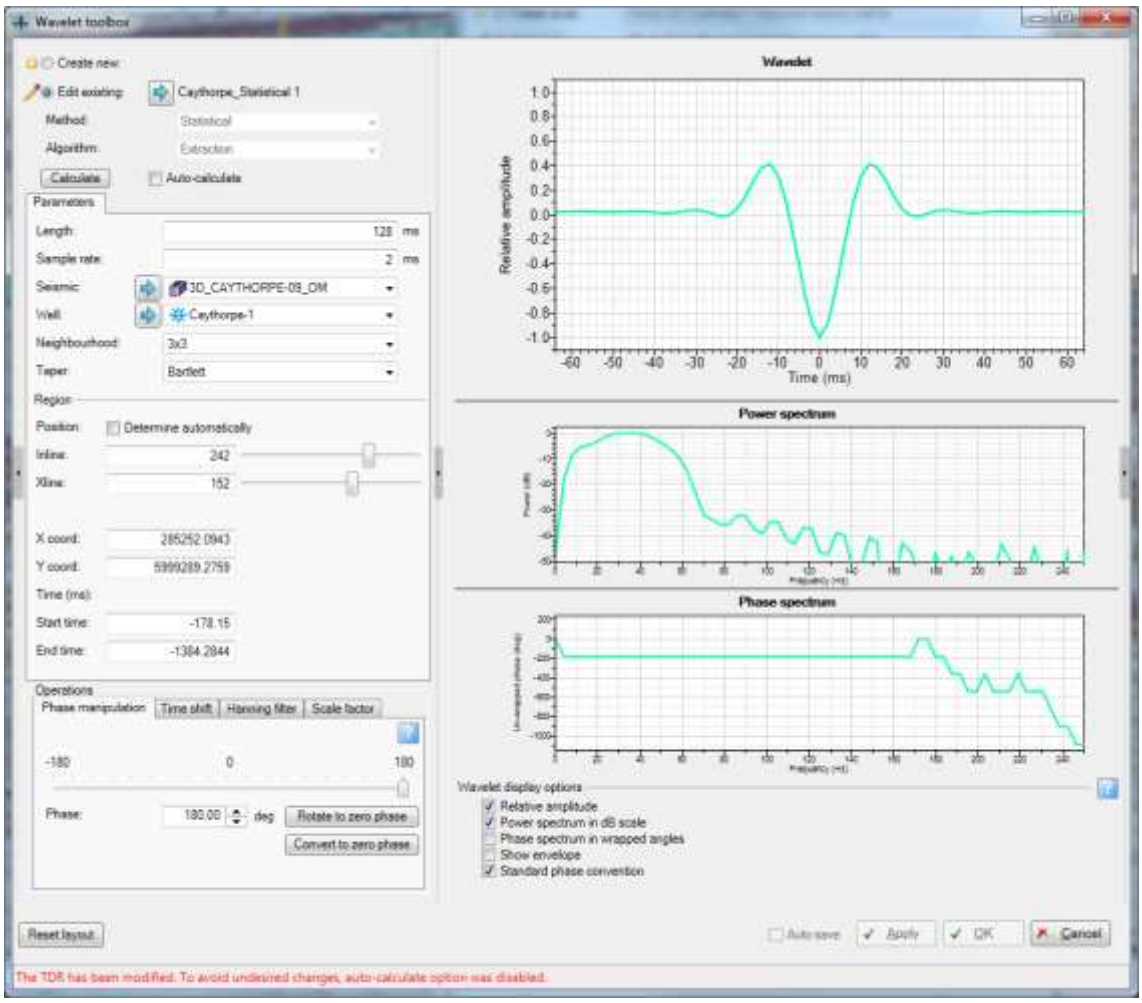

Figure 3.2 Extracted wavelet from Caythorpe 3D survey at Caythorpe-1 well location. Wavelet has been rotated 180 degrees to conform to European polarity convention.

The onshore Caythorpe-1 synthetic well tie (Figure 3.3) and offshore 42/27b-2 well (Figure 3.4) were used as the definitive ties for identifying reflectors to interpret in this project as they provide good synthetic matches through good quality 3D seismic and well log data. Caythorpe-1 well has the benefit of the only well fulfilling these criteria that has a vertical borehole trajectory and therefore greatly improving the prospect of an accurate well tie at this location. Bulk shifts of -2.46ms for Caythorpe-1 and 8.99ms for 42/27b-2 were required to tie the synthetic traces to the seismic volumes.

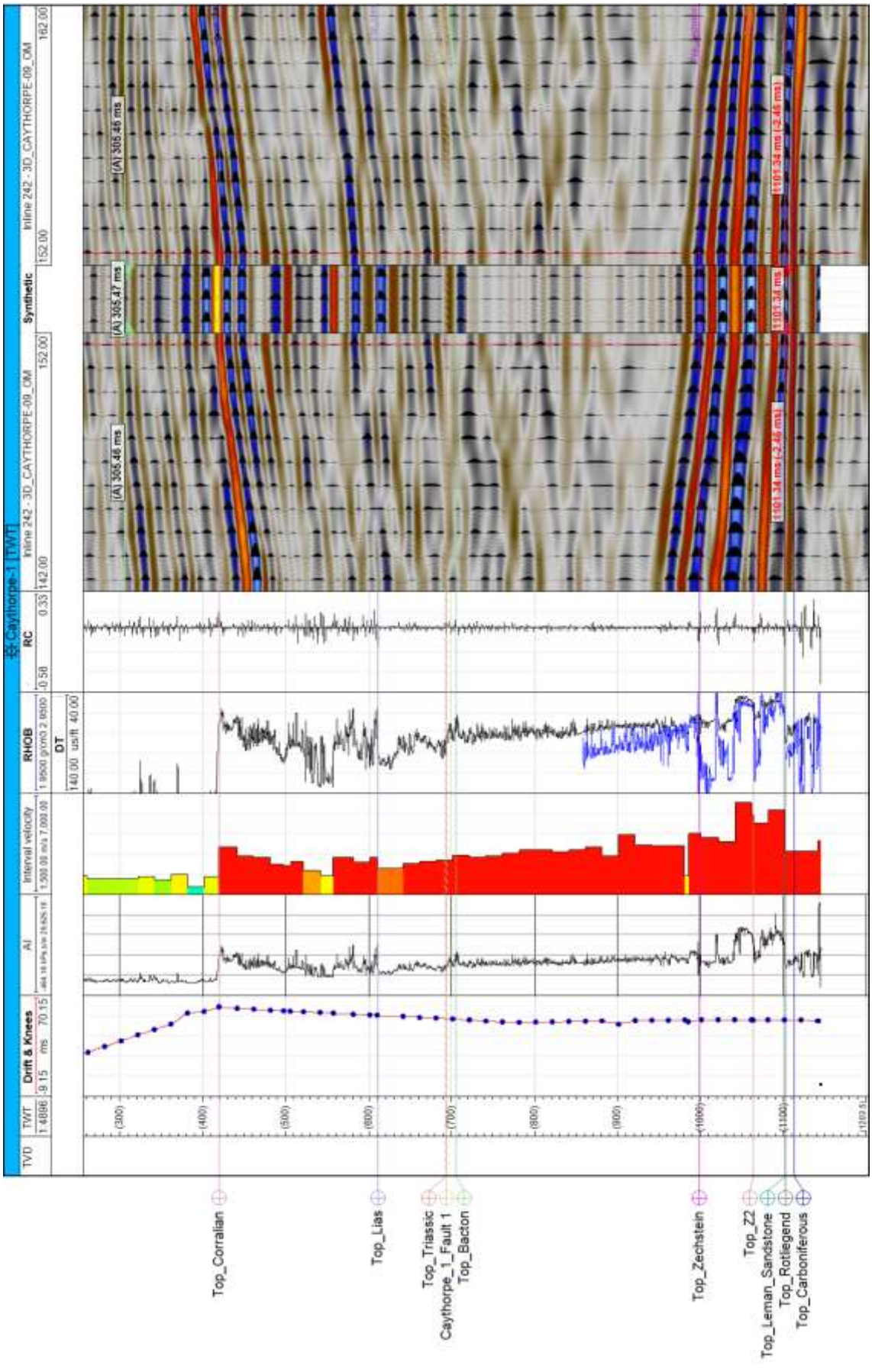

Figure 3.3 Caythorpe-1 well to seismic synthetic tie. -2.46 ms bulk shift required.

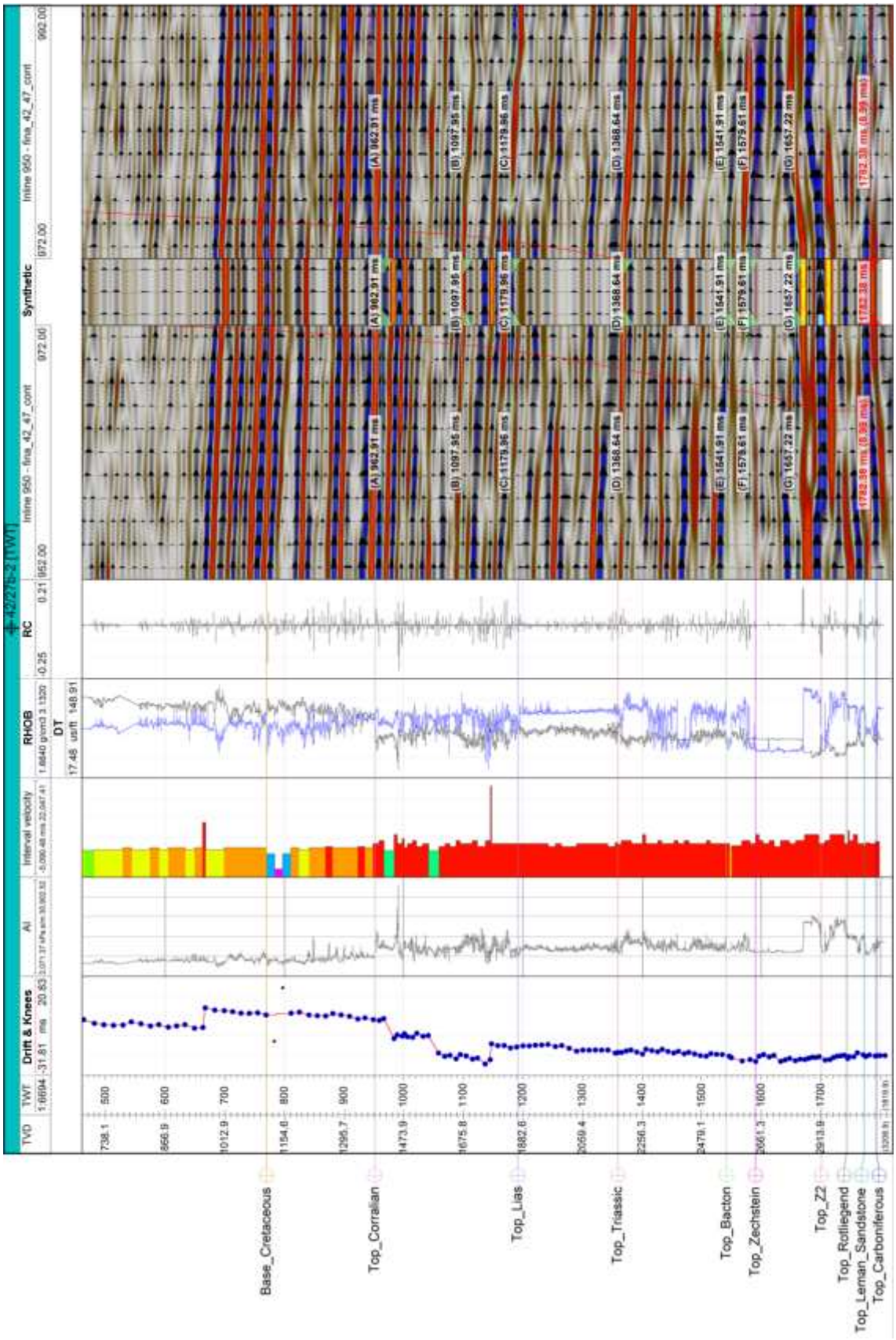

Figure 3.4 42/27b-2 well to seismic synthetic tie. 8.99 ms bulk shift required. Note edited checkshot points below base Cretaceous. These points created artificial reflectors on the synthetic and were manually removed to improve the tie in this section. These anomalous values are assumed errors in the source data. .

3.3 Interpreted Seismic Reflectors

The tied seismic reflector surfaces interpreted for this study are shown in Table 3.1. These surfaces have been chosen as they are represented by strong acoustic impedance contrasts, are continuously interpretable reflectors of regional extent and represent major changes in sedimentation and/or regionally important tectonic events.

Table 3.1 Table of tied seismic reflectors picked. See Figure 1.3 for stratigraphic interval definition.

Surface	Reflector Type	Picked Colour	Stratigraphic Interval	Comments
			Water Column	
Sea Bed	Trough	Dark Blue		No log coverage to generate synthetic. Inferred from seismic polarity
			Chalk	
Base Chalk	Peak	Turqouise		Defined from 42/27a-1
			Cromer Knoll	
Base Cretaceous	Peak	Lime Green		Defined from 42/27b-2
			Humber Group	
Top Corallian	Trough	White		Defined from Caythorpe-1
			West Sole Group	
Top Lias	Peak	Light Blue		Defined from Caythorpe-1
			Lias	
Top Triassic	Trough	Salmon		Defined from Caythorpe-1
			Haighsborough Group	
Top Bacton	Peak	Light Green		Defined from Caythorpe-1
			Bacton Group	
Top Zechstein	Peak	Pink		Defined from Caythorpe-1
			Zechstein Z5-Z2	
Top Z2 / Stassfurt Halite	Peak	Aqua		Defined from Caythorpe-1
			Zechstein Z2-Z1 to Carboniferous	
Rotliegend / Base Permian Unconformity	Peak	Yellow		Defined from Caythorpe-1

The base Permian unconformity / top Carboniferous is represented by a trough in the synthetics for Caythorpe-1 well and in 42/27b-2. In 42/27a-1 it is represented as a peak due to the absence of Leman Sandstone in this well. Because of this geologically derived

polarity reversal and the fact that the base Permian unconformity trough is often difficult to accurately resolve, the peak of the directly overlying reflector (which represents Leman Sandstone where it is present and base Permian unconformity where it is absent) has been used as a proxy, regionally traceable seismic reflector for the base Permian unconformity.

A seismic inline intersection of the Caythorpe 3D volume through the Caythorpe-1 well with the Caythorpe-1 synthetic overlay and picked seismic reflectors is shown in Figure 3.5.

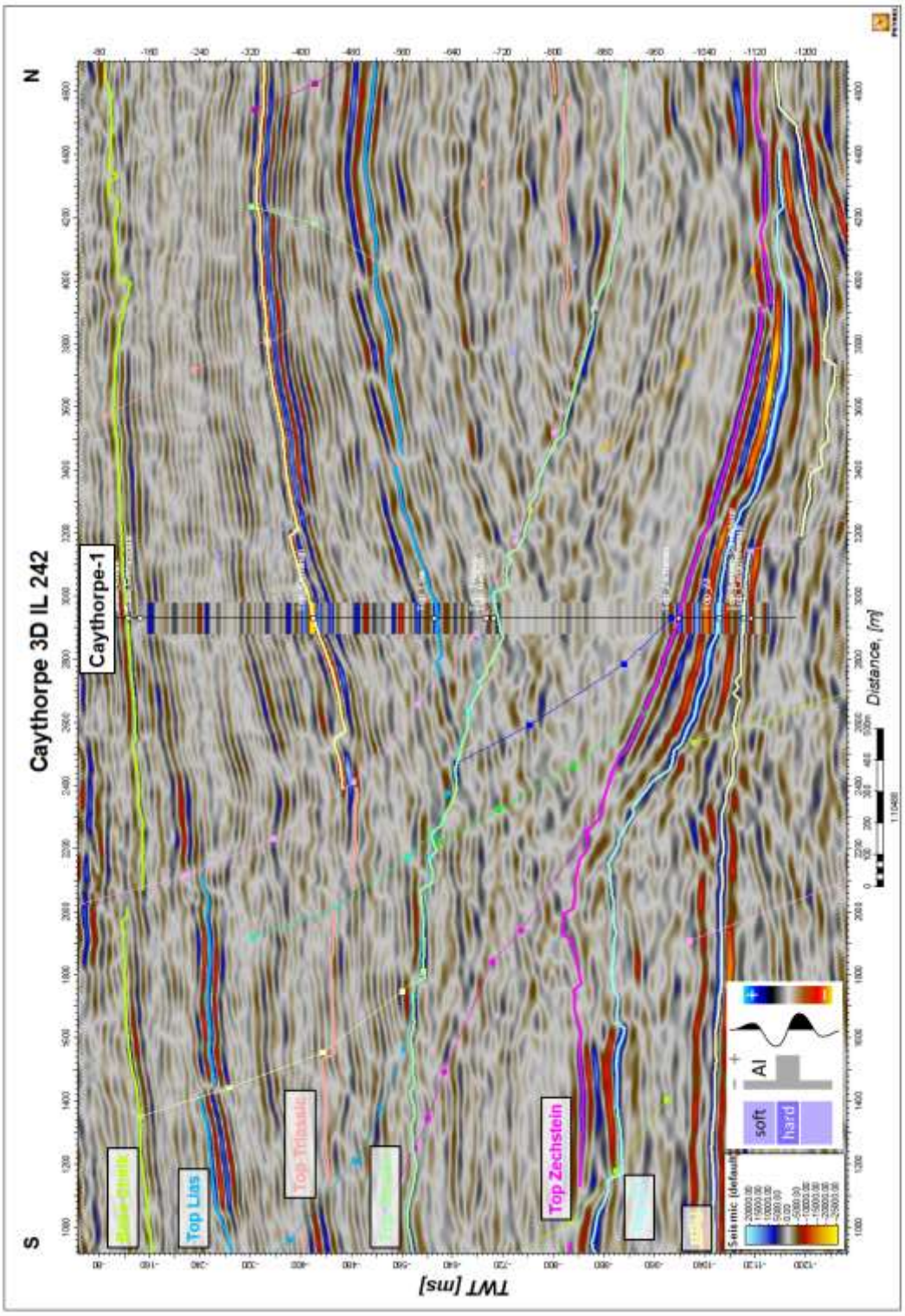

Figure 3.5 Caythorpe 3D IL 242 intersection through Caythorpe-1 well with synthetic seismic overlay and picked seismic reflectors. Two times vertical exaggeration. Data courtesy of UKOGL.

3.4 Time Domain Interpretation

3.4.1 Two-Way Travel Time Structure Gridding

Two-way travel time (TWTT) structure grids were created for each picked seismic horizon listed in Table 3.1 and are included as map plots in Appendix A, for reference.

These surfaces were generated by gridding the seismic interpretation at a cell size of 50m x 50m, using the Petrel seismic interpretation software's default convergent interpolation gridding algorithm. This cell size was selected as a balance to capture the fine scale detail of the 3D survey interpretation without introducing an unacceptable number of gridding artefacts over the more sparse 2D interpretations.

3.4.2 Time Isochore Mapping

Regional isochore maps in time were generated for each stratigraphic interval documented in Table 3.1 and, in addition, for the Cretaceous, Jurassic, Triassic and Permian geological time periods.

Isochore maps were generated in the Petrel seismic interpretation software by subtracting the corresponding top TWTT seismic grid from the base for each interval creating contour maps of equal true vertical thickness in time. For reference, plots of these maps are included in Appendix B.

3.5 Depth Domain Interpretation

3.5.1 Time to Depth Conversion

The seismic datasets used in this study are all in the time domain. As the study area has been structurally inverted and contains highly variable thicknesses of clastics, carbonates and evaporite (Figure 3.5) a robust depth conversion is required to resolve the extreme lateral and vertical velocity contrasts associated with these features and to generate accurate depth structure maps. To achieve this, a $V_0 - K$ depth conversion methodology (Marsden 1992) was adopted based on functions of interval velocity for each mapped seismic interval. This method involved first compiling the tied checkshot depth and time values for the top and base of each stratigraphic interval for twelve wells, shown in Figure 3.6.

Well	Datum		Sea Bed		Base Chalk		Base Cretaceous		Corrallian		Lias		Triassic		Bacton		Zechstein		Z2		BPU	
	TVDSS	2WT	TVDSS	2WT	TVDSS	2WT	TVDSS	2WT	TVDSS	2WT	TVDSS	2WT	TVDSS	2WT	TVDSS	2WT	TVDSS	2WT	TVDSS	2WT	TVDSS	2WT
Caythorpe-1	0	0	0	0	194.79	0.12631	223.5	0.1453	543.78	0.41941	864.43	0.61111	991.53	0.69305	1013.48	0.70533	1591.99	0.99858	1759.63	1.06638	1891	1.1134
Rudston-1	0	0	0	0	207.95	0.11823	207.95	0.11823	255.73	0.15909	459.94	0.29606	490.12	0.31767	678.18	0.42883	1257	0.75596	1421.59	0.82342	1887.02	1.01666
Rudston-2	0	0	0	0	232.9	0.1012	232.9	0.1012	314.58	0.17287	514.65	0.30267	755.46	0.48563	1029.51	0.65993	1281.76	0.83759	1547.65	0.9795	1875.18	1.11456
Willows-1	0	0	0	0	122.1	0.0599	332.77	0.28673	#N/A	#N/A	471.34	0.42483	662.2	0.52746	902.62	0.65495	1498.82	0.95391	1711.38	1.04576	2140.78	1.21608
Hunmanby-1	0	0	0	0	0	0	#N/A	#N/A	#N/A	#N/A	316.9	0.30201	568.1	0.48641	833.3	0.63373	1431.5	0.93819	1619.98	1.00722	2113.3	1.21798
42/26-1	0	0	47.85	0.062795	669.34	0.41794	1138.73	0.774	#N/A	#N/A	1345.99	0.91081	1394.76	0.943	1461.82	0.971	2122.62	1.285	2548.43	1.4496	2745.64	1.527
42/27a-1	0	0	55.17	0.072402	602.84	0.36818	758.55	0.51053	894.46	0.63028	1021.18	0.6959	1081.18	0.72866	1444.98	0.93337	2269.45	1.34126	2521.42	1.45588	2928.22	1.63581
42/27a-3	0	0	54.79	0.071903	613.02	0.40241	797	0.55437	874.96	0.61247	1012.37	0.68859	1260.66	0.83468	1382.52	0.89508	2144.63	1.27326	2404.97	1.3941	3010.65	1.66404
42/27b-2	0	0	54.25	0.071194	415.01	0.27253	1073.14	0.77147	1332.67	0.95258	1827.53	1.19207	2128.49	1.36234	2528.2	1.54546	2592.09	1.58988	2876.06	1.69499	3110.35	1.79491
42/28-2	0	0	51.82	0.068005	863.78	0.54248	1122.32	0.73038	1180.18	0.76842	#N/A	#N/A	1461.78	0.94245	1812.05	1.13023	2481.98	1.46933	2725.22	1.56919	3016.61	1.69257
42/28a-4	0	0	53.34	0.07	630.68	0.40411	901.73	0.61799	1026.54	0.71192	1335	0.86364	1558.12	1.01297	1797.53	1.14973	2419.96	1.43399	2579.31	1.50199	3112.03	1.7137
41/24a-2	0	0	50.01	0.06563	#N/A	#N/A	#N/A	#N/A	#N/A	#N/A	50.01	0.06563	157.51	0.16444	450.01	0.32611	986.01	0.5973	1166.01	0.68277	1762.01	0.92932

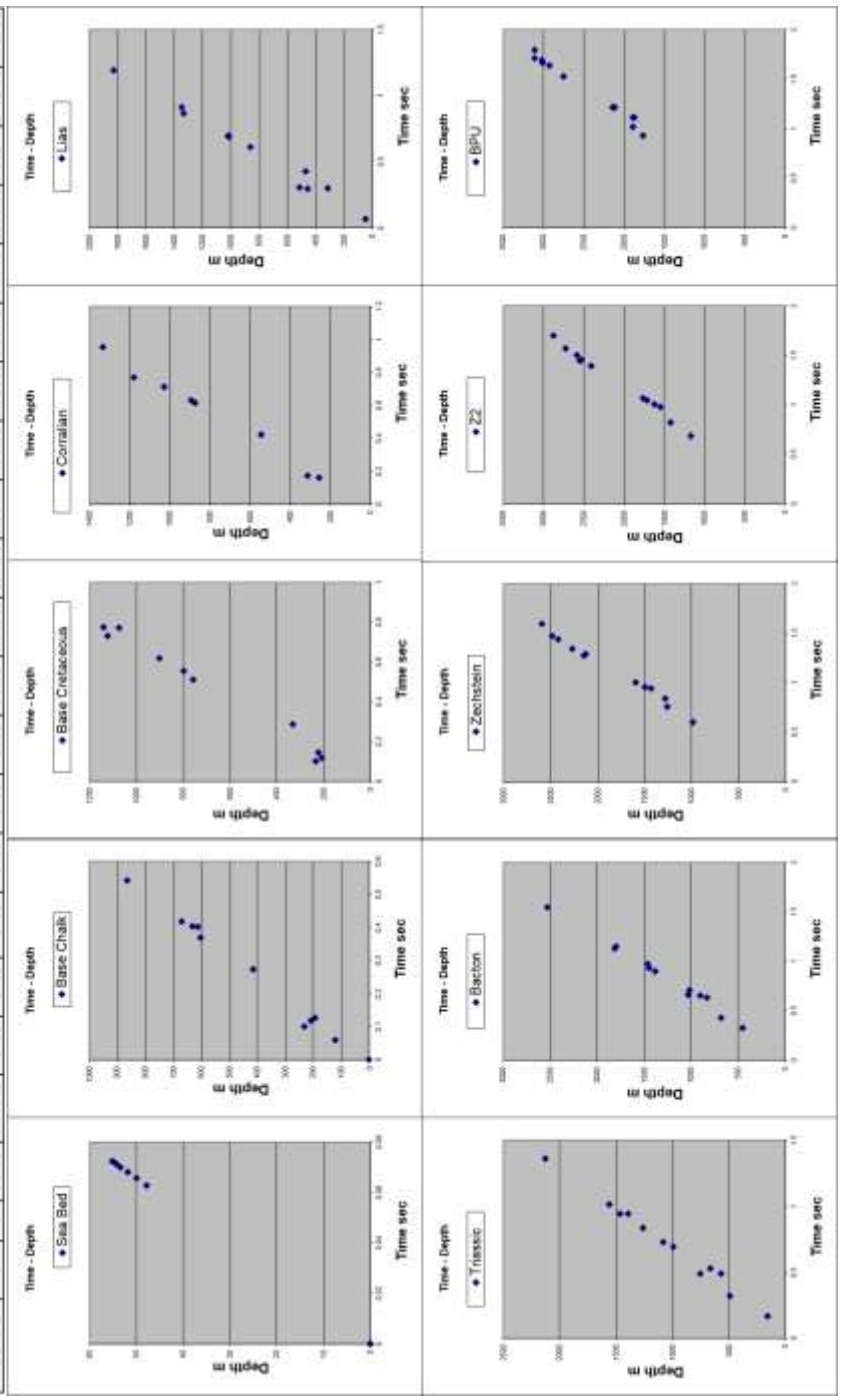

Figure 3.6 Compiled tied checkshot time / depth values for each mapped seismic reflector from twelve wells used in depth conversion. Depth values are TVDSS metres and time values are TWT in seconds.

From the compiled tied checkshot data, multiple V_0-K functions of interval velocity for each mapped seismic interval can be investigated. This process involves cross plotting isochron Δz against isopach Δz (Figure 3.7), interval velocity against formation mid-point time (Figure 3.8) and interval velocity against mid-point depth (Figure 3.9) from the tied checkshot data from each well for each seismic interval. V_0 (intercept) and K (gradient) is then derived through the regression analysis for each cross plot and these values can be integrated into a time to depth function depending on the type of cross plots and the regression analysis employed.

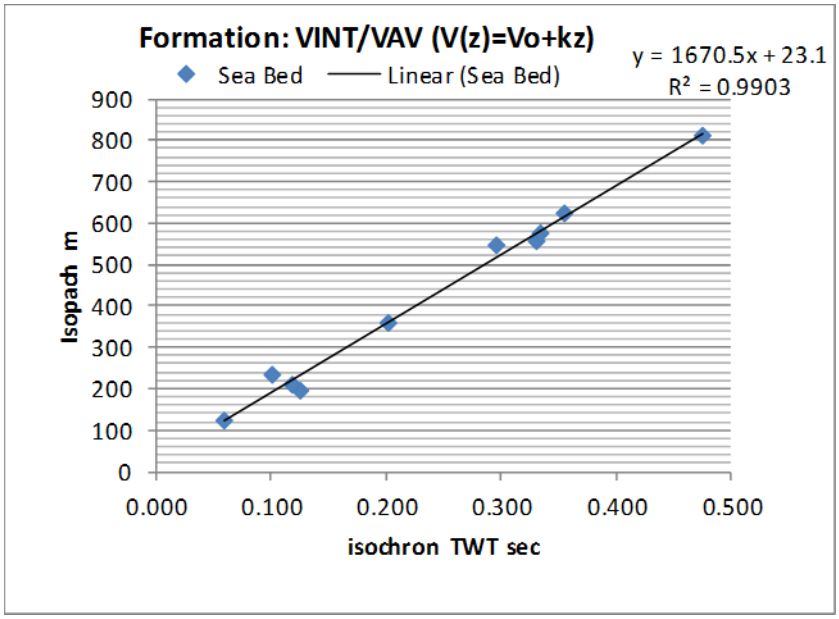

Figure 3.7 Cretaceous Chalk interval Isopach / Isochron cross plot showing linear regression and derived Vo and k values

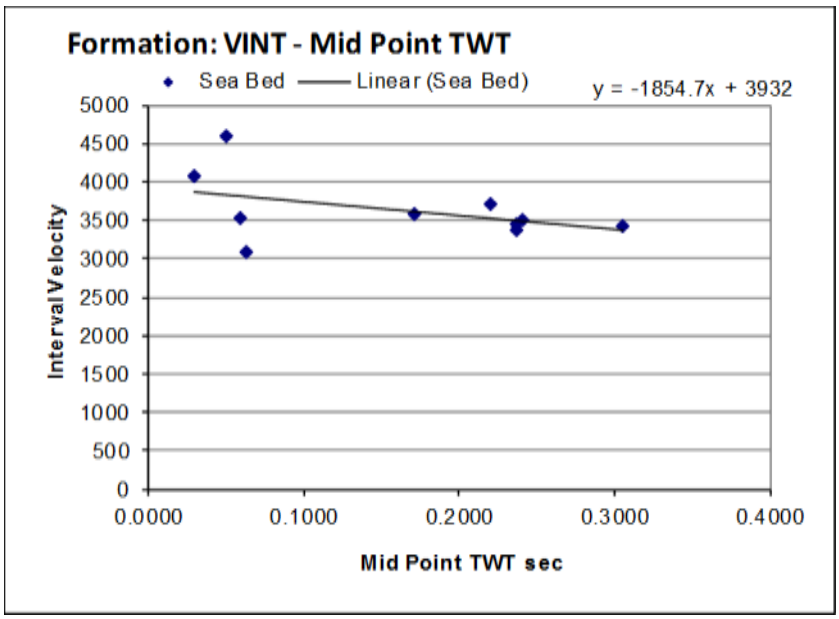

Figure 3.8 Cretaceous Chalk interval mid-point TWT / interval velocity cross plot showing regression and derived Vo and k values

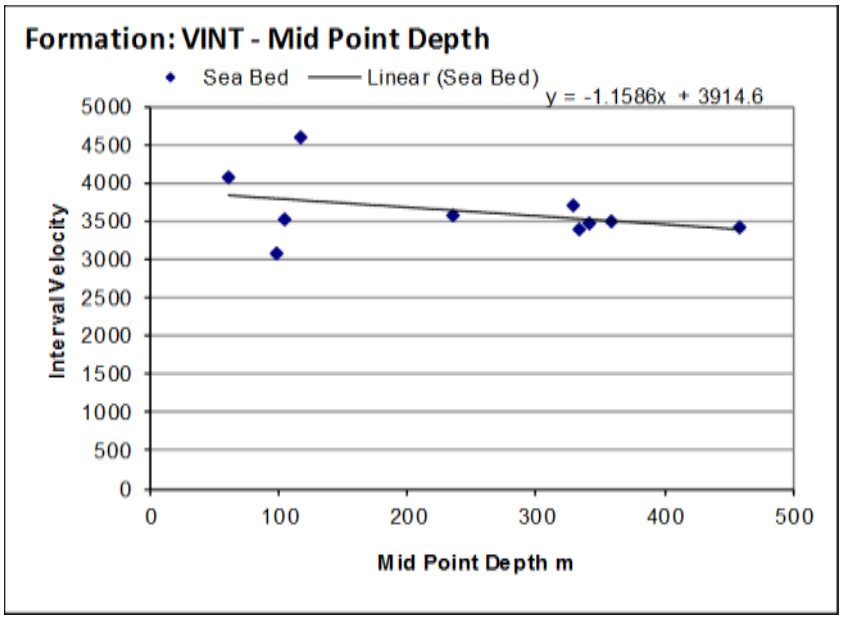

Figure 3.9 Cretaceous Chalk interval mid-point depth / interval velocity cross plot showing regression and derived Vo and k values

The isopach depth values derived from each function are then compared with the true isopach depth values at each well location to calculate the correlation coefficient, standard deviation and RMS error. The formula resulting in the lowest RMS error between the calculated isopach depth and true isopach depth for each interval was selected to depth convert that interval, resulting in a series of depth isochores. This is documented in Table 3.2. The tied checkshot interval velocity cross plots, regression analyses, depth

conversion functions and modelled Δz versus true Δz error analyses for each seismic interval are included for reference in Appendix C.

Depth surface maps are then created by summing each depth isochore map down to each reference surface.

This depth conversion approach is suitable for the study area as it takes in account velocity variations due to lateral variations in both formation burial depth and formation thickness.

Table 3.2 Depth conversion methods for each mapped interval

Mapped Interval / Time Isochore	Function	Correlation Coefficient	Standard Deviation	Mean	RMS Error	Formula
Water Column	Constant sea water velocity = 1524ms	-	-	-	-	Δz = VINT * ΔT / 2
Chalk	Isopach / Isochron (Linear)	0.995	21.543	0.002	21.543	Δz = Vo + k * ΔT
Cromer Knoll	Mid-Point Time	0.991	25.716	-4.273	26.068	Δz = (Vo + k * Tmid) * ΔT / 2
Humber Group	Mid-Point Time	0.997	7.569	-2.395	7.939	Δz = (Vo + k * Tmid) * ΔT / 2
West Sole Group	Mid-Point Time	0.998	10.212	-2.062	10.418	Δz = (Vo + k * Tmid) * ΔT / 2
Lias	Mid-Point Time	0.981	18.388	-2.643	18.577	Δz = (Vo + k * Tmid) * ΔT / 2
Haighsborough Group	Mid-Point Time	0.988	18.825	-5.482	19.607	Δz = (Vo + k * Tmid) * ΔT / 2
Bacton Group	Isopach / Isochron (Linear)	0.982	37.831	0.003	37.831	Δz = Vo + k * ΔT
Zechstein Z5-Z2	Mid-Point Time	0.940	25.583	-3.009	25.759	Δz = (Vo + k * Tmid) * ΔT / 2
Zechstein Z2-Z1 to Carboniferous	Isopach / Isochron (2nd Order Polynomial)	0.994	16.612	-0.006	16.612	Δz = Vo * ΔT + k * ΔT^ 2

3.5.2 Depth Surface to Well Tie and Tied Depth Structure Grids

Any well data points on the V_0 – k cross plots which do not sit exactly on the regression line will result in the calculated depth surface values at these well locations being different to those seen in the well. To correct this, the error between the depth surfaces and the well top picks at each well location was calculated, gridded and applied to each depth structure grids, creating well top tied depth surfaces. The calculated well tie error and correction for each depth structure grid is included in Appendix D.

Regional tied depth structure grids for each mapped seismic horizon are included in Appendix E.

CHAPTER 4. TECTONO-STRATIGRAPHIC EVOLUTION OF THE STUDY AREA

4.1 Introduction

The interpreted subsurface dataset forms the basis on which to construct a new structural and stratigraphic geological history for the study area. This chapter presents the geological model defined in this study for each mapped seismic interval from the end Carboniferous / Base Permian Unconformity through to the Upper Cretaceous, which subcrops in the area. The main aims of this section are to present a unified geological model that is unconstrained by the coastline, identify the tectonic regime present in the study area and identify any kinematic controls on sedimentation and facies distribution.

4.2 Late Carboniferous / Base Permian Unconformity and Upper Permian Rotliegend Group

The nature of the contact between the Carboniferous and Upper Permian Rotliegend Group is known to be unconformable from onshore mapping and is marked by erosional truncation of folded and tilted carboniferous strata (Figure 4.1).

The unconformity is represented on the seismic dataset where it is again represented by angular truncation of Carboniferous reflectors against the Base Permian Unconformity throughout the study area (Figure 4.2), interpreted to result from Late Carboniferous Variscan uplift and levelling of the Carboniferous topography in the study area. Upper Permian Rotliegend Group units directly overly the unconformity surface. The Rotliegend and underlying Carboniferous are offset by many planar faults that appear to be a mostly extensional displacement sense although relatively poor seismic quality at this level precludes a definitive answer (Figure 4.2). Rotliegend sedimentation and deformation is related to the development of the Southern Permian Basin through crustal thermal subsidence and extension driven by intramontane collapse of the Variscan Orogen and north – south intracratonic rifting (Gast, *et al*. 2010).

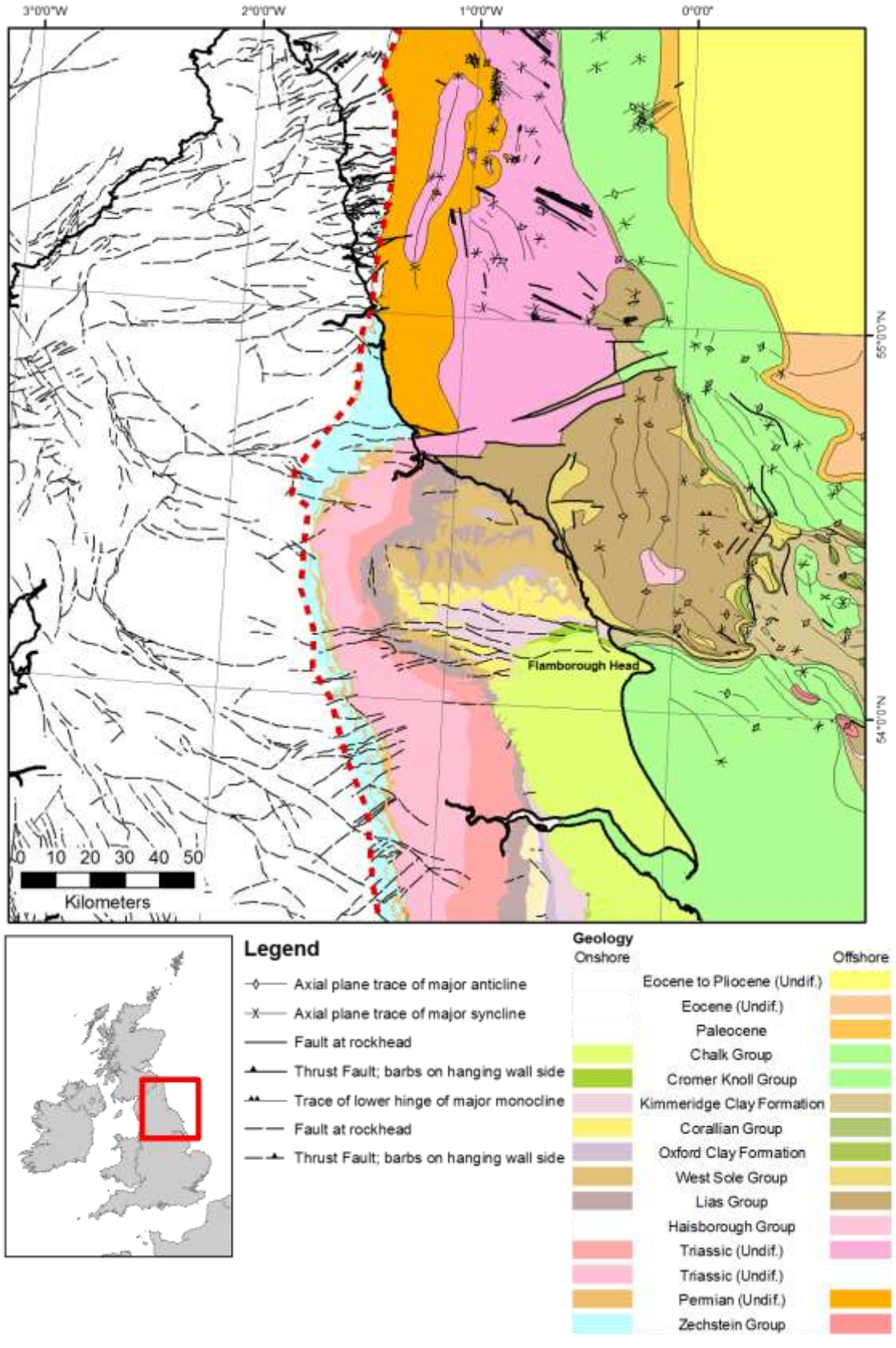

Figure 4.1 Geological map of east-central UK with Carboniferous - Permian unconformity shown as dashed red line. Stratigraphy older than Permian not shown. Data courtesy of British Geological Survey.

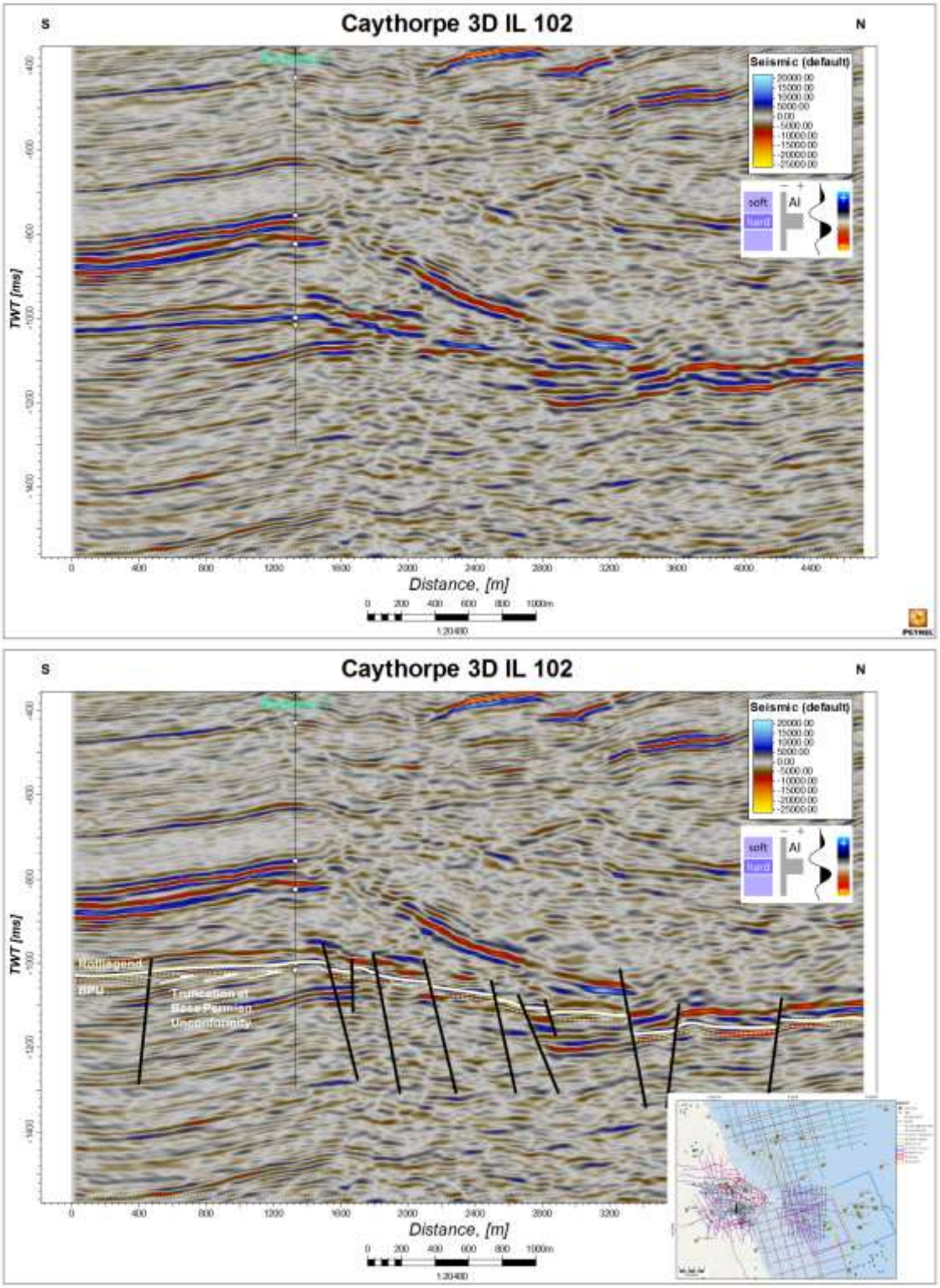

Figure 4.2 (Above) north – south striking un-interpreted Caythorpe 3D IL 102 S-N line through Rudstone-1 well. (Below) interpreted section at Base Permian Unconformity level highlighting truncation of Carboniferous reflectors by BPU and planar faulting of BPU and overlying Rotliegend. Two times vertical exaggeration. Inset map shows line location. Data courtesy of UKOGL.

Rotliegend level fault orientations are broadly west to east across the dataset (Figure 4.3), mirroring the west to east trend of the Vale of Pickering – Flamborough Head Fault Zone (Figure 1.2), (Starmer 2008). This trend can be traced from the onshore to the offshore

via a series of planar dip-slip faults, which throw to the north, from just north of the Caythorpe-1 well eastwards underneath Bridlington and extend offshore to just north of the 42/27b-2 well (Figure 4.3 (shown by red arrows)). Onshore, this fault system has been previously termed the Langtoft Fault (Kirby & Swallow 1987). The Langtoft Fault System may be linked by relay structures that are not resolvable due to the low seismic quality at this level. The west to east striking fault systems are inferred to represent a west to east trending hinge zone between the northern margin of the buoyant granite cored Market Weighton Block to the south and the less stable Cleveland Basin to the north (Kent 1980).

In the onshore, to the north of the Langtoft Fault and in the vicinity of the Hunmanby-1 well, a major planar dip-slip fault system which throws to the south can be identified (Figure 4.3 (shown by white arrows) and Figure 4.4). This fault has been previously termed the Bempton Fault (Kirby & Swallow 1987) and, like the Langtoft Fault, appears to be present and extend into the offshore (Figure 4.3).

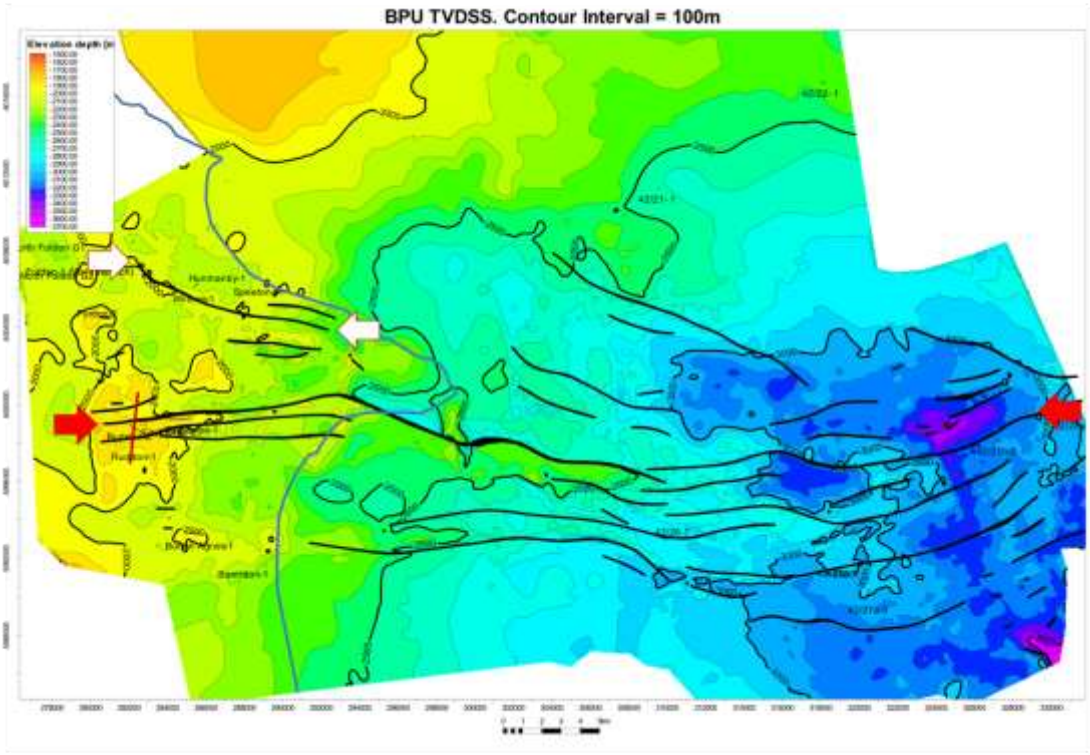

Figure 4.3 Depth structure grid of Base Permian Unconformity showing fault pattern. Red arrows denote location of Langtoft Fault System. White arrows denote location of Bempton Fault System. Red line shows location of seismic line in Figure 4.2. Blue line marks coastline. Pink line shows location of composite seismic line in Figure 4.4. See Appendix E-11 for large scale plot.

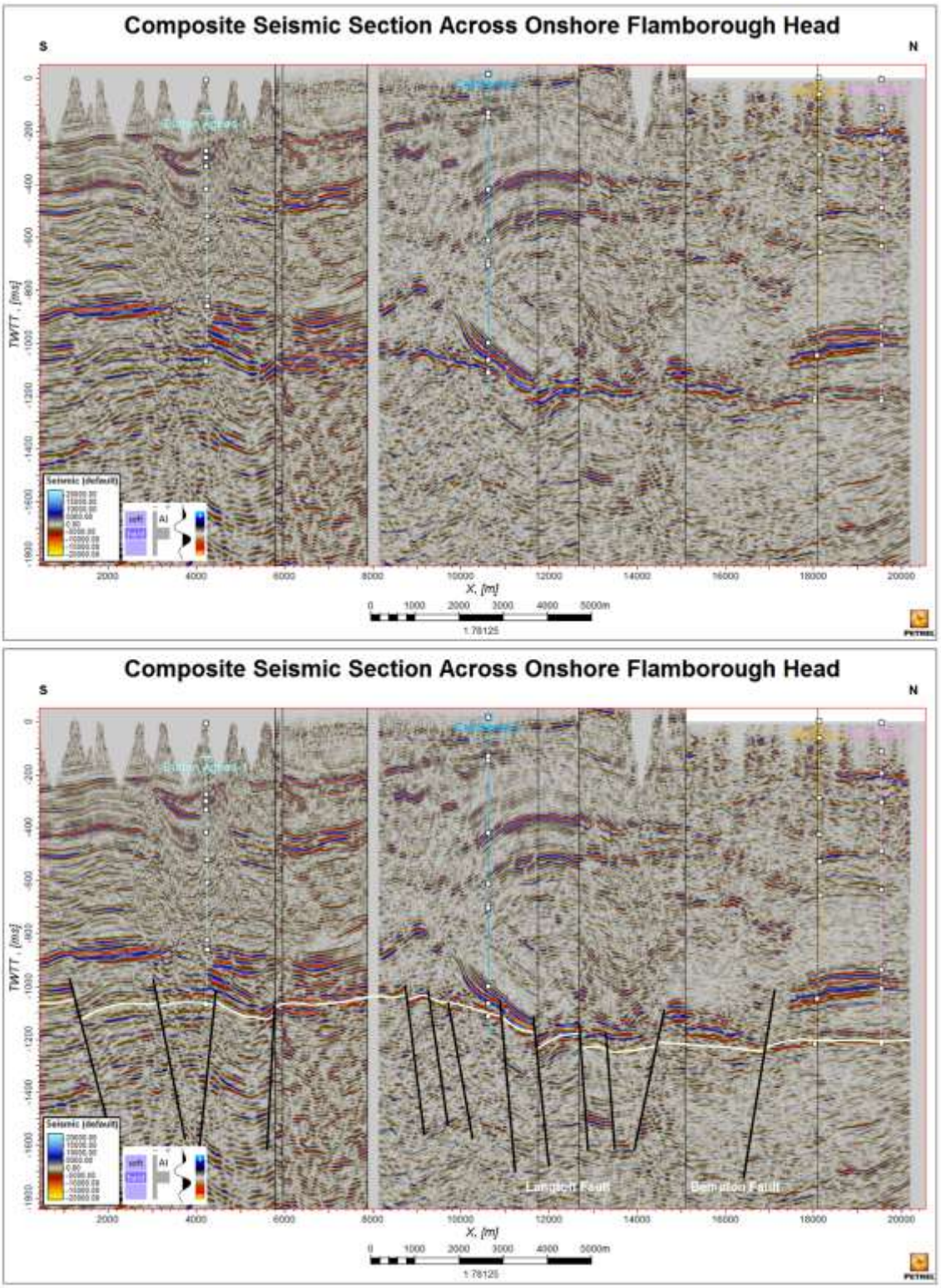

Figure 4.4 (Above) un-interpreted south to north composite seismic line across onshore Flamborough Head, intersecting through Burton Agnes-1, Caythorpe-1, Willows-1 and Hunmanby-1 wells. (Below) interpretation of same line showing Top Rotliegend / Base Permian Unconformity horizon, fault displacements and location of Langtoft and Bempton Faults. See Figure 4.3 for section location. Six times vertical resolution. Data courtesy of UKOGL.

Towards the north of the dataset, where the effects of the Market Weighton Block – Cleveland Basin hinge zone are reduced, several north-west to south east trending faults have been interpreted (Figure 4.3). Faults with this orientation may represent basement

inherited Tornquist Trend features. The mapped Flamborough Head fault trends are proposed to link up with the basement inherited Dowsing Fault Zone at the eastern margin of the Market Weighton Block granite (Figure 4.5).

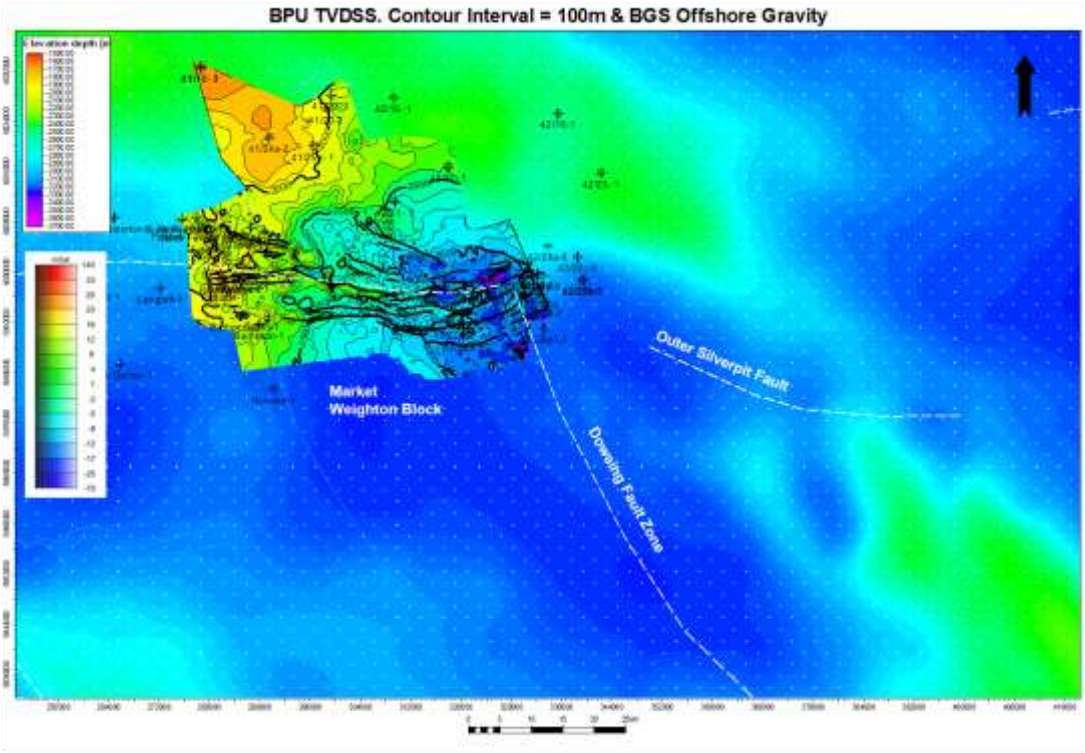

Figure 4.5 Base Permian Unconformity contoured depth structure grid and fault polygons overlain on offshore gravity. Upper, elevation depth colour bar is legend for Base Permian Unconformity structure grid. Lower, colour bar is legend for offshore gravity. Blue colours represent negative gravity anomalies that are attributed to the large Devonian granite situated below the Market Weighton Block. White dashed lines are regional tectonic features as defined by the British Geological Survey. Data courtesy of British Geological Survey.

The described geometries of the faulting at Rotliegend and deeper levels across Flamborough Head strongly suggests that a post Permian dip-slip tectonic regime is the dominant process that has created this deformation style. By using the criteria defined by Harding (1990), (outlined in Section 2.4.2 above), a strike-slip tectonic regime can be ruled out based on the following observations:

- A narrow, long, straight, central, solitary master fault at depth or a linear throughgoing solitary zone of deformation is not observed (Figure 4.3, Figure 4.5).

- Neither positive nor negative flower structures are observed on vertical seismic sections (Figure 4.2, Figure 4.4).

Permian Rotliegend Group sedimentation shows a trend of excellent reservoir quality (up to 20% effective porosity and over 100mD permeability at the Caythorpe gas field (Kelt UK Ltd. 1991)), with coarse clastics of the Leman Sandstone Formation in the south of the dataset (Figure 4.6), passing into fine grained, non-reservoir silts and mudstones of the Silverpit Claystone Formation to the north (Figure 4.7). This observation is consistent with published material (Underhill 2003) and the observed facies changes are proposed to represent a paleogeographical change at the time of deposition from arid, continental fluvial and aeolian dune deposition of the Leman Sandstone Formation in the south to the development of a desert lake setting further north, in which the mudstones and evaporites of the Silverpit Claystone Formation were deposited (Figure 4.8 and Figure 4.9), (Gast, *et al*. 2010).

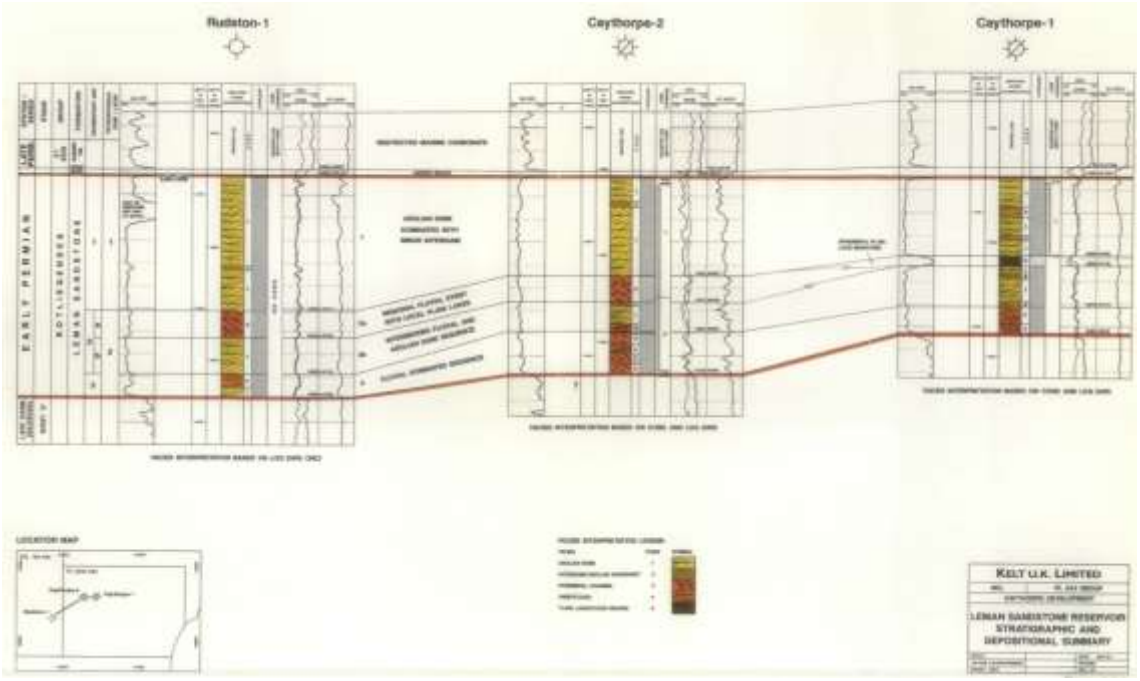

Figure 4.6 Rotliegend Leman Sandstone Formation facies characterisation onshore Flamborough Head, in the Caythorpe field area (Kelt UK Ltd. 1991)

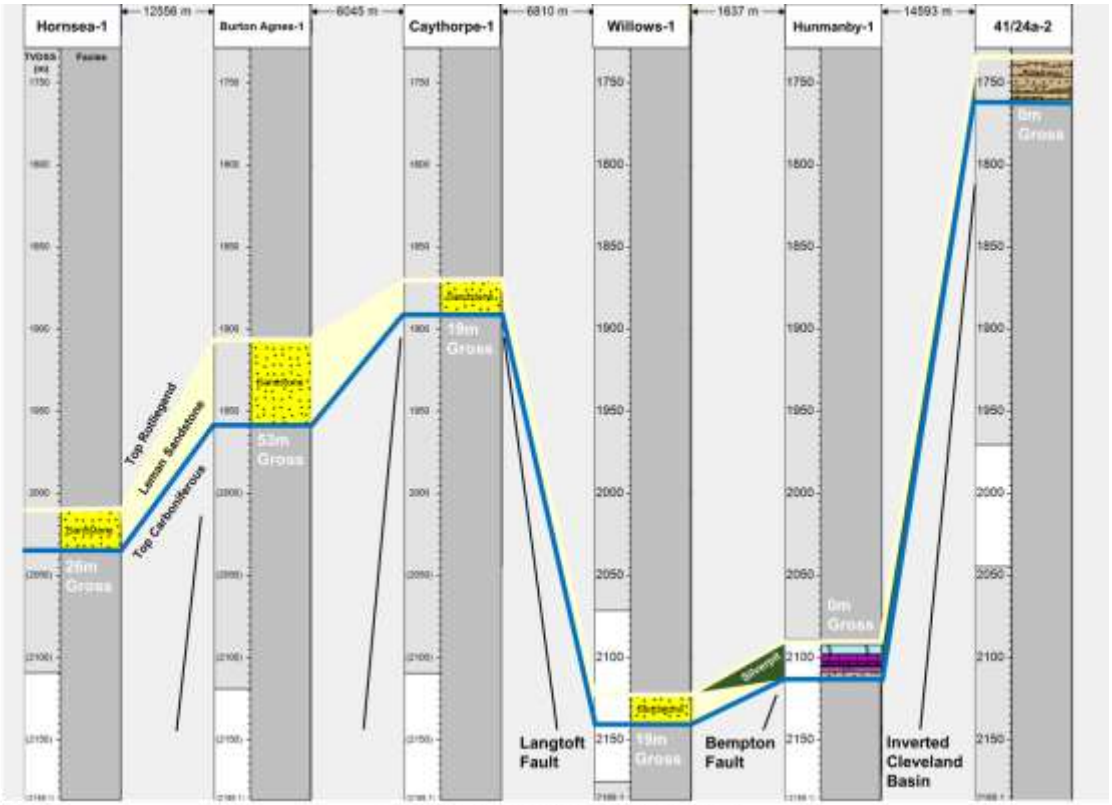

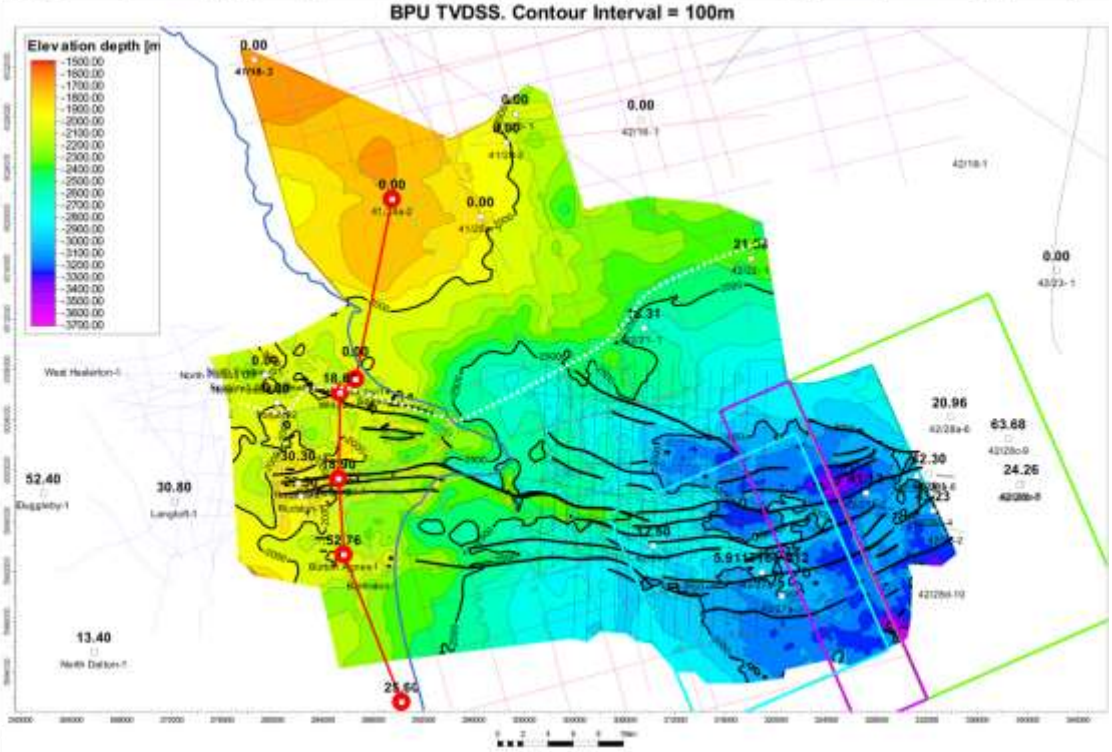

Figure 4.7 (Above) Rotliegend level well correlation in metres TVDSS across the Flamborough Head Fault Zone. Transition from Leman Sandstone Formation to Silverpit Claystone Formation occurs between the Langtoft and Bempton faults. Composite log is not available for Willows-1 so lithology is inferred from mud log. Well operator suggested low porosity in this interval so might represent a transition zone at this location. (Below) Base Permian Unconformity depth surface map in metres TVDSS showing Leman Sandstone isochore thickness values, proposed Leman Sandstone – Silverpit Formation facies boundary line in white, coastline in blue, fault polygons in black and cross section line in red.

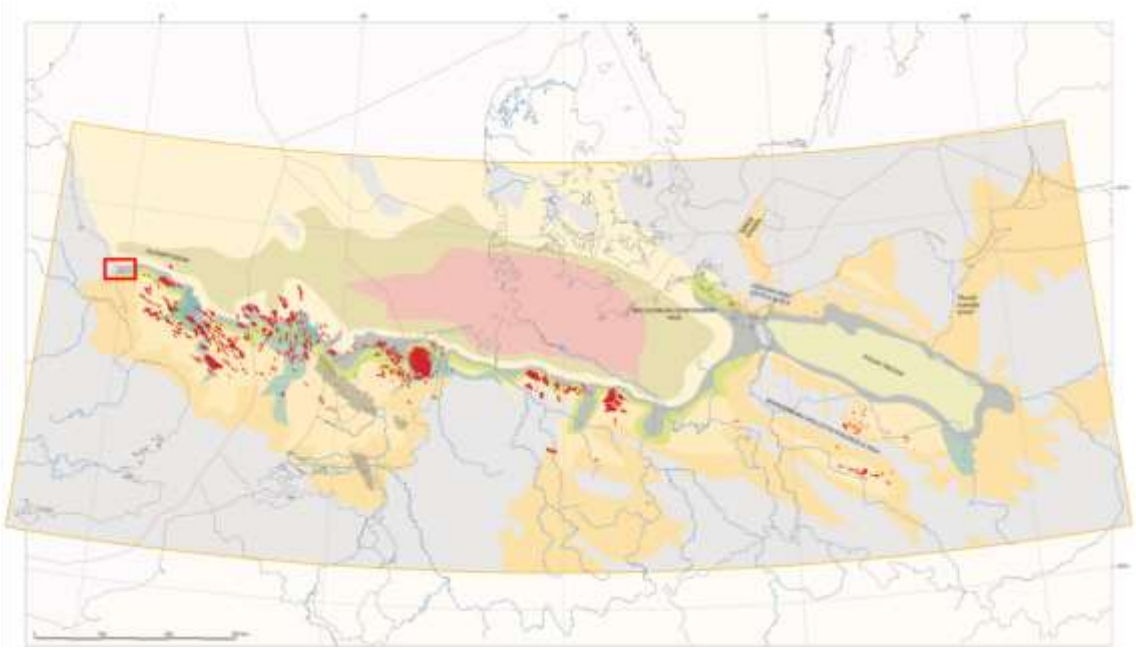

Figure 4.8 Reservoir facies distribution of the lower part of the Leman Sandstone Formation. Fields with Rotliegend reservoirs shown. Study area shown as red box. Legend shown in Figure 4.9. Modified after Gast, et al. (2010).

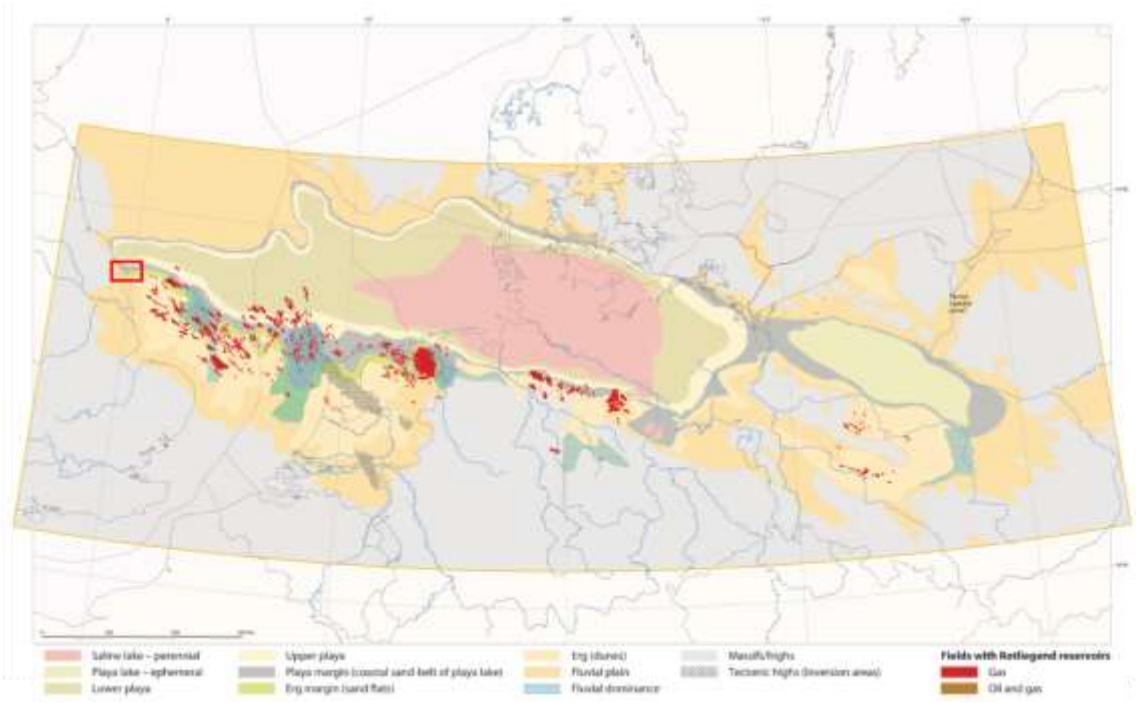

Figure 4.9 Reservoir facies distribution of the upper part of the Leman Sandstone Formation. Fields with Rotliegend reservoirs shown. Study area shown as red box. Modified after Gast, et al. (2010).

The location of the Leman Sandstone Formation to Silverpit Claystone Formation facies boundary appears to be co-incident with the location of the Flamborough Head Fault Zone (Figure 4.7). This important observation suggests that, at this location, Permian Rotliegend Group reservoir deposition has been structurally controlled by the Langtoft and Bempton faults of the Flamborough Head Fault Zone. It is proposed that active

extensional faulting across the Flamborough Head Fault Zone during the Rotliegend created a paleo-topographic low to the north and in the hanging wall of this fault system, which facilitated the formation of a desert lake environment and thus the deposition of the Silverpit Claystone Formation. The fining and thinning of the Leman Sandstone Formation across the Flamborough Head Fault Zone, in particular at the poor quality, low porosity reservoir encountered at Willows-1 well (Rigzone 2006) and development of non-reservoir evaporites and claystones of the Hunmanby-1 well (Figure 4.7), could represent the development of a desert sabkha reservoir waste zone across the fault zone (Figure 4.7 and Figure 4.10).

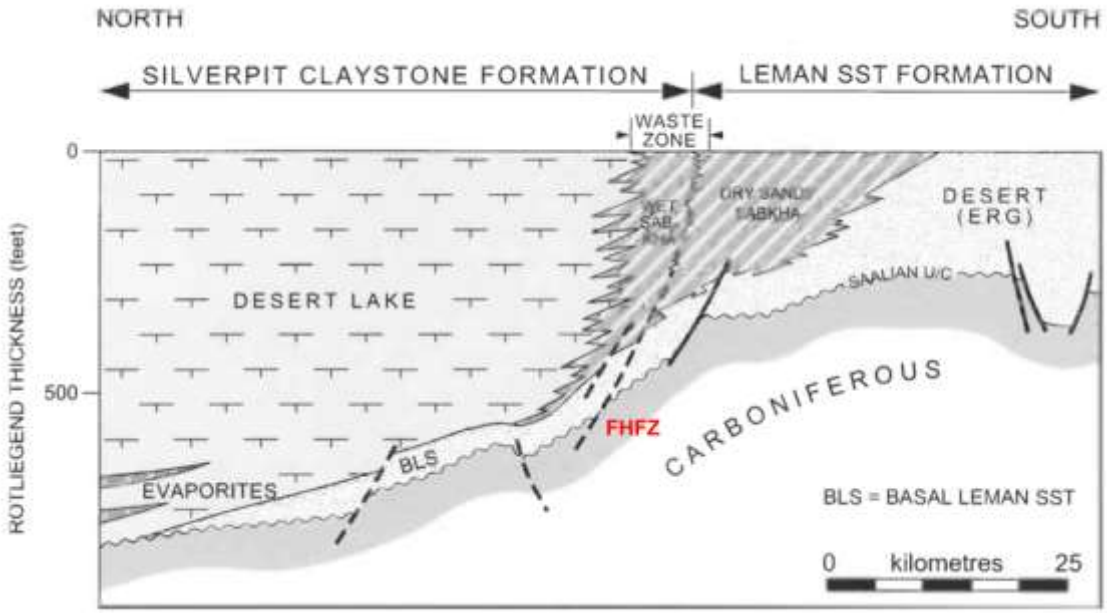

Figure 4.10 Tectonic control of Flamborough Head Fault Zone (FHFZ) on Rotliegend facies development. Aeolian and fluvial sandstones of the Leman Sandstone Formation are deposited on the southern footwall of the FHFZ and over the Market Weighton Block. Desert lake, Silverpit Claystone Formation mudstones and evaporites are deposited in the hanging wall of the Cleveland Basin with a desert sabkha and reservoir waste zone developed across the FHFZ. Modified after Underhill (2003).

4.3 Upper Permian Zechstein Group

The carbonate and evaporitic facies of the Zechstein Group overlie the Rotliegend Group and represent a period of major marine transgression with cyclic periods of marine incursion, regression and evaporation (Underhill 2003). Rapid flooding of the low-lying late Permian topography, through a major transgression from the Barents Sea, brought fully marine conditions to the entire Northern and Southern Permian Basins, marking the onset of Zechstein Group deposition (Peryt, *et al*. 2010). The base of the interval displays a general seismic character of bright, layer-parallel reflectors that drape over the Rotliegend, creating a disconformable boundary (Figure 4.11). These represent the

carbonate to anhydritic facies of the Z1 – Z2 Zechstein groups, the Kupfershiefer, Zechsteinkalk, Werraanhydrit, Hauptdolomit and Basalanhydrit formations (Figure 4.12).

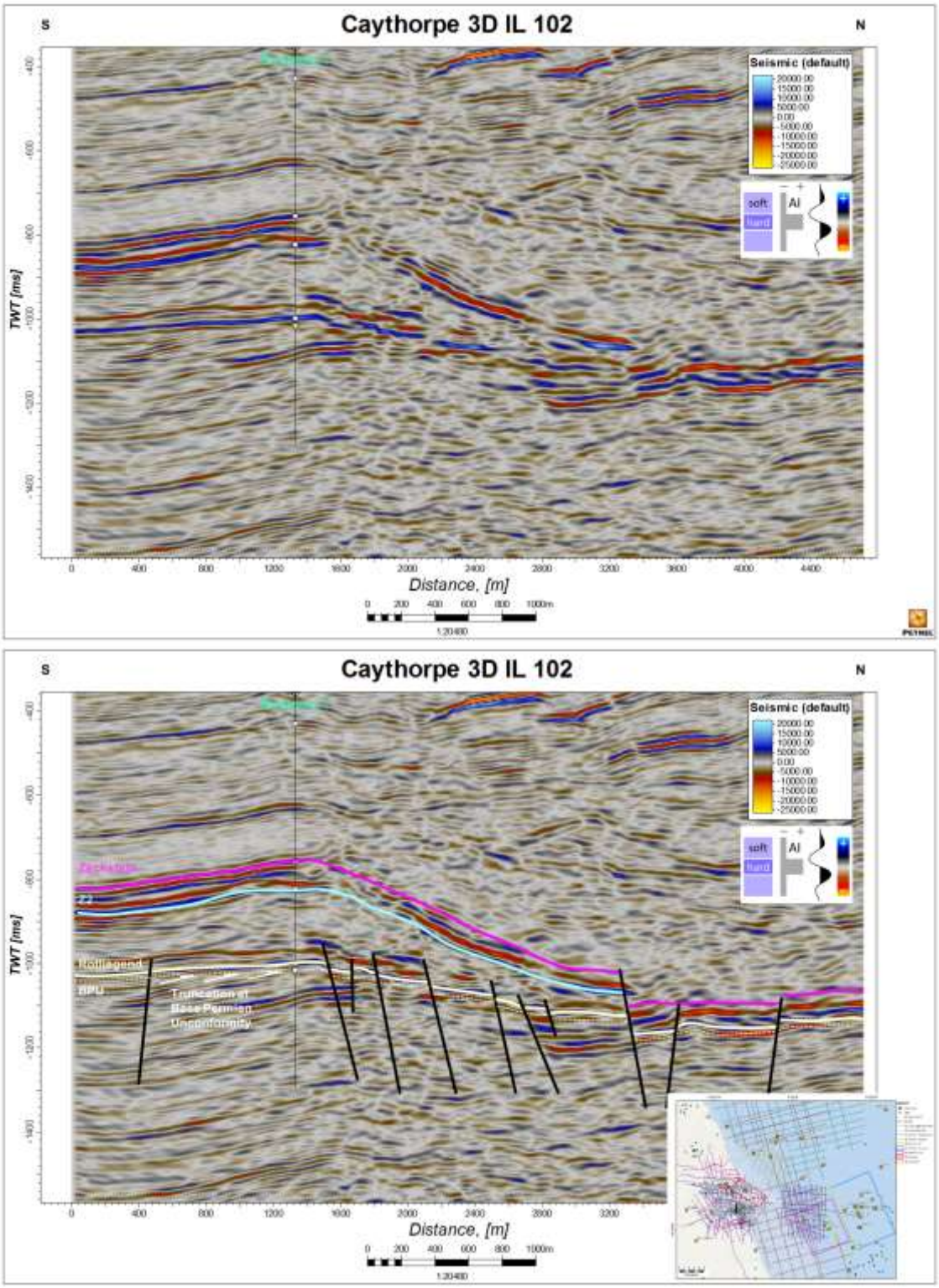

Figure 4.11 (Above) north – south striking un-interpreted Caythorpe 3D IL 102 S-N line through Rudstone-1 well. (Below) interpreted section up to top Zechstein level showing Z2 and Top Zechstein seismic picks, thickness variations of Z2 Stassfurt Halite, fault offset to the base Z2 (yellow arrow) and zone of complete salt evacuation. Two times vertical exaggeration. Inset shows line location. Data courtesy of UKOGL

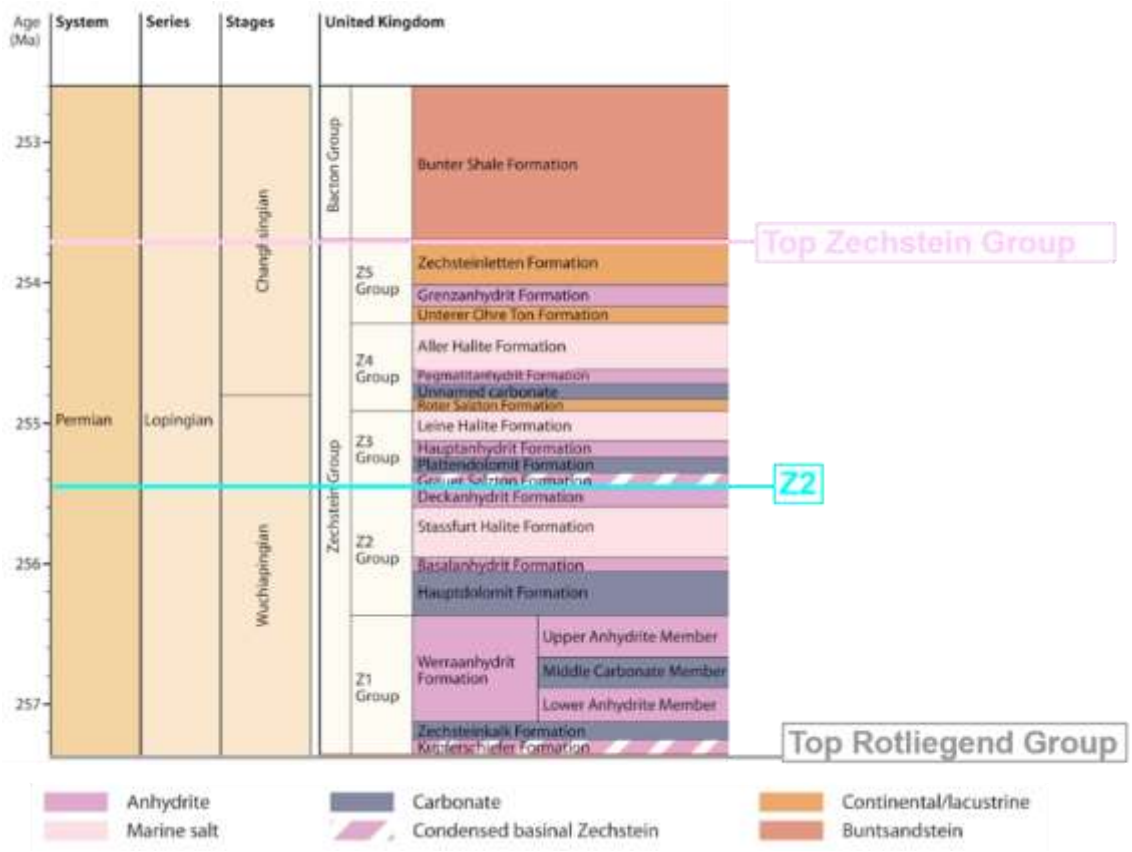

Figure 4.12 Zechstein stratigraphy with Z2 and Top Zechstein seismic picks shown. Modified after Peryt, et al. (2010)

An interval of low seismic resolution containing chaotic and discontinuous reflectors directly overlies the Z1 and lower Z2 carbonate and anhydrite reflectors (Figure 4.11). This interval represents the Z2 Stassfurt Halite formation (Figure 4.12) which marks the first major evaporation phase in the Zechstein. The top of the Z2 Group, represented by the Deckanydrit Formation, is a regionally interpreted seismic reflection horizon in this study (Figure 4.11, Figure 4.13). The overlying Z3 to Z5 Groups of the Grauer Salzton, Plattendolomit, Hauptanhydrit, Liene Halite, Roter Salzton, Pegmatitanhydtrit, Aller Halite, Unterer Ohre Ton, Grenzanhydtrit and Zechsteinletten formations represent continuing cycles of transgression, regression and evaporation (Figure 4.12). Due to the presence of layered carbonates and anhydrites in this interval, the seismic character displays a return to strong layer parallel reflectors. The top of this interval is a regionally interpreted seismic reflector in this study, representing the top of the Zechstein Group (Figure 4.11, Figure 4.13).

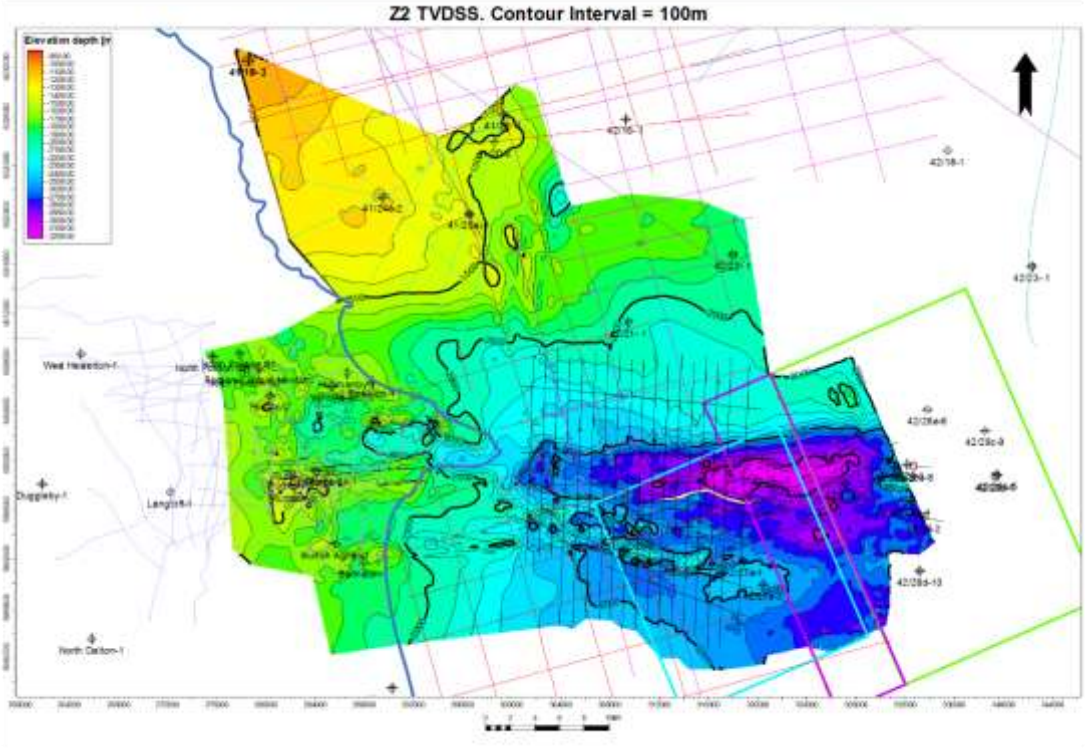

Figure 4.13 Well-tied Z2 depth surface grid, metres TVDSS. Coastline shown as blue line. See Appendix E-10 for large-scale plot.

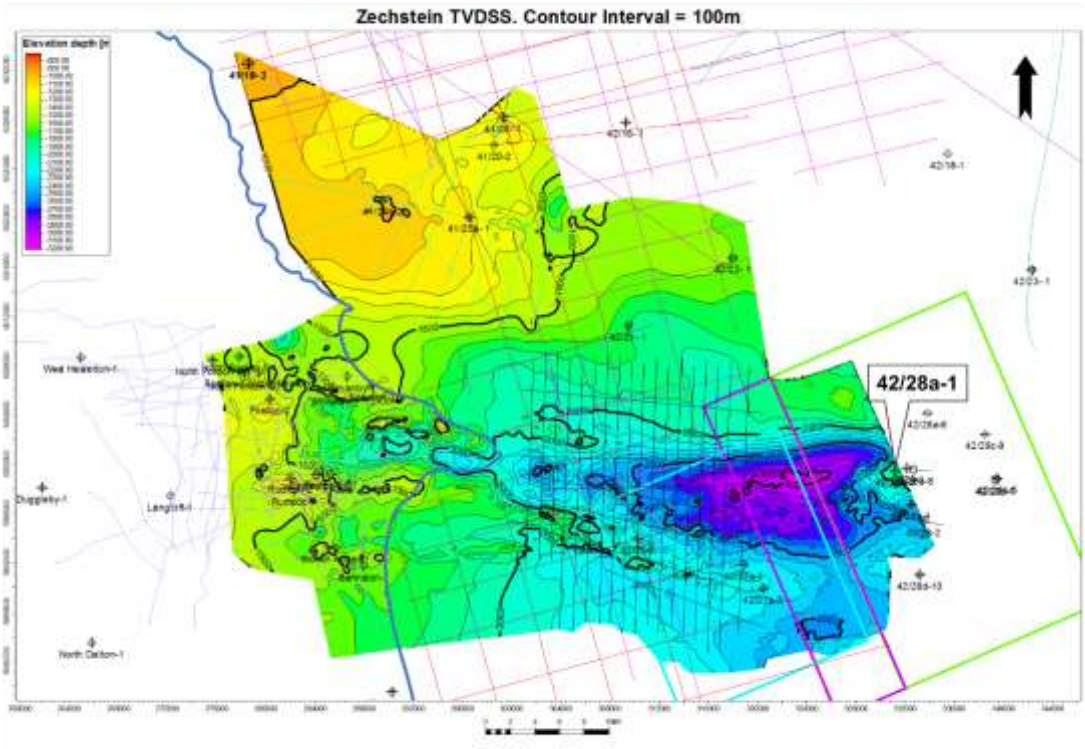

Figure 4.14 Well-tied Zechstein depth surface grid, metres TVDSS. Significant shallowing in the vicinity of 42/28a-1 well records onset of Zechstein salt diapirism. Coastline shown as blue line. See Appendix E-9 for large-scale plot.

Isochore maps (Figure 4.15, Figure 4.16) and vertical seismic sections (Figure 4.11) for the Z1 – Z2 interval show significant thickness variations across the study area, recording post depositional subsurface movement of the Z2 Stassfurt Halite. Z2 salt thickness west to east across the study area ranges from 320m at Burton Agnes-1 in the west to 860m at well 42/28b-7 in the east, where Zechstein salt diapirs occur (Figure 4.17). The presence of large Zechstein salt diapirs in the east of the dataset suggests a broadly west to east movement sense of the salt, from the basin margin to the centre, with complete salt evacuation and touchdown of the Z3 – Z5 directly onto the Rotliegend units occurring across Flamborough Head and into the offshore (Figure 4.11; Figure 4.14; Figure 4.15' Figure 4.16 and Figure 4.17). The zone of Z2 salt withdrawal overlies and runs parallel to the Carboniferous to Rotliegend Flamborough Head Fault Zone faults with these faults also displacing the Zechstein up to the base of the Z2 Stassfurt Halite, suggesting a possible tectonic control to initiation of salt movement (Figure 4.11).

Zechstein Group evaporites are found to be present across the entire study area, indicating that the study area was located in the main basinal part of the Zechstein Sea salt basin and resulting in the deposition of the observed thick halite intervals (Figure 4.18), (Smith, *et al*. 1992). Regional onshore mapping confirms that the Zechstein salt basin margin is located approximately 25km to the west of Flamborough Head (Figure 4.18). The Zechstein basin margin represents a shallowing from open marine conditions to a coastal lagoonal complex and is marked by a depositional facies change from halite to equivalent basin margin slope to shelf carbonates (Figure 4.18 and (Figure 4.19), (Stewart, *et al*. 1996). The Zechstein basin margin is aligned broadly north-west to south-east (Figure 4.18), suggesting a basement inherited Tornquist trend control to the basin margin as opposed control from the west to east trending Flamborough Head Fault Zone, which the Zechstein margin overprints.

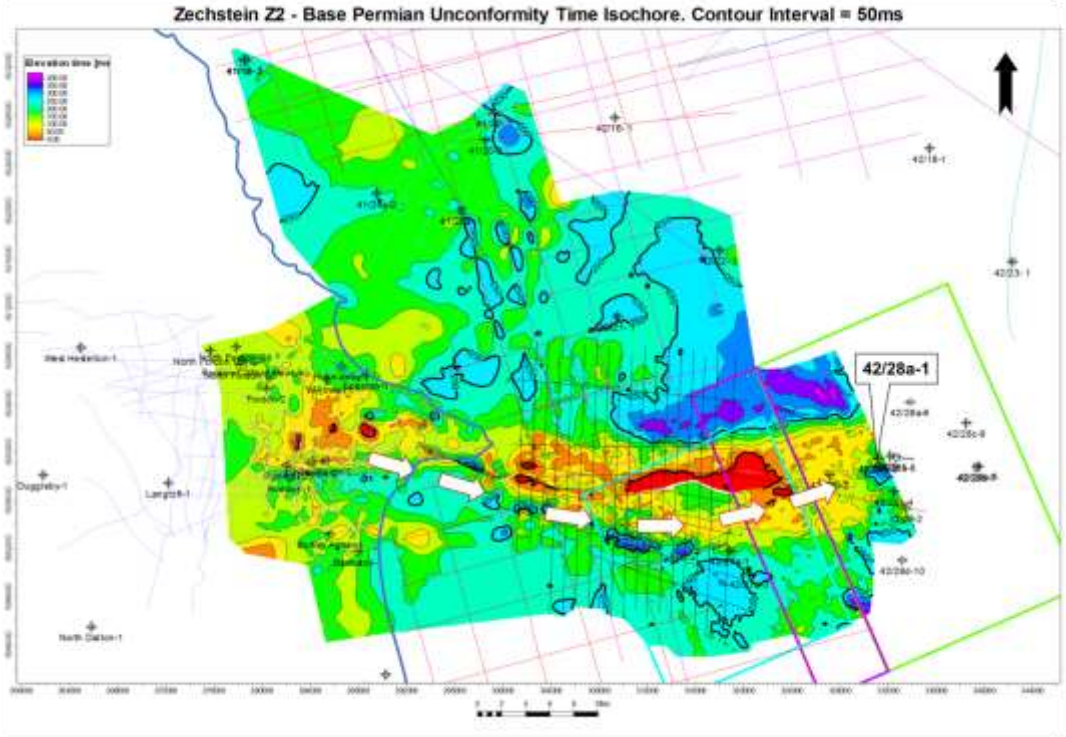

Figure 4.15 Z1- Z2 time isochore, milliseconds TWTT. Red colour and zero contour indicate zone of complete salt withdrawal. Rapid thickening in the vicinity of the 42/28a-1 well represents onset of Zechstein salt diapirism. White arrows represent proposed Z2 halite migration direction.. See Appendix B-11 for large-scale plot.

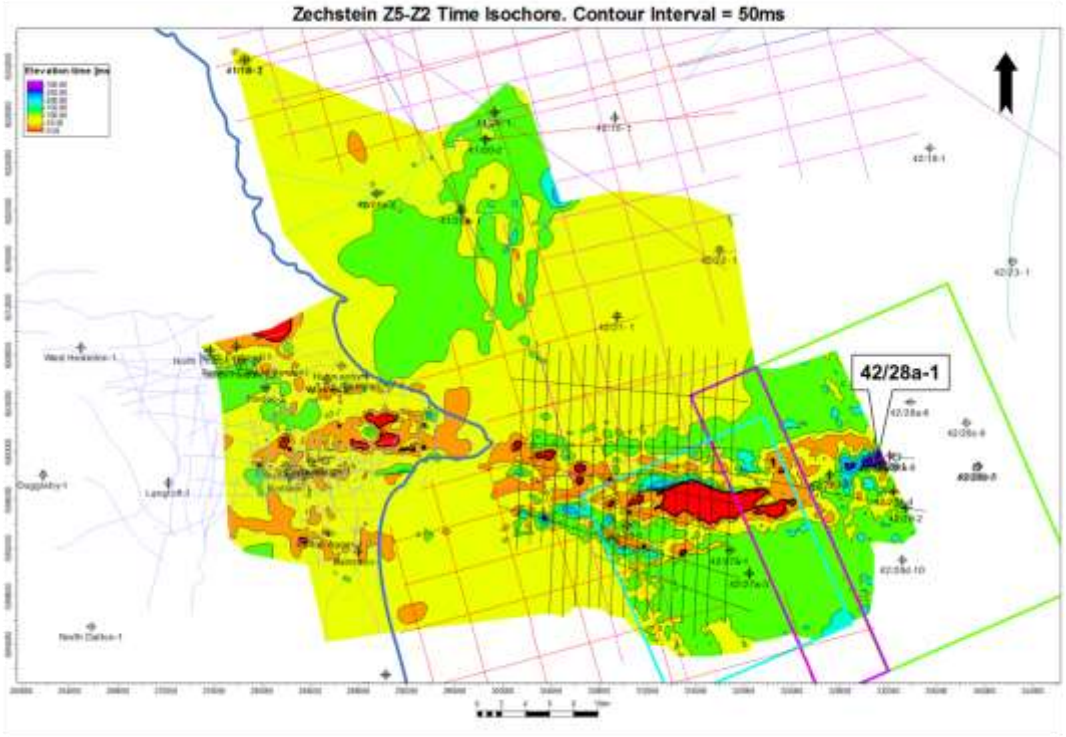

Figure 4.16 Z5- Z3 time isochore, milliseconds TWTT. Red colour and zero contour indicate zone of complete salt withdrawal. Rapid thickening in the vicinity of the 42/28a-1 well represents onset of Zechstein salt diapirism. See Appendix B-10 for large-scale plot.

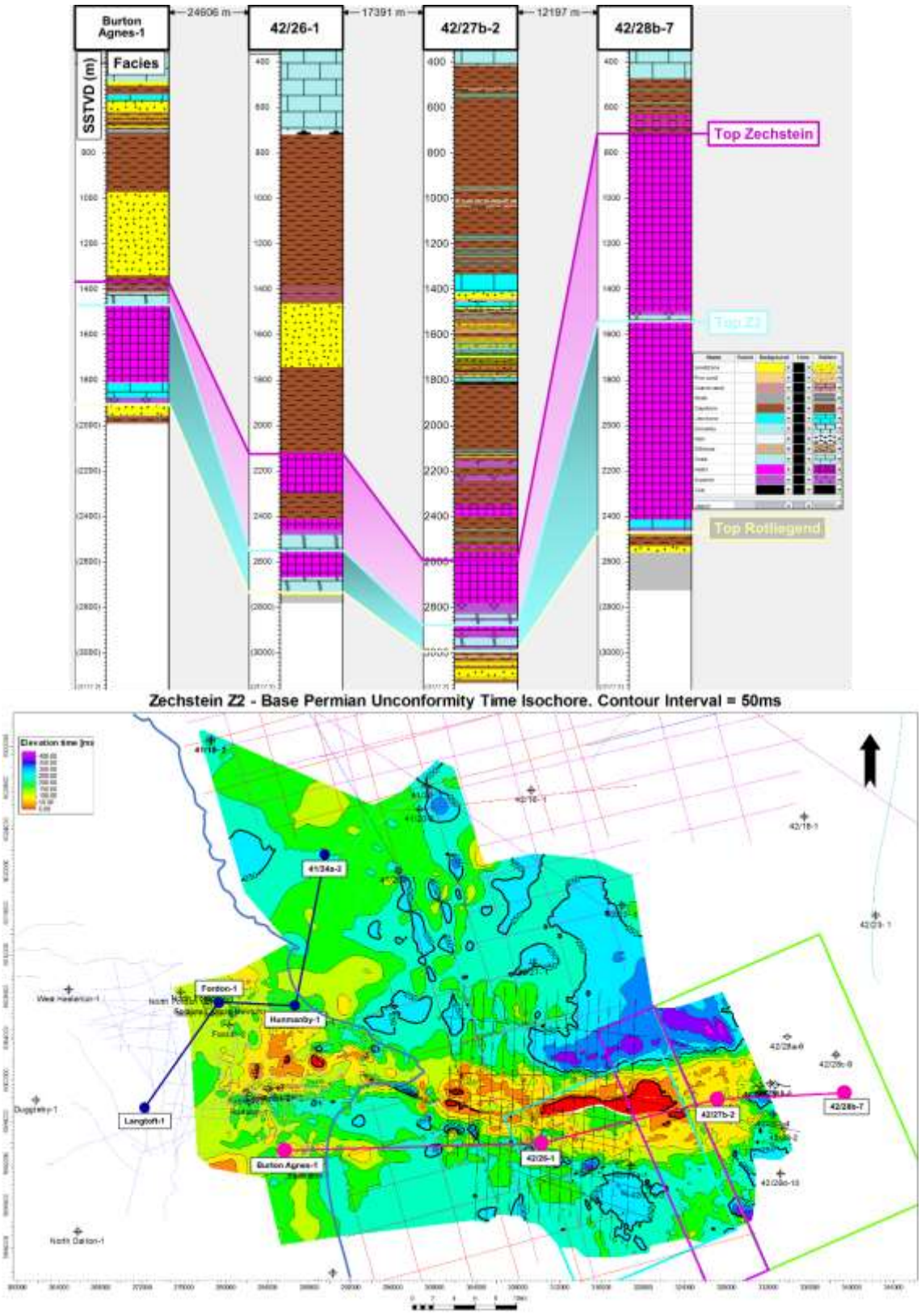

Figure 4.17 (Above) well correlation of the Zechstein units across the dataset in metres TVDSS showing interpreted facies and Zechstein salt diapirism in the east of the study area at well 42/28b-7. (Below) Z2 – Base Permian Unconformity time isochore map with pink line showing well correlation location for this figure. Blue line represents the line of section location for the well correlation shown in Figure 4.19.

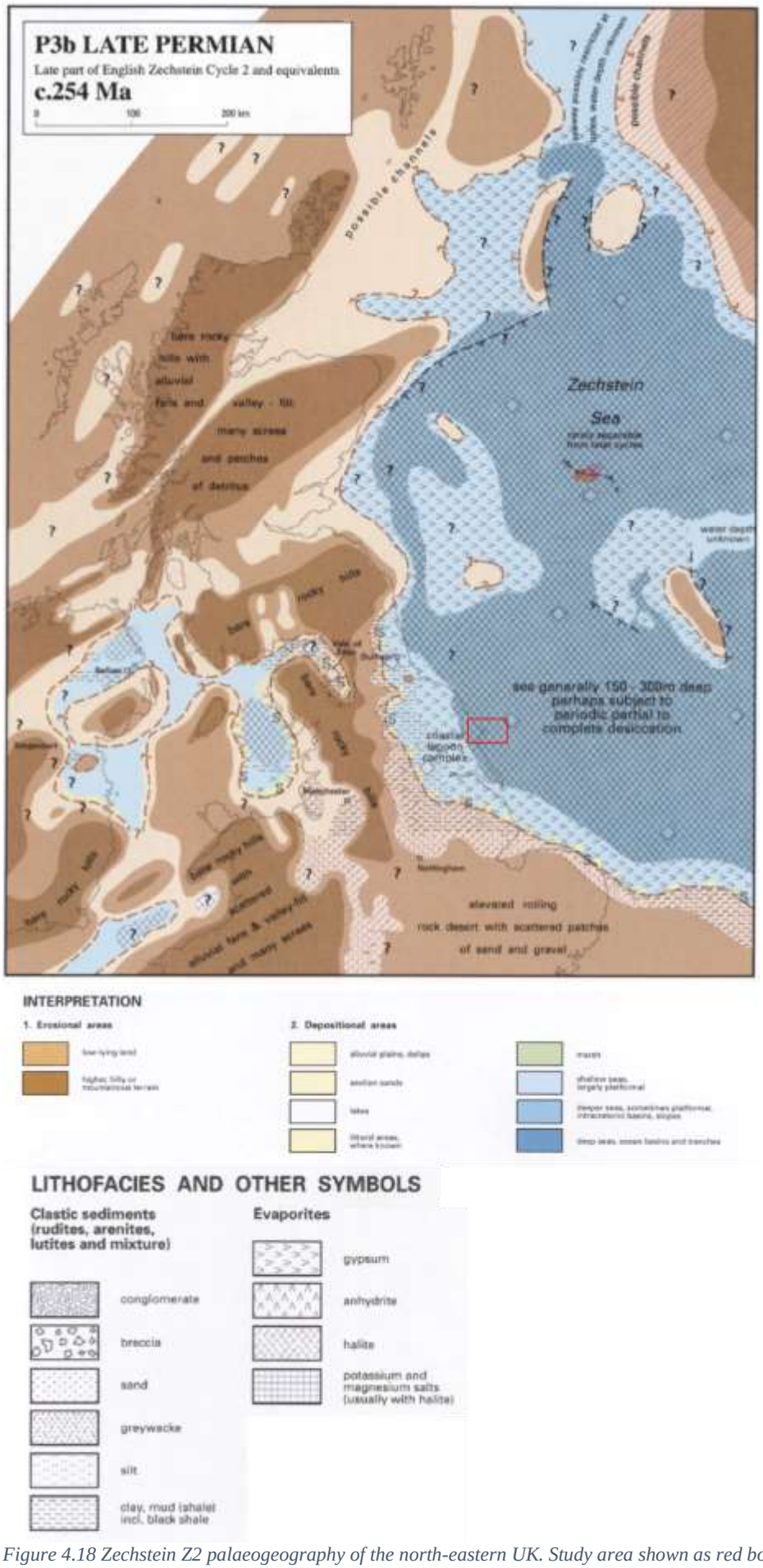

Figure 4.18 Zechstein Z2 palaeogeography of the north-eastern UK. Study area shown as red box. Note the north-west to south-east trend of the Zechstein basin margin. Modified after Smith, et al. (1992).

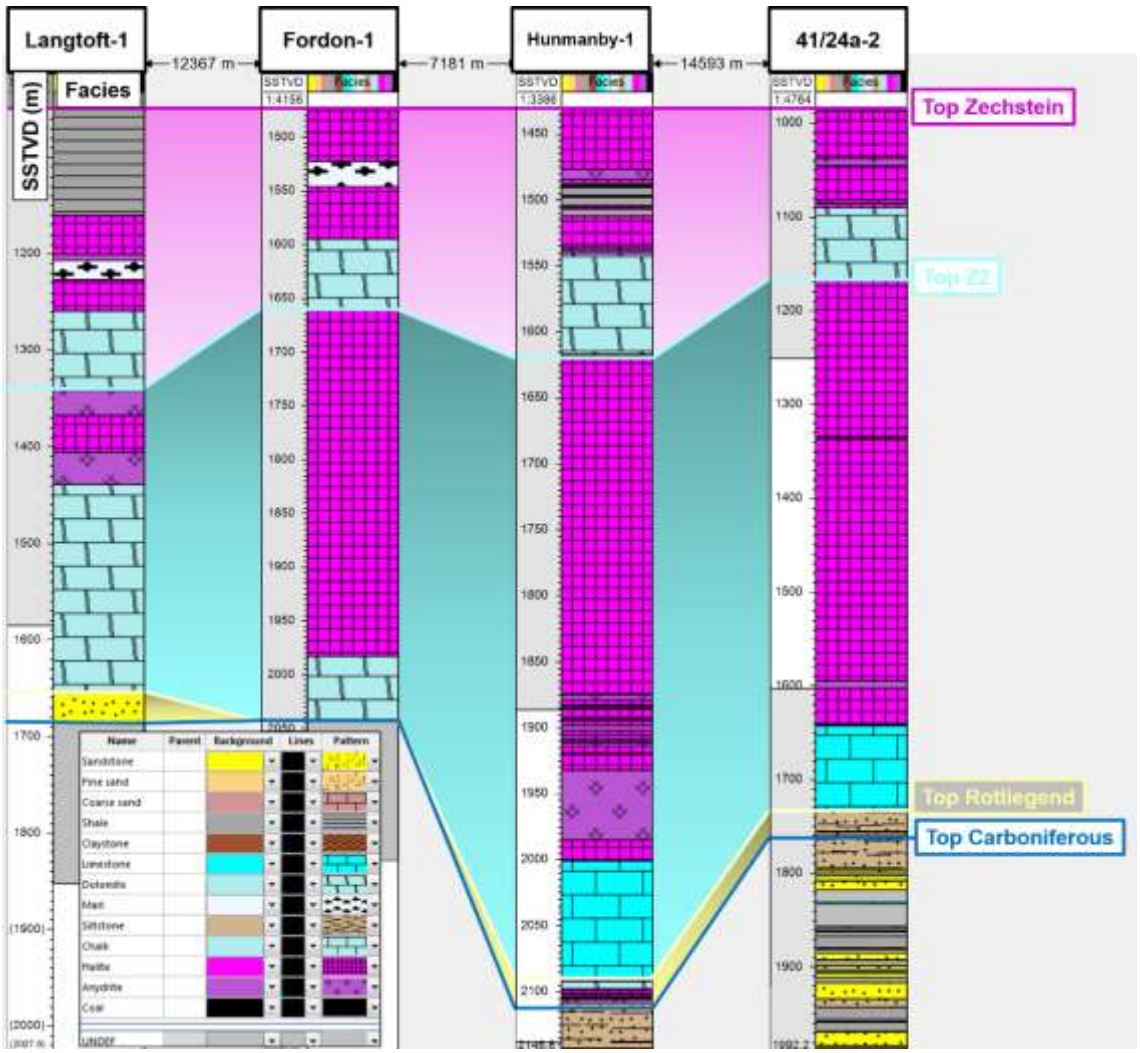

Figure 4.19 SW (Langtoft-1)-NE (41/24a-2) striking well correlation from onshore to offshore highlighting the facies change from of the Z2 unit from predominantly carbonates of the proximal shelf to slope in the west of the study area to thick halites of the basinal setting to the east. See Figure 4.17 for line of section location.

4.4 Triassic

4.4.1 Bacton Group

Intraplate extension and gradual subsidence continued from the Permian into the Triassic, with deposition of the continental clastics of the Bunter Shale and Sandstone Formations of the Bacton Group, marking a transition from evaporitic sabkha sedimentation of the Zechstein Group to fluvial, lacustrine and playa deposits of the Bacton Group (Figure 4.20 and Figure 4.21), (Bachmann, *et al*. 2010). Triassic seismic reflectors are conformable with the underlying Zechstein Group carbonate reflectors, suggesting uninterrupted subsidence and sedimentation from the Permian and into the Triassic without any significant depositional hiatus, marked by a disconformable lithostratigraphic boundary (Figure 4.22). The top of the Bacton Group is a regionally interpreted seismic reflector in this study (Figure 4.22 and Figure 4.23). The Bacton Group interval is

seismically transparent due to the relatively homogenous sandstone composition of this unit, with little acoustic impedance variation throughout, and has a geometry that mirrors the topography of the underlying Zechstein Group units (Figure 4.22).

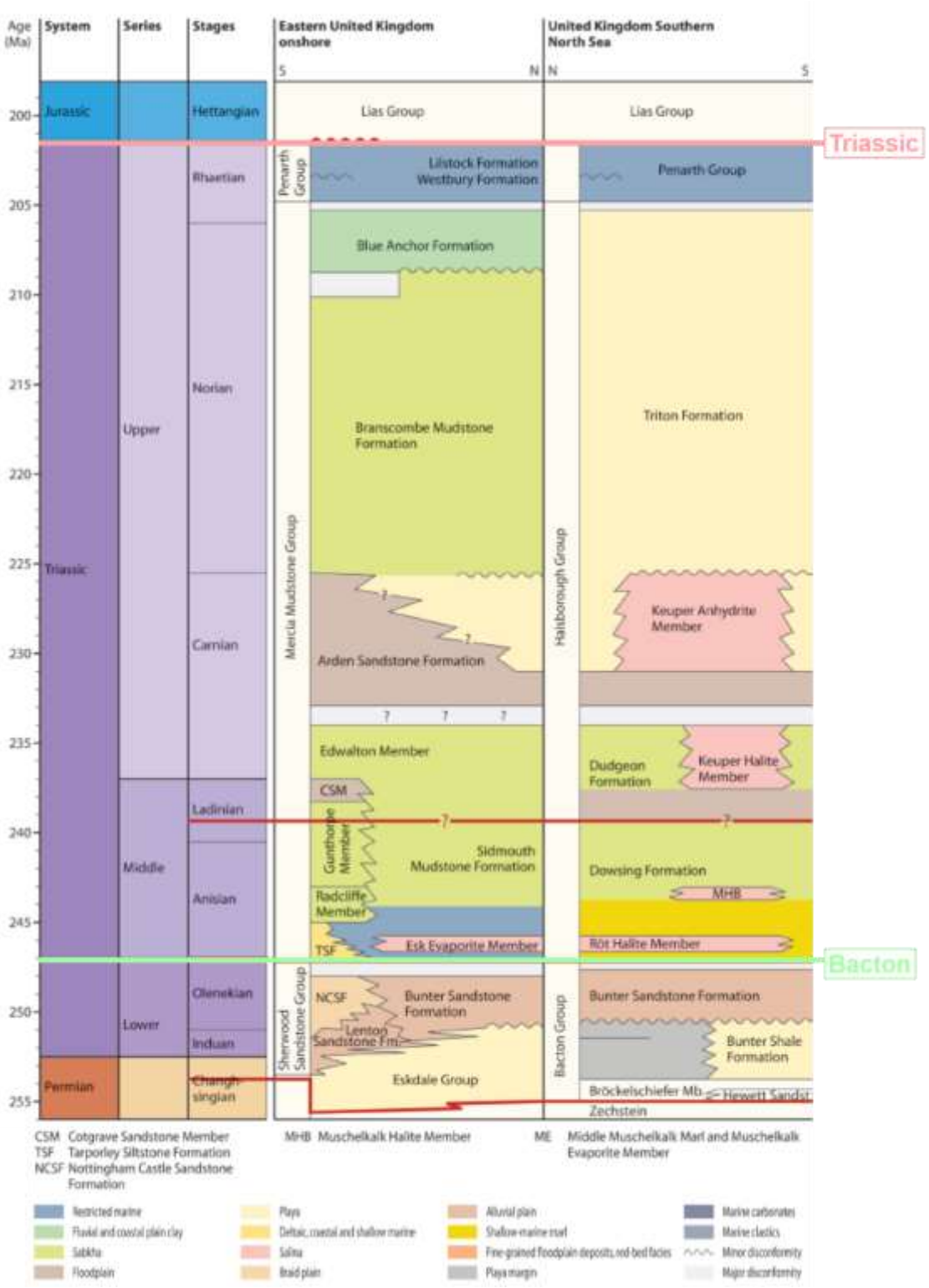

Figure 4.20 Triassic stratigraphy with Bacton and Triassic seismic picks shown. Modified after Bachmann, et al. (2010)

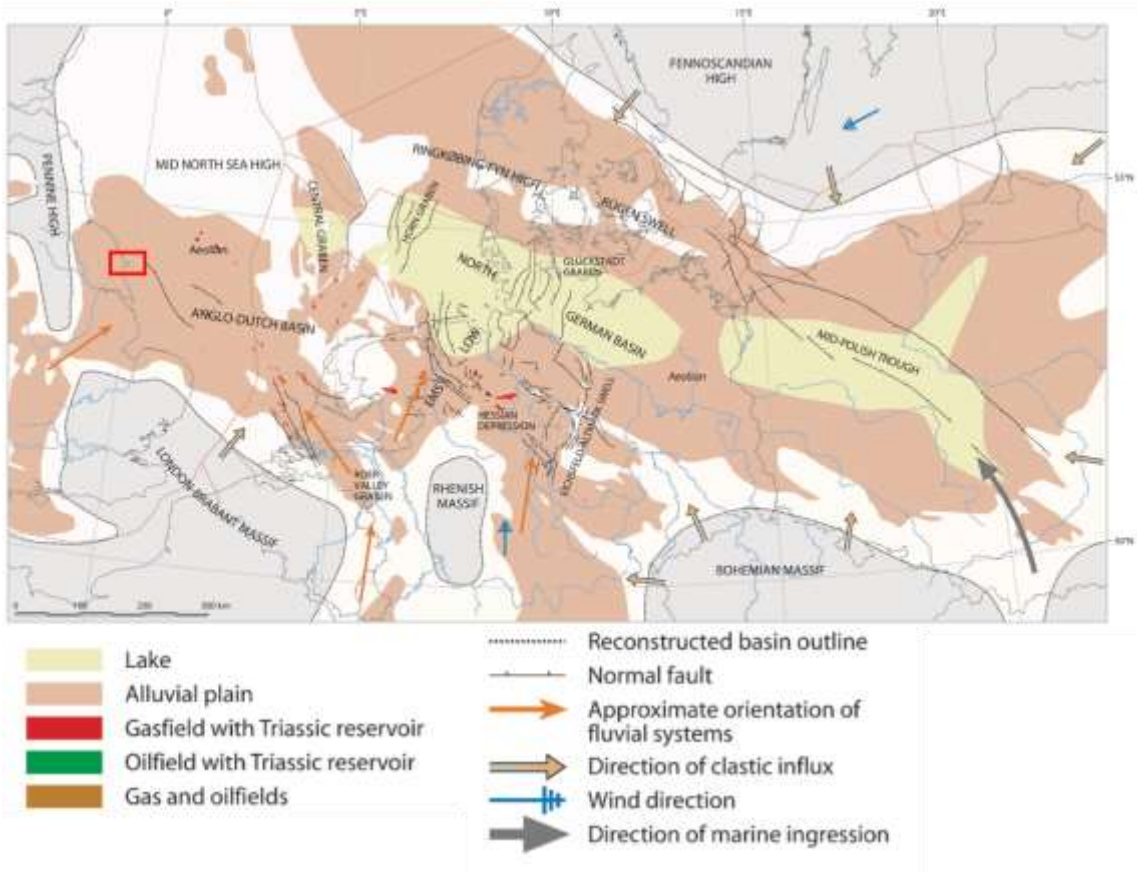

Figure 4.21 Palaeogeographic map showing the distribution of depocentres and facies of the Bunter Sandstone of the Bacton Group across the South Permian Basin (Lower Triassic- Olenekian to earliest Middle Triassic- Anisian (Middle Triassic). Study area shown as red box. Modified after Bachmann, et al. (2010)

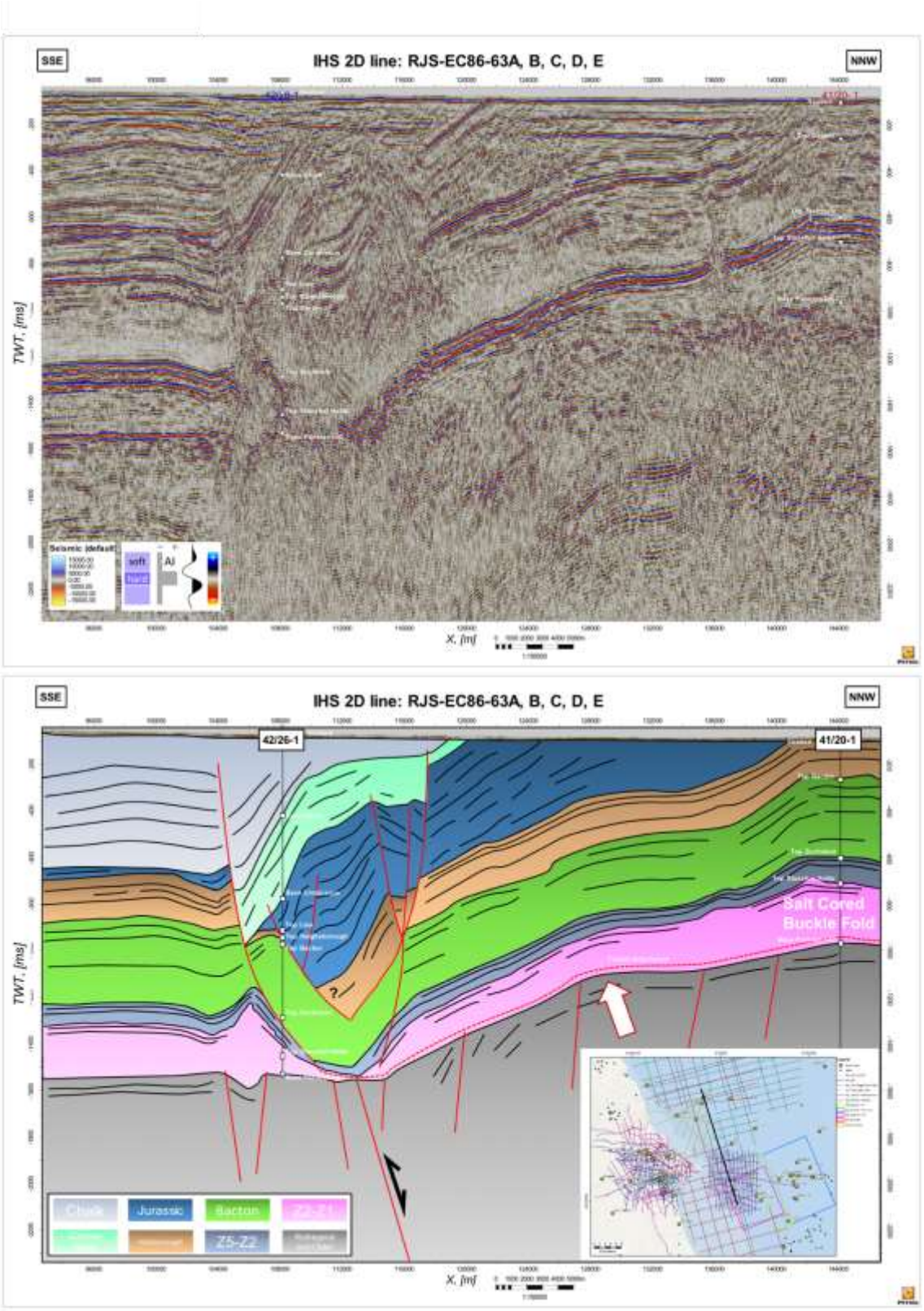

Figure 4.22 (Above) SSE – NNW striking un-interpreted Regional IHS 2D line RJS-EC86-63A,B,C,D,E (Below) interpreted geo-seismic section of same line. Inset shows line location. Note uniform thickness of Bacton and Haisborough units between Market Weighton Block footwall and Cleveland Basin hanging wall; the transparent nature of Bacton unit; extensional listric faulting that detaches into Zechstein and Triassic evaporites and geometry that mirrors the underlying Zechstein. Also note the postulated development of salt cored buckle fold in the post salt cover at well 41/20-1 that may have developed in response to basinward movement of the cover during basin inversion (see Chapter 5.2.5 below for discussion). "?" highlights regions of uncertain interpretation. Fifteen times vertical exaggeration. Data courtesy of IHS.

Isochore maps (Figure 4.24), well correlations (Figure 4.26) and regional seismic reflection profiles (Figure 4.22) show that the Bacton Group is of relatively uniform thickness south from the Market Weighton Block and north to the Cleveland Basin. True vertical time isochore thicknesses of around 380ms are observed in the extreme north and south of the dataset, either side of the Flamborough Head Fault Zone (Figure 4.24). Well top depth isochores also mirror this trend with 620m of Lower Triassic measured in Hornsea-1 well and 660m recorded in well 41/20-1 (Figure 4.25). This uniform thickness implies that the deposition of the Lower Triassic pre-dates the formation of the Cleveland Basin and represents a pre-rift tectono-stratigraphic unit. Thinning of the unit through extensional faults, which sole out into a detachment within the Zechstein Group is evident across the Flamborough Head Fault Zone (Figure 4.22 and Figure 4.24). Figure 4.24 also shows thinning of the Bacton Group in the extreme east of the dataset. This is the result of underlying Zechstein Group salt diapirism, which has pierced and displaced Triassic units.

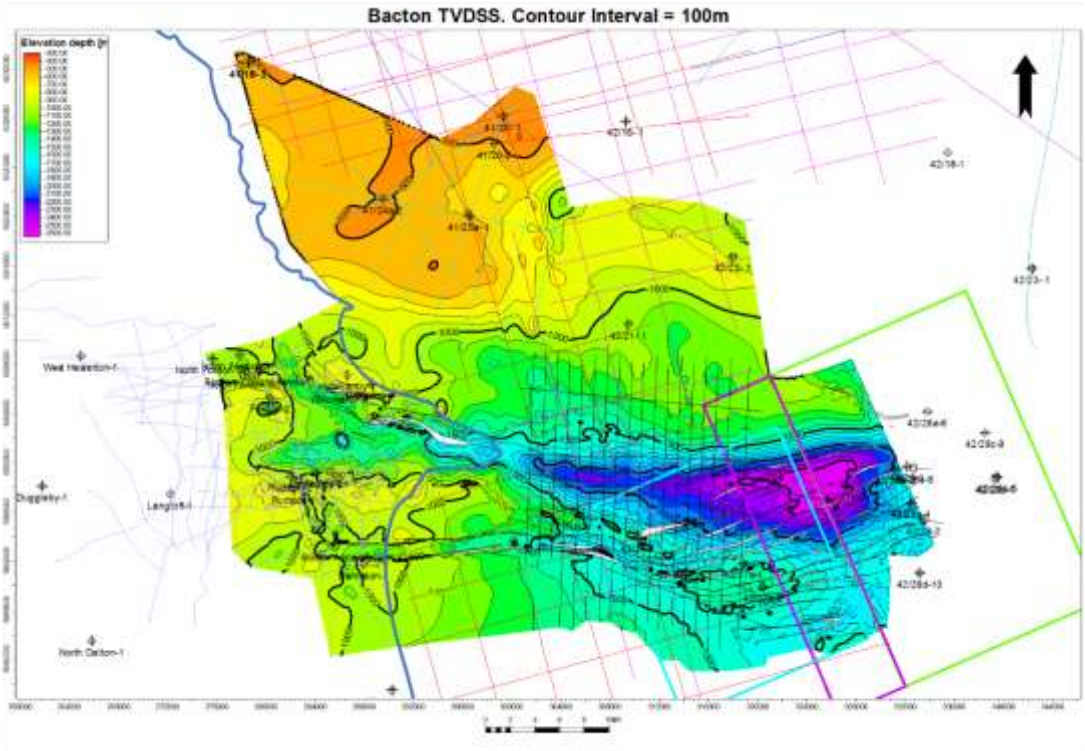

Figure 4.23 Well-tied Bacton depth surface grid, metres TVDSS. See Appendix E-8 for large-scale plot.

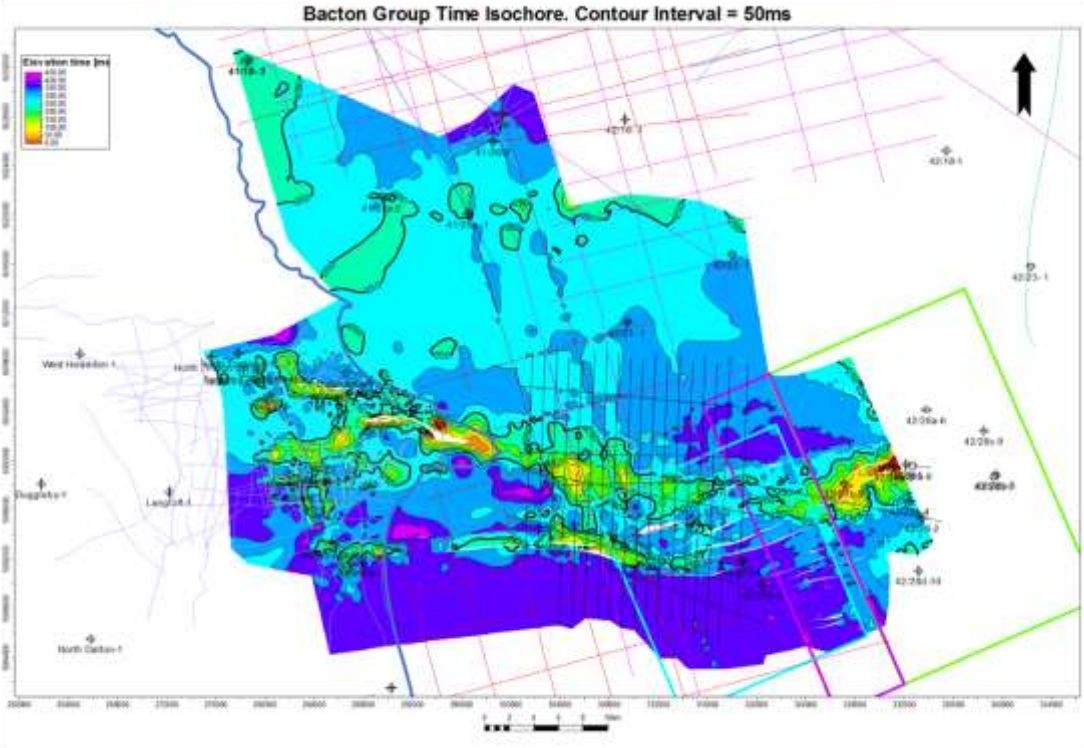

Figure 4.24 Bacton Group time isochore, milliseconds TWTT. Note thinning of the unit above zones of Zechstein Group salt evacuation due to associated stretching. Thinning in the extreme east of the dataset is due to Zechstein salt diapirism piercing and displacing the Triassic. See Appendix B-9 for large-scale plot.

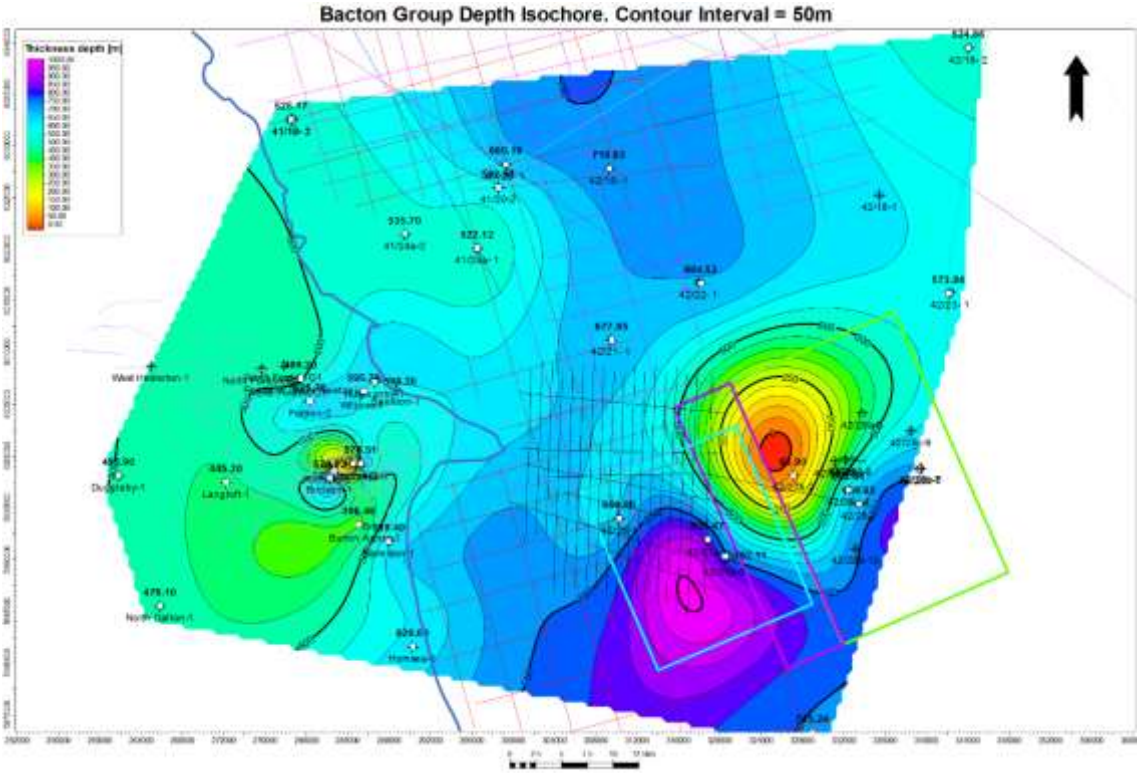

Figure 4.25 Bacton Group depth isochore from well tops in metres.

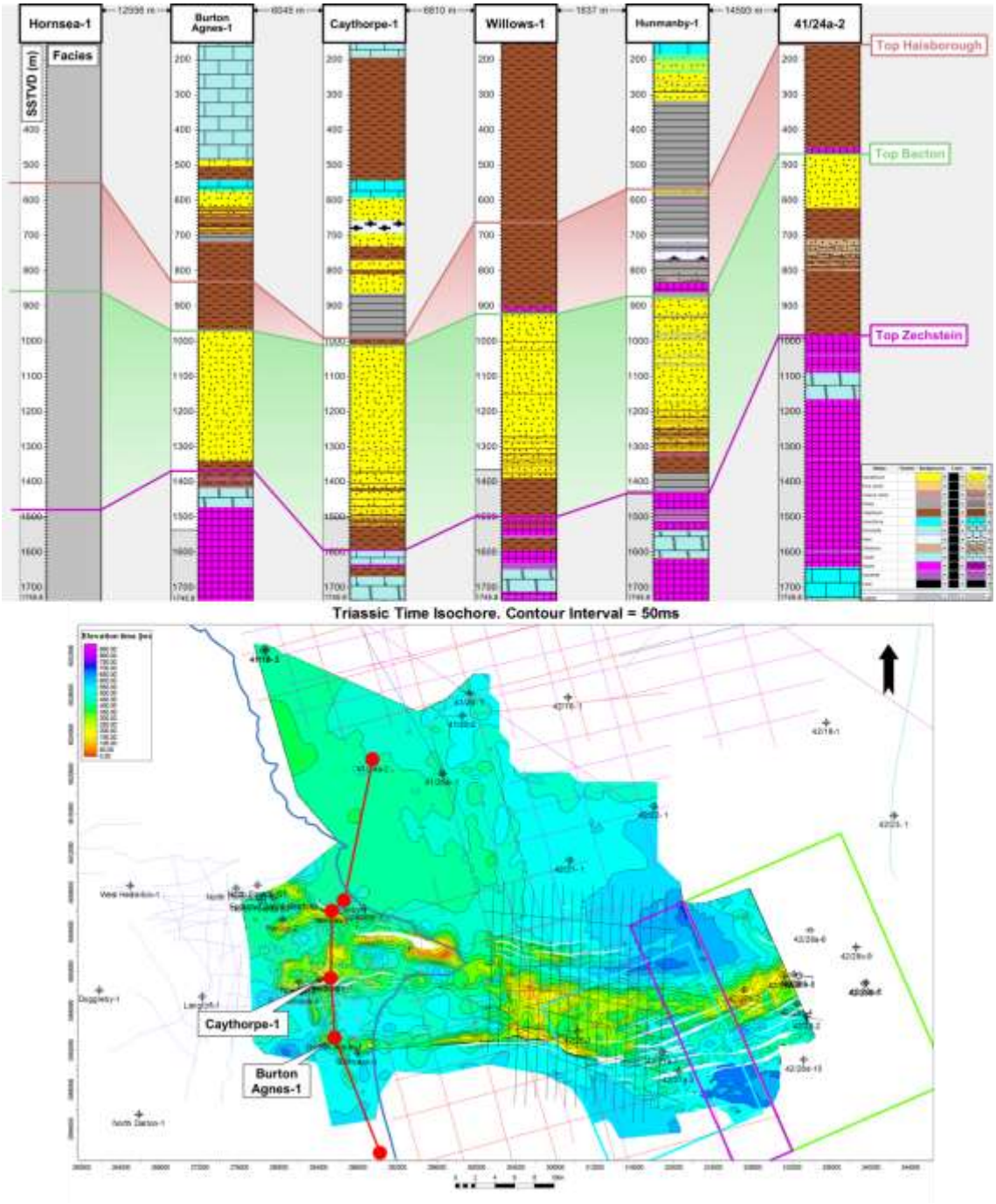

Figure 4.26 (Above) well correlation of the Triassic units across the Flamborough Head Fault Zone in metres TVDSS showing interpreted facies. Note Upper Triassic section thinning in Burton Agnes-1 and Caythorpe-1 is due to section being faulted out and not representative of true stratigraphic thickness. (Below) Triassic time isochore map showing well correlation location.

Geometries for the faults that displace the Bacton Group unit mirror the broad west to east trend observed in the Carboniferous to Rotliegend Group aged faults (Figure 4.23). However, these faults, rather than being planar, are listric in nature and do not appear to be hard linked to the underlying planar Carboniferous to Rotliegend faults but instead sole out into detachments within Zechstein Group evaporitic units (Figure 4.22), implying a thin-skinned tectonic regime for the post Zechstein Group stratigraphy.

4.4.2 Haisborough Group

The Middle to Upper Triassic Haisborough Group directly overlies the Lower Triassic Bacton Group and represents a continuation of continental red bed sedimentation with the deposition of the desert sabkha to playa Dudgeon, Dowsing and Triton formations interspersed with the evaporitic units of the Röt Halite, Muschelkalk Halite, Keuper Halite and Keuper Anhydrite members (Figure 4.20). This sequence is capped by the lacustrine fine clastics and mudstones of the Penarth Group. The acoustic boundary of this unit with the overlying Lower Jurassic Lias Group provides a regionally interpreted top Triassic seismic marker (Figure 4.22 and Figure 4.28).

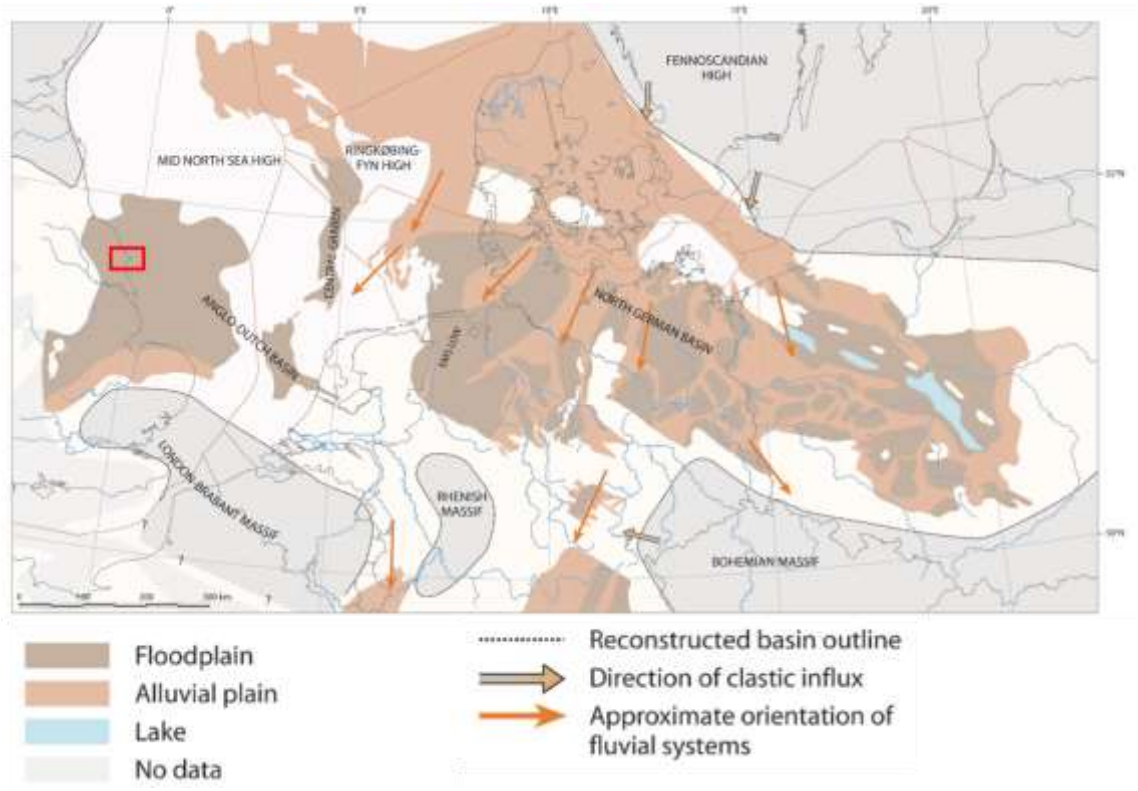

Figure 4.27 Palaeogeographic map showing the distribution of depocentres and facies of Carnian aged rock units of the Haisborough Group. Study area shown as red box. Modified after Bachmann, et al. (2010).

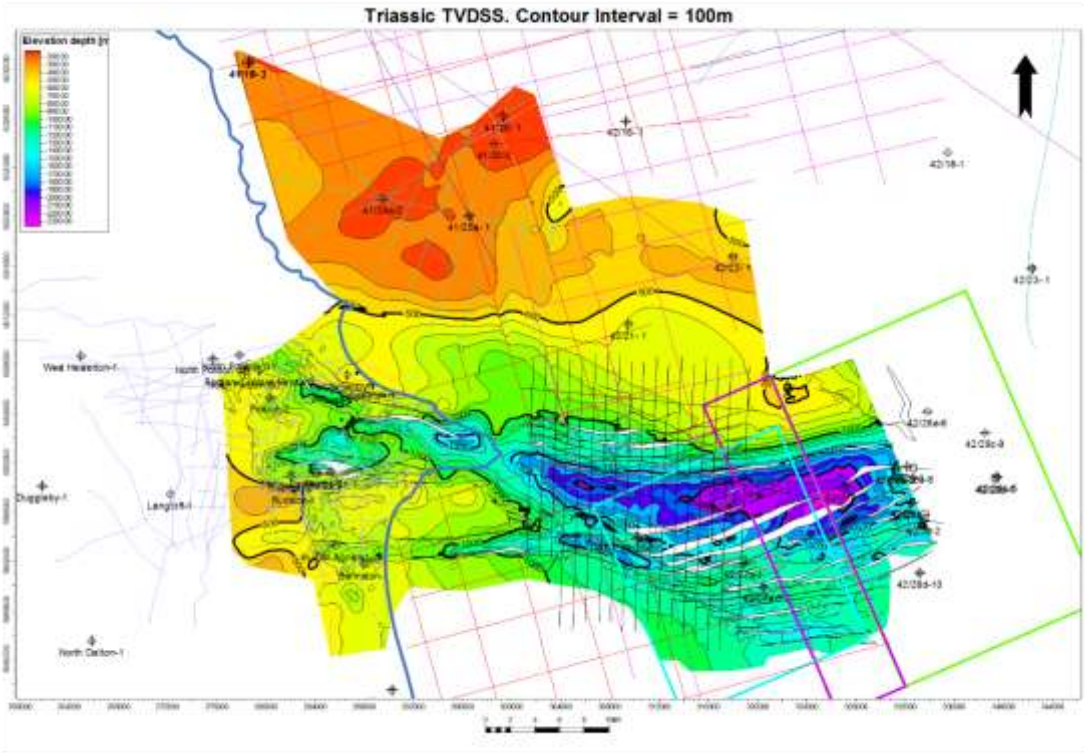

Figure 4.28 Well-tied Triassic depth surface grid, metres TVDSS. See Appendix E-7 for large-scale plot.

The more heterogeneous lithologies of the Haisborough Group compared to the underlying Bacton Group results in greater acoustic impedance contrasts and hence stronger seismic reflectors within this unit, particularly the evaporitic intervals of the Röt Halite, Muschelkalk Halite, Keuper Halite and Keuper Anhydrite (Figure 4.22).

Haisborough Group isochores (Figure 4.29), well correlations (Figure 4.26) and regional seismic profiles (Figure 4.22) show a similar unit thickness geometry to that seen in the underlying Bacton Group, with a relatively uniform formation thickness from the Market Weighton Block in the south to the Cleveland Basin in the north and thinning through extensional faulting above Zechstein Group salt evacuation zones. True vertical time thickness for the Haisborough Group is around 150ms both to the north and to the south of the Flamborough Head Fault Zone (Figure 4.29). Well top isochores of 310m at Hornsea-1 and 348m at well 41/20-2 also follow this trend (Figure 4.30). This suggest that north to south across the study area, the Triassic interval (Bacton and Haisborough Groups) was deposited prior to formation of the Cleveland Basin and represents a pre-rift stratigraphic interval, as there are no significant thickness variations from the Market Weighton Block to the Cleveland Basin (Figure 4.31, Figure 4.32).

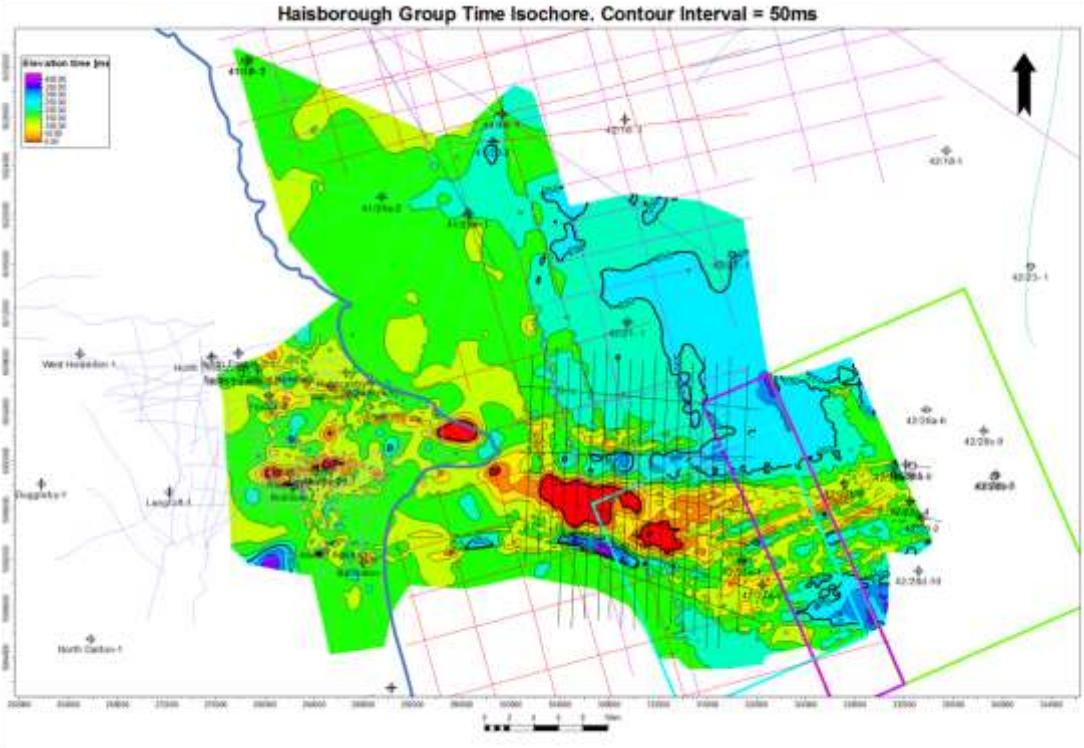

Figure 4.29 Haisborough Group time isochore, milliseconds TWTT. Note thinning of the unit above zones of Zechstein salt evacuation due to associated stretching. See Appendix B-8 for large-scale plot.

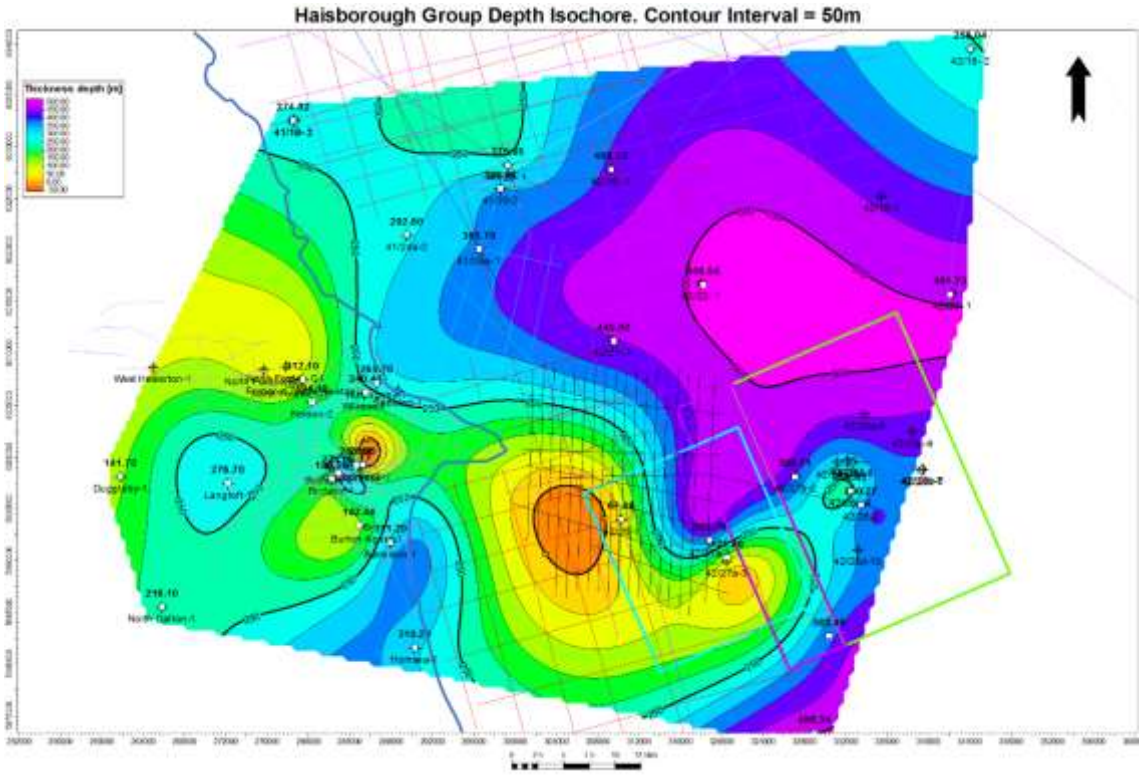

Figure 4.30 Haisborough Group depth isochore from well tops in metres.

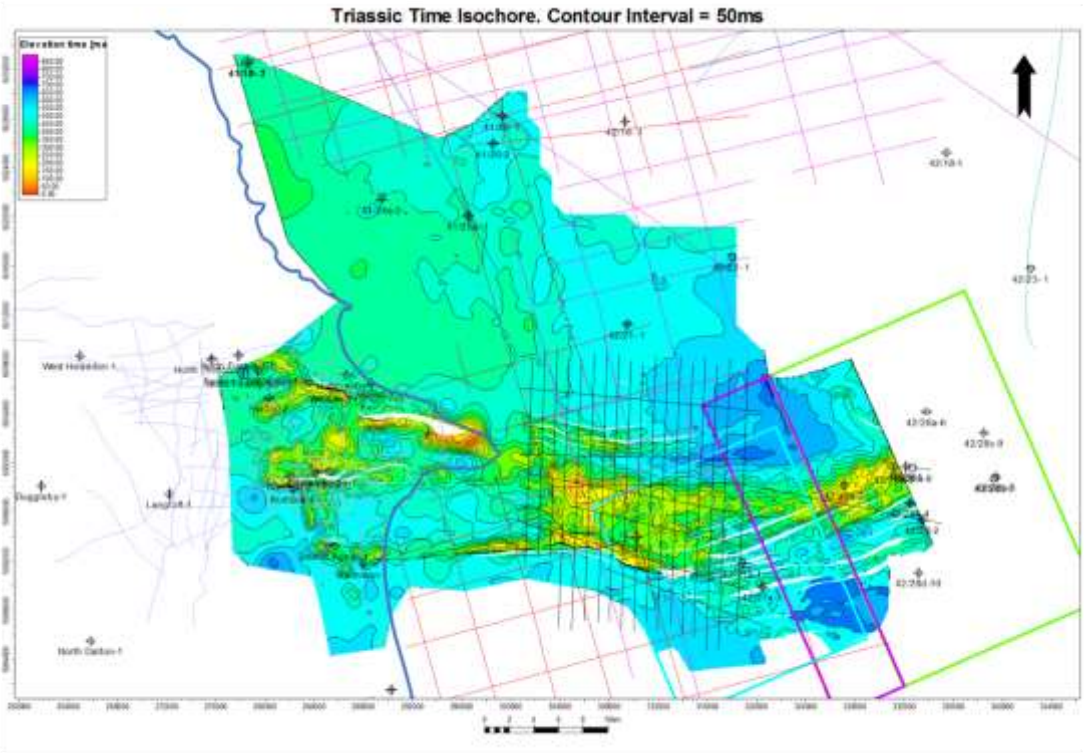

Figure 4.31 Triassic time isochore, milliseconds TWTT. See Appendix B-14 for large-scale plot.

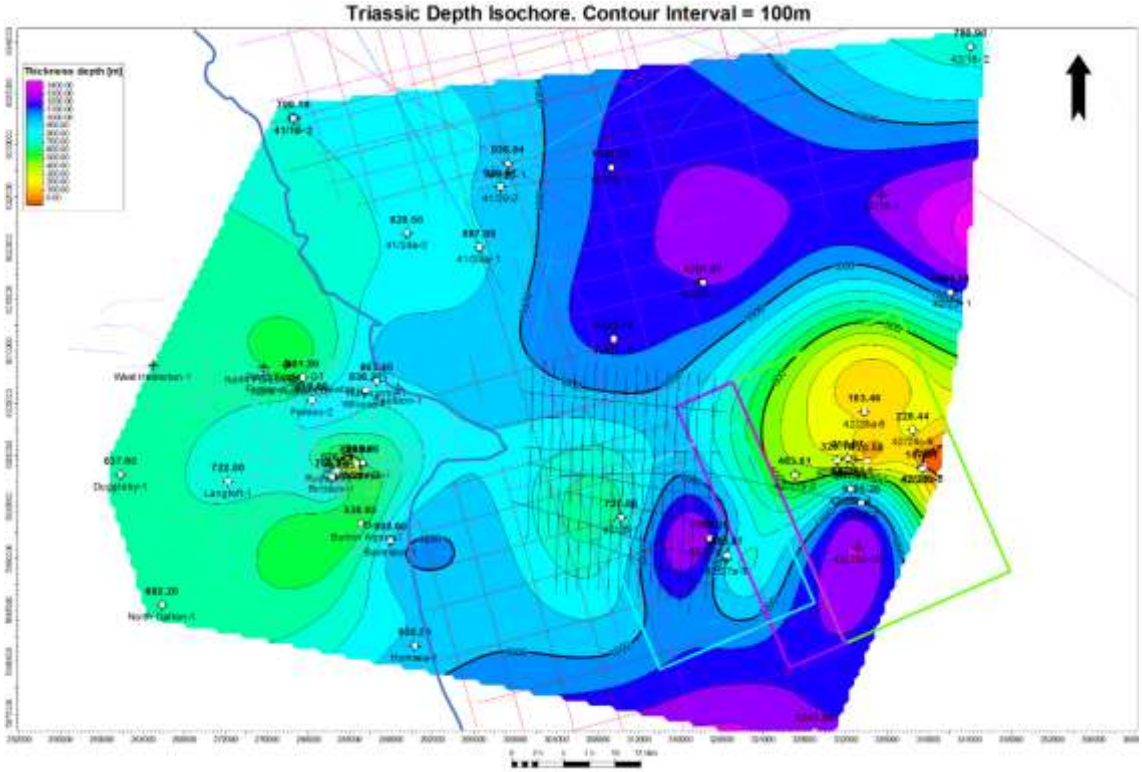

Figure 4.32 Triassic depth isochore from well tops in metres. Note general trend of thickening of section from west to east. Isochore thin in east of dataset in vicinity of 42/28a-6 well is due to underlying Zechstein salt diapir piercing and displacing the Triassic.

Isochore maps of the Haisborough Group from well tops show that, in the greater study area, there is a thickening of section from west to east with 142m recorded at Duggleby-1 compared to 492m at well 42/23-1 (Figure 4.30). This trend is also reflected in a broadly west to east composite seismic profile across the hanging wall of the Flamborough Head Fault Zone where there is a very subtle, apparent time thickening of the Haisborough Group to the east (Figure 4.33). This suggests a Late Triassic depocenter situated to the east of Flamborough Head, in the Sole Pit Trough to Anglo Dutch Basins (Stewart & Coward, 1995). This depocenter was controlled by subsidence due to extensional faulting, replacing the thermal subsidence of the Lower Triassic (Stewart & Coward 1995) and may have been controlled by decoupled subsidence due to extensional movements on NW-SE striking basement orientated Tornquist trend faults (Figure 4.21). Late Triassic extension was also accompanied by the initiation of Late Triassic salt tectonics with the development of salt swells of this age observed in the Sole Pit Trough, to the east and seaboard of Flamborough Head (Stewart & Coward 1995).

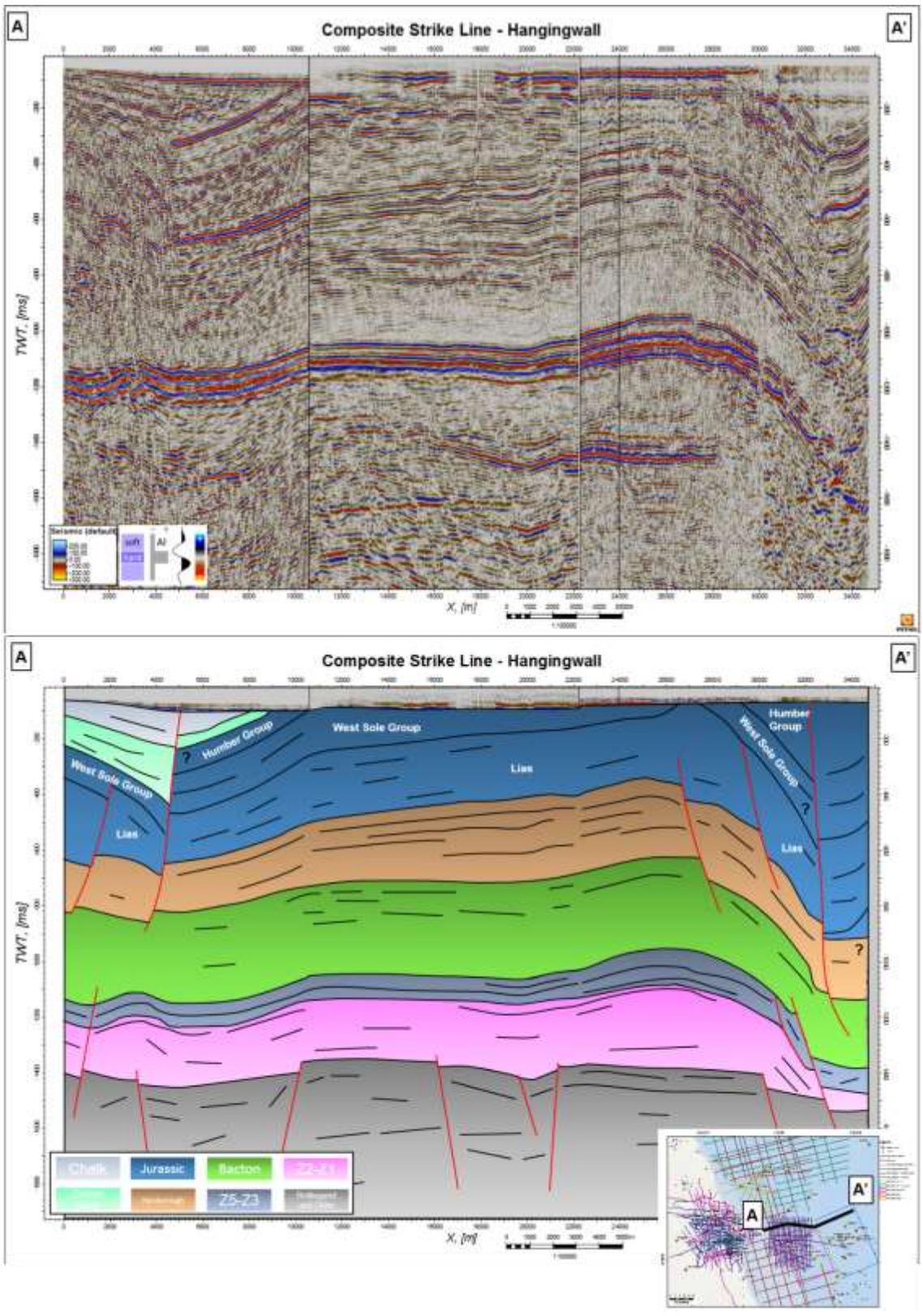

Figure 4.33 (Above) West to east striking composite strike seismic profile through the hanging wall of the Flamborough Head Fault system. (Below) Geoseismic interpretation of same line. Note possible thickening of Upper Triassic Haisborough Group from west to east. Inset shows line location. Twelve times vertical exaggeration. Data courtesy of IHS, BP and Total.

As seen from the Haisborough Group depth structure map in Figure 4.28 and the vertical seismic profile in Figure 4.22, the faults that displace this unit are a continuation of the

listric, collapse faults that displace the underlying Bacton Group. These listric faults are shown to detach along regionally extensive Zechstein Group and Triassic evaporites, specifically the basal Haisborough Group Röt Halite Member, providing more evidence towards a detached post rift sequence (Figure 4.22).

4.5 Jurassic

4.5.1 Lias Group

The Early Jurassic Lias Group represents the first major marine incursion into the basin and is represented by the deposition of marine claystones in the study area (Figure 4.34, Figure 4.35). Gradual, tectonically quiescent extensional subsidence and marine conditions continued throughout the lower Jurassic until an abrupt shallowing of the system occurred at the end of the Lias, attributed to the onset of Middle Jurassic thermal doming of the Central North Sea Dome, that created the Mid-Cimmerian Unconformity and was centred upon what subsequently became the trilete rift system of the North Sea during the upper Jurassic (Underhill & Partington 1993; Underhill 2003). This event provides a regionally interpretable seismic reflector at the top of the Lias Group (Figure 4.36).

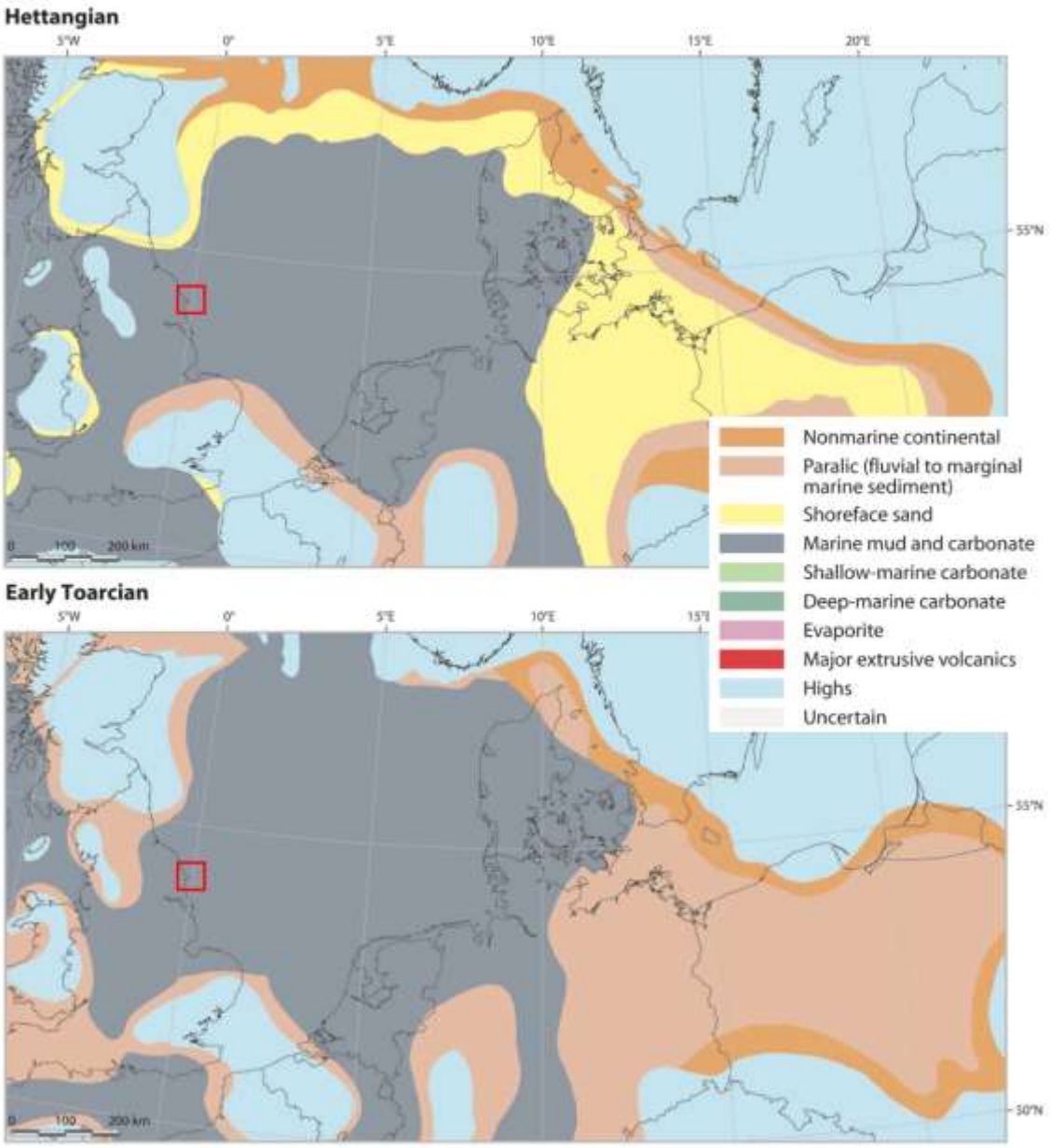

Figure 4.34 Lower Jurassic Lias Group palaeogeography. Study area shown as red box. See Figure 4.35 for Stage age clarification. Modified after Lott, et al. (2010).

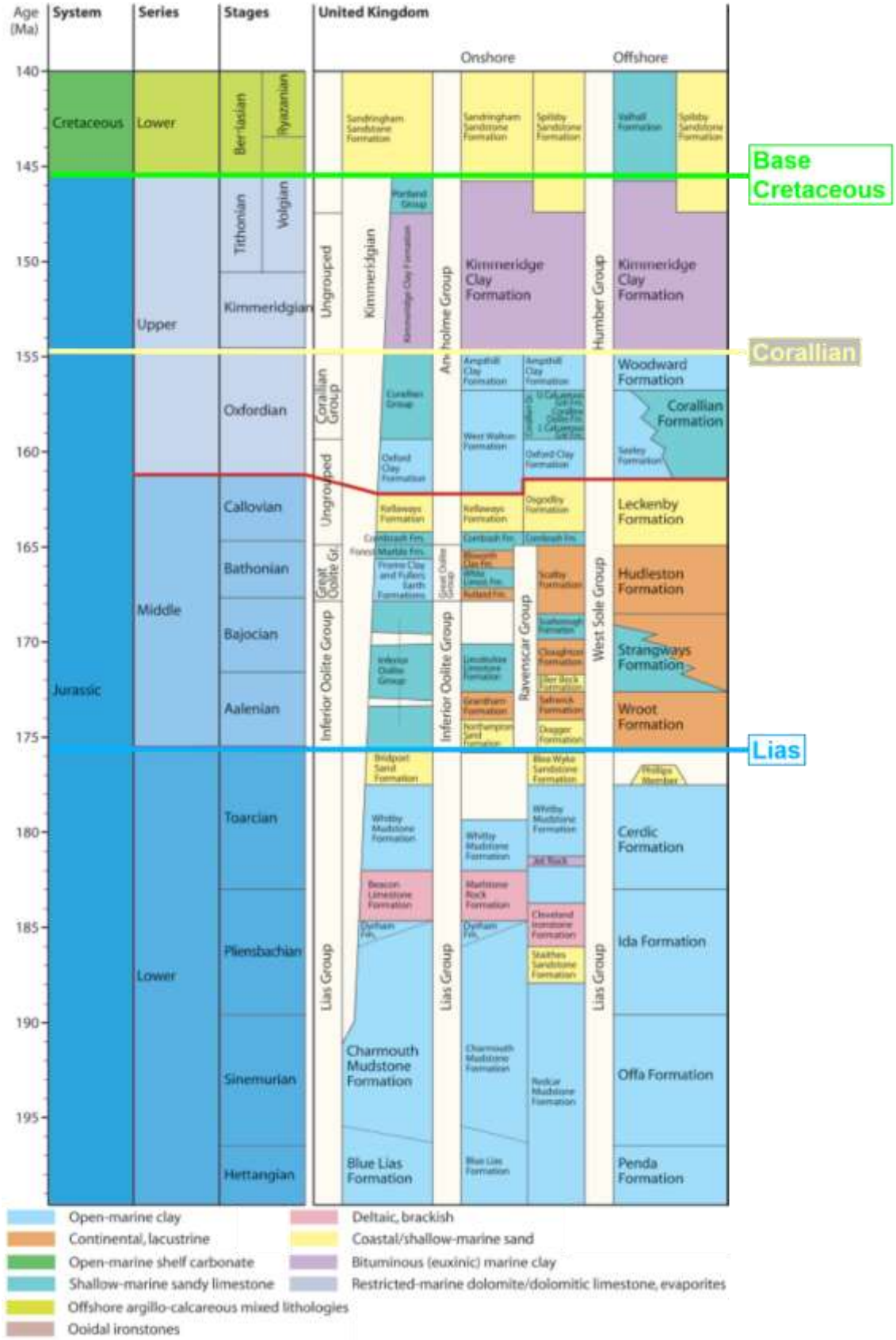

Figure 4.35 Jurassic stratigraphy with Lias, Corallian and Base Cretaceous seismic picks shown. Modified after Lott, et al. (2010).

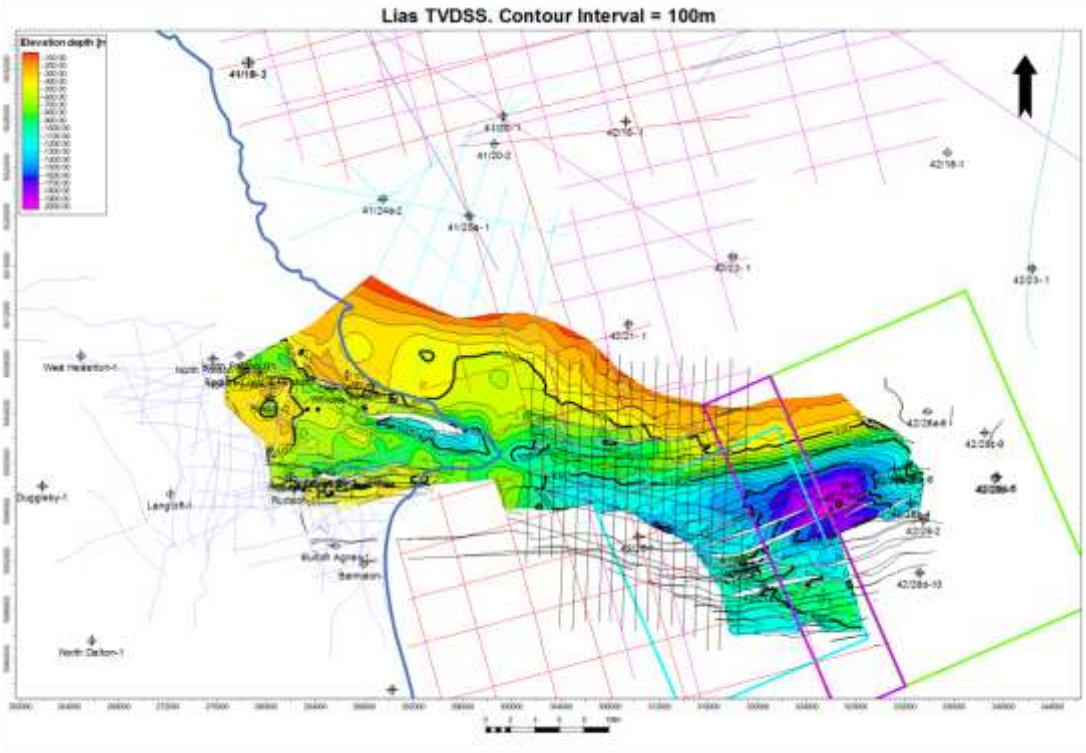

Figure 4.36 Well-tied Lias depth surface grid, metres TVDSS. Northern limit of interpretation marks seabed subcrop. All other limits are interpretation clips. See Appendix E-6 for large-scale plot.

As documented in Section 1.5, post Triassic thermal relaxation and differential movement across the Market Weighton Block resulted in the creation of accommodation space to the north, leading to the creation of the Cleveland Basin. The Flamborough Head Fault Zone acts as a hinge zone between the stable Market Weighton Block and the subsiding Cleveland Basin. Isochore maps of the Lias Group (Figure 4.38), regional seismic profiles (Figure 4.40) and well correlations (Figure 4.41) reflect this by recording a unit thickening of the Lias Group in the hanging wall of west to east trending listric faults of the Flamborough Head Graben System and condensation in the footwall, across the Market Weighton Block, suggesting a syn-tectonic control on sedimentation across the Flamborough Head Fault Zone at this time. True vertical time thickness of the Lias Group section grows from less than 150ms south of the Flamborough Head Fault Zone to more than 450ms in the north (Figure 4.38). Well isochores also show this trend across the Flamborough Head Fault Zone, with a minimum thickness of 43m recorded in Hornsea-1 and a maximum thickness of 925m recorded in the 42/28a-6 well (Figure 4.39). The observation that the hanging wall of the Flamborough Head Graben System lies to the north towards the Cleveland Basin with the footwall to the south towards the Market Weighton Block discounts the interpretation of Kirby & Swallow (1987) who propose that the inverse is true across Flamborough Head (Figure 1.5).

Although it is proposed that tectonic subsidence in the study area from the Early Jurassic onwards has been primarily the result of intraplate extension at basement level Flamborough Head Fault Zone faults, there is evidence from seismic profiles of the influence of salt tectonics from this time. Syn-depositional, west to east trending listric faulting across the Flamborough Head Fault Zone within the Upper Triassic and Lower Jurassic creates a series of domino fault blocks in the Lias and Upper Triassic Haisborough Group, which have a multiple detachments in the Triassic Keuper Halite, Röt Halite and Zechstein Group evaporites, creating a ramp – flat extensional decollement (Figure 4.40). The observed detached ramp – flat basement / cover fault relationship is similar to analogue models that involve a viscous layer (Richard, 1991; Stewart & Coward, 1995; Stewart, *et al*. 1996). These models show that, in the presence of a ductile layer (i.e. salt) between the basement and the cover, the fault systems in the cover are located horizontally offset towards the basement footwall and away from the basement fault crest (Stewart & Coward 1995), (Figure 4.37). This type of basement / cover relationship identified at Flamborough Head has been documented elsewhere in the Southern North Sea, such the Dowsing Peripheral Graben System and the UK Continental shelf, such as the Central North Sea and the Irish Sea basins (Stewart & Coward 1995).

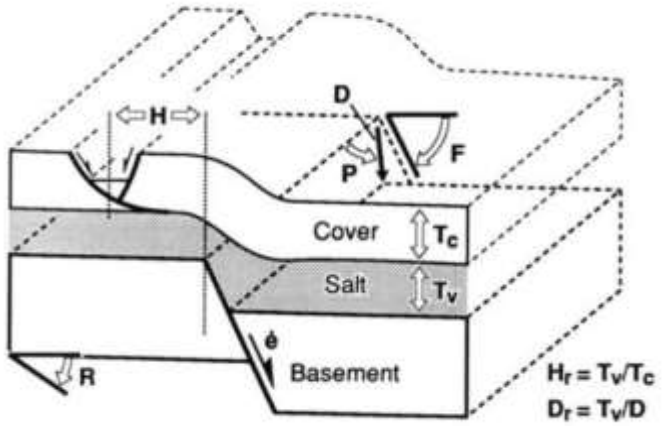

Figure 4.37 Model showing a ramp - flat basement to cover fault relationship and offset of cover listric faults from planar basement faults. Factors influencing magnitude of offset ratio are: thickness ratio H_r; displacement ratio D_r; displacement vector P; basement dip F; displacement rate ė and regional dip R (Stewart & Coward 1995)

It is proposed that from the Late Triassic to Early Jurassic, basinal tilt to the north-east was achieved by subsidence due to basement extension. This provided a smooth north-easterly dipping slope at the top Permian salt level, with salt moving from the Zechstein carbonate shelf edge (Figure 4.18) towards the basin centre and actively shaping to the evolving faulted topography at Rotliegend level (Stewart & Coward 1995). A de-coupled

post-salt section was free to slide due to gravity along this tilted detachment surface towards the centre of the Cleveland Basin (Stewart & Coward 1995). This has resulted in the creation of an Early Jurassic and younger decoupled collapse graben system characterised by domino fault blocks above the Flamborough Head Fault Zone and which stretches from the onshore to the offshore (Figure 4.36, Figure 4.38 and Figure 4.40). Sedimentary fill of the graben system was controlled by listric faults that detach into Triassic and Permian salt and were formed as a response to extension due to basinward gravity sliding of the decoupled post Permian salt section (Figure 4.40). Extension in the Flamborough Head Graben System was balanced by folding within the centre of the basin and extension in the pre-salt section (Stewart & Coward 1995).

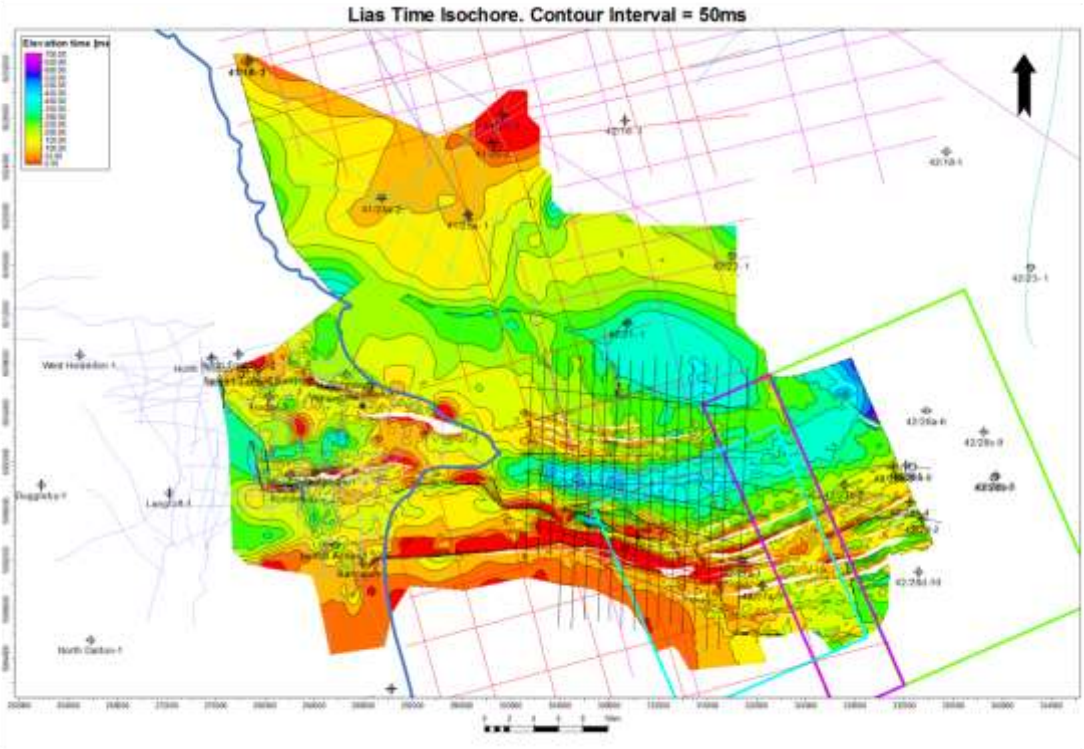

Figure 4.38 Lias Group time isochore, milliseconds TWTT. Note thickening of section and creation of a west to east half graben structure in the immediate hanging wall of the Flamborough Head Fault Zone. Condensation of section is apparent to south and truncation through basin inversion to the north from thinning of the isochore. See Appendix B-7 for large-scale plot.

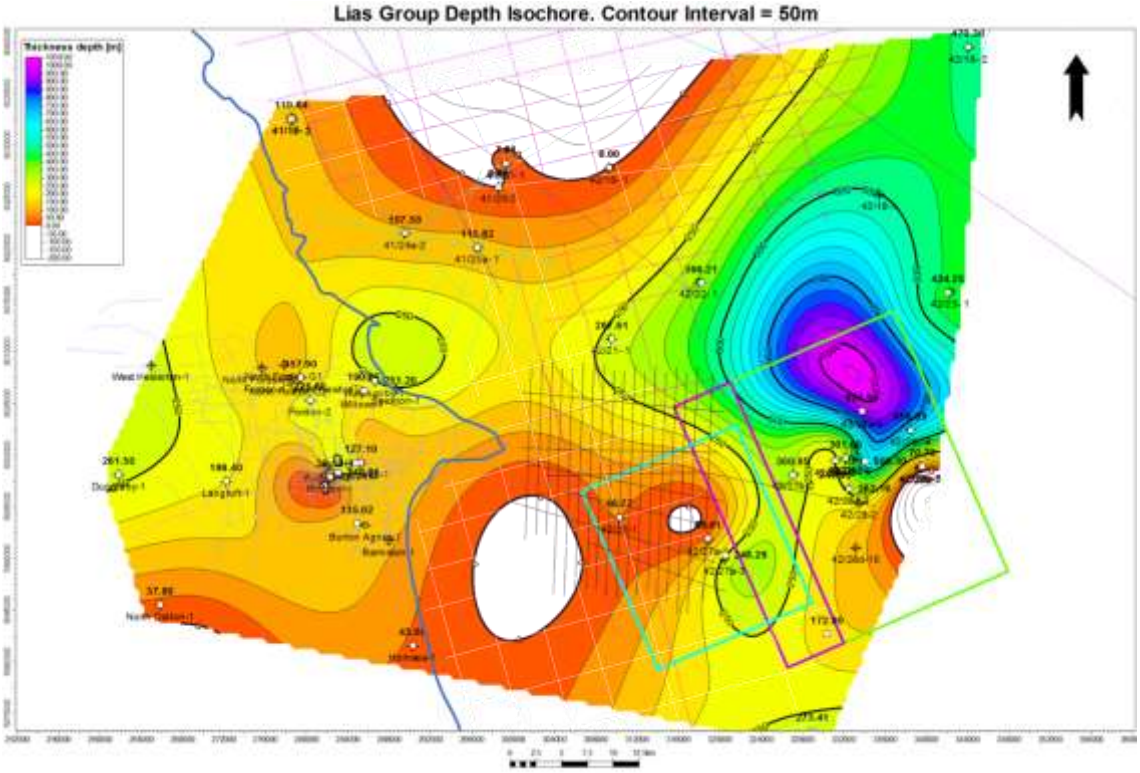

Figure 4.39 Lias Group depth isochore from well tops in metres.

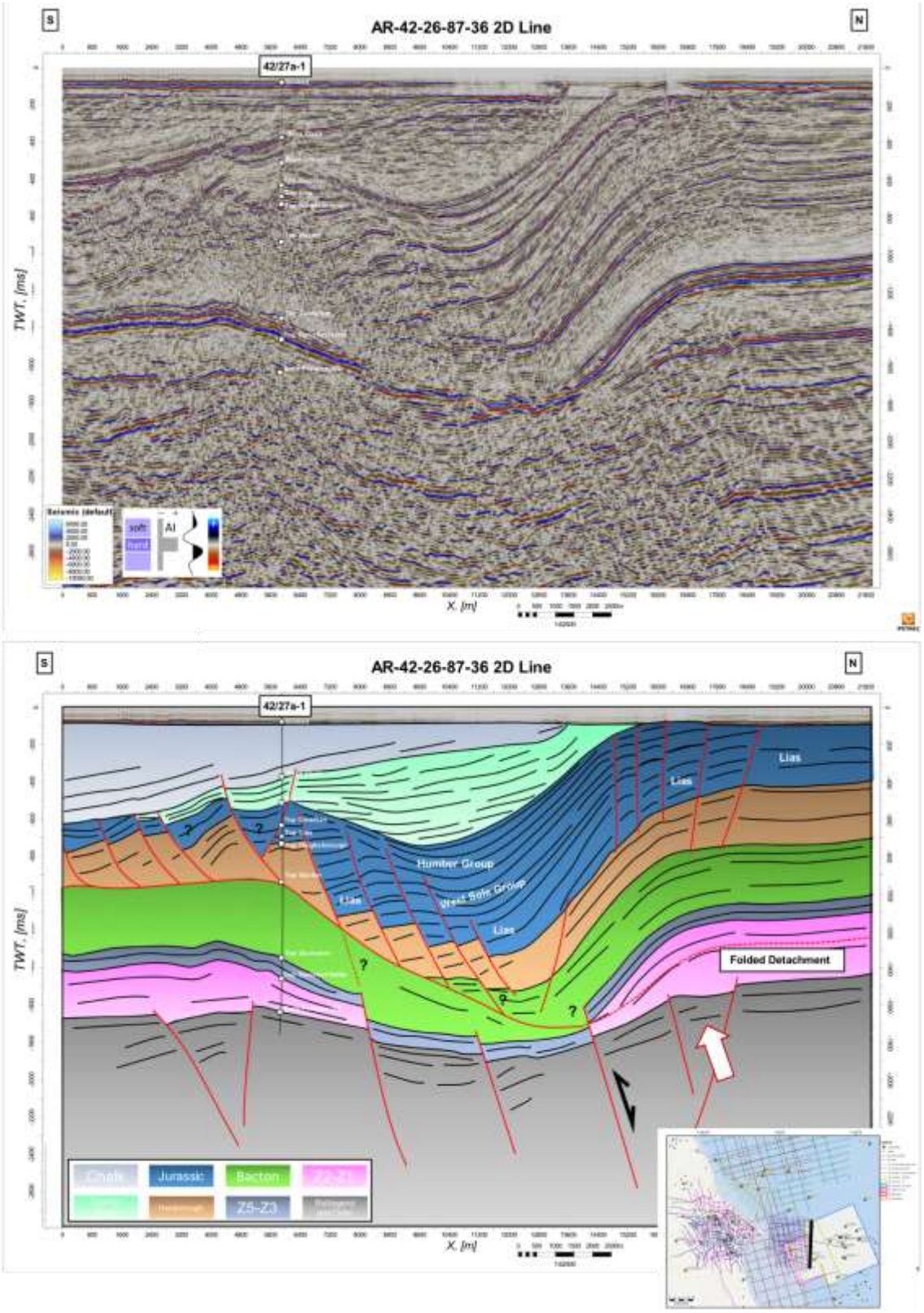

Figure 4.40 (Above) South to north striking un-interpreted regional 2D line AR-42-26-87-36 (Below) interpreted geo-seismic section of same line. Inset shows line location. Note thickening of Lias and Jurassic section into the hanging wall of the Flamborough Head Fault System and condensation to the south in the footwall; domino faulting of Jurassic and Triassic units onto a Röt Halite detachment which then detaches onto Zechstein evaporites; antithetic faults in the hanging wall which detach onto Upper Triassic evaporites and erosional truncation of Jurassic units into the Cleveland Basin in the north due to post depositional uplift, shown by white arrow. Five times vertical exaggeration. Data courtesy of BP.

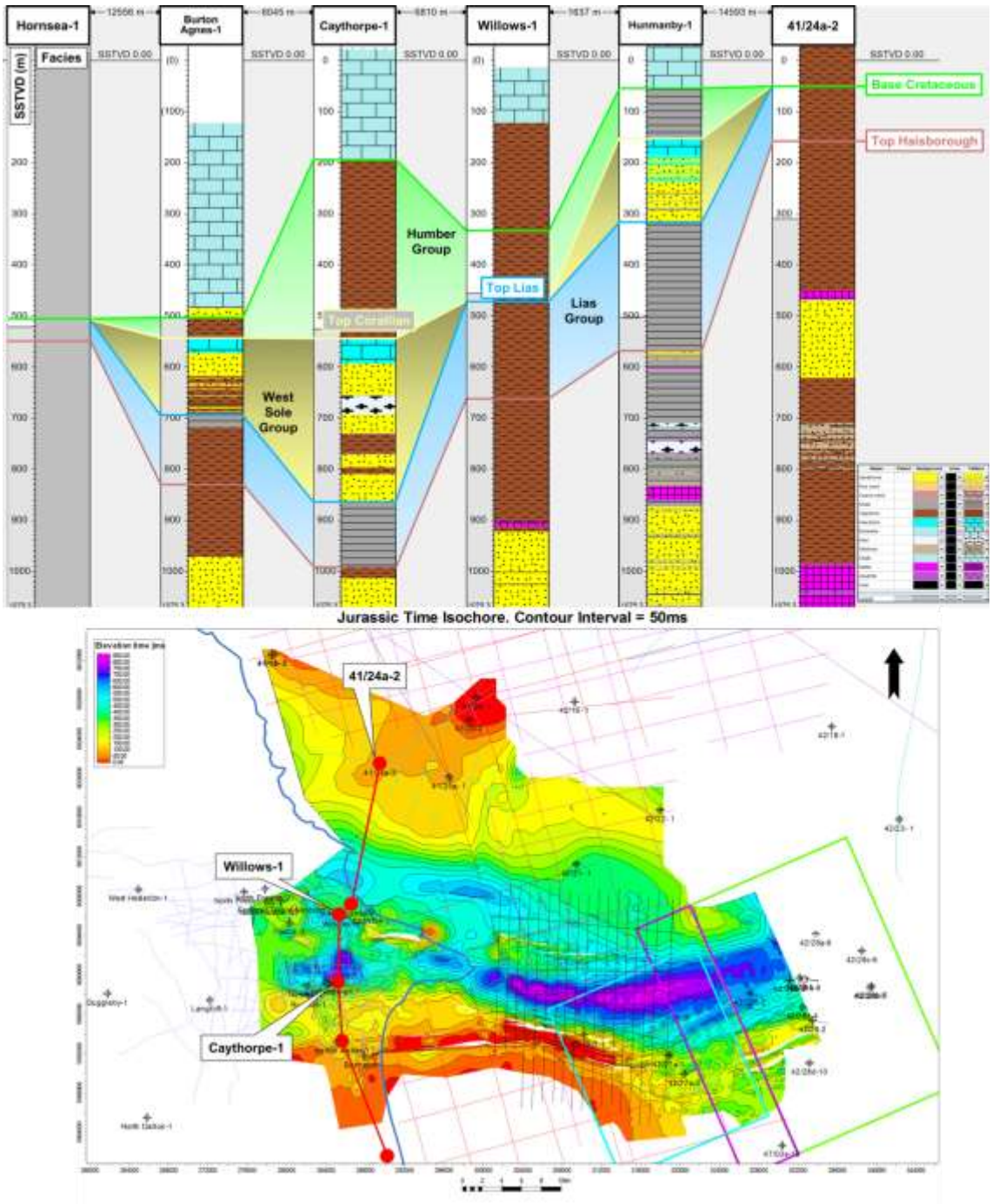

Figure 4.41 (Above) well correlation of the Jurassic units across the Flamborough Head Fault Zone in metres TVDSS showing interpreted facies. Note Lias section thinning in Caythorpe-1 and absence of West Sole in Willows-1 is due to section being faulted out and not representative of true stratigraphic thickness. Thinning of Lias at 41/24a-2 is result of truncation through inversion of the Cleveland Basin (Below) Triassic time isochore map showing well correlation location.

Isochore thinning of the Lower Jurassic (and subsequent younger Jurassic units) occurs to the north of the dataset, into the Cleveland Basin (Figure 4.38) with Lias Group units exposed at the seabed (Figure 4.40). This is related to post-depositional truncation as a result of tectonic inversion of the Cleveland Basin during the Cenozoic and therefore a true depositional thickness of Lias Group and younger Jurassic units is not preserved in the Cleveland Basin within the study area.

4.5.2 West Sole Group

Regional uplift in the Middle Jurassic due to the thermal effects of the Central North Sea Dome resulted in a switch from the marine transgressive setting of the Lias Group to the regressive regime of the West Sole Group, with the deposition of non-marine fluvio-deltaic coarse-grained clastics and associated fine-grained paralic sediments (Lott, et al., 2010) (Figure 4.35, Figure 4.41 and Figure 4.42).

Deflation and collapse of the dome in at the start of the Late Jurassic, from the Callovian to Oxfordian, saw a new transgressive cycle start with a marine incursion back into the basin (Lott, *et al*. 2010). The establishment of marine conditions saw the development of the regionally extensive Corallian carbonates during the Oxfordian. As this rock unit displays a strong acoustic impedance contrast across the entire seismic dataset, it was picked as a proxy to the top of the West Sole Group (Figure 4.35, Figure 4.40 and Figure 4.43).

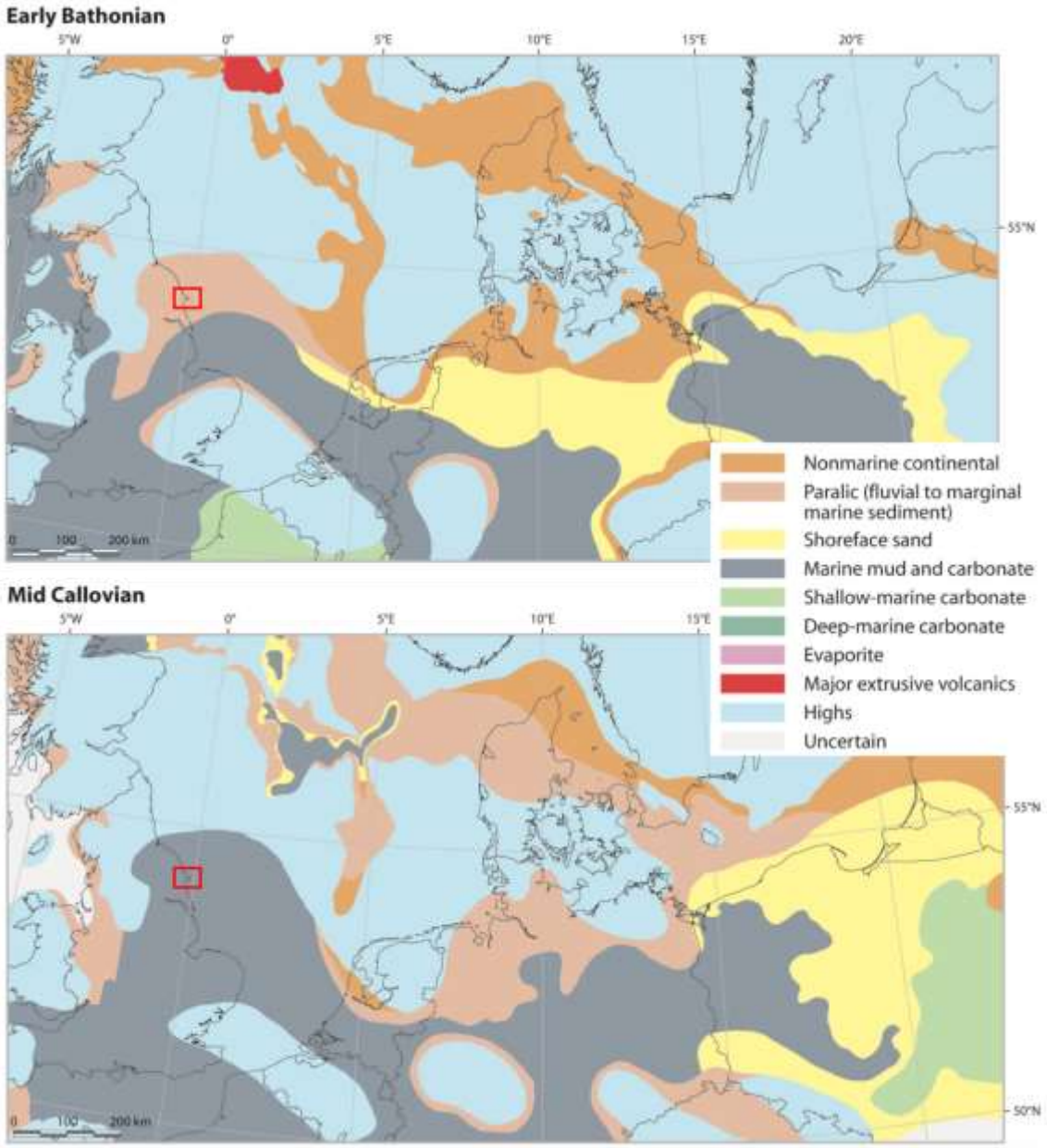

Figure 4.42 Middle Jurassic West Sole Group palaeogeography. Study area shown as red box. See Figure 4.35 for stage age clarification. Modified after Lott, et al. (2010)

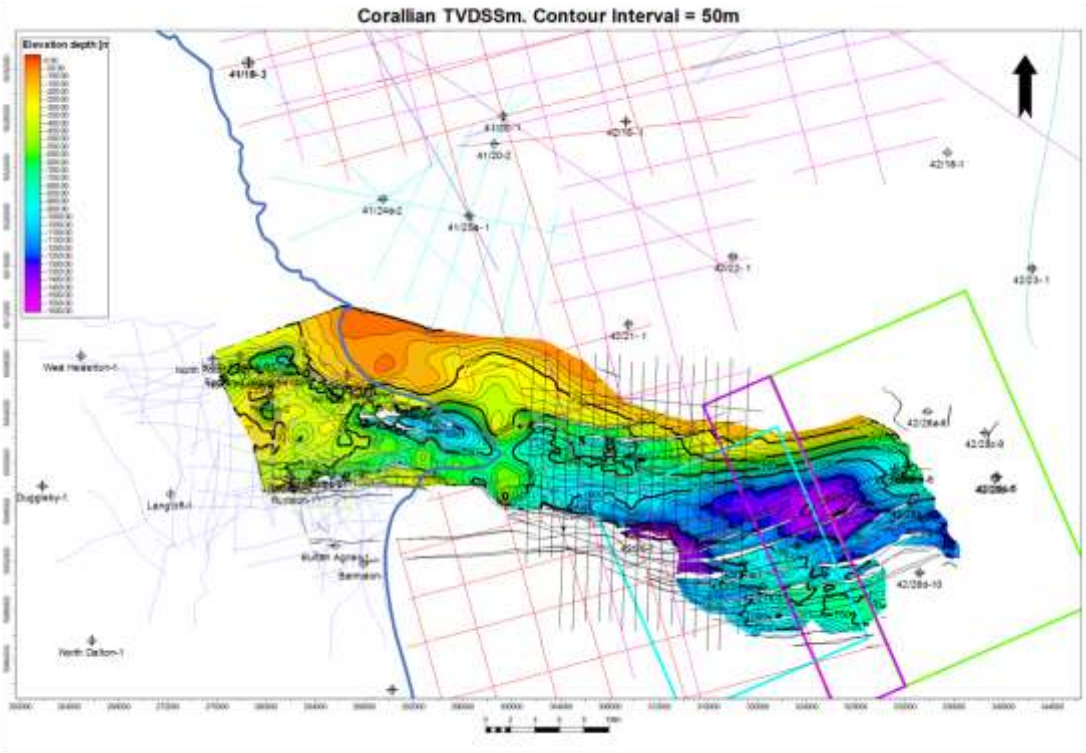

Figure 4.43 Well-tied Corallian depth surface grid, metres TVDSS. Northern limit of interpretation marks seabed subcrop. All other limits are interpretation clips. See Appendix E-5 for large-scale plot.

Isochore maps (Figure 4.44) and well correlations (Figure 4.41) for the West Sole Group document a Middle Jurassic interval that is approximately half the total thickness of the Lower Jurassic Lias Group (maximum vertical time thickness of 250ms and 450ms, respectively). This trend is reflected in encountered well sections, with a maximum Lias Group thickness of 925m recorded in the 42/28a-6 well (Figure 4.39) and a maximum West Sole Group thickness of 495m recorded in the 42/27b-2 well (Figure 4.45). These observations suggest that subsidence slowed down in the Cleveland Basin during the Middle Jurassic due to the thermal uplift effects of the Central North Sea Dome. Active extension on the detached listric faults that displace this unit was still occurring during deposition, with growth of section evident in the immediate fault hanging walls of the faults (Figure 4.40 and Figure 4.44).

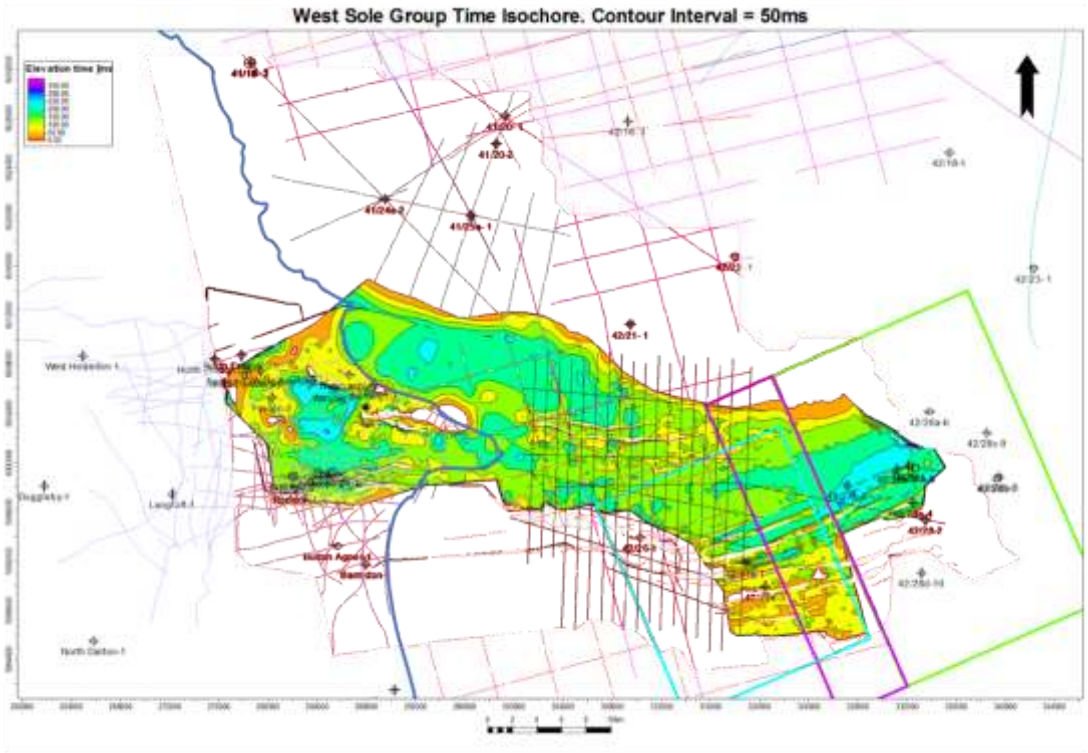

Figure 4.44 West Sole Group time isochore, milliseconds TWTT. See Appendix B-6 for large-scale plot.

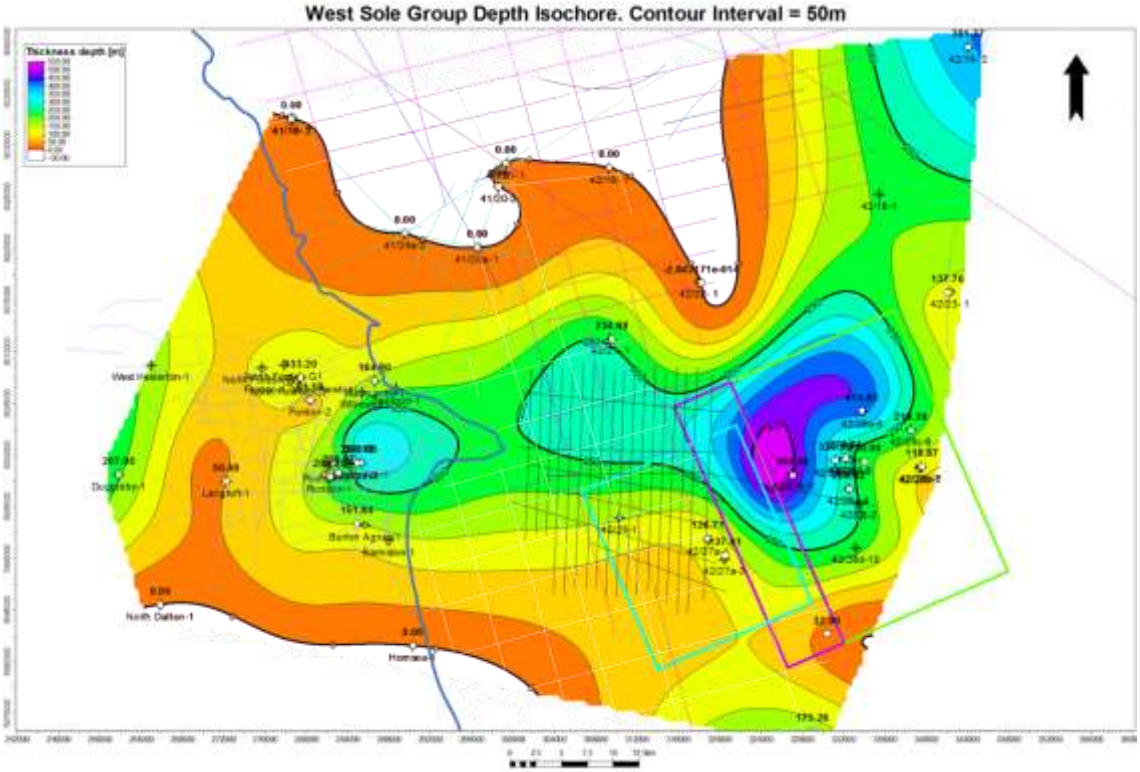

Figure 4.45 West Sole Group depth isochore from well tops in metres.

The Middle Jurassic also saw renewed movement of the Peak Trough, an actively subsiding NNW-SSE striking graben during the Jurassic (Milsom & Rawson 1989; Powell 2010), (Figure 4.46). Faulting of the Peak Trough is postulated to have

commenced during the Triassic and Lower Jurassic, with facies changes and thickness increases from the flanks into the Peak Trough are recorded in the Upper Lias, Toarcian (Milsom & Rawson 1989; Powell 2010). Middle Jurassic rejuvenation of the Peak Trough is well recognised regionally, with syn-sedimentary faulting recorded at outcrop on the Peak Fault at Ravenscar (Figure 4.46). Here, high net to gross Aalenian to Bathonian aged Ravenscar Group (West Sole Group age equivalent), (Figure 4.35) fluvial clastics are preserved in the hanging wall of the Peak Fault, whereas Lower Jurassic, thinner, low net to gross, fine grained overbank distal shale facies of the Staithes Sandstone Formation is present in the footwall (Figure 4.47).

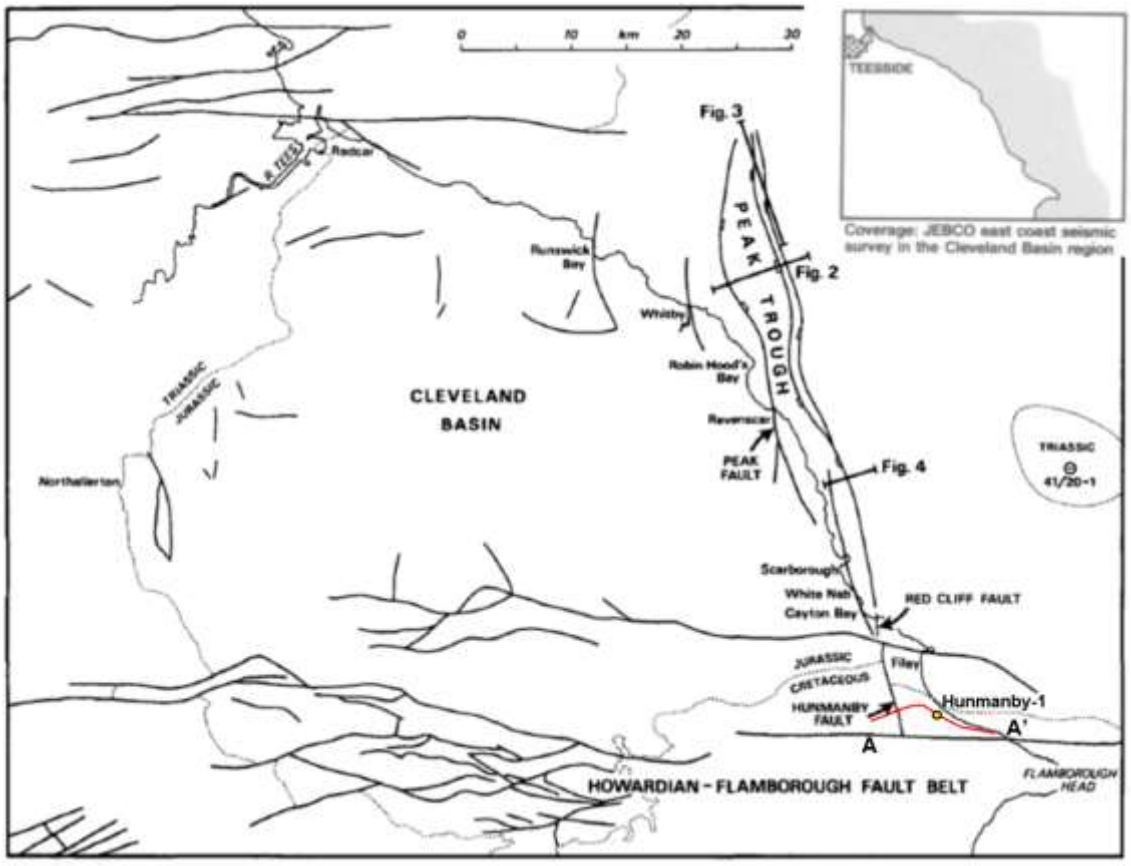

Figure 4.46 Map of North Yorkshire coast and greater Cleveland Basin showing the location of the N-S trending Peak Trough in relation to the W-E trending Flamborough Head Fault Zone. Red line shows location for seismic profile in Figure 4.49. Modified after Milsom & Rawson (1989).

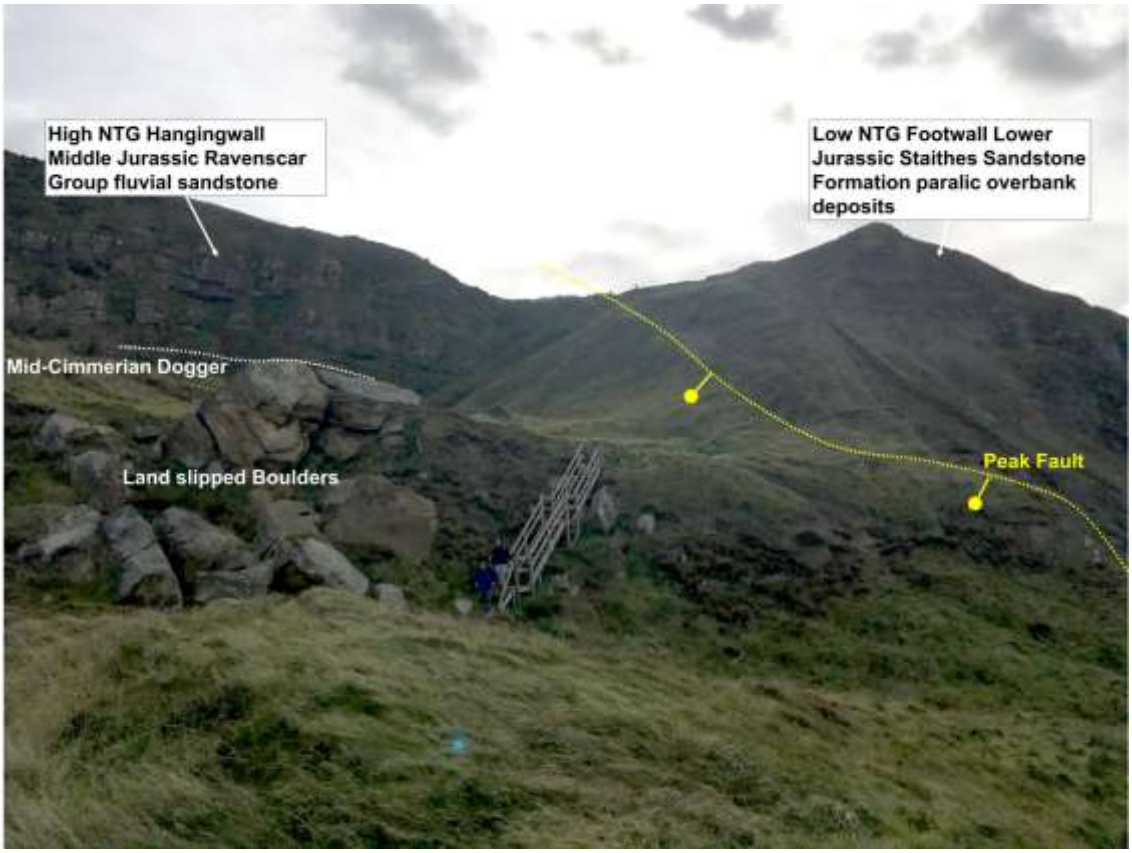

Figure 4.47 Field photograph of the Peak Fault at Ravenscar, showing syn-sedimentary relationship of high net to gross fluvial sandstones deposited in the hanging wall of the fault (Peak Trough) compared to the age equivalent low net to gross distal shales in the footwall. Photograph view orientation is approximately to the SW.

The middle Jurassic rejuvenation of the Peak Trough faults is postulated to be due to extension in response to the rising Central North Sea Dome, in a process that is analogous to the formation of radial expansion faults above a rising salt diapir (Fossen 2010).

Subsurface mapping of offshore 2D seismic to the north of the study area demonstrates that the Peak Trough faults are listric in nature, having multi-level detachments within Triassic and Permian Zechstein Group salt layers (Milsom & Rawson 1989), similar to the mapped listric faults of the Flamborough Head Graben System. This important observation, combined with the NNW-SSE geometries of the Peak Trough fault system and the Zechstein shelf edge suggests a Zechstein Group salt control to the development of western flank of the Peak Trough (Figure 4.48). In this proposed model, the facies change from thick mobile evaporites of the Zechstein salt basin to basin-margin carbonates and evaporites at the slope to shelf edge (Figure 4.19) acts as a natural zone of weakness along which the western flank of the Peak Trough faults have centred. It is proposed that the basin margin facies acts as a pin in the footwall and the mobile

evaporites of the salt basin accommodates listric detachments into the basin in the hanging wall.

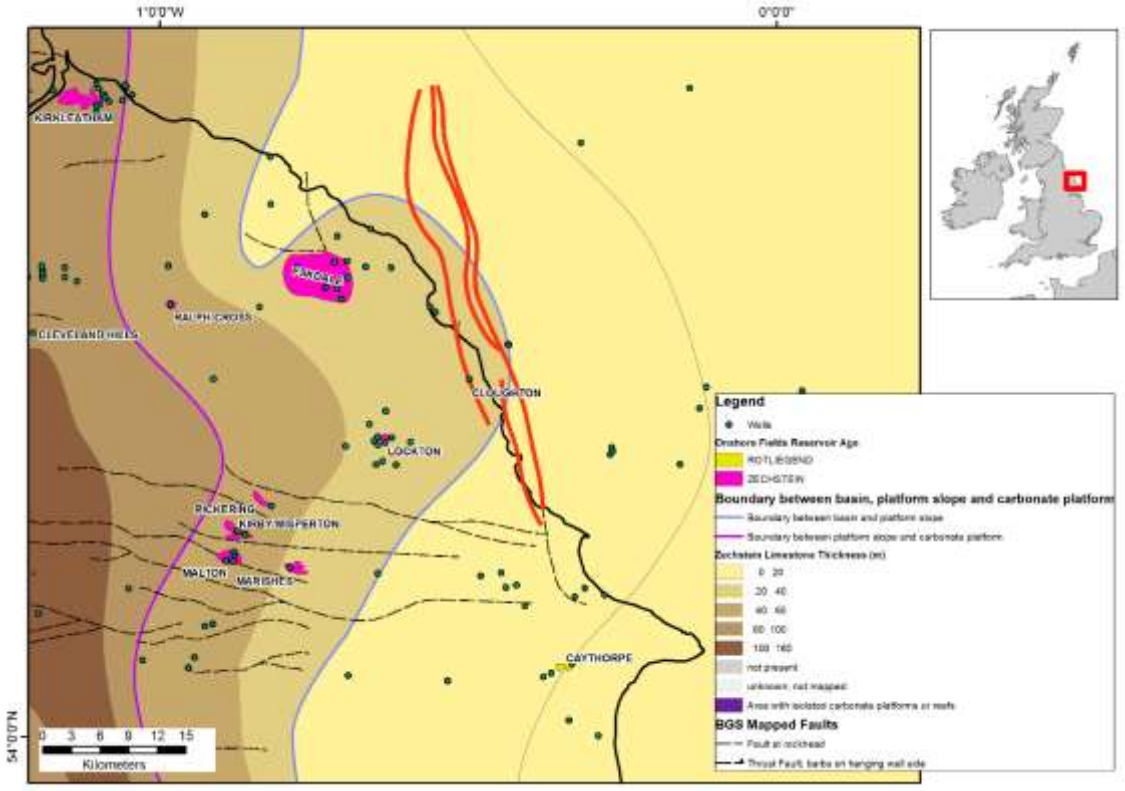

Figure 4.48 Structural features, with Peak Trough faults, as mapped by Milson & Rawson (1989), highlighted in red and overlain on Z2 group carbonate thickness map with boundary line between basin and platform edge marking facies transition from thick evaporites in the basin (right of line) to carbonates and evaporites on the platform (left of line). Note distribution of Z2 carbonate reservoir gas fields restricted to the Z2 carbonate platform. Modified after Peryt, et al. (2010) and Milsom & Rawson (1989) with additional data courtesy of Oil & Gas Authority and British Geological Survey.

The southern extension of the eastern flank fault of the Peak Trough extends into the study area as the Hunmanby Fault (Figure 4.46). The Hunmanby Fault is situated at the extreme northern edge of the onshore seismic data, at the poor quality western edge of the Bempton 3D survey and is only crossed by two 2D seismic profiles, precluding detailed subsurface mapping of this feature on this dataset. A composite 2D seismic profile that crosses the Hunmanby Fault and ties the Hunmanby-1 well is shown in Figure 4.49. Extrapolation of reflectors from Hunmanby-1 well across the Hunmanby Fault is challenging due to poor well control in the fault hanging wall the and poorly resolved steep dipping seismic reflectors. However, it can be noted that the Hunmanby Fault is a listric fault that throws to the west and is decoupled from the underlying Rotliegend faults, detaching into Zechstein Group evaporites.

Syn-tectonic stratal thickening in the West Sole, Humber and Cromer Knoll Groups can be tentatively identified on seismic data (Figure 4.49). Thickening of the Humber Group by 46m and of the Cromer Knoll Group by 280m across the Hunmanby Fault between Hunmanby-1 and Fordon-1 suggests continued movement on the Hunmanby Fault through the Late Jurassic and Early Cretaceous which has been noted by others (Milsom & Rawson 1989), possibly through deflation of the Central North Sea Thermal Dome and Late Jurassic rifting – Early Cretaceous thermal subsidence. Seismic profiles also show that The Hunmanby Fault was active in the Cenozoic, as it throws the Upper Cretaceous Chalk Group against the Lower Cretaceous Cromer Knoll Group. It has been proposed that this occurred as a result of Cenozoic inversion of the Cleveland Basin (Milsom & Rawson 1989).

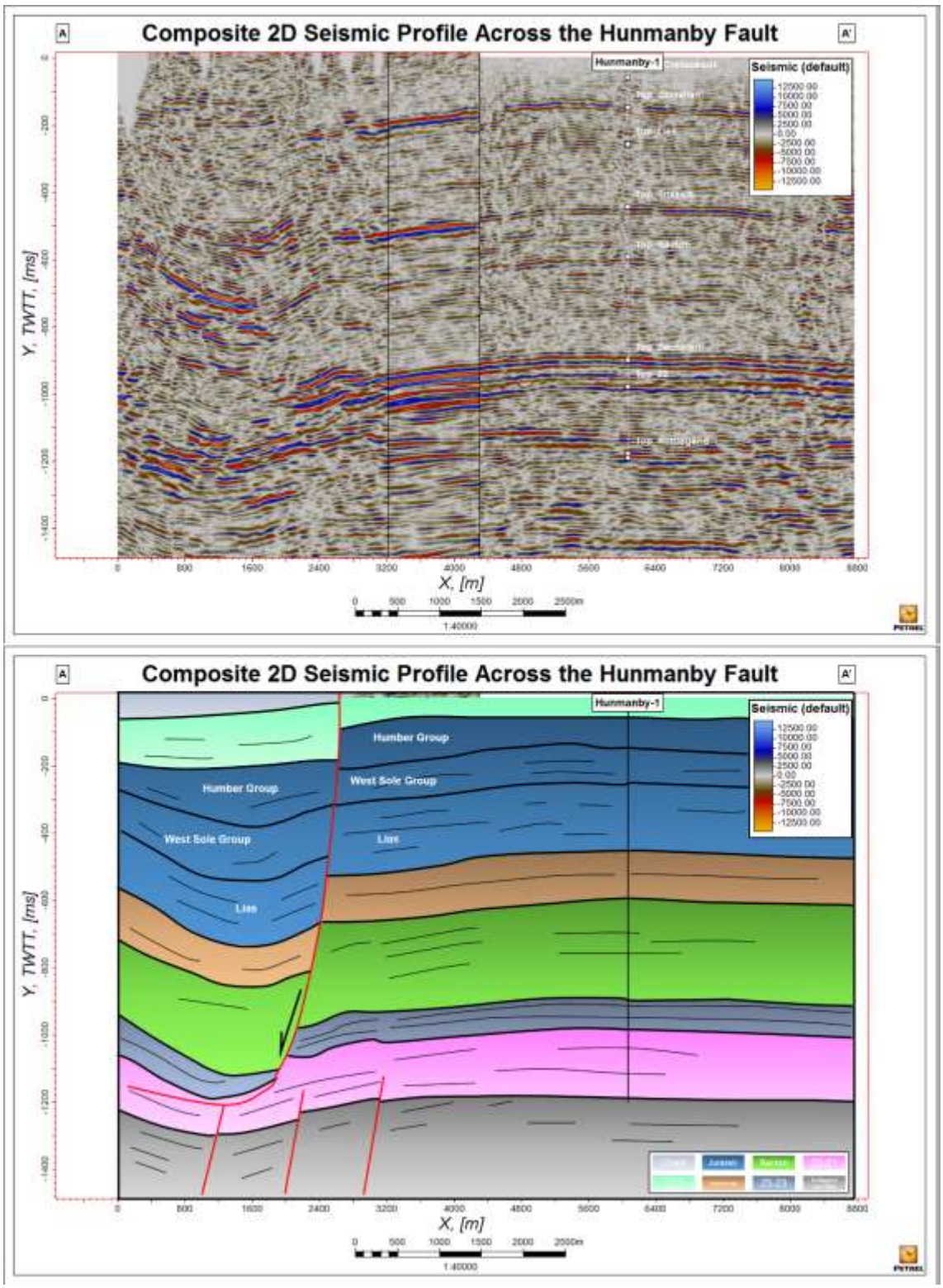

Figure 4.49 (Above) un-interpreted composite 2D seismic profile across the Hunmanby Fault. Four times vertical exaggeration. (Below) interpretation of same line. Note syn-depositional thickening of Middle and Late Jurassic and Lower Cretaceous across the Hunmanby Fault. See Figure 4.46 for seismic profile location. Data courtesy of UKOGL.

4.5.3 Humber Group

The collapse of the Central North Sea thermal dome at the end of the Middle Jurassic to start of the Late Jurassic and rifting associated with the breakup of Pangea and continuing

opening of the central Atlantic Ocean resulted in rejuvenated extension, creation of accommodation space and the onset of a new eustatic marine transgressive system and open marine incursion of the Late Jurassic (Lott, *et al*. 2010). The stratigraphy of the Humber Group in the study area is composed of Oxfordian aged marine claystones of the Oxford Clay and higher energy shallow marine sandstones and carbonates of the Corallian Group, suggesting a brief period of eustatic sea level rise during the late Oxfordian. A major eustatic sea level rise and marine flooding of the study area resumed during the Kimmeridgian to Tithonian with the deposition of the regional extensive marine claystones of the Kimmeridge Clay Formation (Figure 4.35, Figure 4.50).

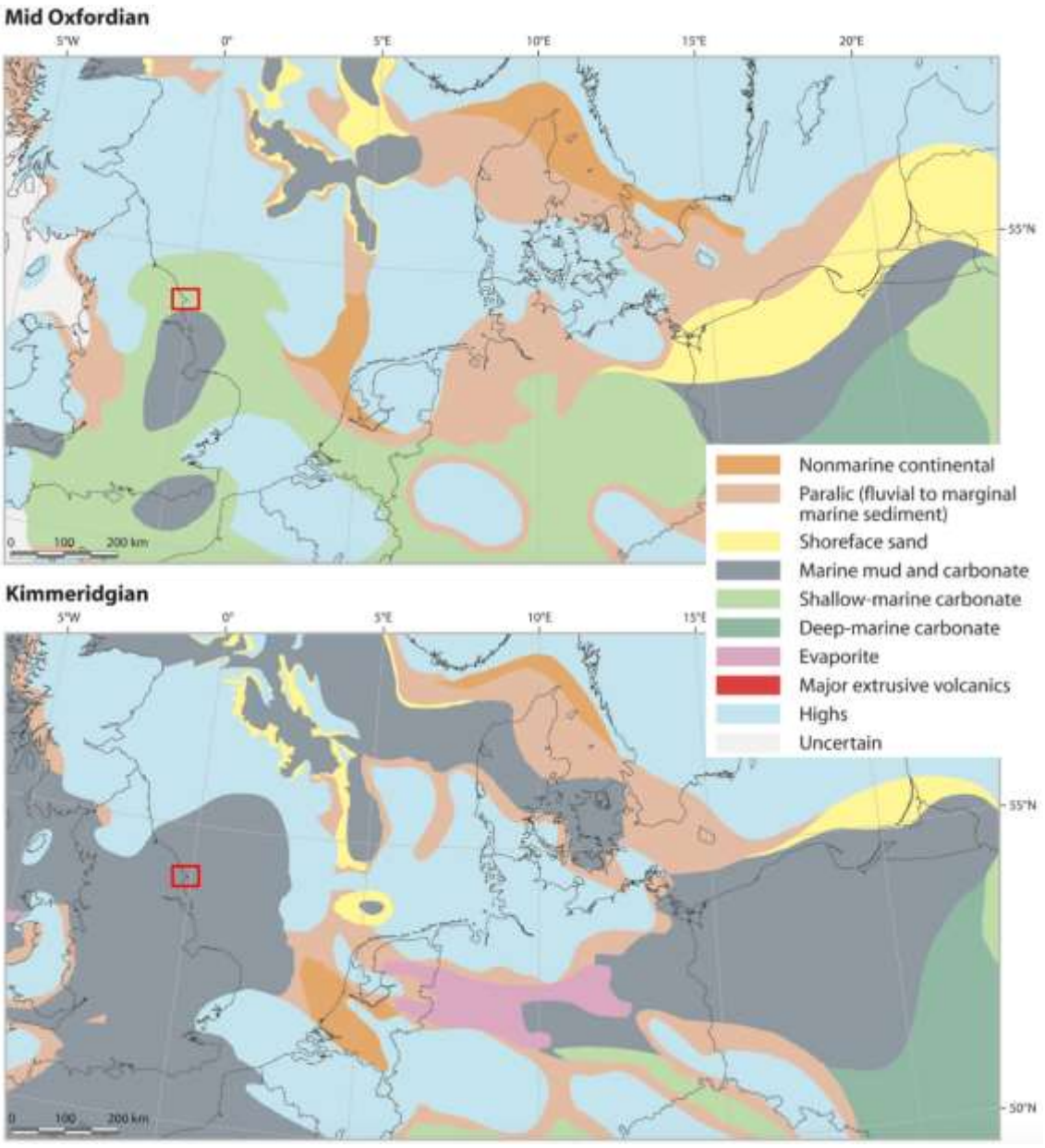

Figure 4.50 Late Jurassic palaeogeography. Study area shown as red box. See Figure 4.35 for stage age clarification. Modified after Lott, et al. (2010).

Late Jurassic rifting continued until the start of the Cretaceous, when the tectonic regime transitioned from active rifting to a post rift thermal sag phase (Vejbaek, *et al*. 2010). This transition is represented by the Base Cretaceous Unconformity, which provides the regionally interpretable seismic reflector for the top of the Humber Group litho-stratigraphic package (Figure 4.40 and Figure 4.51).

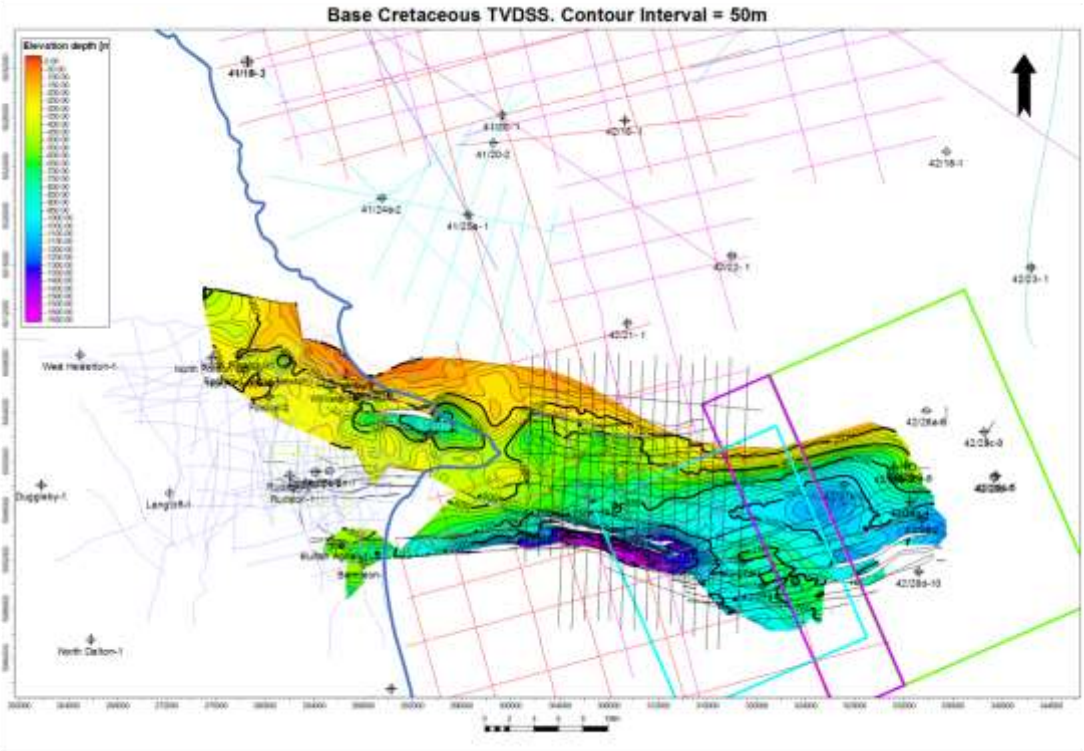

Figure 4.51 Well-tied Base Cretaceous tied depth surface grid, metres TVDSS. See Appendix E-4 for large-scale plot.

Humber Group isochore maps (Figure 4.53), well correlations (Figure 4.41) and vertical seismic profiles (Figure 4.40) document the renewed syn-extensional deposition for this unit, with observable section growth in the immediate hanging wall of the detached listric faults of the Flamborough Head Fault Zone. Renewed Late Jurassic extension on these salt-detached listric faults, combined with sediment gravity loading effects, is inferred to have initiated movement of the salt, creating roll-over anticlines of the Early and Middle Jurassic units in listric fault hanging walls (Figure 4.52).

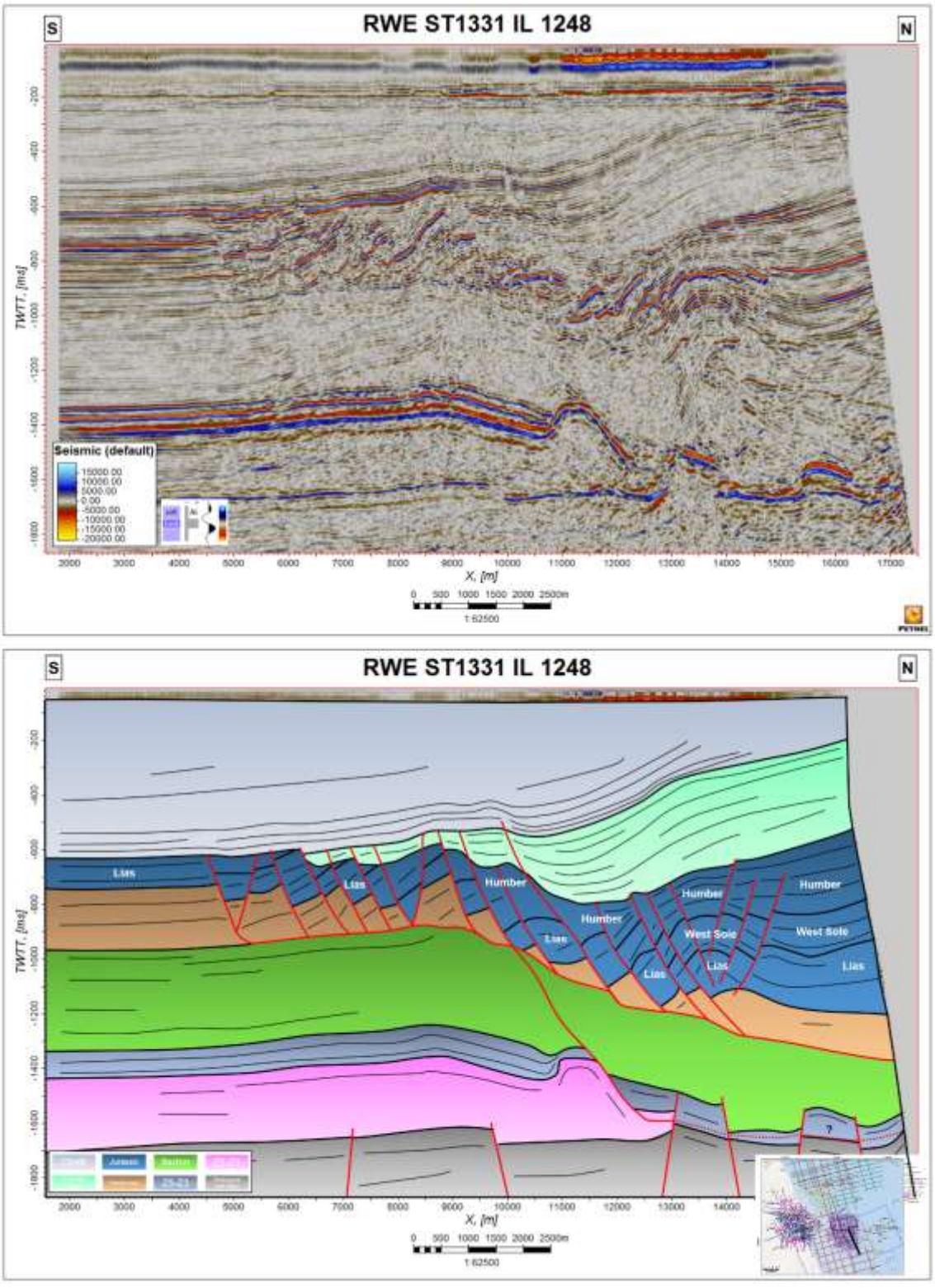

Figure 4.52 (Above) South to north striking un-interpreted IL 1248 of RWE ST1331 3D survey. (Below) same line with interpretation overlay showing rollover anticlines in hanging walls of listric faults and dual Triassic / Permian salt detachments. Five times vertical exaggeration. Data courtesy of Ineos Industries.

A maximum vertical time thickness of 350ms is reached across the Humber Group compared with 250ms and 450ms for the West Sole and Lias Groups, respectively. This trend is reflected in offshore wells with a maximum Humber Group thickness of 395m

recorded in the 42/28c-9 (Figure 4.54), maximum West Sole Group thickness of 495m recorded in the 42/27b-2 well (Figure 4.45) and a maximum Lias Group thickness of 925m recorded in the 42/28a-6 well (Figure 4.39). These observations point to maximum subsidence and extension during the Early Jurassic Lias in the Cleveland Basin, with renewed rifting and subsidence during the Late Jurassic. This suggests that the formation of the Cleveland Basin pre-dates the formation of the tripartite rift systems of the Moray Firth, Viking and Central Grabens, whose genesis is intrinsically linked to the collapse of the Central North Sea Dome during the Late Jurassic. The formation of an Early Jurassic graben structure in the study area, controlled by west to east striking listric faults that detach on to a mobile salt substrate is comparable with the timing and formation mechanism of the Wessex Basin (Butler 1998).

Isochore maps for the complete Jurassic interval (Figure 4.55, Figure 4.56) illustrate the syn-tectonic sedimentary nature for this interval with the creation of a west to east striking graben system across the Flamborough Head Fault Zone in the hanging wall of west to east striking listric normal faults that detach into both Triassic and Permian evaporitic intervals. Total Jurassic thickness increases from 43m at Hornsea-1 in the Market Weighton Block to 1661m at well 42/28a-6 within the Flamborough Head Fault Zone graben system (Figure 4.56). Active rift faulting and associated syn-rift sedimentation commenced in the Early Jurassic, continuing until the end of the Late Jurassic.

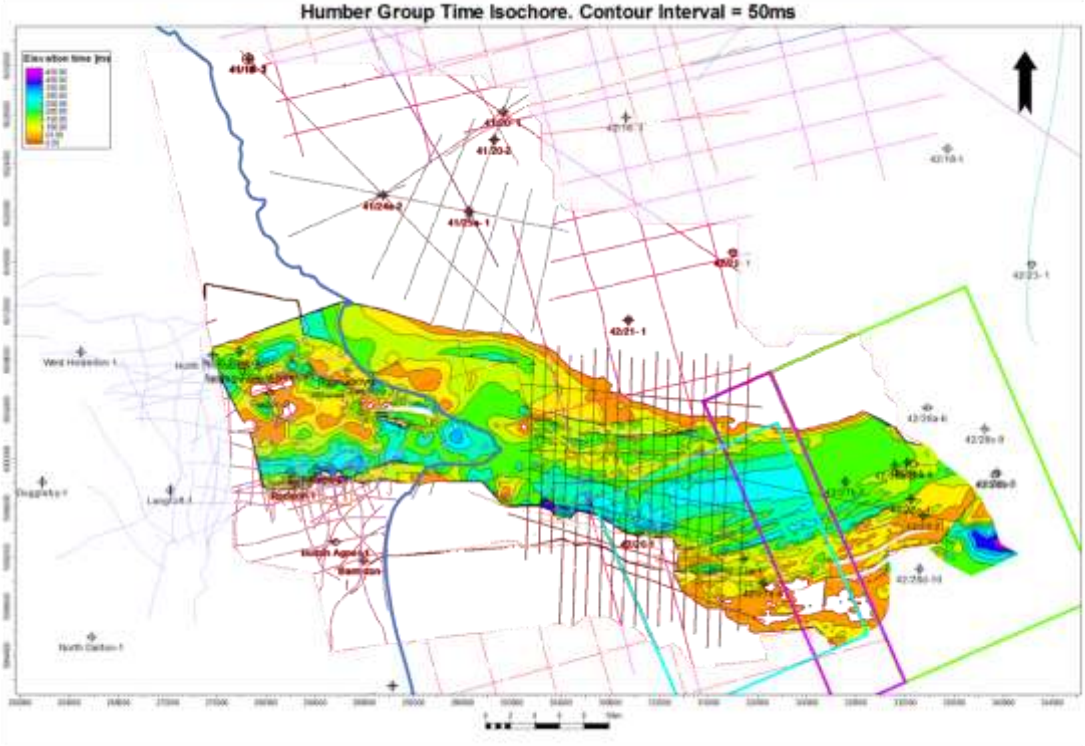

Figure 4.53 Humber Group time isochore, milliseconds TWTT. See Appendix B-5 for large-scale plot.

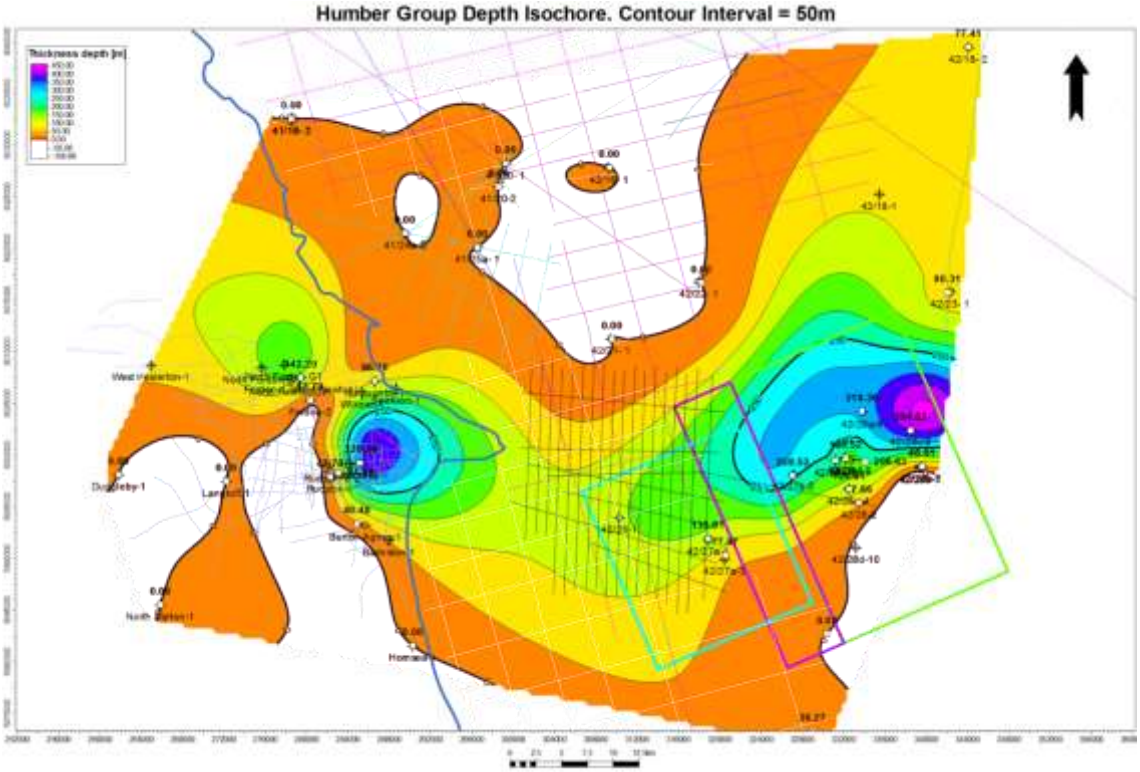

Figure 4.54 Humber Group depth isochore from well tops in metres.

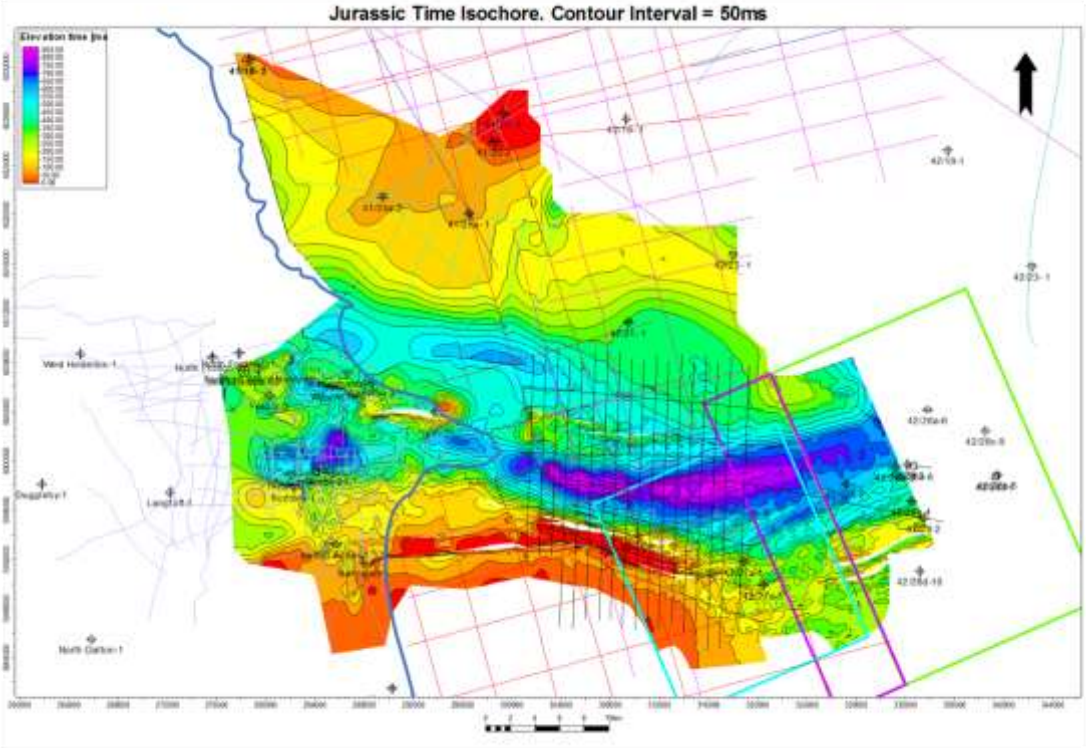

Figure 4.55 Jurassic time isochore, milliseconds TWTT. See Appendix B-13 for large-scale plot.

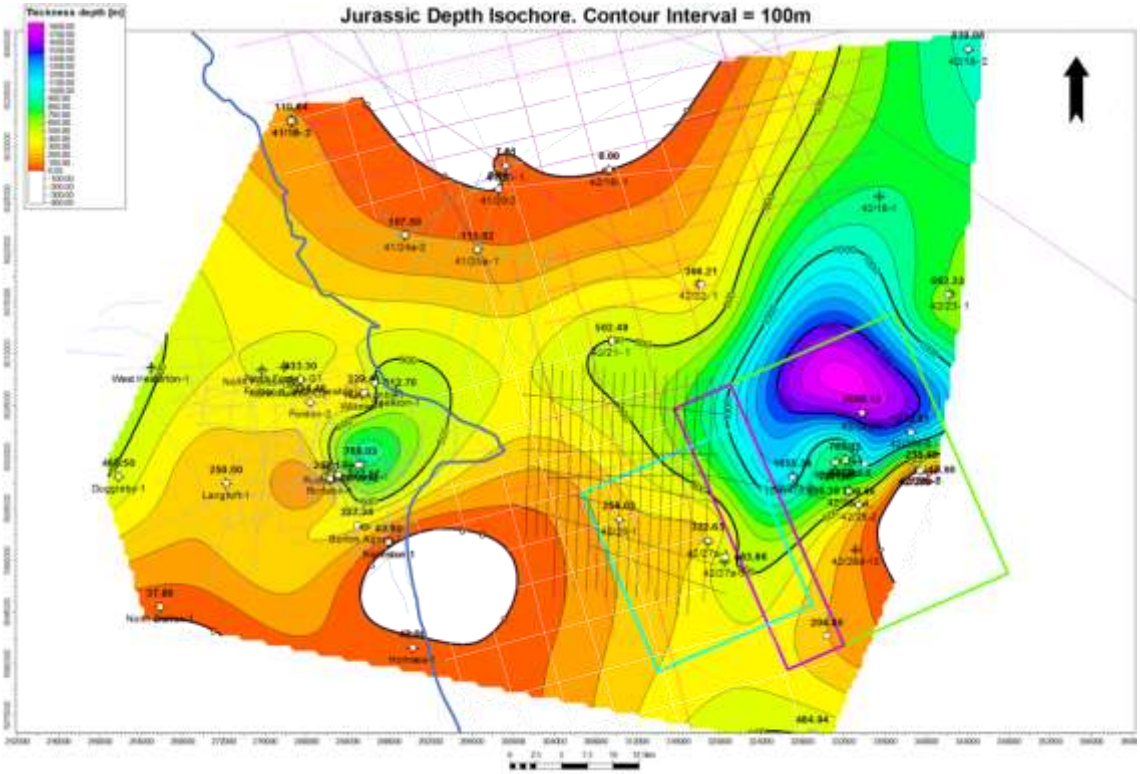

Figure 4.56 Jurassic depth isochore from well tops in metres.

4.6 Cretaceous

4.6.1 Cromer Knoll Group

Regional extension ceased in the North Sea during the Late Jurassic, with a transition to regional intra plate subsidence due to post rift thermal lithospheric cooling (Vejbaek, *et al*. 2010). The Base Cretaceous Unconformity (BCU) marks this transition and provides a regional seismic reflector for interpretation (Figure 4.51). The unconformable nature of this boundary is evident through truncation of underlying Jurassic sediments (Figure 4.52, Figure 4.59). Post rift subsidence coupled with eustatic sea level rise led to a continued transgression in the Lower Cretaceous with an open marine environment established and the deposition of marls of the Speeton Clay Formation deposited across the study area (Vejbaek, *et al*. 2010), (Figure 4.57, Figure 4.58).

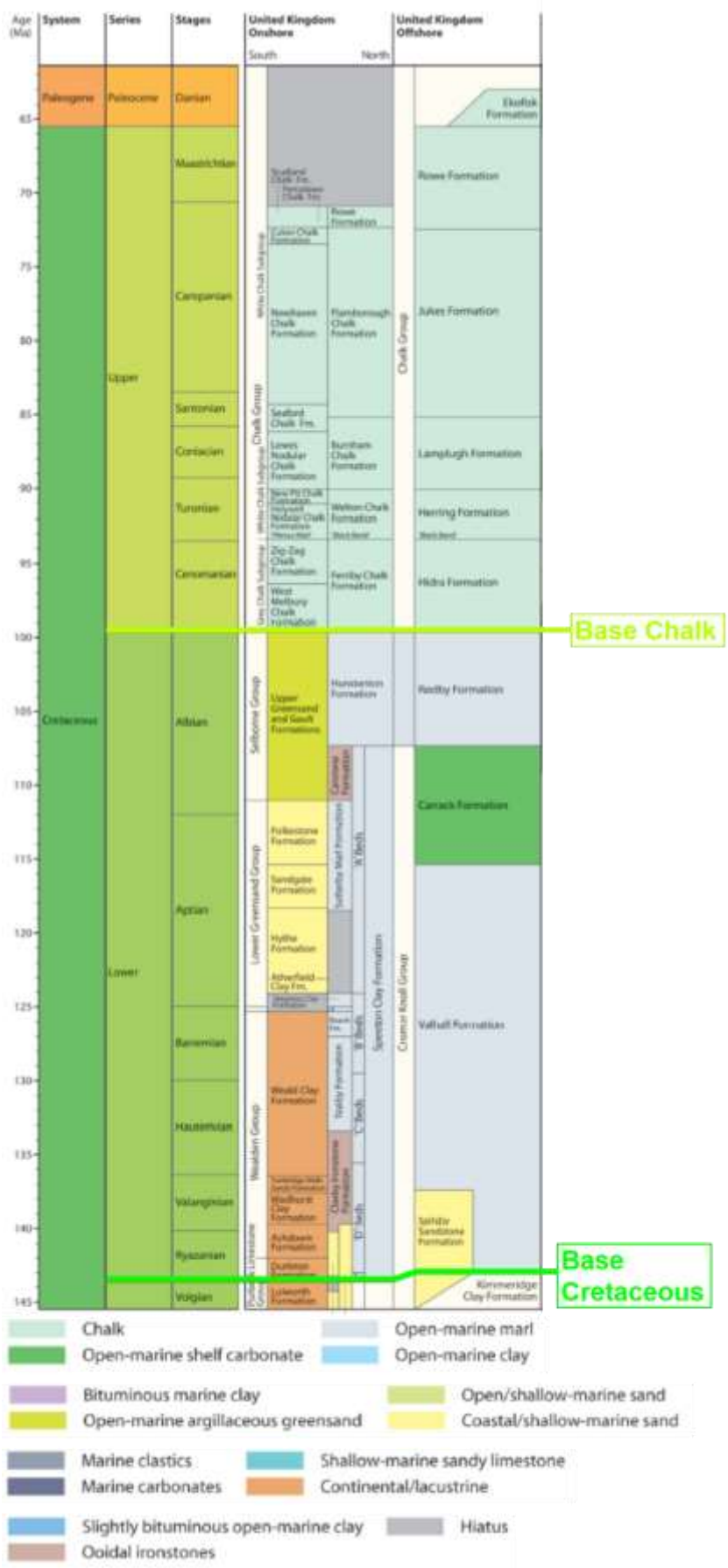

Figure 4.57 Cretaceous stratigraphy with Base Cretaceous and Base Chalk seismic picks shown. Modified after Vejbaek, et al. (2010)

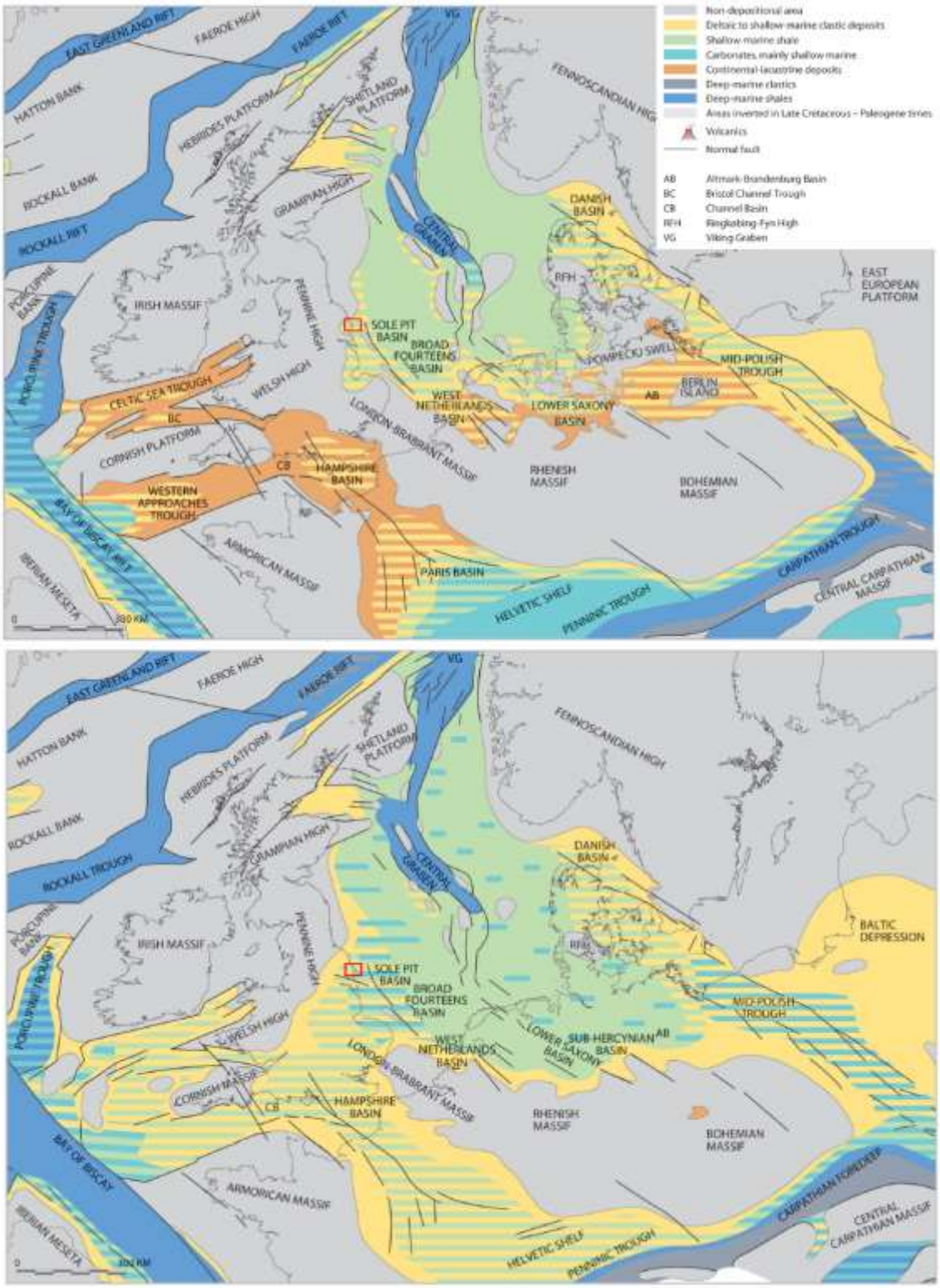

Figure 4.58 Palaeogeography for (above) Berriasian to Barremian times and (below) Aptian to Albian times. Study area shown as red box. See Figure 4.58 for stage age clarification. Modified after Vejbaek, et al. (2010).

The juxtaposition of Lower Cretaceous Cromer Knoll Group Speeton Clay marine marls and Upper Jurassic Kimmeridge Clay Formation marine claystones results in a low acoustic impedance contrast, resulting in a poorly resolvable seismic reflector between these lithologies in places (Figure 4.59).

The majority of interpreted faults terminate at the Base Cretaceous Unconformity, confirming a cessation of rifting in the Lower Cretaceous and the deposition of the Cromer Knoll Group as a post rift tectono-stratigraphic unit (Figure 4.59). Subsidence at this time appears to be strongly influenced by a period of renewed or accelerated Zechstein Group salt movement in the Late Jurassic and through into the Lower Cretaceous. This has resulted in a syn-halokinetic, "canoe" shaped Cromer Knoll Group which is situated directly above the zone of Zechstein Group Z2 salt withdrawal, overburden touch down and the detached Jurassic graben system, showing evidence of growth during deposition and onlap against the Base Cretaceous Unconformity palaeo-topography (Figure 4.59, Figure 4.60 and Figure 4.61). The vertical time thickness for this "canoe" package reaches a maximum of 550ms (Figure 4.60) and the maximum well thickness of 658m is recorded in well 42/27b-2 (Figure 4.62).

The observed halokinesis controlled deposition of the Cromer Knoll Group in this study contradicts previously published work in the Flamborough Head area, which suggests that the deposition of this unit is primarily tectonically controlled (Kirby & Swallow 1987).

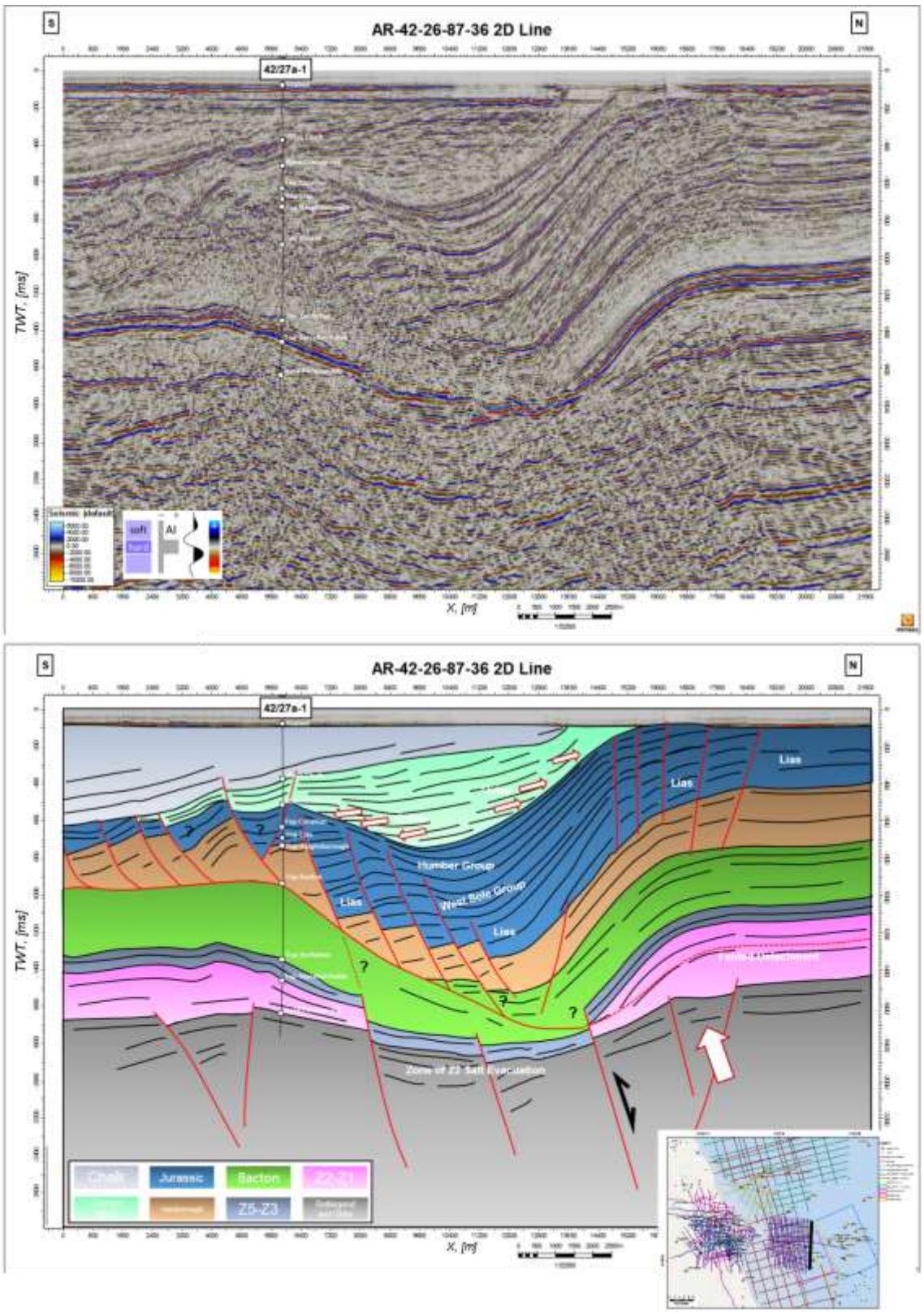

Figure 4.59 (Above) South to north striking un-interpreted regional 2D line AR-42-26-87-36 (Below) interpreted geo-seismic section of same line. Inset shows line location. Note white arrows highlighting onlap of Cromer Knoll Group reflectors against Base Cretaceous Unconformity, poor resolution of Base Cretaceous Unconformity to the south of 42/27a-1 well and position of Cromer Knoll depocenter directly above zone of Zechstein Z2 salt withdrawal. Five times vertical exaggeration. Data courtesy of BP.

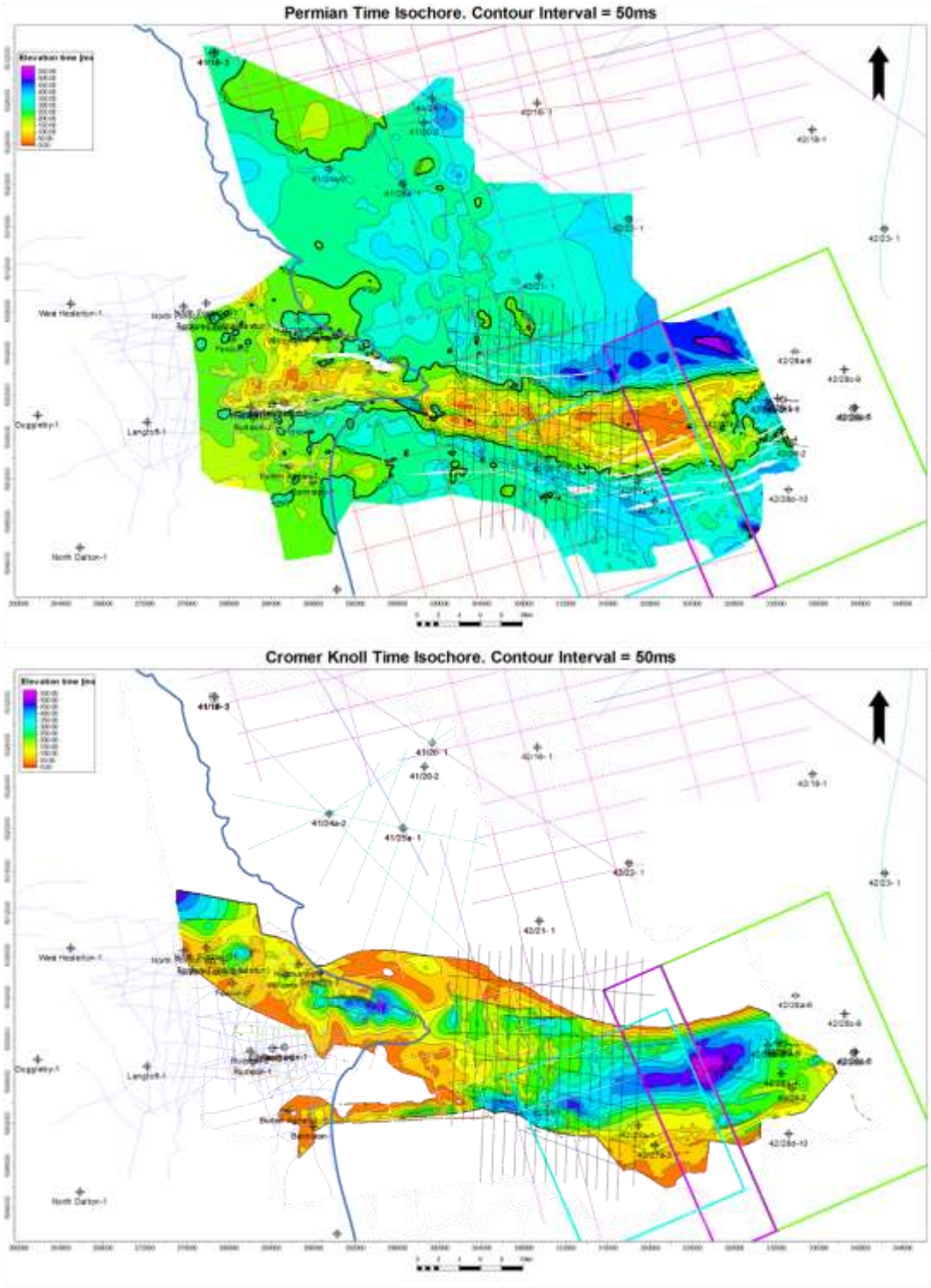

Figure 4.60 (Above) Permian (mainly Zechstein) time isochore, milliseconds TWTT. (Below) Cromer Knoll time isochore, milliseconds TWTT. Note the spatial relationship between where the Zechstein has thinned due to salt withdrawal and maximum Cromer Knoll deposition has occurred. See Appendix B-4 for large-scale plots.

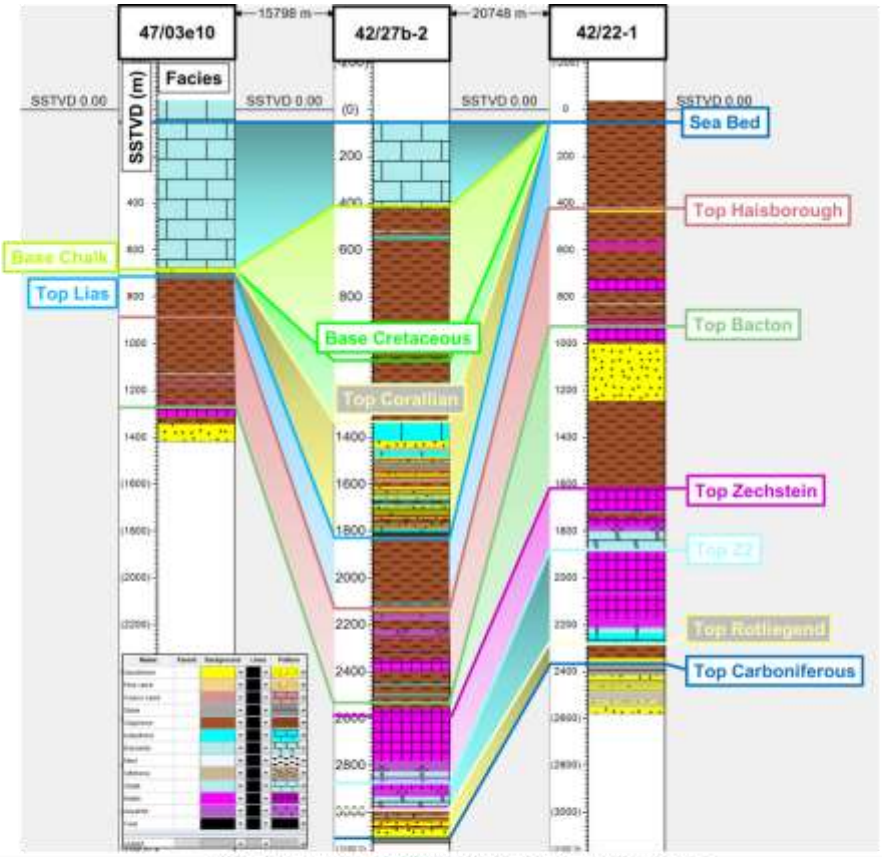

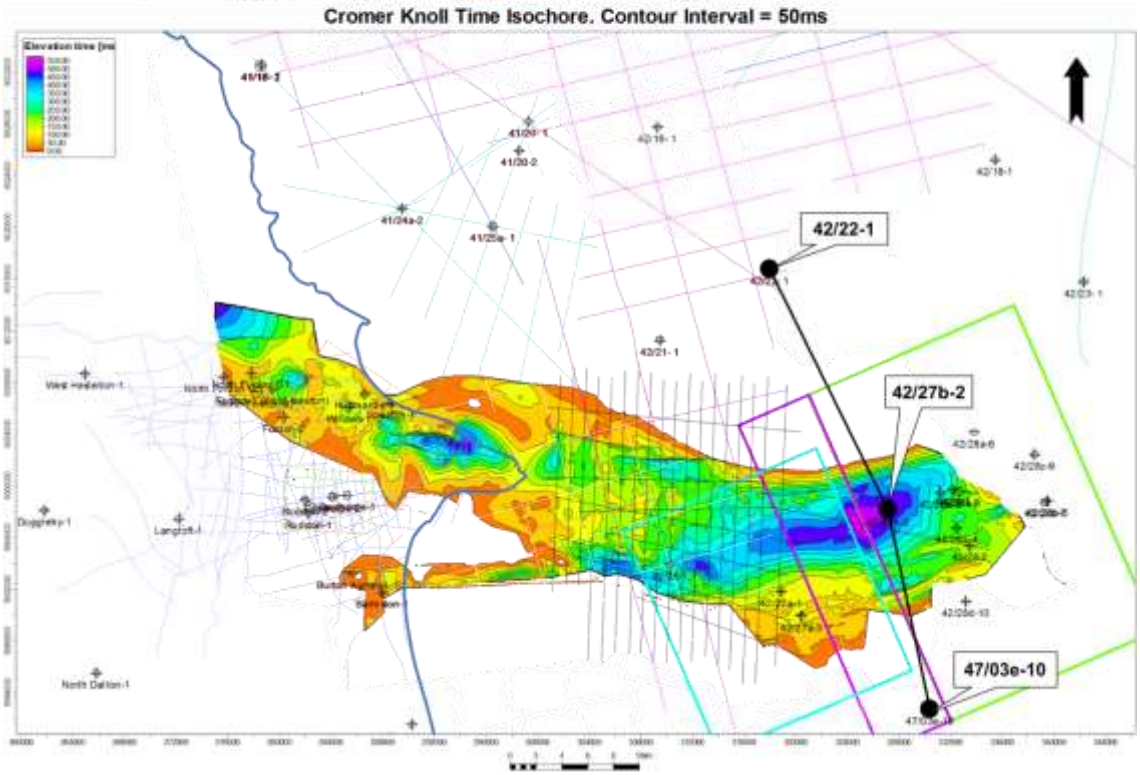

Figure 4.61 (Above) well correlation across the Flamborough Head Fault Zone in metres TVDSS showing interpreted facies. Note development of Cromer Knoll Group above a zone of thin, evacuated Z2 salt. (Below) Cromer Knoll time isochore map showing well correlation location.

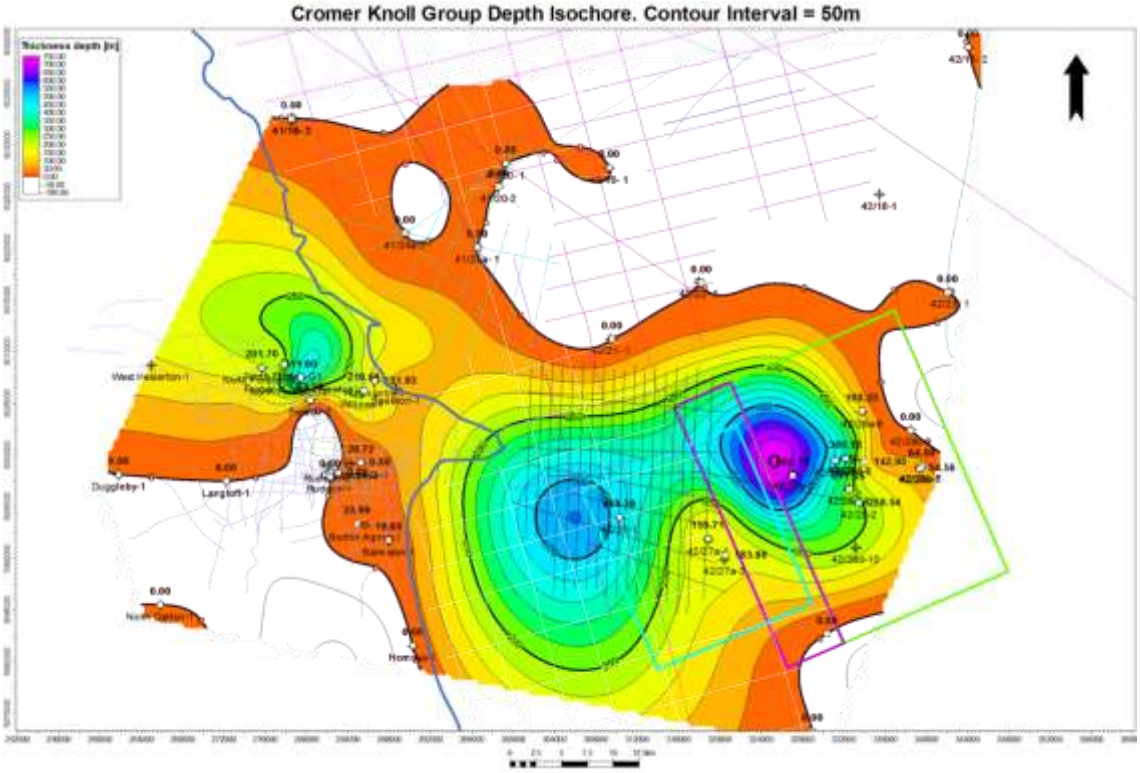

Figure 4.62 Cromer Knoll Group depth isochore from well tops in metres.

4.6.2 Chalk Group

A major global eustatic sea level rise in the Upper Cretaceous resulted in open marine pelagic conditions and the deposition of the Chalk Group, which overlies the Lower Cretaceous Cromer Knoll Group marls and forms the youngest preserved lithostratigraphic unit within the study area (Vejbaek, *et al*. 2010), (Figure 4.57, Figure 4.63). The boundary between the Cromer Knoll and Chalk Groups represents a regionally interpretable seismic pick across the dataset (Figure 4.57, Figure 4.59 Figure 4.61 and Figure 4.64). The nature of this boundary appears to be unconformable in the south of the dataset, with angular truncation of underlying Jurassic reflections beneath lower angled Upper Cretaceous Chalk Group reflectors, observed on seismic profiles to becoming disconformable to the north (Figure 4.52, Figure 4.59). In the 47/08e10 and 47/02-1 wells, Upper Cretaceous Chalks unconformably overlie Middle Jurassic West Sole and Upper Jurassic Humber Groups, respectively (Figure 4.62). This could suggest a period of localised uplift and erosion between the Lower and Upper Cretaceous, with increased erosion on the footwall flanks of the decoupled Flamborough Head Fault Zone graben system. This is compared to the immediate hanging wall to the north, where Lower Cretaceous and Upper Jurassic section is preserved and to the Market Weighton Block to the south, which has Humber Group sediments preserved at well 47/02-1. Due to the documented halokinetic depositional nature of the Lower Cretaceous Cromer Knoll Group, an alternative interpretation could be that erosion of Jurassic sediments occurred

as a result of Late Cimmerian tectonic events at the Base Cretaceous Unconformity which exposed the footwall of the Flamborough Head Fault Zone Graben and led to disconformable deposition of the Cromer Knoll Group in the immediate hanging wall. Subsequent flooding of the basin and chalk deposition during the Late Cretaceous, possibly preceded by middle Cretaceous uplift that masked the effects of the Late Cimmerian uplift, resulting in the present day observed Upper Cretaceous / Jurassic juxtaposition.

Middle Cretaceous uplift has been recorded elsewhere in the Southern North Sea, with combined apatite fission track (AFTA) and vitrinite reflectance (VR) well data suggesting a middle Cretaceous exhumation event beginning between 120 and 93 Ma (Green, Duddy, & Japsen, 2017). However, Green *et al.* (2017) suggest that, based on AFTA and VR well data, middle Cretaceous uplift is restricted to a region east of the Sole Pit Trough. Additionally, the same authors do not recognise an episode of Early Cretaceous exhumation using this technique. Therefore, this suggests that, in the study area, and based on the seismic and well data, Cretaceous uplift has occurred that is not represented locally by AFTA and VR results, possibly due to under sampling of wells in the Green *et al*. (2017) study or that exhumation at these times has been overprinted by Late Cretaceous to Cenozoic burial (Green, *et al*. 2017).

Uplift at this time has attributed to reactivation of NW – SE striking basement trends (such as the Tornquist trend fault zone) through NW – SE transpression, the result of far-field stresses from the onset of subduction along the northern Tethyan margin in southern Europe and the opening of the Bay of Biscay through sea-floor spreading (Vejbaek, *et al*. 2010).

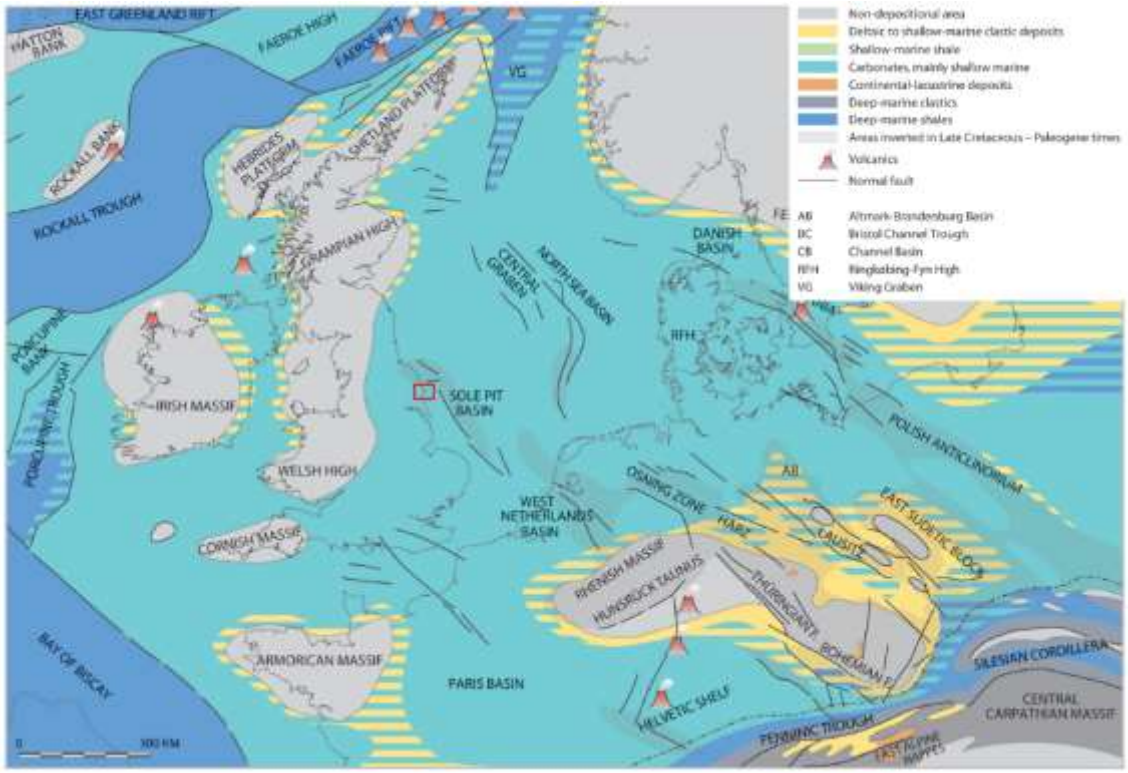

Figure 4.63 Palaeogeography for Cenomanian to Danian times. Study area shown as red box. Modified after Vejbaek, et al. (2010).

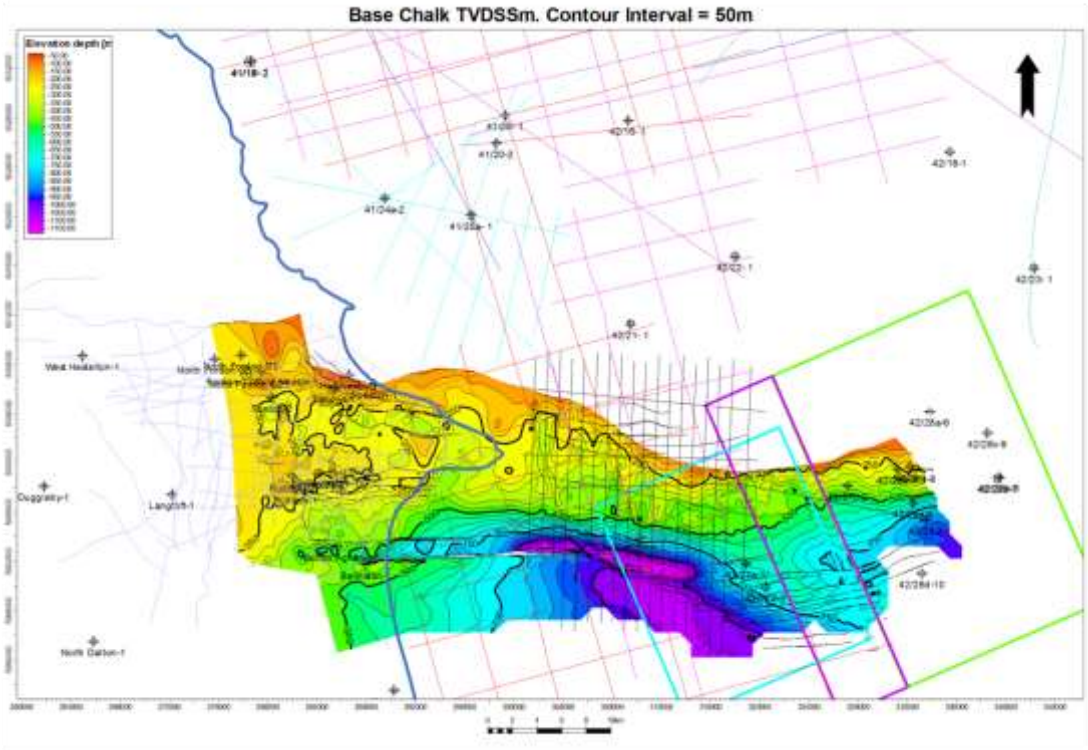

Figure 4.64 Well-tied Upper Cretaceous Chalk depth surface grid, metres TVDSS. Absence of data to north is due to erosional truncation through tertiary inversion. Southern limit is an interpretation clip. See Appendix E-3 for large-scale plot.

The Upper Cretaceous Chalk Group is characterised by inclined, laterally continuous seismic reflectors (Figure 4.59). The inclination of chalk seismic reflectors suggests that post depositional tilt and inversion in the Cenozoic has completely removed Upper Cretaceous Chalk in the north of the dataset and into the Cleveland Basin with the chalk sub-cropping the seabed in a west to east orientation (and dipping to the south) above the Bempton Fault of the Flamborough Head Fault Zone (Figure 4.59, Figure 4.64, Figure 4.65 and Figure 4.69). The Chalk Group reaches a maximum vertical time thickness of over 650ms (Figure 4.65) and a maximum recorded well thickness of 812m in well 42/28-2 (Figure 4.66) thinning in a wedge to zero at its seabed subcrop. This suggests that at least 800m of Chalk Group sediments have been removed across Flamborough Head during post depositional inversion.

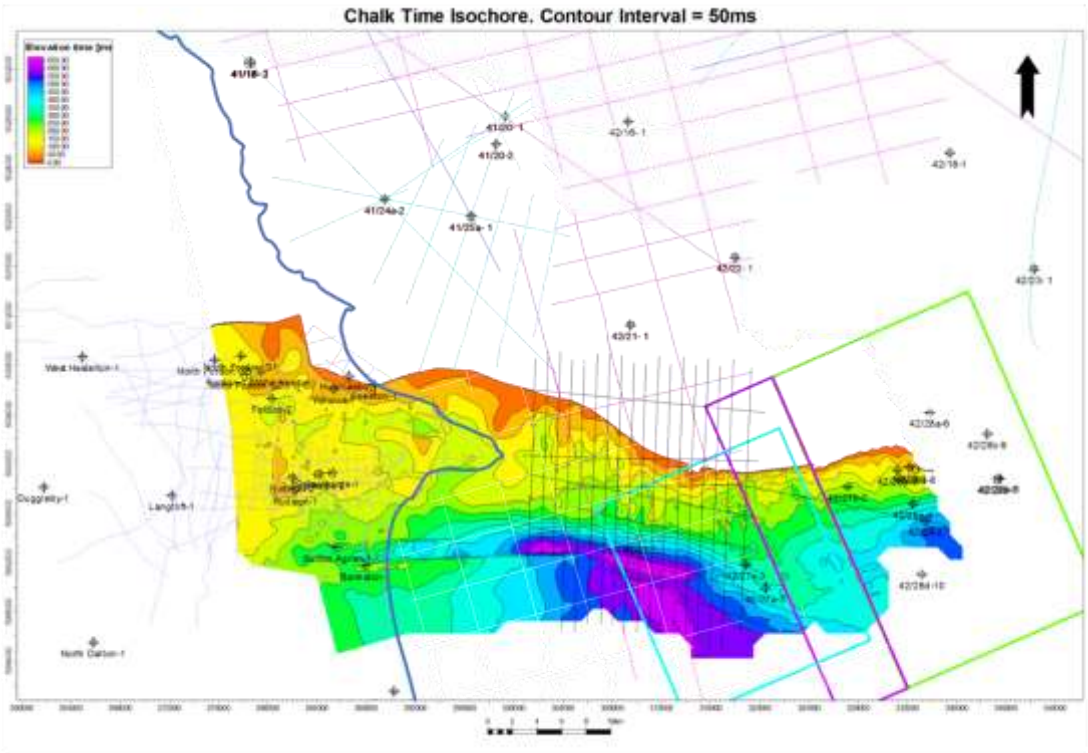

Figure 4.65 Chalk Group time isochore, milliseconds TWTT. See Appendix B-3 for large-scale plot.

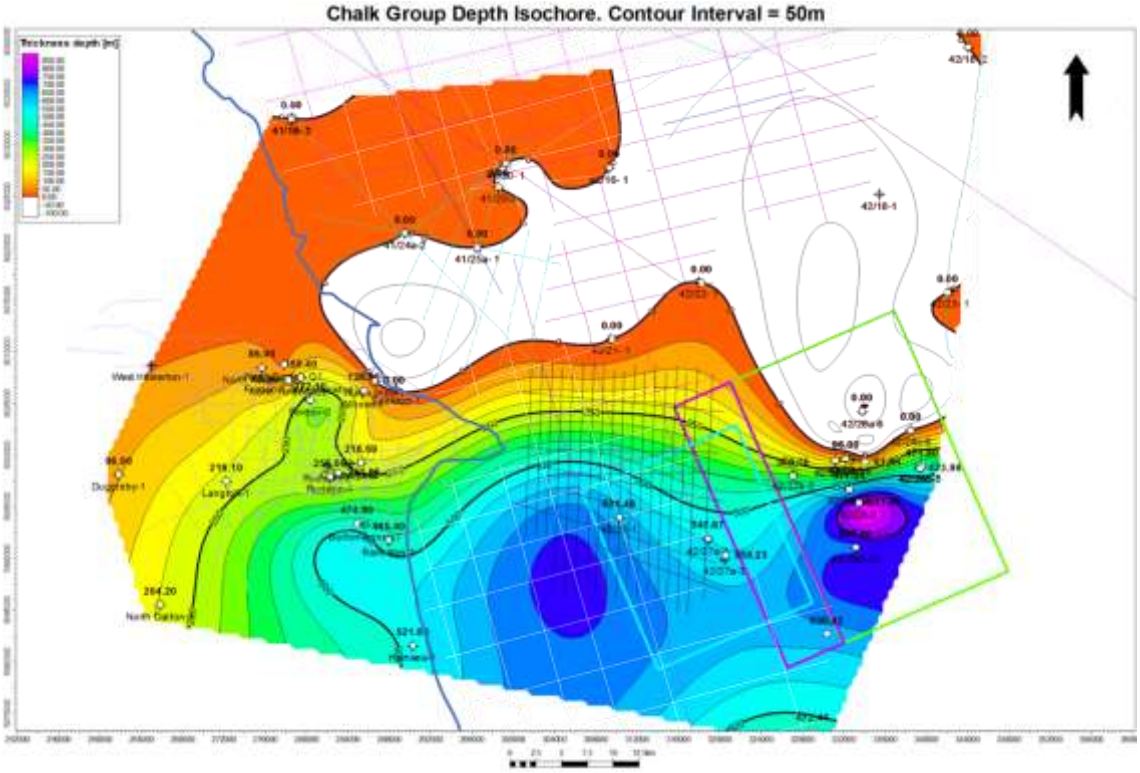

Figure 4.66 Chalk Group depth isochore from well tops in metres.

4.7 Cenozoic

No lithostratigraphic units younger than the Upper Cretaceous have been preserved across Flamborough Head and the study area therefore precluding any analysis of the Cenozoic depositional history. Cenozoic strata are preserved elsewhere in the Southern North Sea, most notably at the Flamborough Tertiary outlier, located 50km from the Flamborough Head coastline, where up to 700m of Cenozoic deposits are located and are believed to be the remnants of a more extensive Paleogene cover that reached over 2,000m thickness in the centre of the Southern North Sea basin (Stewart & Bailey 1996).

Removal of Cenozoic sediments regionally and across the study area is the product of major regional and local basin reconfiguration events that affected the British Isles post-Upper Cretaceous Chalk Group deposition. On the regional scale, the British Isles were subjected to a regional tilt to the south-east during the Paleocene, attributed to the initiation of the proto-Iceland hotspot in the North Atlantic (Underhill 2003). The effects of Cenozoic regional tilt is evident both on a small scale within the study area, with the highest topography of regional seismic surfaces seen in the north west and lowest topography in the south east (Figure 4.67) and on a greater scale from composite regional seismic profiles which clearly show a tilting of strata to the south-east (Figure 4.68). On the local scale, post-Upper Cretaceous Chalk Group uplift and inversion of the Cleveland Basin has affected the north of the study area, with erosion down to the Lower Jurassic

Lias Group in the hanging wall of the Flamborough Head Graben System (Figure 4.69). This structural inversion of the Cleveland Basin relative to the Market Weighton Block is clearly defined on regional composite seismic profiles (Figure 4.70).

The removal of Cenozoic sediments across Flamborough Head from during this inversion also precludes analysis of Cenozoic uplift history through seismic reflection interpretation alone and will therefore be discussed in detail in Chapter 5 below.

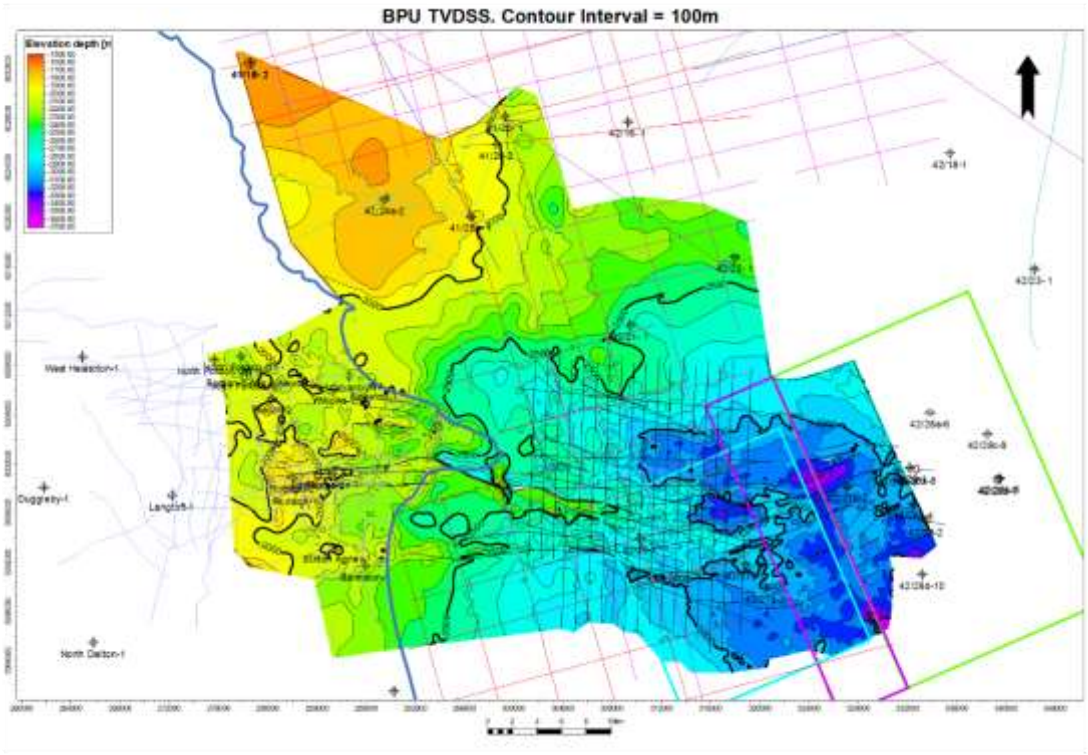

Figure 4.67 Base Permian unconformity depth map in metres TVDSS. Note evidence of tilt to the SE with highest structural elevation in the NW and lowest in the SE

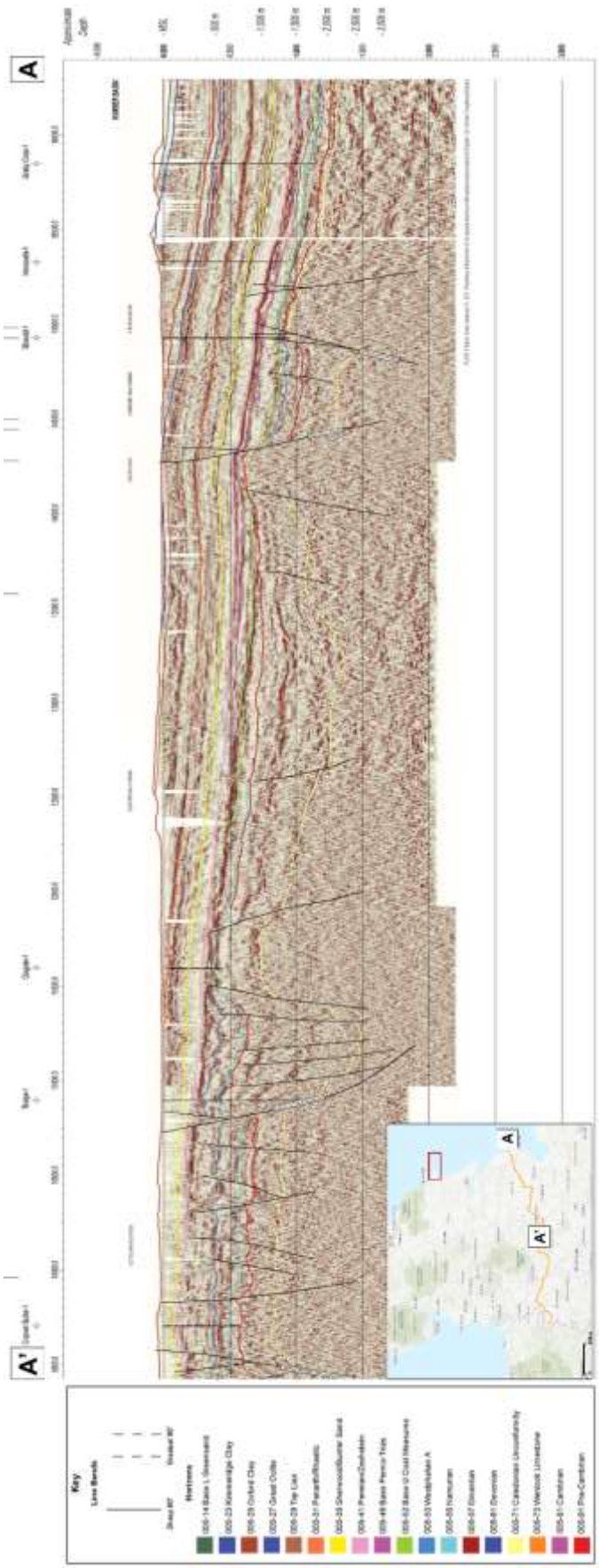

Figure 4.68 West to east striking regional 2D seismic profile with UKOGL interpretation. Note clearly defined easterly tilt of strata. Inset shows line location relative to Flamborough Head study area (red box). Modified after Butler & Jamieson (2013).

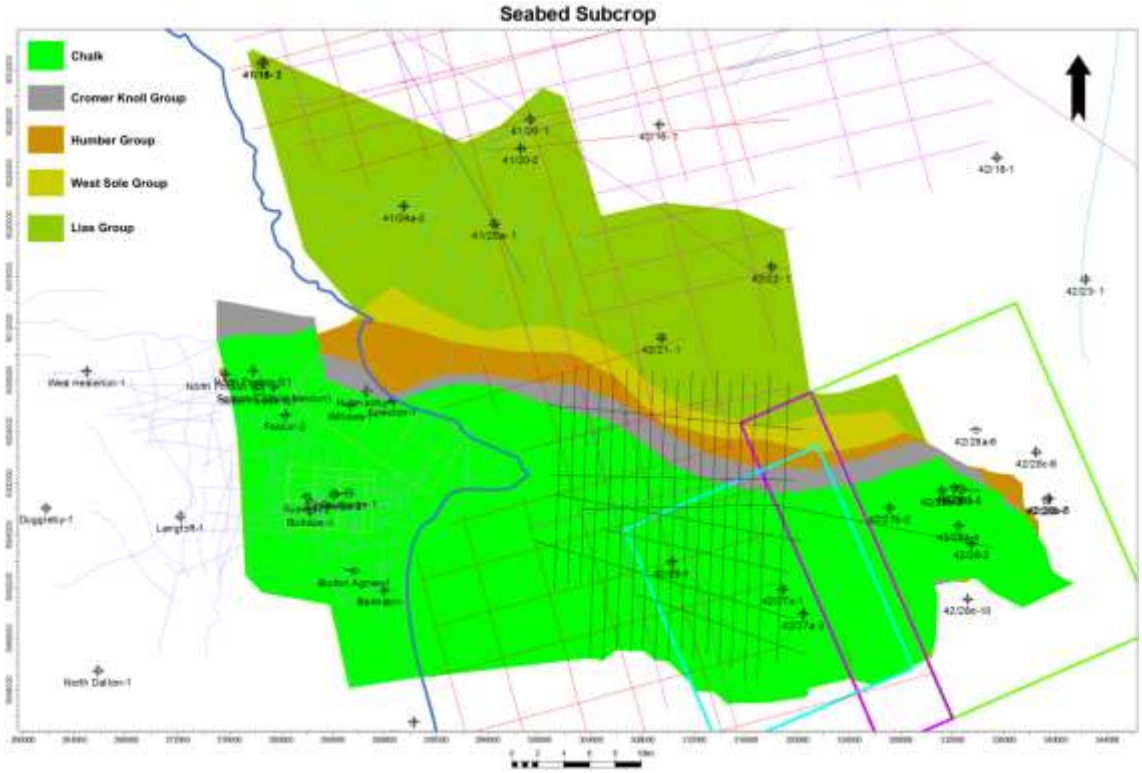

Figure 4.69 Interpreted seabed subcrop map. Edge limits of polygons represent interpretation clip rather than extent of rock units.

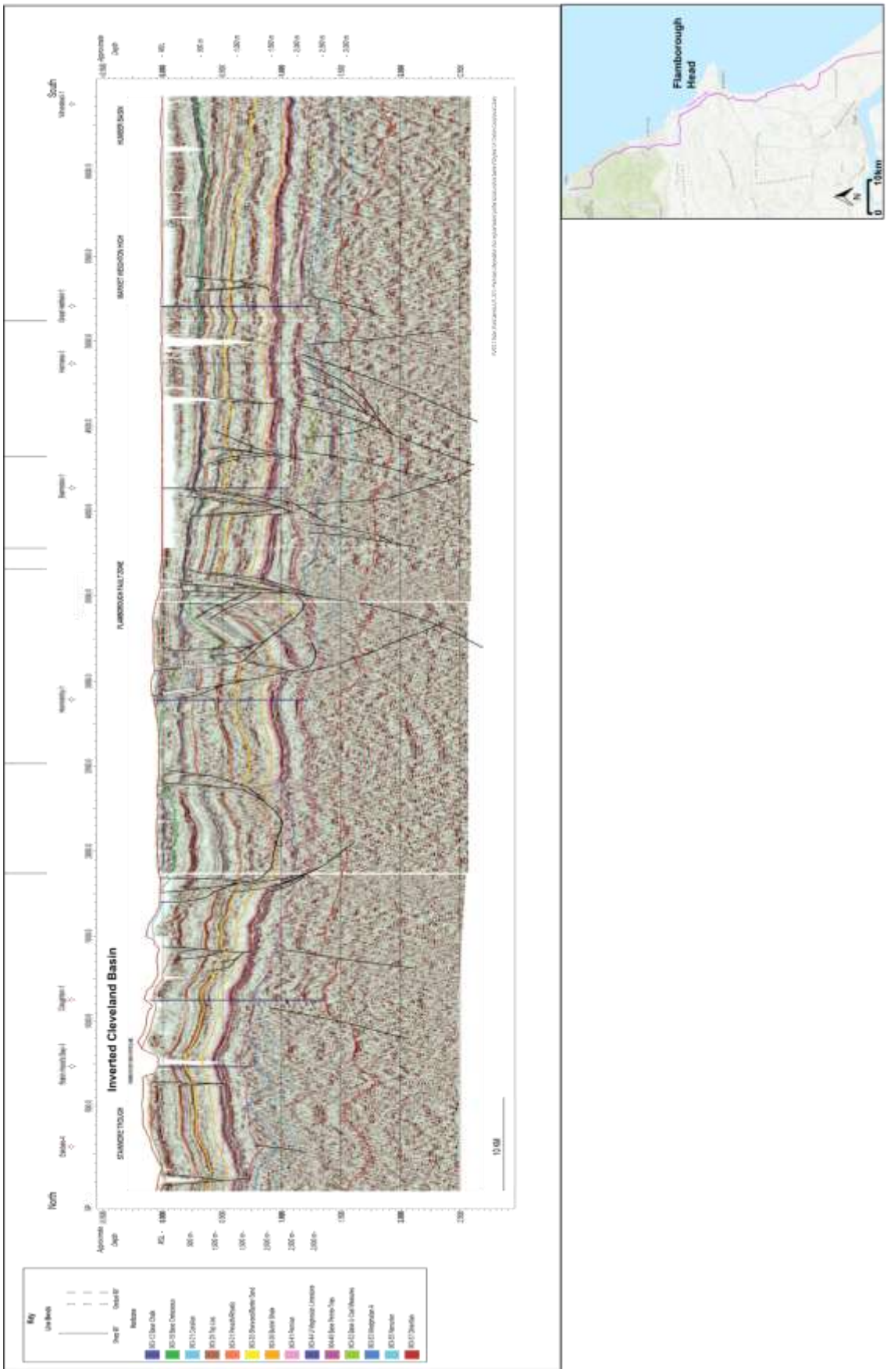

Figure 4.70 North to south striking regional interpreted seismic line highlighting the structural inversion of Cleveland Basin relative to the Market Weighton Block. Inset displays line location. Modified after Butler & Jamieson (2013).

4.8 Conclusions

In summary, the geological history of Flamborough Head area can be broadly defined as two periods of major tectonic inversion and basin reconfiguration, one at the end of the Carboniferous, attributed to Variscan uplift, and another post Upper Cretaceous Chalk Group deposition. Sandwiched between these two regional tectonic uplift events is a period of relatively continuous sedimentation of carbonates, evaporites and siliciclastics from the Permian to the Upper Cretaceous, punctuated by hiatuses during the mid and late Cimmerian and the mid-Cretaceous. A schematic summary of the structural evolution across the Flamborough Head Disturbance is shown in Figure 4.71.

Intraplate extension in the Lower Permian resulted in the formation of the North and South Permian Basin and the deposition of the arid, continental Rotliegend Group (Figure 4.71a). This creates a pattern of west to east trending planar faults in the Permo-Carboniferous pre-salt that extend from onshore Flamborough Head into the offshore, marking the hinge zone boundary between the Market Weighton Block and the Cleveland Basin. Displacement sense on these pre-salt faults appears to be predominantly normal, with little observed evidence to support a strike-slip tectonic regime. These faults may have been active during Permian Rotliegend Group deposition and controlled the distribution of the Leman Sandstone Formation hydrocarbon reservoir unit and the Silverpit Claystone Formation caprock unit (Figure 4.71a). Thermal subsidence in the Upper Permian led to the development of an evaporitic basin characterised by repeated cycles of marine incursion, regression and evaporation (Figure 4.71b).

Intraplate extension and thermal subsidence in the Triassic resulted in continental red bed deposition of the Bacton and Haisborough Groups, forming a pre-rift succession (Figure 4.71c). Basin tilt to the north east during the Late Triassic due to basement extension initiated Permian Zechstein Group salt movement and the creation of the detached post-salt listric faults and a post salt cover sequence that is free to move on Zechstein Group salt in relation to the basement (Figure 4.71d). A Late Triassic depocenter was developed to the east of the study area, in the Sole Pit Trough.

Continued detached listric faulting in the Lower Jurassic created a west to east trending Mesozoic graben system and onset of the creation of the Cleveland Basin, characterised by Lower Jurassic syn-rift deposition of the Lias Group marine marls (Figure 4.71e). The decoupled post-salt graben is characterised by a northward throwing main west to east

striking listric faults system and a southward throwing antithetic listric system that both detach into both Permian and Triassic evaporite units, creating a thin-skinned extensional system. The timing and physical nature of Cleveland Basin formation bears strong resemblances to the Wessex Basin. Regional uplift in the Middle Jurassic, due to the thermal effects of the rising Central North Sea Dome, resulted in marine regression and deposition of West Sole Group fluvio-deltaic sediments and the rejuvenation of the NNW-SSE striking Peak Trough collapse graben, visible in the west of the dataset. It is proposed that the Zechstein shelf edge played a part in controlling the distribution of Peak Trough Faulting. Intraplate extension in the Late Jurassic, coupled with a major marine transgression, led to the deposition of the Kimmeridge Clay Formation of the Humber Group.

Extensional faulting ceased in the Late Jurassic and was replaced by thermal subsidence and rift infill. A period of post-rift halokinesis through Permian Zechstein Group salt withdrawal and diapirism created a "canoe"-shaped depression above the Mesozoic Graben, which was filled by Lower Cretaceous post-rift – syn-halokinetic deposits (Figure 4.71f). A major marine transgression in the Upper Cretaceous resulted in the widespread deposition of the Chalk Group (Figure 4.71g).

Regional and local scale basin reconfiguration episodes post Upper Cretaceous Chalk deposition imparted a regional south-easterly tilt to the UK and uplifted and inverted the Cleveland Basin, folding the post-Carboniferous strata into a monocline, with erosion completely removing the Chalk Group north of Flamborough Head and eroding down to Lower Jurassic Lias Group units while also inverting and folding the Zechstein Group salt detachment of the Flamborough Head Graben System (Figure 4.71h). The influence of regional tilting is recorded across the entire dataset, whereas only the Cleveland Basin and the hanging-wall of the Flamborough Head Fault System displays evidence of deformation associated with inversion, with the footwall basement and cover faults appearing to have remained in net extension (Figure 4.71h).

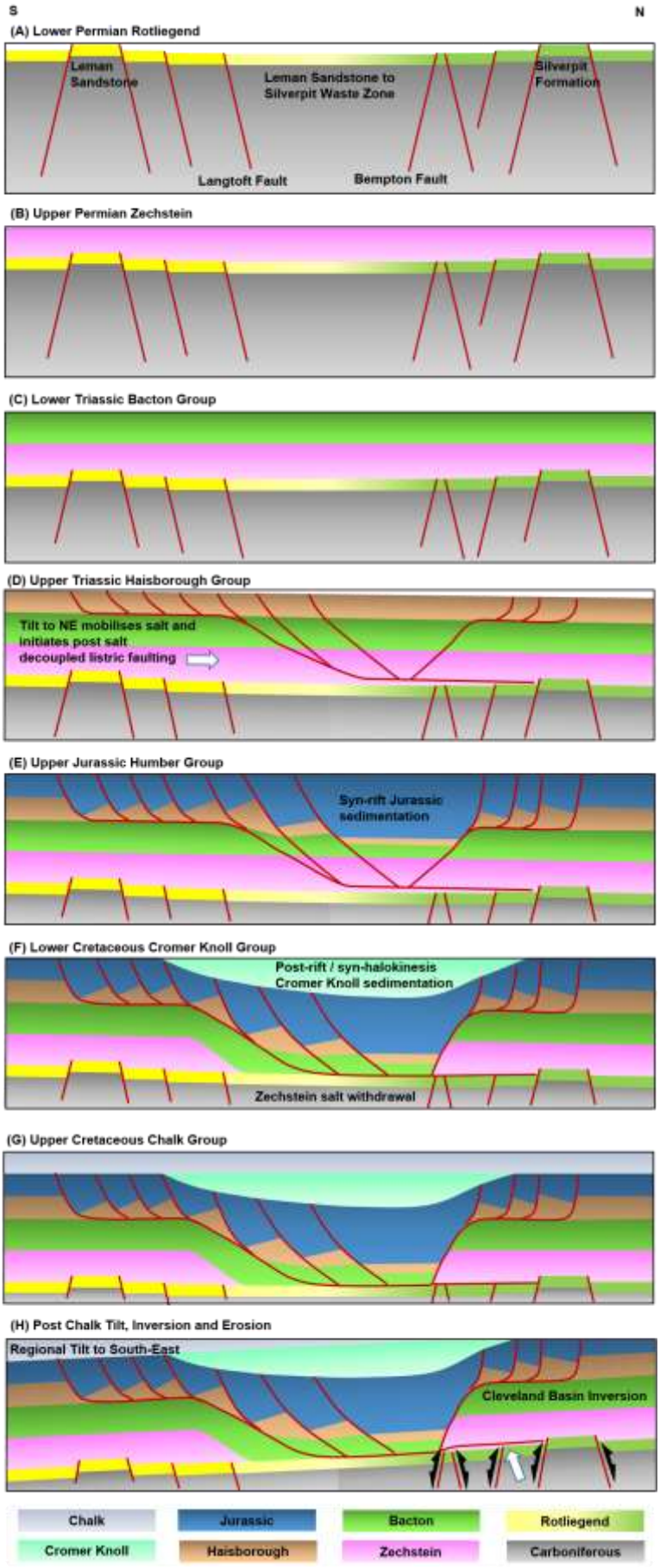

Figure 4.71 Structural evolution history of Flamborough Head region. Not to scale.

CHAPTER 5. DISCUSSION

5.1 Timing, Magnitude and Genesis of Uplift

As described and documented in Chapter 4, following the deposition of the Upper Cretaceous Chalk Group, the study area has been affected by regional uplift and tilt to the south-east and structural inversion of the Cleveland Basin. The impact of regional tilting clearly extends across the entire dataset, as evident by the ubiquitous inclined seismic reflectors across all stratigraphic levels, and also based on evidence from onshore geological mapping and regional seismic profiles (Figure 4.68). The effects of uplift resulting in basin inversion are shown to have a more localised influence, restricted to the hanging wall of the Flamborough Head Fault Zone and northwards into the Cleveland Basin. The footwall of the Flamborough Head Fault Zone appears to be undisturbed by the effects of structural inversion and with basement and cover faults remaining in net extension. The differences in the geographical distribution of the deformation associated with regional tilting and basin inversion strongly suggests that these are two discrete, basin reconfiguration episodes that have impacted upon the study area. Constraining the timing and magnitude of Cenozoic south-easterly regional tilt and basin uplift and structural inversion in the Southern North Sea has been attempted in previous research, often with conflicting results. For instance, regional south-easterly tilting of the UK has been dated from the late Maastrichtian (Cope 1994; Stewart & Bailey 1996) to the Paleocene (Underhill 2003; Gale & Lovell 2017) and undefined Cenozoic (Kirby & Swallow 1987). A late Maastrichtian age for the initiation of regional tilt is based upon the absence of late Maastrichtian strata across Britain and Northern Ireland and is inferred to have occurred in response to the development of a conceptual mantle hotspot beneath the Irish Sea, at this time (Cope 1994). Evidence for regional tilt being initiated during the Paleocene is more robust, as it can be attributed to the development of the known proto-Iceland hotspot and tilting, and exhumation at this time can also be used to explain the easterly sediment dispersal of Paleocene aged submarine fans into the North Sea Basin and the provenance of hinterland that acted as a sediment source (Underhill 2003). Further constraining the age of regional tilt, based on the interpreted dataset used in this study, is difficult due to the aforementioned loss of post-Chalk Group stratigraphy. A Paleocene aged regional tilt and exhumation would also be consistent with a regional exhumation event recognised from apatite fission track analysis of borehole samples from the Southern North Sea that has been dated as Paleocene (Green, *et al*. 2017).

Based on seismic reflection and borehole interpretation, it has been proposed that the Sole Pit Basin was inverted in the Late Cretaceous (Glennie & Boegner 1981), further refined to occurring between the Turonian and Campanian, and inversion was repeated again in the Oligocene, resulting in a total uplift of 1,500m (van Hoorn 1987). An Eocene to Oligocene age for the main phase of inversion of the Sole Pit Basin has also been proposed (Ziegler 1989). Through the interpretation of seismic reflection and borehole biostratigraphy data of an outlier of Cenozoic sediments, called the Flamborough Tertiary Outlier, inversion events have been proposed during the intra-Campanian, late Maastrichtian and intra-Miocene (Stewart & Bailey 1996). Subsurface study of East Yorkshire and Lincolnshire has suggested a late Cretaceous to early Cenozoic age for the inversion of the Cleveland Basin (Kent 1980). Previous work involving the interpretation of an onshore 2D seismic profile across Flamborough Head has proposed a late Cretaceous inversion of the Cleveland Basin and eastward tilting during the Cenozoic (Kirby & Swallow 1987). Study of deformation structures in the Upper Cretaceous Chalk Group outcrops at Flamborough Head has led to the proposal of a Cenozoic age for the development of tilting and the structural inversion of the Cleveland Basin, with both features being contemporaneous (Starmer 1995; 2008 and 2013). Research involving the integration of apatite fission track analysis (AFTA) and vitrinite reflectance (VR) from Southern North Sea wells suggests uplift occurring in the mid-Cretaceous (beginning between 120 and 93 Ma), the mid-Paleocene (beginning between 63 and 59 Ma) and in the early Miocene (beginning between 22 and 15 Ma) (Green, *et al*. 2017) with estimated Cenozoic exhumation of over two kilometres in the Southern North Sea (Hillis, *et al*. 2008).

Although the estimated timings for the onset of exhumation varies between researchers, it is clear that most recognise a complex and multiple-phase uplift history for the Southern North Sea. The tectonic processes and stress regimes that have resulted in reported uplift events are discussed below.

5.2 Inversion Kinematics and Analogues

The structural kinematics and the stress regimes that have ultimately caused the uplift and tectonic inversion are also subject to debate. Glennie & Boegner (1981) attribute Late Cretaceous inversion of the Sole Pit Basin to east-west compression encompassing left-lateral fault movement followed by north-south right-lateral movement based on evidence of observed drag folds and Riedel shears associated with major faults. Van Hoorn (1987)

also observes right-lateral wrench-induced flower structure fault systems at the Rotliegend level in the Sole Pit Basin. Glennie & Boegner (1981), attribute this multiple-phase timing to far field compressive stresses associated with North Atlantic opening events for their earlier recorded uplift phase and right-lateral movements resulting from stresses associated with the Alpine orogeny for their second recorded exhumation episode.

Kent (1980) has proposed that late Cretaceous to early Cenozoic inversion of the Cleveland Basin is the result of a short-lived compressional phase associated with a transition from a dextral to sinistral stress regime in northern Europe at this time, taking advantage of existing lines of weakness, particularly deep-seated faults. Kent (1980) argues that geometrical reconstructions do not suggest that significant shortening has taken place in the Cleveland Basin and that the widely varying range of strike of inverted troughs from north-south to east-west rules out simple lateral compression. Based on sparse borehole coverage at the time, Kent (1980) also proposes a "double inversion" event whereby a Late Carboniferous Variscan uplift event that removed significant amounts of Westphalian Group strata in the Cleveland Basin area relative to the Market Weighton Block, was focussed along the same structural trends as the Cenozoic structural inversion (Figure 5.1). Although the Base Permian Unconformity map, derived from borehole data and shown in Figure 5.1 demonstrates increased erosion of Upper Carboniferous strata within the Cleveland Basin area, it is difficult to validate from the poor quality seismic data at this level, the Kent (1980) hypothesis that Variscan inversion was focussed along the same structural trends as the Cenozoic inversion from the poor quality seismic data at this level is challenging. Seismic profiles appear to highlight the increased deformation of Carboniferous reflectors in the footwall of the Flamborough Head Fault Zone, relative to the hanging wall (Figure 4.2 and Figure 4.4), tentatively suggesting that Variscan fold generation and subsequent levelling occurred independently of the Flamborough Head Fault Zone. However, the proposition that the Market Weighton Block granite was emplaced during late Caledonian (early Devonian) times (Donato 1993), prior to Variscan inversion and that it imparted a tectonic control on Carboniferous sedimentation (Bott, *et al*. 1978) suggests that it could potentially influence Variscan inversion by acting as a buttress during structural inversion of the Flamborough Head Fault Zone. This would therefore inhibit deformation in the footwall of the Carboniferous Cleveland Basin. This proposal, combined with the observation that Variscan compression in northern England is expressed as large-scale anticlines within

the hanging walls of basin bounding faults (Fraser & Gawthorpe 2003) adds weight to Kent's (1980) "double inversion" hypothesis in this area.

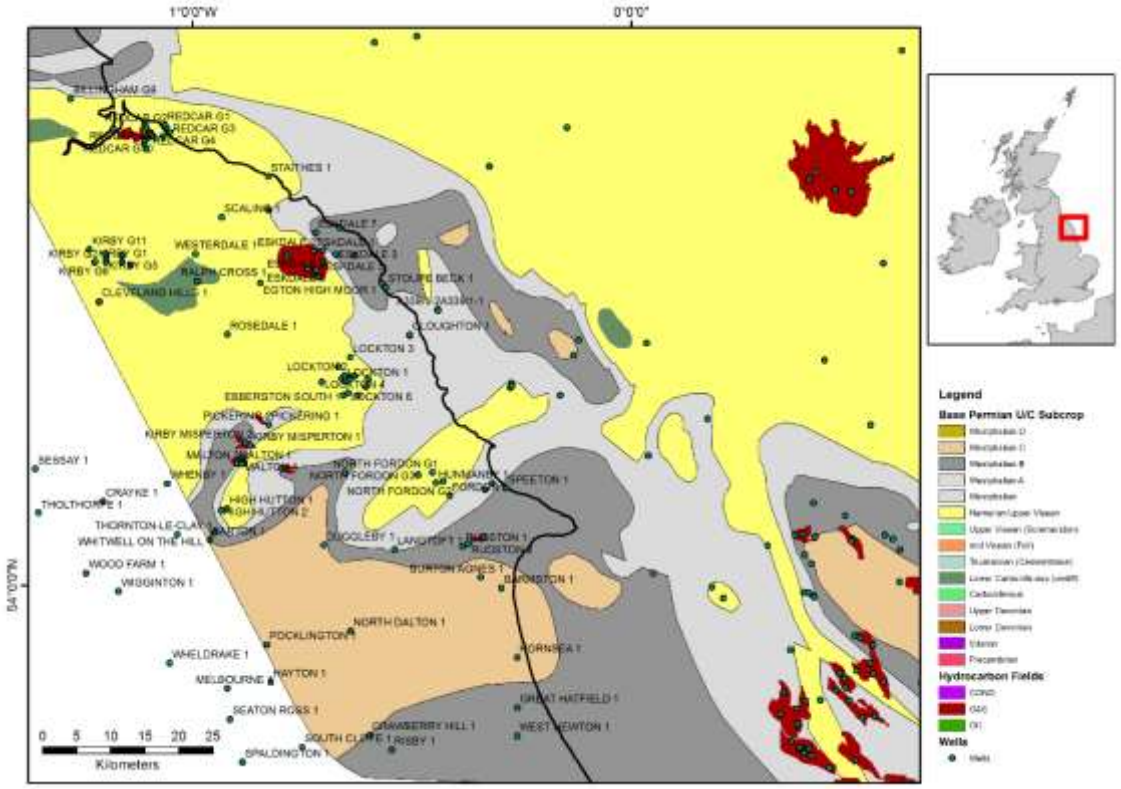

Figure 5.1 Base Permian Unconformity subcrop map highlighting removal of Upper Carboniferous Westphalian Group strata in the Flamborough Head / Cleveland Basin region relative to the Market Weighton Block in the south. Data courtesy of British Geological Survey and Oil & Gas Authority.

In their investigation of an onshore 2D seismic profile at Flamborough Head, Kirby & Swallow (1987) recognise the effects of structural inversion of the Cleveland Basin and regional tilting, but do not satisfactorily address the genesis of each. The authors propose that deformation seen at outcrop at Flamborough Head may be the result of transcurrent reactivation of the Bempton Fault of the Flamborough Head Graben System. This inference is based on the authors' observation of an interlocking, arcuate fault distribution in plan view along with splaying of faults (Kirby & Swallow 1987). Kirby & Swallow (1987) also recognise that Late Cretaceous sinistral transpression and inversion occurred on the Dowsing Fault Zone in the Sole Pit Trough (Glennie & Boegner 1981) but do not correlate this event with uplift at Flamborough Head, but instead attempt to relate it to the onset of extensional faulting at this location. The authors use the age discrepancy between Late Cretaceous sinistral transpression at the Dowsing Fault Zone and earlier Mesozoic extensional faulting at Flamborough Head to rule out a relationship between transcurrent

motion on the Dowsing Fault Zone and the initiation of extensional faulting at Flamborough Head.

Field observations of deformation in the Upper Cretaceous Chalk Group at Selwicks Bay (Starmer 1995), Staple Newk (Starmer 2008) and Dykes Head (Starmer 2013) at Flamborough Head has led that author to derive a complex multiple-phase uplift history. Starmer (1995, 2008, and 2013) uses the Kirby & Swallow (1987) subsurface interpretation as a control on the interpretation of his field observations but also attempts to relate the observed field deformation to regional events. For instance, Starmer (1995, 2008, and 2013) infers that deformation observed in the Chalk Group outcrop at Selwicks Bay, such as NNW-SSE buckles with localised overturned folds and minor thrusting, is the result of sinistral reactivation of the pre-Chalk Group E-W Flamborough Head fault complex, specifically the Langtoft Fault. This reactivation is proposed to be a response to ENE-WSW compression due to Late Cretaceous to Paleocene sinistral transpression along the Dowsing Fault Zone, inversion of the Sole Pit Basin and N-S to NNE-SSW folding in the Cleveland Basin (Starmer, 1995; 2008 and 2013). Starmer also interprets a younger phase of compressive deformation in the Chalk Group represented by broadly E-W folding and N-S thrusting being caused by dextral transpressional reactivation of the Bempton Fault, as a response to N-S Oligocene aged Alpine compression. Starmer (1995) infers a period of post-Alpine tension from observed N-S faulting that is the result of E-W tension related to easterly tilting due to North Sea subsidence. This fault system underwent dextral strike-slip motion, the result in a switch to N-S tension as a result a of structural inversion of the Cleveland Basin, causing hinging across the Flamborough Head Fault Zone and a tilt to the south that was superimposed onto a regional tilt (Starmer 1995) that has been described above.

Based on their AFTA and VR analysis of Southern North Sea well samples, Green *et al.* (2017) postulate that mid-Cretaceous exhumation is the result of intra-plate compression related to a global-scale plate reorganisation. The same authors also propose that their identified Paleocene exhumation is the result of intra-plate compression related to regional tectonic events, because it is recorded across different regions. They propose that this regional extent of the Paleocene uplift evidence discounts uplift due to an igneous plate underpinning related to the Iceland Plume (Jones, *et al*. 2002) as the major contributor to Cenozoic exhumation. This is because the observed amount of Paleocene exhumation affects a wider area than predicated from igneous plate underplating (Hillis,

et al. 2008). Hillis *et al.* (2008) state that the timing and lack of structural control of Paleocene exhumation in the Southern North Sea is consistent with Iceland Plume plate underplating as a cause and cannot be ruled out, but that a regional component is also required due to the observed compressional structures. However, recent seismic interpretation in the Moray Firth Basin shows clear evidence of early Cenozoic uplift in the form of a pronounced easterly dip of the basin that has been attributed to the development of the proto-Iceland plume on the Atlantic Margin (Guariguata-Rojas & Underhill 2017). Hillis *et al* (2008) suggest that strain partitioning between the crust and the lithospheric mantle (heterogeneous lithospheric shortening) may represent the regional component of Cenozoic uplift in the Southern North Sea. The regional cause of the Neogene exhumation in the Southern North Sea as recorded from AFT analysis of well samples is unclear, but may either be a result of strain partitioning between the crust and the mantle or a dynamic topographic response to convective flow in the upper mantle beneath the Atlantic margin (Hillis, *et al*. 2008).

It is clear, from the evidence documented above, that there are a range of hypotheses for the causal effects of basin tilt, uplift and structural inversion in the Southern North Sea and Cleveland Basin and that no definitive answer has been presented. The absence of any Cenozoic aged units across the study area precludes any seismic-based validation of Cenozoic uplift. The presence of inclined bedding plane reflectors in the Upper Cretaceous Chalk and older strata, and the clearly defined south-easterly basinal dip seen locally in the study area (Figure 5.2 and Figure 5.3) and more regionally (Figure 4.68), is evidence of a far-reaching tilting and exhumation event that has been variously dated as initiating in the Late Cretaceous (Cope 1994; Stewart & Bailey 1996) and Early Cenozoic (Underhill 2003; Guariguata-Rojas & Underhill 2017); (Green, *et al*. 2017). Based on the available data, the onset of regional titling that affected the Flamborough Head study area can only definitively be described as occurring post Upper Cretaceous Chalk Group deposition.

Structural inversion of the study area is documented in the seismic dataset by the recognition of the geometric characteristics of inversion structures as defined by Cooper & Warren (2010). These criteria include the observation that the hanging wall of the Flamborough Head Fault Zone has risen vertically to now sit structurally higher than the footwall, and the formation of an eroded, asymmetric monocline focussed over the syn-rift depocenter and facing the footwall (Figure 5.2), (Cooper & Warren 2010). The

complete removal of the post-rift Upper Cretaceous Chalk Group and erosion down to the syn-rift Lias Group levels over the Cleveland Basin is evidence that structural inversion of the Cleveland Basin also occurred after the deposition of Upper Cretaceous Chalk Group (Figure 5.2, Figure 5.3 and Figure 5.4). Further refinement of this age of basin inversion, based on the available data is not possible and thus no new data can be obtained from this study to further challenge the previously documented hypotheses on constraining the Cenozoic uplift ages in the Flamborough Head – Southern North Sea areas. However, the mechanisms of regional tilt and basin inversion observed across Flamborough Head and the Cleveland Basin, as suggested from seismic profile data and by relating to analogues of uplift and basin inversion from elsewhere in the UK, can be investigated and are described below.

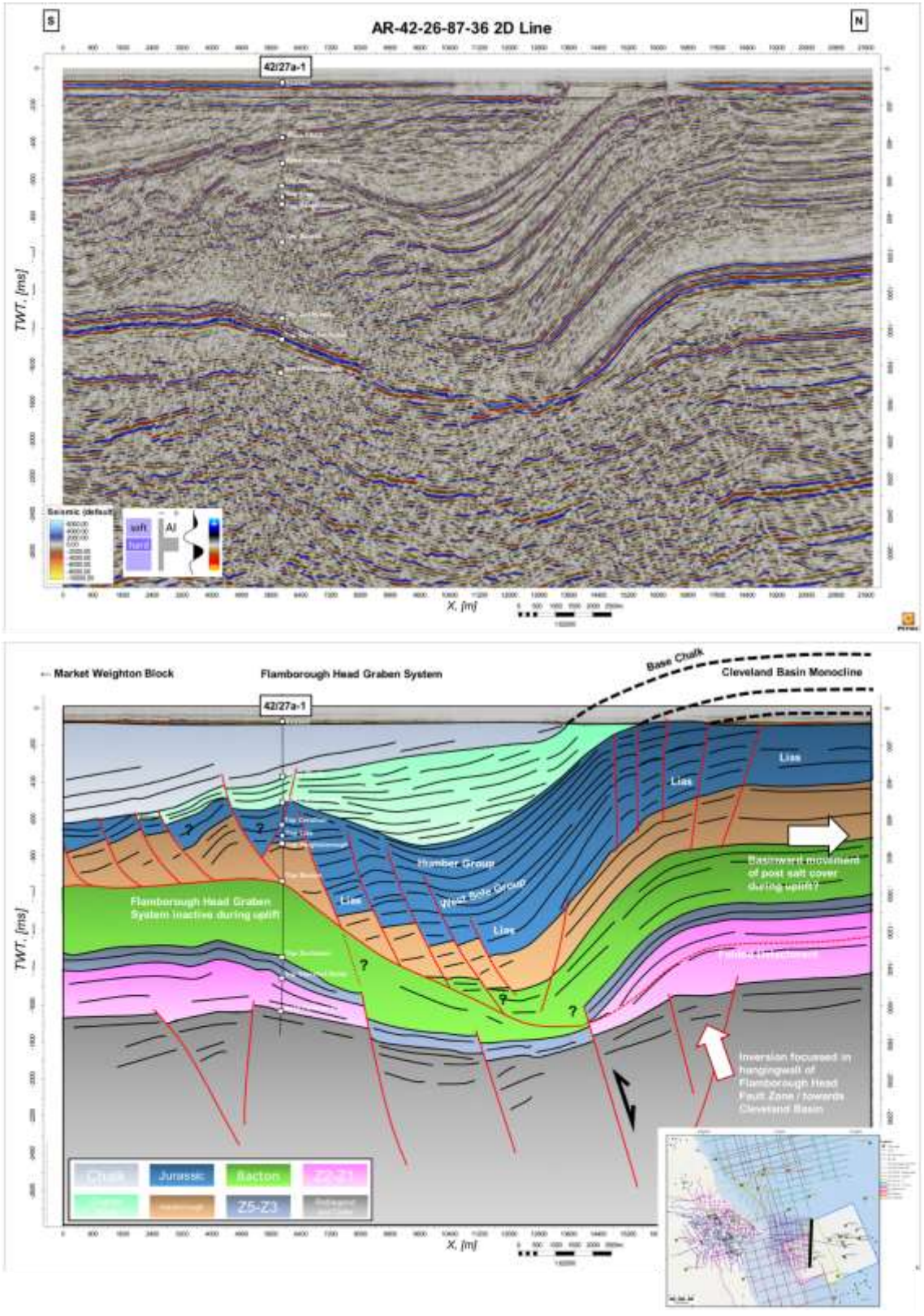

Figure 5.2 (Above) South to north striking un-interpreted 2D seismic line AR-42-26-87-36. (Below) Geoseismic interpretation of same line showing proposed "basin focussed" inversion across Flamborough Head and monoclinal folding of Upper Cretaceous Chalk and post salt cover during uplift. Inset shows line location. Note location of folded Flamborough Head Graben System detachment fault at the north of the line, at approximately 1,300ms TWTT. Five times vertical exaggeration. Data courtesy of BP.

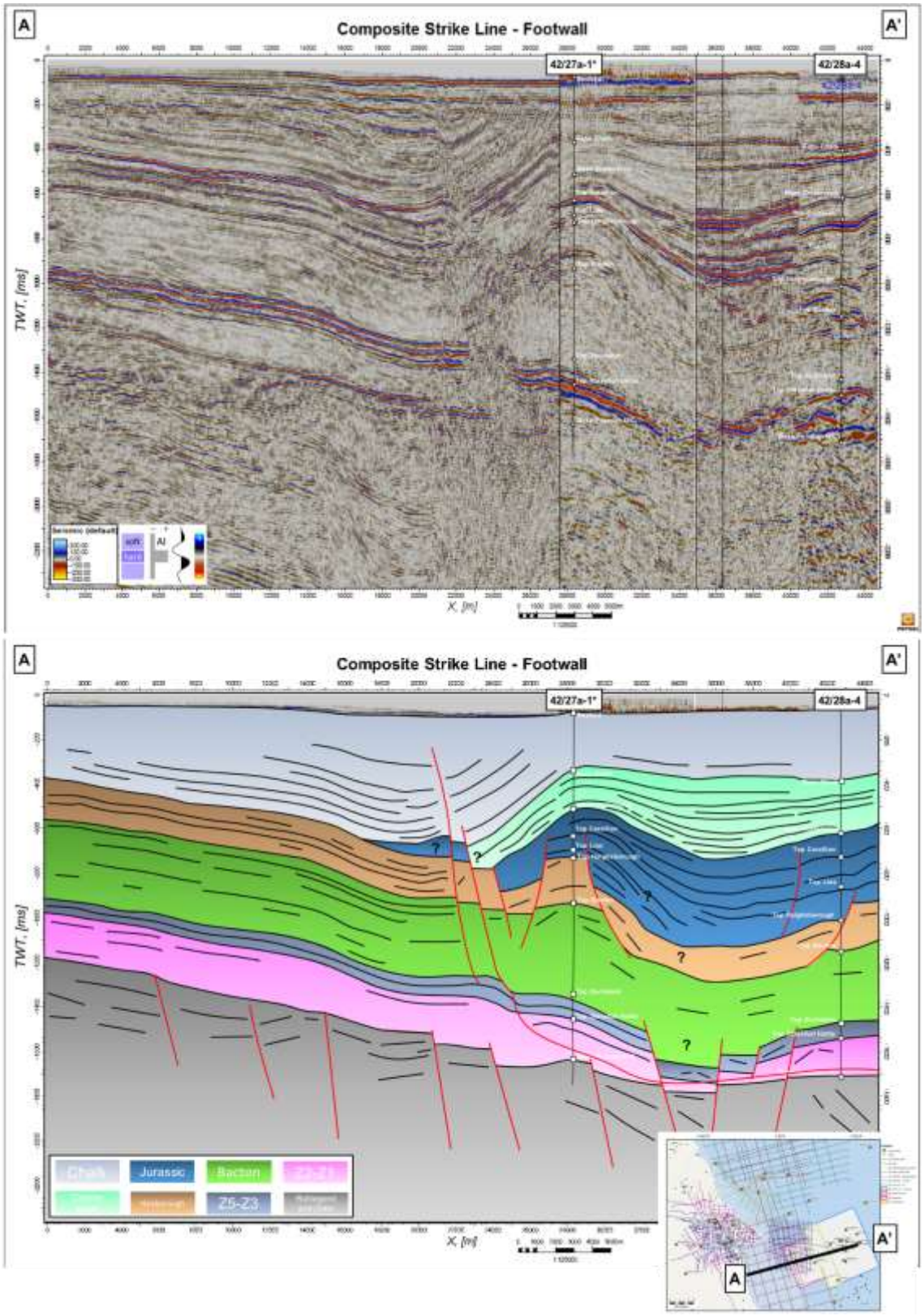

*Figure 5.3 (Above) WNW-ENE striking composite seismic profile across the footwall of the Flamborough Head Fault Zone, at approximately 33,000m offset. (Below) Geoseismic interpretation of the same line. Note regional tilt down to the south east. Twelve times vertical exaggeration. * denotes projected well. Data courtesy of IHS, BP and Total.*

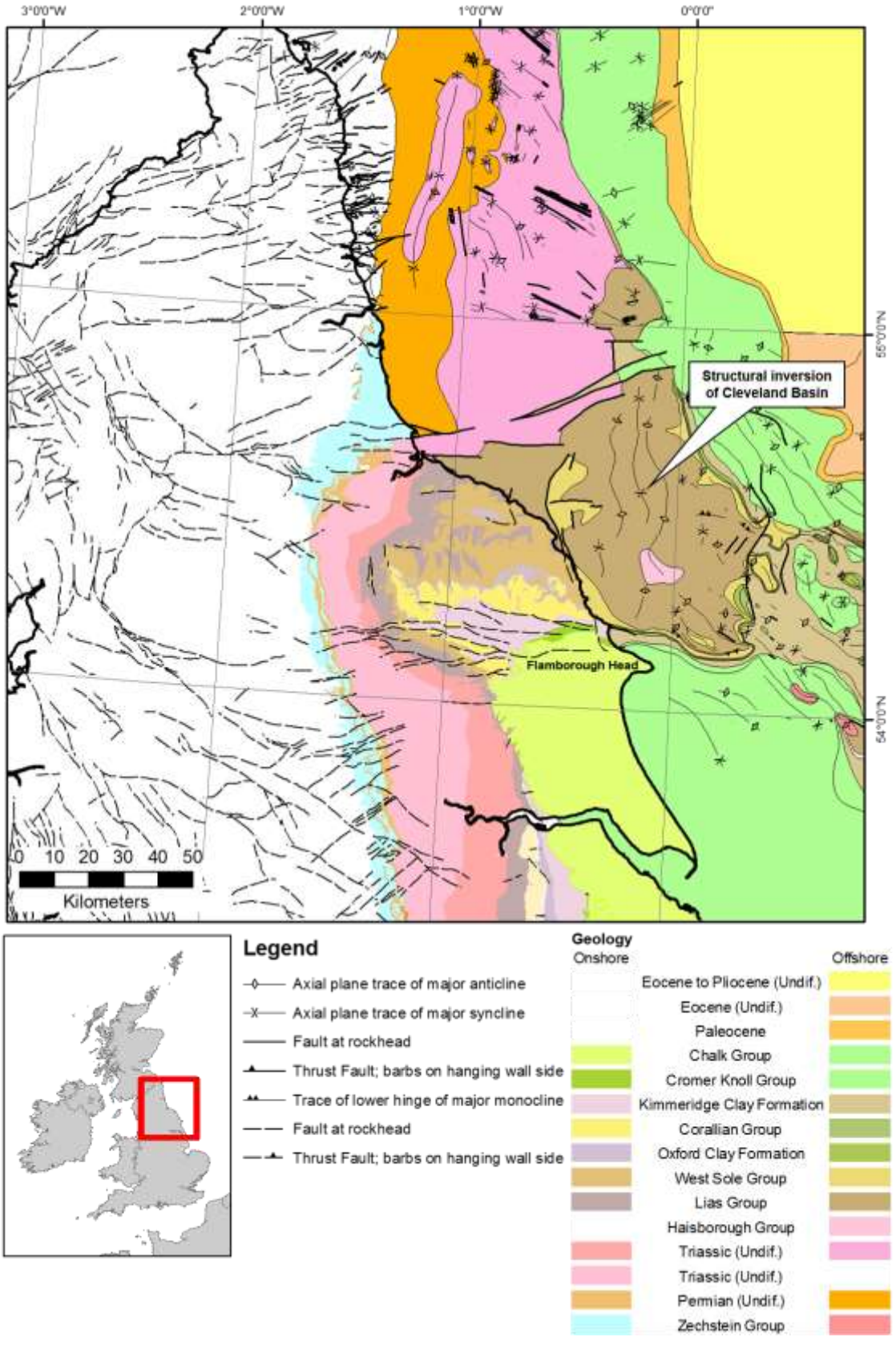

Figure 5.4 Bedrock geology and seabed subcrop map demonstrating the erosion down to Lower Jurassic and Upper Triassic strata over the Cleveland Basin in response to structural inversion. Stratigraphy older than Permian not shown. Data courtesy of the British Geological Survey.

5.2.1 Southern North Sea Analogue

Although, the effects of post Upper Cretaceous Chalk Group tilt and inversion across Flamborough Head are clear from the observations detailed above, Figure 5.2 also shows that the decoupled post salt Mesozoic graben system remains in net extension at present day. This phenomenon has also been recorded in the decoupled Mesozoic Dowsing Graben System that overlies the Dowsing Fault Zone, pointing to a Permian salt influence on inversion as well as extension (Stewart & Coward 1995), (Chapter 4). Stewart & Coward (1995) have shown that, although 3,000ft of reverse movement has occurred on the Dowsing Fault Zone, reverse displacement did not propagate up through the Zechstein Group salt into the decoupled Dowsing Graben System (Figure 5.5). Their observations suggest that the pre-salt basement has been shortened by reverse faulting while the post salt cover has been shortened by buckle folding (Figure 5.5). Experimental models have shown that in the presence of a sufficiently thick ductile layer (e.g. salt) shortening of pre-ductile units does not result in the propagation of reverse faulting through the ductile layer into the post-ductile units. Instead, shortening is accommodated by gentle monoclinal folding of the post-ductile layers and by lateral flow in the ductile layer (Richard 1991). The same study and observations from seismic profiles across the Sole Pit Basin (van Hoorn 1987) and the Dowsing Fault Zone (Stewart, *et al*. 1996) show that, where salt is thin or absent then hard linkage between the post-salt cover and pre-salt basement occurs with reverse displacement of basement faults being propagated to cover faults during inversion.

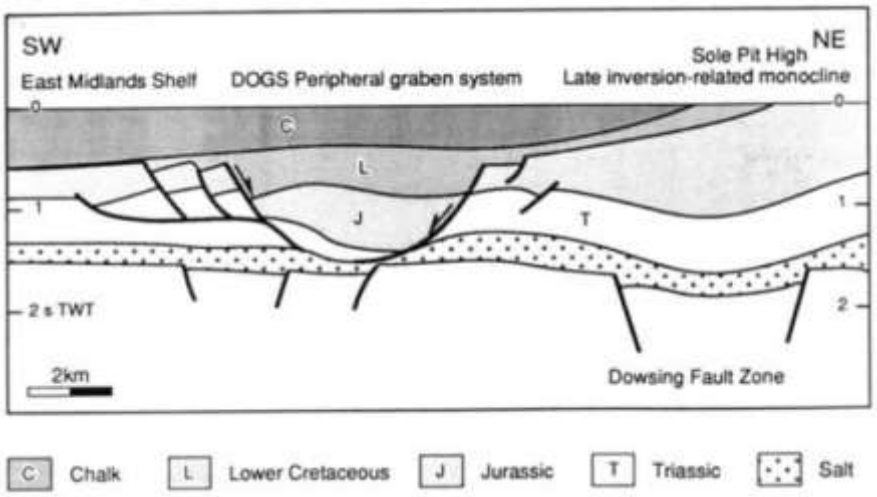

Figure 5.5 Interpreted seismic line across the west margin of southern North Sea, passing over the Dowsing Graben System and the Dowsing Fault Zone. Figure highlights the decoupled pre and post salt sections and tilt and inversion of the Sole Pit High (Stewart & Coward 1995).

It has been proposed that the preservation of extensional geometries within the detached Dowsing Graben System, while the pre-salt basement faults of the Dowsing Fault Zone are being shortened, is compensated by basinward translation of decoupled post-salt section relative to the basement, which itself is balanced by shortening in the cover on the eastern side of the Sole Pit High through detached salt cored buckle folding (Stewart & Coward, 1995; Stewart, *et al*. 1996), (Figure 5.6).

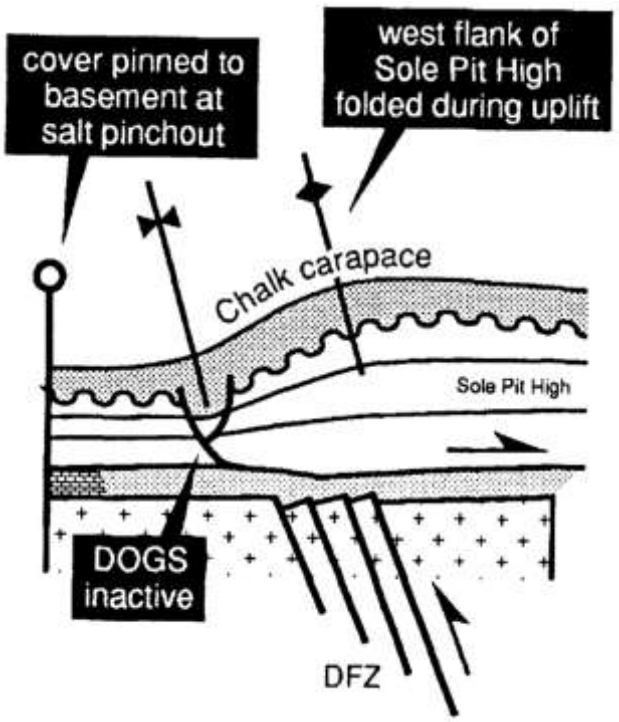

Figure 5.6 Inversion kinematics of the Dowsing Fault Zone. Reverse movements on basement faults are inferred from monoclinal folding of post salt cover. The extensional Dowsing Graben System (DOGS) was not reactivated during inversion, suggesting basinwards movement of the Sole Pit High post-salt cover relative to the basement. The cover is pinned to the west, where Zechstein Group facies change from evaporites to carbonates (Stewart, et al. 1996).

5.2.2 Wessex Basin Analogue

As well as similarities with the structural inversion patterns seen along the Dowsing Fault Zone and the Sole Pit High, tectonic uplift at Flamborough Head also bears a resemblance to styles identified at the Weymouth Anticline in the Wessex Basin (Figure 5.7). In this analogue, the decoupled basement – cover system consists of a Lower Triassic Bunter Group "basement" with an overlying Upper Triassic to Cretaceous cover, with Upper Triassic evaporites acting as the decoupling layer (Butler 1998); (Harvey & Stewart 1998); (Underhill & Stoneley 1998)

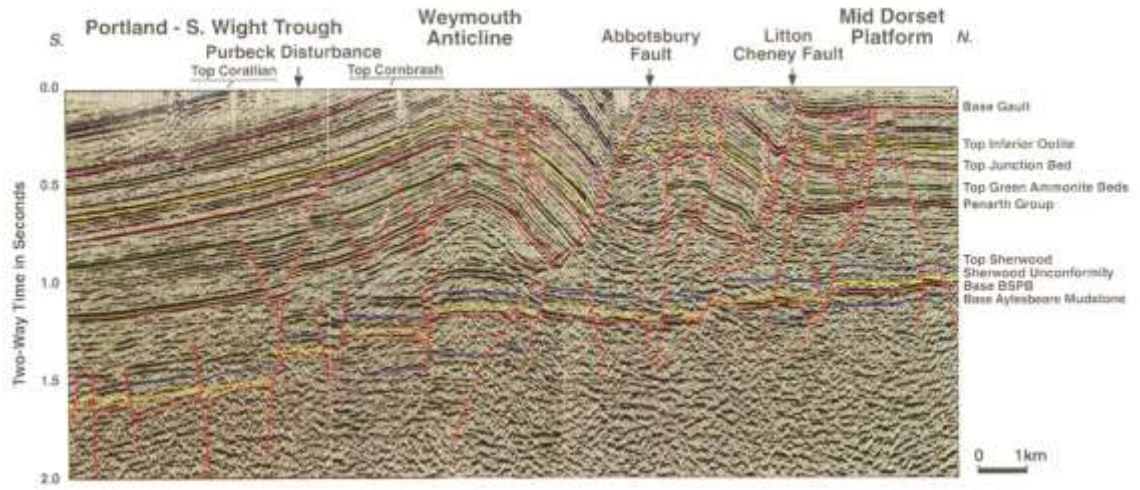

Figure 5.7 South to north striking regional seismic profile across the Weymouth Anticline in the Wessex Basin, illustrating the formation of a hanging wall monocline in a decoupled basement – cover setting (with Triassic salt acting as the detachment layer) through reverse sense structural inversion of basement faults. Note the preservation of extensional geometries in the footwall cover fault system (Butler 1998).

The Weymouth Anticline formed through the structural inversion of decoupled, pre-salt planar faults during Cenozoic intraplate contraction (Underhill & Stoneley 1998); (Butler 1998). This inversion episode resulted in the creation of an anticline in the hanging wall of a post-salt cover, west to east trending listric fault complex while the footwall section has remained undisturbed (Figure 5.7). In this Wessex Basin example, the pattern of observed deformation is proposed to be the result of the footwall of the fault system acting as a buttress during the reactivation of pre-existing planar extensional faults, with strain being taken up through deformation of an incompetent former syn-rift package within the hanging wall (Figure 5.7), (Underhill & Stoneley 1998; Underhill & Paterson 1998).

5.2.3 Weald Basin Analogue

Structural inversion of an onshore UK, Mesozoic basin due to intra-plate compressional stresses is also recorded in the Weald Basin, across the Weald Anticlinorium, which can also provide an analogue to the structural inversion of the Cleveland Basin (Figure 5.8). The Weald Basin forms an easterly extension to the Wessex Basin, forming during the early Mesozoic through subsidence driven by thermal relaxation driven subsidence but recording a main syn-extension depositional period in the Upper Jurassic and Lower Cretaceous, in contrast to the Lower Mesozoic depocenter in the Wessex Basin (Butler & Pullan 1990).

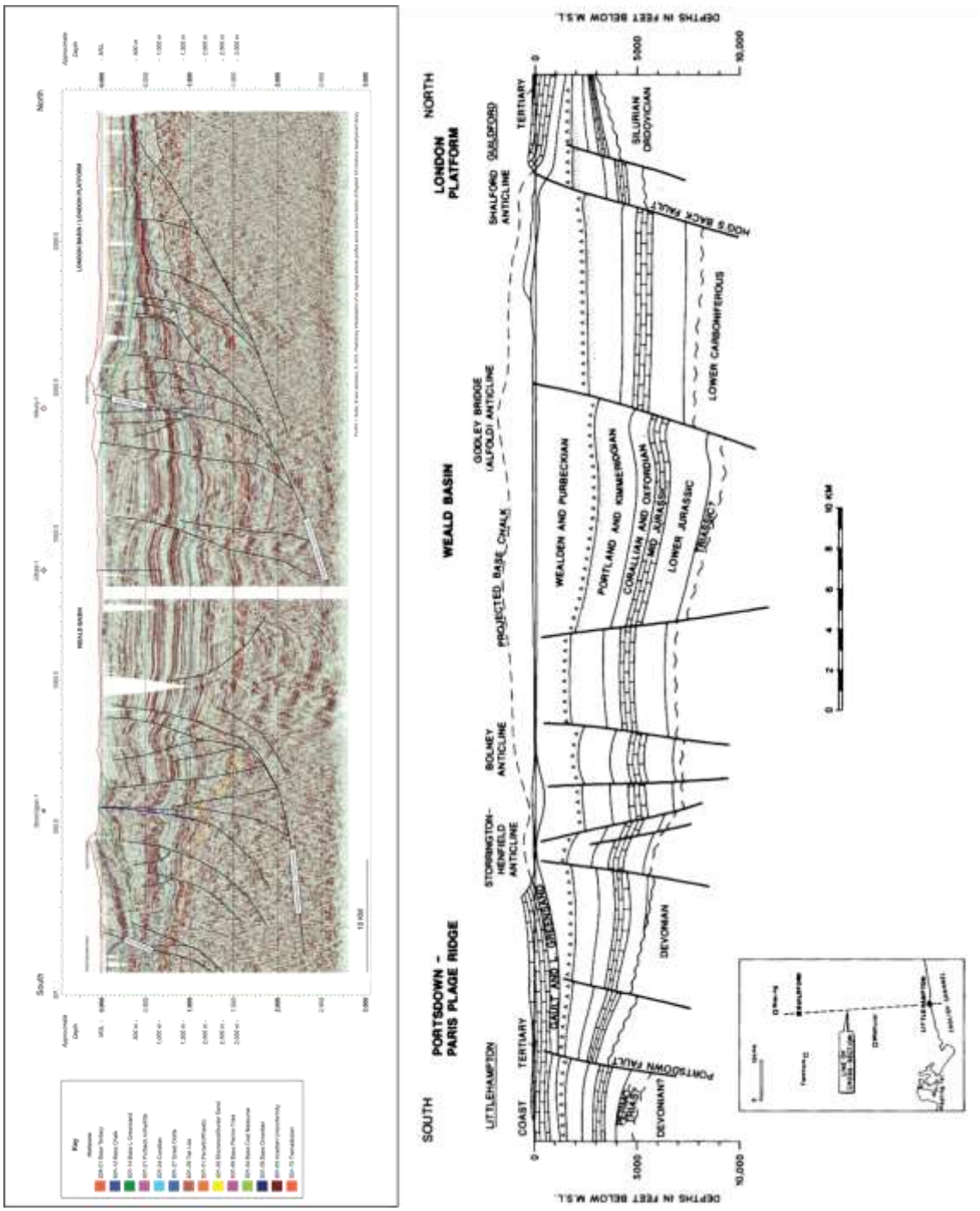

Figure 5.8 (Left) South to north striking regional interpreted seismic profile through the Weald Basin (Butler & Jamieson 2013). (Right) Geological cross section along same line orientation (Butler & Pullan 1990). Note general eroded anticlinorium shape of the inverted Weald Basin and general association of internal deformation and secondary anticline formation with basin margin and internal faults.

Tectonic uplift and structural inversion of the Weald Basin occurred during the Cenozoic and is characterised by a broad regional uplift resulting in the creation of the Weald Anticlinorium superimposed with local areas of intense compressional deformation in the form of tight anticlines and reverse faults, attributed to local uplift along pre-existing, Hercynian structural trends (Butler & Pullan 1990). The genesis of these intense deformation zones is mostly restricted to hanging wall blocks and inferred to be the result

of footwall highs acting as buttresses during the reverse reactivation of existing normal faults, against which hanging wall units have been compressed (Butler & Pullan 1990). The recognition that zones of intense deformation related to uplift are not restricted to the Weald Basin suggests that their genesis may be independent of broad regional uplift. It has been proposed that broad uplift in the Weald Basin commenced during the Late Cretaceous with more intense and local fault reactivation and deformation associated with Miocene aged Alpine movements (Butler & Pullan 1990)

5.2.4 Channel Basin Analogue

As detailed above, in the absence of salt (or where it is sufficiently thin) hard linkage between basement and post salt cover faults occurs during inversion, with cover faults being reactivated in a reverse sense. The region of Zechstein Group salt withdrawal underneath the Flamborough Head Fault Zone may have formed a salt weld and a hard linkage pin between the basement and cover (Figure 5.2). Salt weld pinning of pre-salt and post-salt sections during thin-skinned extension has been proposed in a slope-driven extensional setting on the West African Margin (Lundin 1992) and in the Channel Basin (Harvey & Stewart 1998), which provides an additional inversion kinematic analogue to Flamborough Head and the Cleveland Basin. Where salt weld pinning occurs, extension on post-salt cover faults updip of the pin ceases and when this system is inverted, monoclinal folding of the cover occurs in the hanging wall of the cover due to reactivation of basement faults and hard linked cover faults (Figure 5.9).

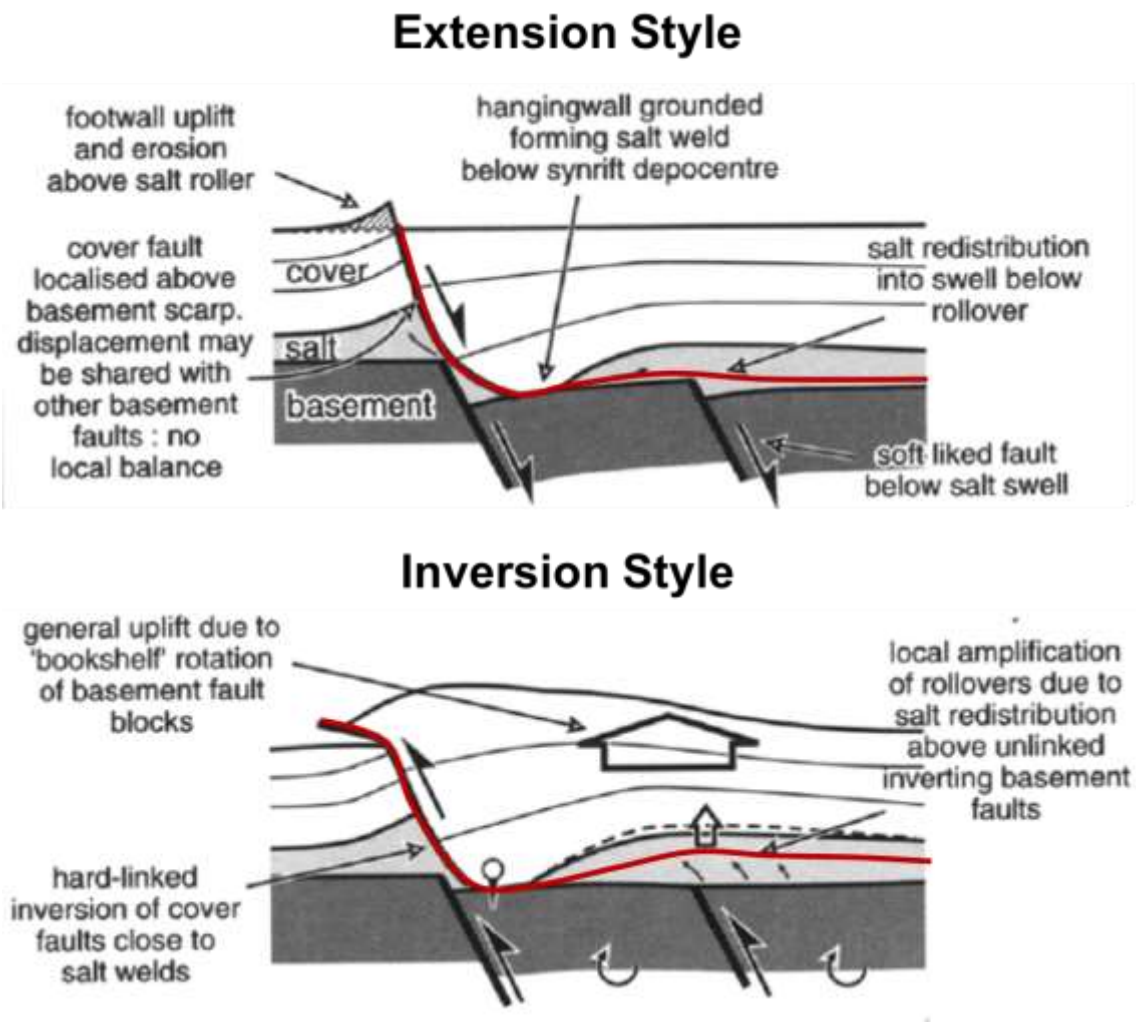

Figure 5.9 Model of extensional cover faulting and inversion for a decoupled system where a salt weld is forming a pin between the basement and cover units. Red line highlights listric detachment into ductile salt layer. Modified after Harvey & Stewart (1998).

The creation of a salt weld and basement – cover pin beneath the Flamborough Head Graben System may have pinned the system during inversion, preserving the extensional nature of the Flamborough Head Graben System and preferentially uplifting and buckling the hanging wall units against this pin (Figure 5.2).

5.2.5 Inversion of the Cleveland Basin

Kinematic mechanisms that have resulted in the inversion of the Cleveland Basin can be proposed, based on the interpreted dataset and regional analogues. As documented in Chapter 4, there is no discernible evidence for strike-slip faulting in the study area, with dip-slip fault displacement being the dominantly observed trend in both the planar pre-salt and listric post salt faults, suggesting dominantly lateral compression resulting in the observed inversion across Flamborough Head. Although basin inversion in the Southern North Sea resulting from transpressional stresses and deformation has been proposed and

summarised above, there are other documented parts of the Southern North Sea where basin inversion appears to be dominantly lateral compression driven (Badley, *et al*. 1989).

Figure 5.2, above displays the interpretation, derived from this study, of the inversion of the southern flank of the Cleveland Basin. In this model, pre-salt planar normal faults of the Flamborough Head Fault Zone have been reactivated through lateral compressive stresses. The presence of the Market Weighton Block buried granite in the footwall of the Flamborough Head Fault Zone (located further to the south, and beyond the line of section shown in Figure 5.2) has not only controlled the creation of the Cleveland Basin through differential subsidence across its northern edge, but has also acted as an effective buttress against which structural inversion is focussed (Figure 5.10). This buttressing by the footwall, as noted in the Wessex Basin analogue, has resulted in strain and deformation being taken up in the hanging wall of the Flamborough Head Fault Zone. The combination of this and the pinning of the cover at the Zechstein Group evaporite-carbonate shelf edge (Figure 5.6), which also acts as a locus of deformation in the cover units, has led to buckling of the post-salt cover and creating the eroded monocline present today. The presence of Permian salt has inhibited reverse movement from propagating into the post-salt cover units and has contributed to buckling of the cover and maintaining the extensional geometries seen in the cover listric faults, as noted in the Southern North Sea Sole Pit High analogue. A potentially unique feature of the structural inversion at Flamborough Head is the interpreted presence of the folded, north-dipping, Flamborough Head Graben System detachment fault (Figure 5.2). This is the Zechstein Group salt detachment of the main Flamborough Head Graben System, listric fault and has folded in response to buckling of the post-salt cover caused by reactivation of the pre-salt planar faults. It is proposed that the folding of this detachment during inversion has, in effect, switched off any lateral movement on this fault and enabled it to act as a pin, focussing deformation in the hanging wall and preserving extensional geometries in the footwall.

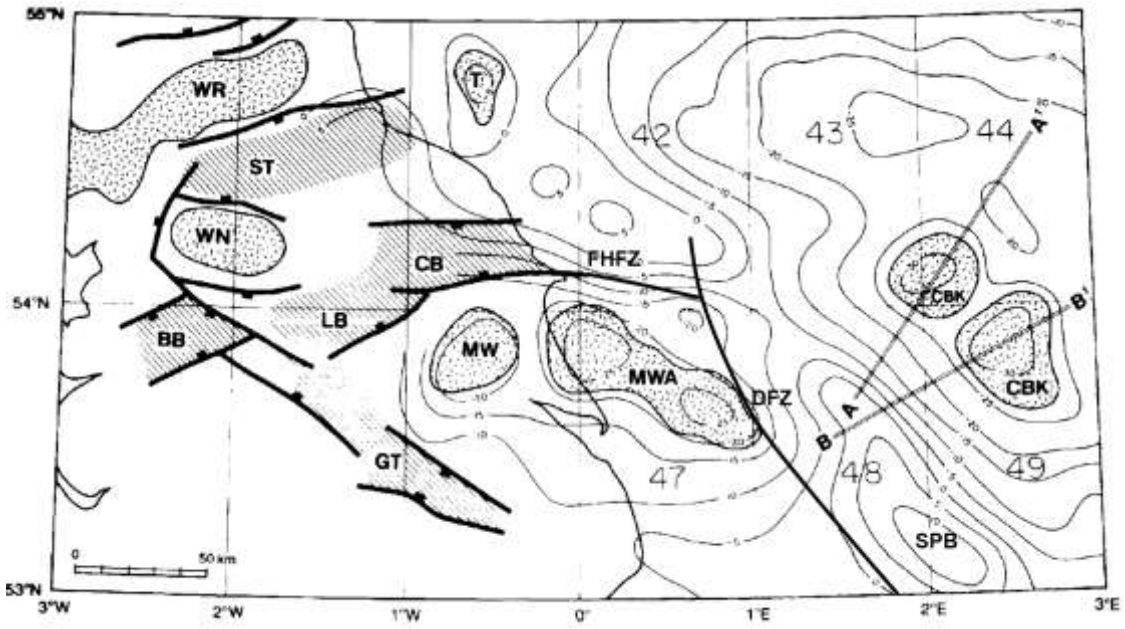

Figure 5.10 Southern North Sea Bouguer gravity anomaly showing location of inferred buried granites at gravity lows (MW, Market Weighton; MWA, Market Weighton Amethyst) and their relationship to sedimentary basins (CB, Cleveland Basin; SPB, Sole Pit Basin) and main tectonic features (FHFZ, Flamborough Head Fault Zone; DFZ, dowsing Fault Zone). Modified after Donato (1993).

As in the case of the Channel Basin analogue described in Section 5.2.4 above, there is a possibility that Zechstein Group salt withdrawal has also acted as a pin, which has focussed inversion-related deformation in the hanging wall of the Flamborough Head Fault System. However, this conceptual model has its challenges: if hard linkage between the basement and cover is occurring through a salt weld at the Flamborough Head Graben System, the reverse sense reactivation of cover faults is not recognised on the seismic dataset, as would be expected from analogue models (Richard 1991) and the harpoon shape adopted by the syn-rift post-salt cover through inversion as shown in Figure 5.9 and Figure 5.11 is not recognised on seismic profiles across Flamborough Head (Figure 5.2).

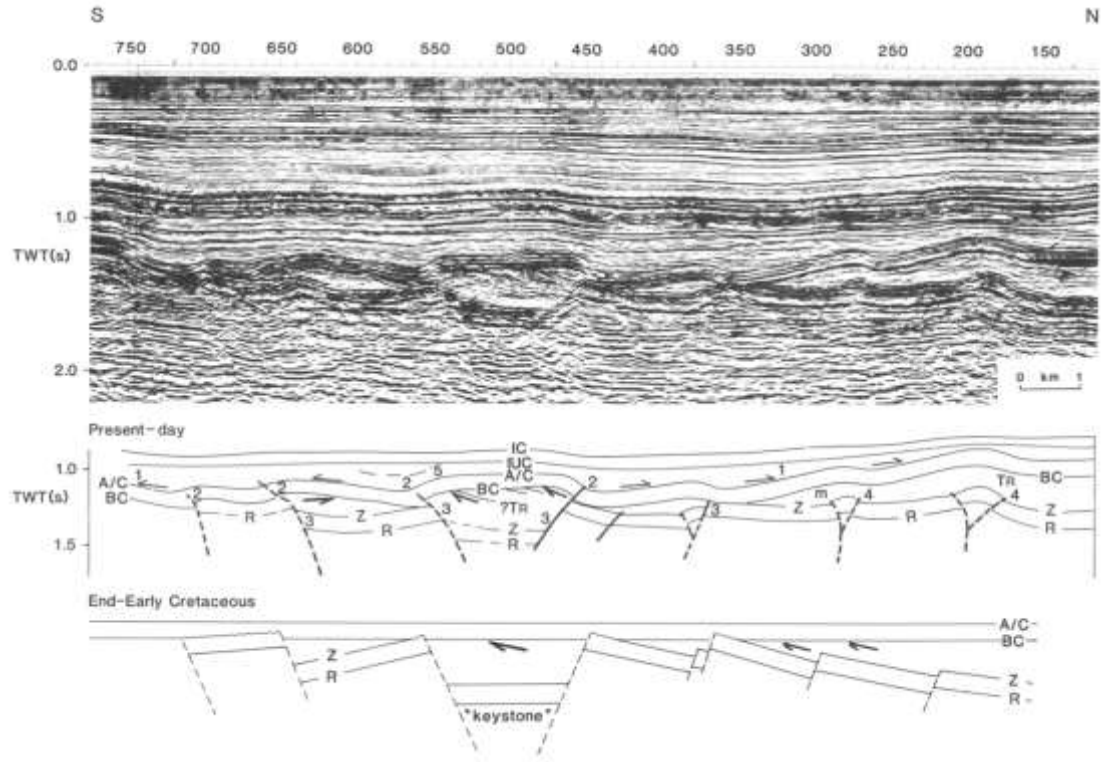

Figure 5.11 South to North striking seismic line across the South Hewett Fault in the Southern North Sea. Below shows present day line section interpretation and end Early Cretaceous tectonic reconstruction. Note the development of classic harpoon shaped geometries of the Jurassic syn-rift units (below the Base Cretaceous reflector: BC) and forced asymmetrical of the overlying Cretaceous post-rift units in response to reverse movement reactivation of pre-existing normal faults (Badley, et al. 1989).

The similarities between the decoupled basement – cover relationship and extensional and inversion characteristics of the Flamborough Head Fault Zone / Flamborough Head Graben System and the Dowsing Fault Zone / Dowsing Graben System are clear (compare Figure 5.2, Figure 5.5 and Figure 5.6). This suggests that a component of the inversion kinematics of the Dowsing Fault Zone and the Sole Pit High as described by Stewart *et al*. (1996) (Figure 5.6) could also be applied to the Flamborough Head Fault Zone and the Cleveland Basin to describe the observed extensional and inversion geometries (Figure 5.2). There is some evidence of balancing for the required basinwards movement of the post-salt cover during basement inversion through the development of a salt-cored buckle fold north of the Flamborough Head Fault Zone at well 41/20-1 (refer to Figure 4.22 in Section 4.4.1 above), in support of the Stewart *et al*., (1996) model. Sequential kinematic restorations of regional seismic profiles would be required to quantitatively support this, which is beyond the scope of this project.

These similarities described above also suggest that the Dowsing Fault Zone and the Flamborough Head Fault Zone are a continuation of the same fault system (contrary to

Kirby and Swallow's (1987) assertion that they are discrete systems), sharing the same extensional and compressional history and basement – cover relationship due to the presence of Permian and Triassic salt units. It is inferred that the presence of the Market Weighton Block granite controls the west to east orientation of the Flamborough Head Fault Zone and the north-west to south-east basement inherited trend of the Dowsing Fault Zone (Donato 1993) and, as documented above, acts as a buttress during intra-plate deformation (Figure 5.10). This observation, along with the similarities between the Flamborough Head Fault Zone and the Dowsing Fault Zone, as described above, points to a shared genesis for both the Cleveland Basin and the Sole Pit Basin.

Regarding the origin of the stress regimes that have resulted in the inversion features seen at the Flamborough Head Fault Zone and the Cleveland Basin, Ziegler (1989) has shown that the pre-existing Permo-Carboniferous fault networks have been reactivated through lateral compressive stresses related to the evolution of the Alpine foreland during the Mesozoic and Cenozoic and with deformation being recorded up to a distance of 1,300km from the Alpine front. This includes basement fault reactivation, inversion and deformation in the Sole Pit Basin, which began an initial phase of inversion during the Late Cretaceous and underwent its main phase of inversion at the Eocene – Oligocene boundary, (Figure 5.12), (Ziegler 1989).

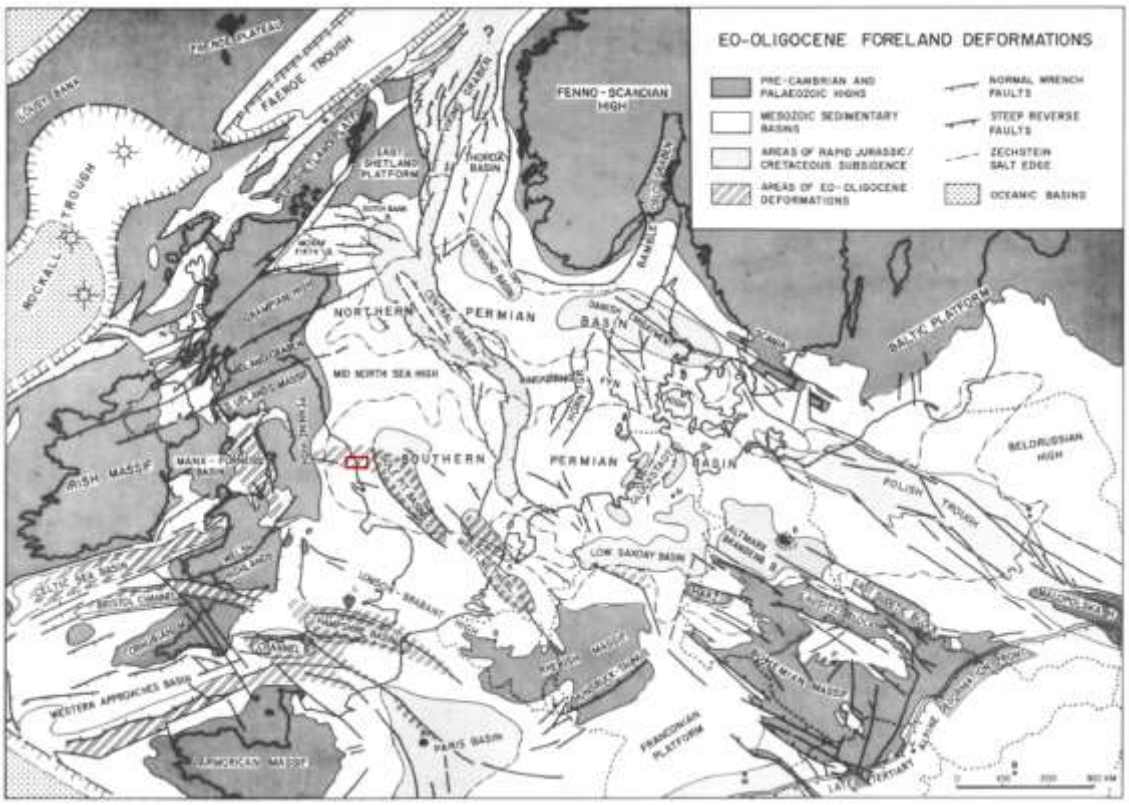

Figure 5.12 Eocene - Oligocene Alpine foreland deformations. Study area shown as red box. Modified after Ziegler (1989)

Alpine-related compression would, in conjunction with rift push from the opening North Atlantic, create a general SE-NW stress field across the North Sea and the eastern UK (Figure 5.13). Ziegler (1989) has highlighted the importance basement faults have had in weakening crustal cohesion of Western Europe, evident from their repeated reactivation throughout the Mesozoic and Cenozoic. Due to this basement inheritance, intra-plate deformation and basement fault reactivation resulting from lateral Alpine-related compression in the orientation described above would result in the inversion axes seen in inverted Mesozoic basins in the UK (Figure 5.13). This broad direction of compression is parallel to the Sole Pit Basin controlling faults, such as the Dowsing Fault Zone, which would result in the positive inversion of the basin through wrenching described by Glennie and Boegner (1981). This compression direction would be less parallel and more at a right angle to the Flamborough Head Fault Zone, which may explain the absence of observed strike-slip faulting and related deformation in the study area. Contractional fault block reactivation along the Flamborough Head Fault Zone could produce the deformation observed in the study area and would give rise to the W-E axis of inversion seen at the Cleveland Basin. This model could also result in the coeval inversion of both the Sole Pit and Cleveland Basins, in the early to mid Cenozoic.

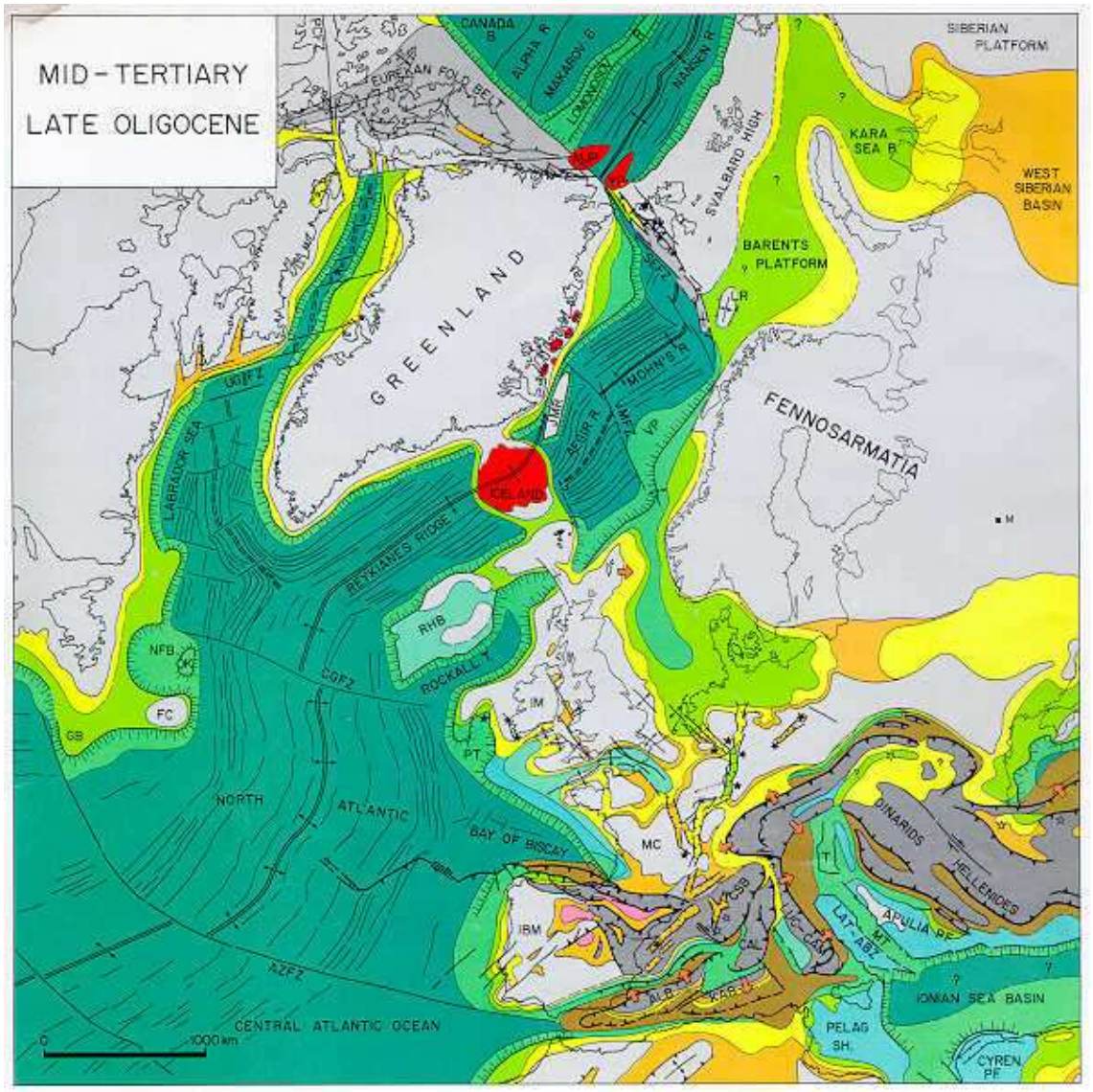

Figure 5.13 Mid-Tertiary, Late Oligocene palaeogeographic-palaeotectonic map (Ziegler 1988)

5.2.6 Conclusions

The discussion above highlights that there are a number of Mesozoic basins from around the UK that have been subjected to regional uplift and structural inversion, dated from the Late Cretaceous to the Cenozoic, that display similar features to those seen at Flamborough Head and the Cleveland Basin. Late Cretaceous to early Cenozoic regional uplift and tilting to the south-east is shown to be basin-independent and affects a broad section of the UK, from the Moray Firth Graben in the north to the Wessex and Weald Basins in the south. Reverse sense structural reactivation of pre-existing normal faults with deformation constrained in their hanging walls, as recognised in these analogues and in the Weald Basin, is shown to superimpose upon the broad regional uplift trends, suggesting a distinctive age and causal mechanism for each of regional uplift and the structural inversion of pre-existing faults.

As noted previously in this section, the evidence for a post-Upper Cretaceous Chalk, regional south-easterly tilting at Flamborough Head is well documented in the subsurface dataset (Figure 5.2 and Figure 5.3), but age refinement of the onset of tilt at Flamborough Head is difficult, due to the absence of any sediments younger than the Upper Cretaceous. However, recent studies on the Cretaceous to Paleogene unconformity in England support a proto-Iceland plume mechanism for regional uplift and tilt at this time, as vertical rather than compressive (i.e. Alpine) forces appear to control the development of the unconformity (Gale & Lovell 2017). This study, in conjunction with the observation of a diachronous genesis for regional uplift and structural inversion at the Weald Basin, suggests that the study area has been affected by two discrete basin reconfiguration episodes after Chalk deposition, in contrast with Starmer (1995, 2008, 2013) who proposes that tilt and inversion seen at Flamborough Head are part of the same event.

Thus, the episodes of basin reconfiguration can be summarised as: (1) regional uplift and tilting due to vertical stresses associated with the thermal effects of the proto-Iceland Plume during the early Cenozoic; (2) reverse sense reactivation of the Flamborough Head Fault Zone as a result of intra-plate deformation from laterally compressive Alpine stresses and rift push from the opening of the North Atlantic. The buried granite at the Market Weighton Block acted as a buttress during compression, which, in conjunction with a cover pin at the Zechstein shelf edge, resulted in the hanging wall deformation of the Flamborough Head Graben System and inversion of the Cleveland Basin. This structural inversion was potentially coeval with the Sole Pit Basin inversion during the Eocene – Oligocene.

5.3 Formation of the Chalk Group Outcrop Deformation

Deformation such as folding and thrusting has been recognised in the Upper Cretaceous Chalk Group outcrop at Flamborough Head for over a century (Figure 5.14), (Philips 1835; Davis 1885; Lamplugh 1895) and has previously been described as a shatter zone (Kirby & Swallow 1987). The deformation features of the Flamborough Head Disturbance have been inferred as resulting from oblique – slip reactivation of the cover faults of the Flamborough Head Fault Zone with a speculative underlying basement fault control (Kent 1980; Kirby & Swallow 1987; Starmer 1995; Starmer 2008 and Starmer 2013). Starmer (1995, 2008, and 2013) has mapped in detail the deformation in the coastal exposures of the Cretaceous Chalk Group at Flamborough Head, proposing ten

stress fields that have led to the creation of the observed deformation structures and attempted to age relate each to regional tectonic trends (Table 5.1).

Figure 5.14 Chalk Group deformation structures at Staple Newk, Flamborough Head. See Figure 1.2 for photograph location (Davis 1885).

Table 5.1 Structural evolution summary of Selwicks Bay, Flamborough Head (Starmer 2008).

STRESS FIELDS	STRUCTURES FORMED	PROBABLE AGE
D1 Compression ENE-WSW to E-W.	**D1** NNW-SSE folds.	**Laramide** (late Maastrichtian -early Paleocene).
D2 General tension (one stage E-W).	**D2** Transverse extensional fractures.	**post-Laramide**
D3		**Alpine** (Oligocene)
D3a Compression N-S (to NNE-SSW).	**D3a** E-W (to ESE-WNW) folds.	
D3b Transpression: N-S compression with E-W sinistral shear.	**D3b** E-W (to ESE-WNW) folds. In north, E-W sinistral shears.	
D3c Transpression: NE-SW compression with NW-SE dextral shear.	**D3c** E-W folds. In south, thrusts to S. In north, thrusts to N and S. N-S Riedel shears.	
D4		**post-Alpine**
D4a Tension E-W. (Tilt S in south).	**D4a** Approx. N-S (NNE-SSW to NNW-SSE) conjugate normal faults. E-W fault in south.	
D4b In south, N-S tension (with tilt to S). In north, transtension: N-S dextral shear with E-W tension.	**D4b** In south, E-W extensional faults in listric fan complex. In north, dextral shear on (D4a) N-S faults.	
D4c Tension N-S.	**D4c** Vertical E-W tension cracks.	

The basis of Starmer's (1995, 2008, and 2013) evaluation is the subsurface interpretation of Flamborough Head by Kirby & Swallow (1987). Both of these interpretations infer a thick-skinned extension and inversion model at Flamborough Head. They rely on the assumption that the observed compressional deformation of the Upper Cretaceous Chalk Group at Flamborough Head is primarily the product of the reactivation of basement and cover faults. Starmer (1995, 2008 and 2013) also attempts to fit his interpretations with the Kirby and Swallow (1987) observation that the dominant throw of the Flamborough Head Graben System is to the south, which is the inverse of what has been shown from this study and the erroneous assumption that southward dipping listric faults are prevailing and are cross cutting the basin bounding northerly dipping listric faults (Figure 5.15). The seismic interpretation resulting from this project show that the post-salt cover section is decoupled from the basement due to the presence of Zechstein Group salt, creating a thin-skinned extensional and compressional system. There is no observable reverse sense reactivation of post-salt cover faults through inversion across Flamborough

Head (at seismic reflection resolution) with analogue modelling providing quantitative evidence to support this (Richard 1991). Therefore, describing the Chalk Group deformation observed at Flamborough Head purely as the product of a complex history of thick-skinned fault reactivations can be ruled out.

An alternative interpretation could be that the deformation is the result of internal stresses acting upon a brittle chalk carapace as the post-salt cover is folded and buckled into a monocline in the hanging wall of the Flamborough Graben System through the reactivation of the decoupled Flamborough Head Fault Zone and inversion of the Cleveland Basin by the model proposed in Section 5.2.5 above (Figure 5.2, Figure 5.6). The creation of this type of deformation in the Upper Cretaceous Chalk Group in response to structural inversion is noted in the Wessex Basin (Butler 1998; Underhill & Paterson 1998) and is shown to result in the low-angle thrusts and significant intra-formational folding there that is also observed in outcrop at Flamborough Head. The steep limb of the chalk monocline has been preferentially eroded during inversion of the Cleveland Basin (but is preserved in underlying post-salt cover units in the subsurface, as shown in Figure 5.2) leaving behind the partly eroded shallow limb that forms the exposures and which has a dip of around 10° south, induced by regional tilt (Starmer 1995).

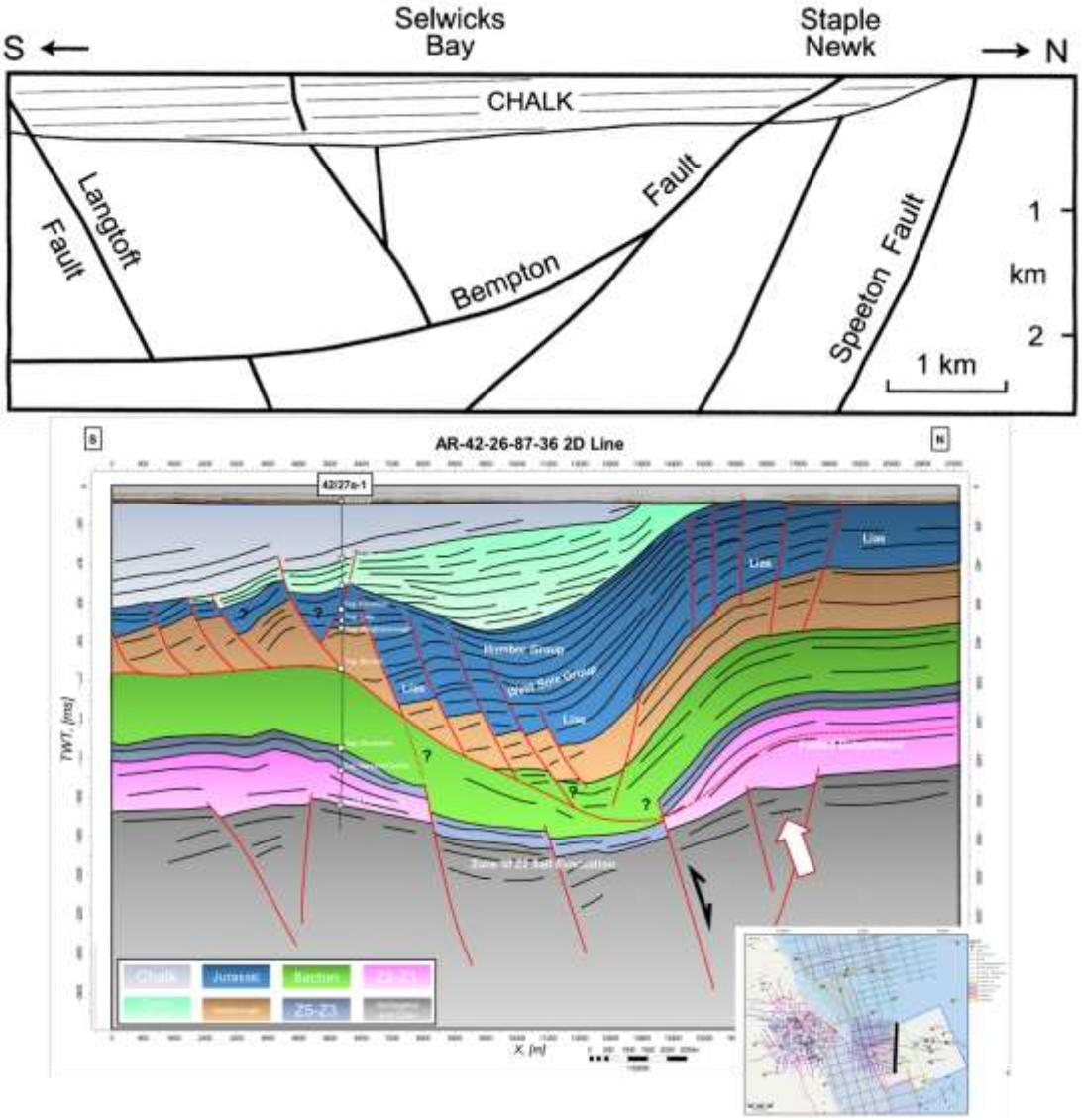

Figure 5.15 (Above) Map of main faults beneath Flamborough Head, based on seismic interpretation by Kirby & Swallow (1987) in Starmer (2008)). Note erroneous major southerly throwing Bempton listric fault cutting the northerly-dipping Langtoft Fault. (Below) Interpreted seismic line from offshore Flamborough Head, showing dominant north dipping listric fault system that detaches into Triassic and Permian salts.

5.4 Implications for Exploration Risk and Hydrocarbon Prospectivity

The primary hydrocarbon play in the Southern North Sea in terms of reserves is Carboniferous-sourced gas reservoired in Permian Rotliegend Group Leman Sandstone Formation and trapped in Permo-Triassic fault block traps and sealed by Upper Permian Zechstein Group evaporites (Figure 5.16). Hydrocarbons sourced from Carboniferous coals and marine shales are the sole productive petroleum system in the basin. This Carboniferous petroleum system also provides hydrocarbons (gas in the case of the Southern North Sea and Cleveland Basins) to secondary but important plays including: Permian Zechstein carbonate reservoirs, trapped in Permo-Triassic fault block traps and sealed by intraformational evaporites; Carboniferous sandstones, trapped in Variscan

structures and sealed by Upper Permian Rotliegend Silver Pit Claystone Formation shales and Upper Permian Zechstein Group evaporites and Triassic Bacton Group Bunter Sandstone Formation reservoirs trapped in salt-cored anticlines and sealed by Triassic Haisborough Group evaporites (Figure 5.16).

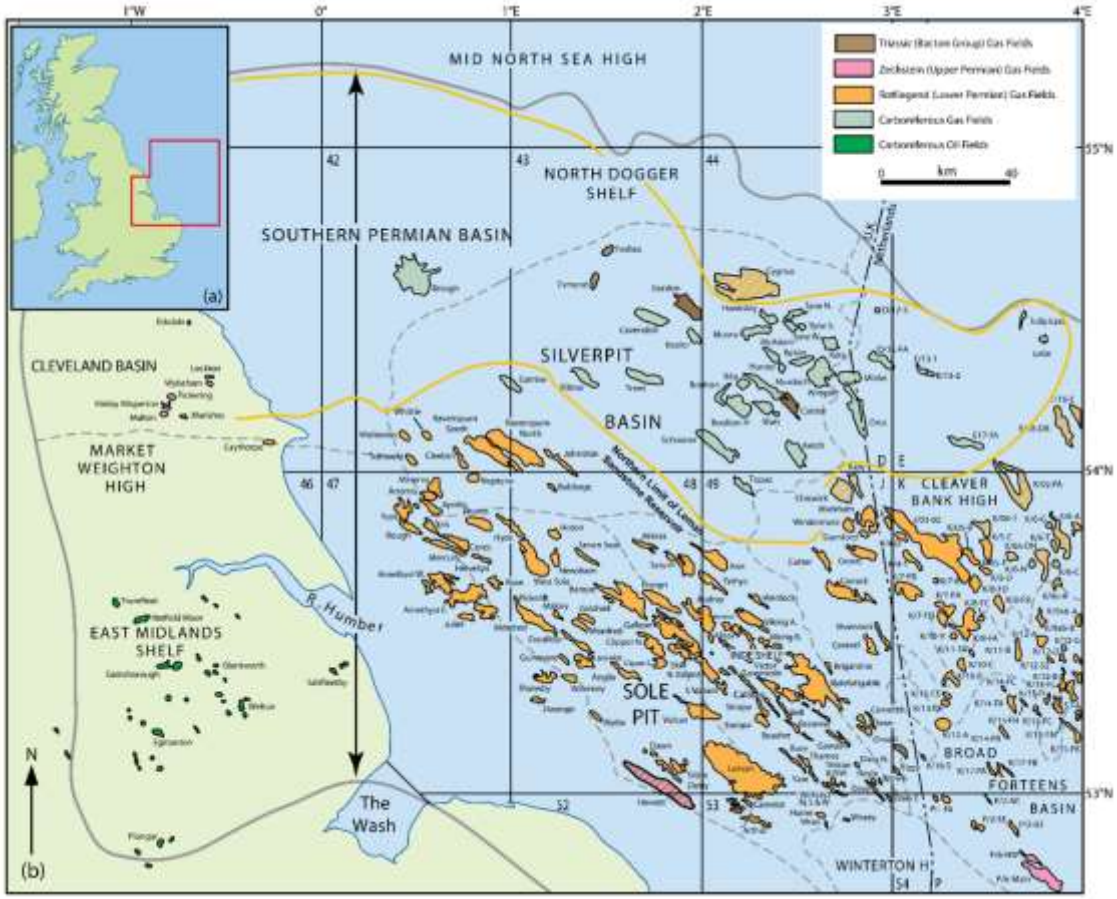

Figure 5.16 Regional map of Southern North Sea basins highlighting productive hydrocarbon fields coloured by reservoir age. The northern limit of the Leman Sandstone formation is depicted as an orange polyline. Modified after Duguid & Underhill (2010).

The principal control on Rotliegend Group hydrocarbon field distribution is the presence or absence of Leman Sandstone Formation reservoir (Figure 5.16). The distribution of the Leman Sandstone Formation in the Southern North Sea is well documented (e.g. Underhill (2003)). However, to date there has been little documented evidence of faulting during Leman Sandstone Formation deposition, with the formation typically draping and filling the topography of the underlying eroded Carboniferous surface (Steele 2017). As described in Chapter 4, it is possible that the Flamborough Head Fault Zone played a role in controlling Leman Sandstone Formation distribution and that the most promising areas for this play lie to the south and in the footwall of the Flamborough Head Fault Zone.

It is important to consider the effects that post Chalk Group regional uplift and tilting and basin inversion has had on the Carboniferous petroleum system. Apatite fission track analysis from wells on the East Midlands Shelf show that maximum burial for Carboniferous source units occurred here during Paleocene burial, prior to the onset of Cenozoic uplift and exhumation (Green, *et al*. 2017). This, in turn, suggests that for the East Midlands shelf, the main period of hydrocarbon generation, expulsion and migration into traps occurred during the Mesozoic and earlier Cenozoic, up until the onset of Cenozoic exhumation, when the petroleum system are switched off. 1D basin modelling for the 41/20-1 well located to the north of Flamborough Head in the offshore Cleveland Basin, confirms that the onset of Cenozoic uplift marks the termination of hydrocarbon generation from Carboniferous source rocks in the study area and greater Cleveland Basin (Figure 5.17 and Figure 5.18).

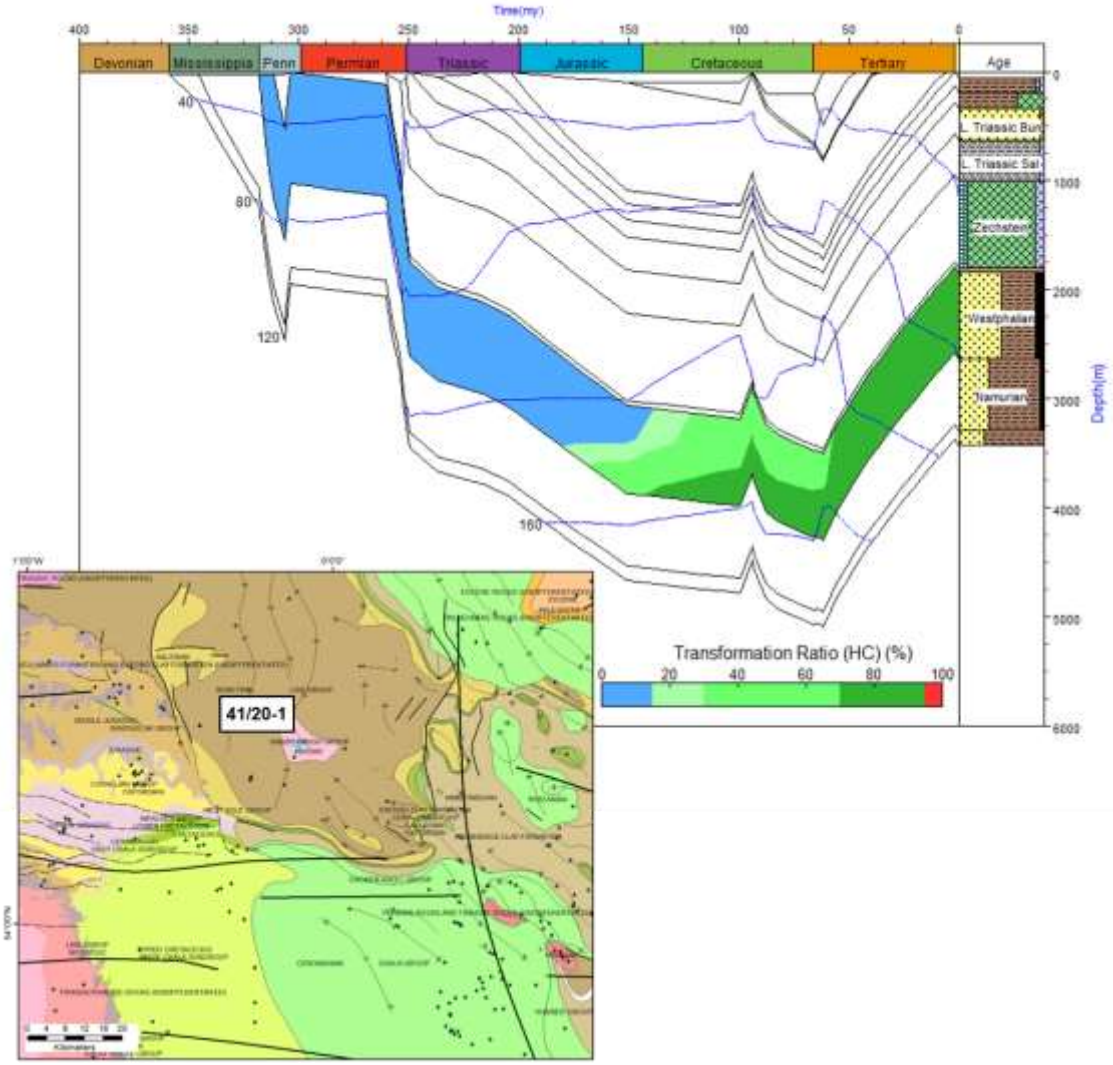

Figure 5.17 Burial history for well 41/20-1 with transformation ratio (the ratio of kerogen in the source rock that has been converted to hydrocarbons) and temperature overlay. Gas generation for a Carboniferous Westphalian source rock commenced during Jurassic burial. An arrest in transformation ratio post Cenozoic uplift relates to the cessation of hydrocarbon generation due to exhumation related basin cooling. Inset shows well location on a surface geological map in relation to Flamborough Head and Cleveland Basin. Data courtesy of British Geological Survey. Note 41/20-1 well is located in a region of maximum uplift of the Cleveland Basin with Triassic Haisborough Group units sub cropping at sea bed.

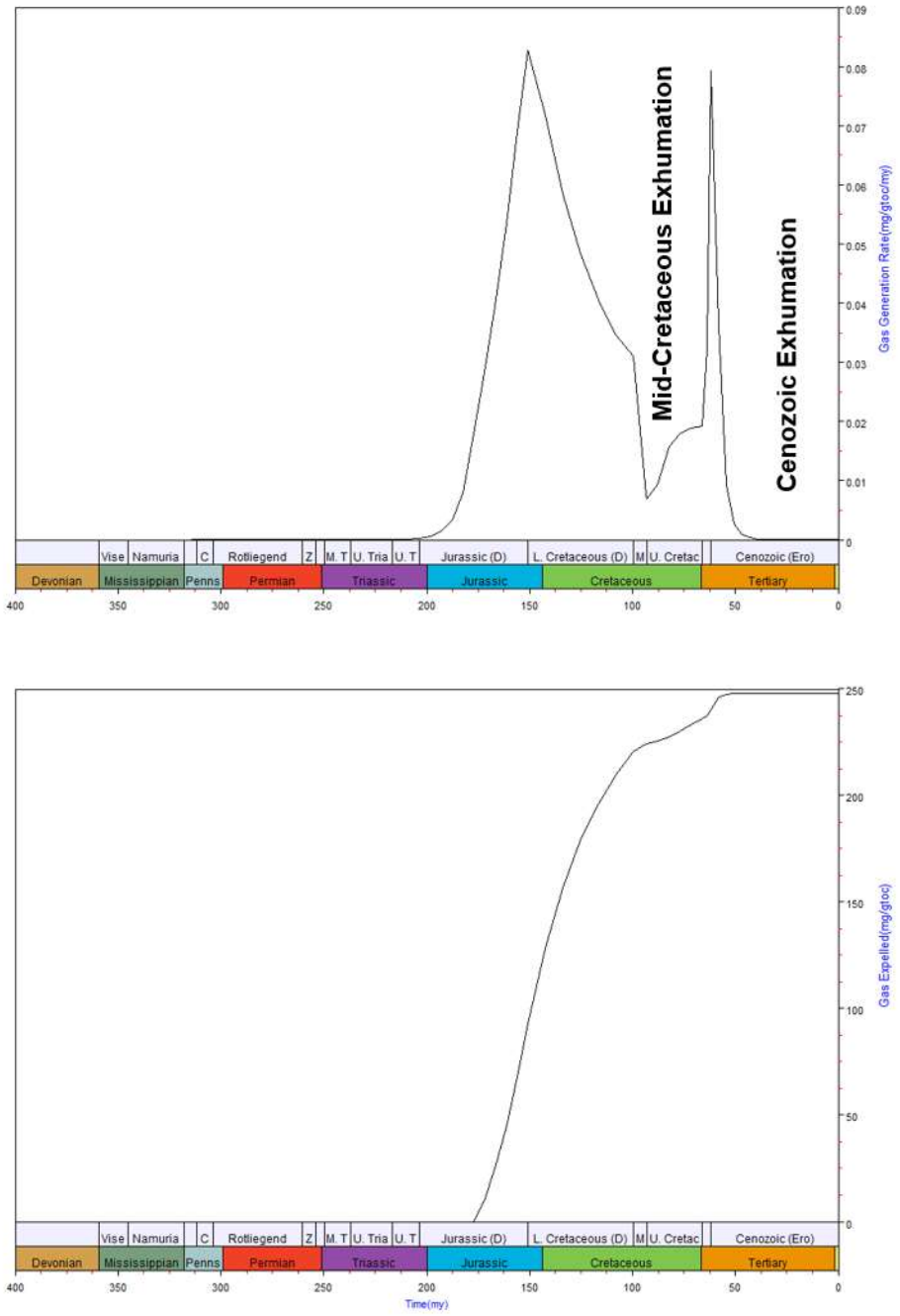

Figure 5.18 (Above) Gas generation rate over time (Below) Cumulative gas expelled over time for a Westphalian source rock in well 41/20-1. Generation reached peak rates in the Late Jurassic – Early Cretaceous and was arrested during a postulated mid Cretaceous exhumation event (Green, et al. 2017). Generation and expulsion continued until the onset of Cenozoic exhumation, after which both ceased and the petroleum system was switched off. The spike in gas generation rate at the onset of Cenozoic exhumation is related to early Cenozoic burial and an increased heat flow at this time due to a rise in global temperatures during the Paleocene, relative to present day (Frakes, et al. 1992).

Cenozoic tilt and uplift has had severe repercussions on the hydrocarbon prospectivity of the Cleveland Basin. Prior to inversion, Carboniferous and Permian structures will have been charged with of hydrocarbons migrating from the Cleveland Basin depocenter in the hanging wall of the Flamborough Head Fault System into the footwall, over the Market

Weighton High. During structural inversion of the Cleveland Basin, any significant trapped accumulations in the hanging wall could have been lost through remobilisation, as trap and seal geometries are modified (Cooper & Warren 2010) whereas accumulations in the un-deformed footwall will remain intact, explaining the present-day distribution of hydrocarbons shown in Figure 5.16, notwithstanding the limits of Rotliegend Group Leman Sandstone Formation reservoir distribution. This pattern of hydrocarbon fill and loss of preservation has been noted in the Wessex Basin, specifically the Wytch Farm oil field. Here, the un-deformed footwall of the Purbeck Fault Zone has retained hydrocarbons but any accumulations in the hanging wall, with the exception of the small Kimmeridge Bay oil field, have been lost through the inversion of the Purbeck Fault Zone and deformation of the hanging wall (Underhill & Stoneley 1998), (Figure 5.19). Similarly, there is a noted absence of significant hydrocarbon accumulations within the central high of the inverted Weald Basin anticlinorium, with present-day accumulations focussed in the un-deformed footwall highs (Butler & Pullan 1990), (Figure 5.20), suggesting widespread remobilisation of hydrocarbons through the Cenozoic inversion of Mesozoic sedimentary basins in the UK.

This pattern of hydrocarbon migration, basin inversion and remobilisation has resulted in only relatively small attic volumes of hydrocarbons remaining in fields reservoired in Carboniferous and Rotliegend Group sandstone and Zechstein Group carbonate structural traps that are capped by the high sealing capacity Zechstein halite. These small, high integrity traps have enabled hydrocarbon retention through Cenozoic tilt and inversion (Figure 5.16). This same process explains the absence of any commercial hydrocarbons in post-salt structures in the Cleveland Basin, that may have initially been charged through the withdrawal and touchdown of Zechstein Group evaporites prior to Cenozoic tilt and uplift. The absence of any onshore hydrocarbon fields to the south, above the Market Weighton Block, is inferred to be due to limited access to charge from productive hydrocarbon source rock kitchens to the north in the Cleveland Basin and east in the Sole Pit Trough (Figure 5.16).

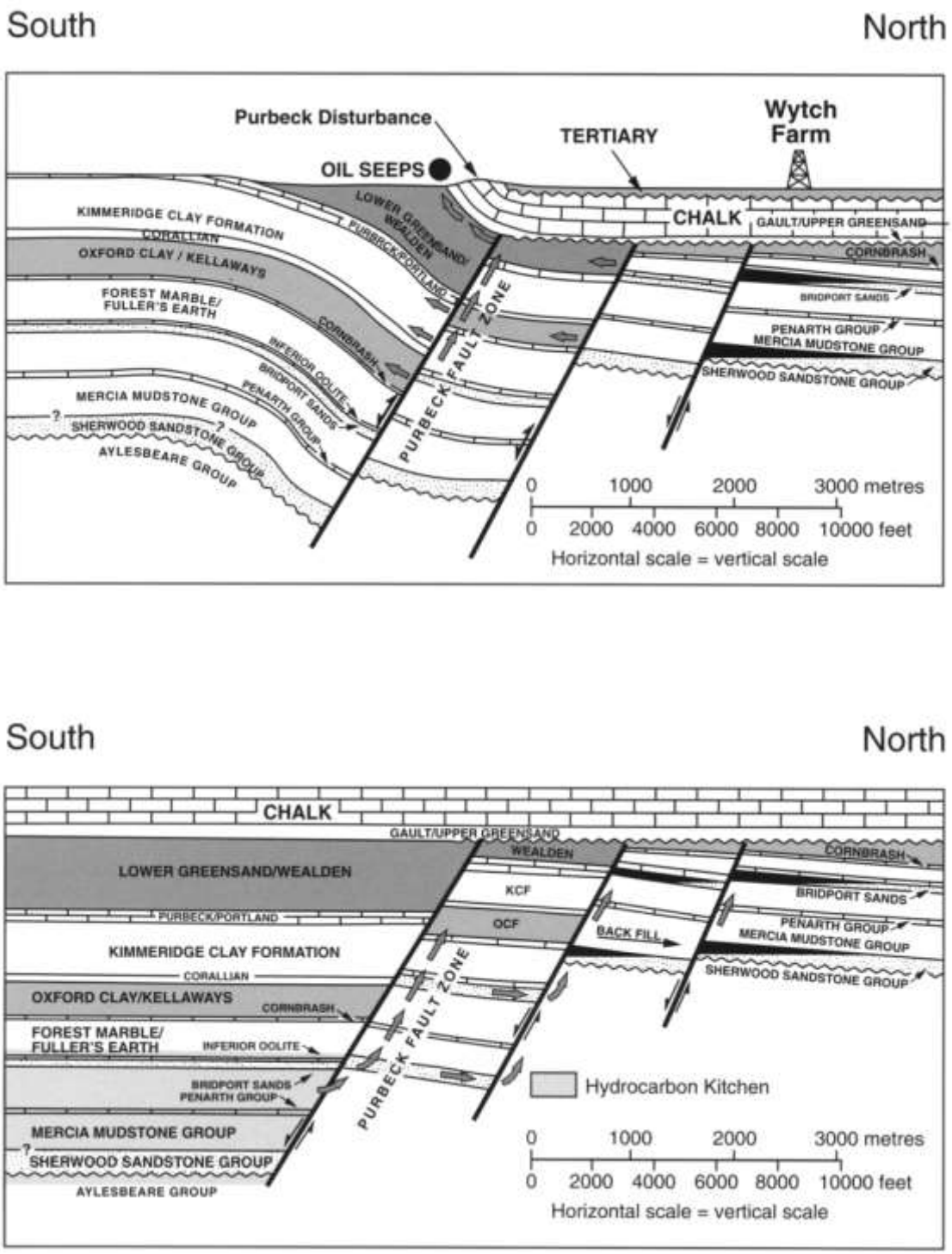

Figure 5.19 South to north present day and restored Late Cretaceous cross-sections through the Wytch Farm oil field highlighting the main controls on hydrocarbon migration and preservation in the area (Underhill & Stoneley 1998).

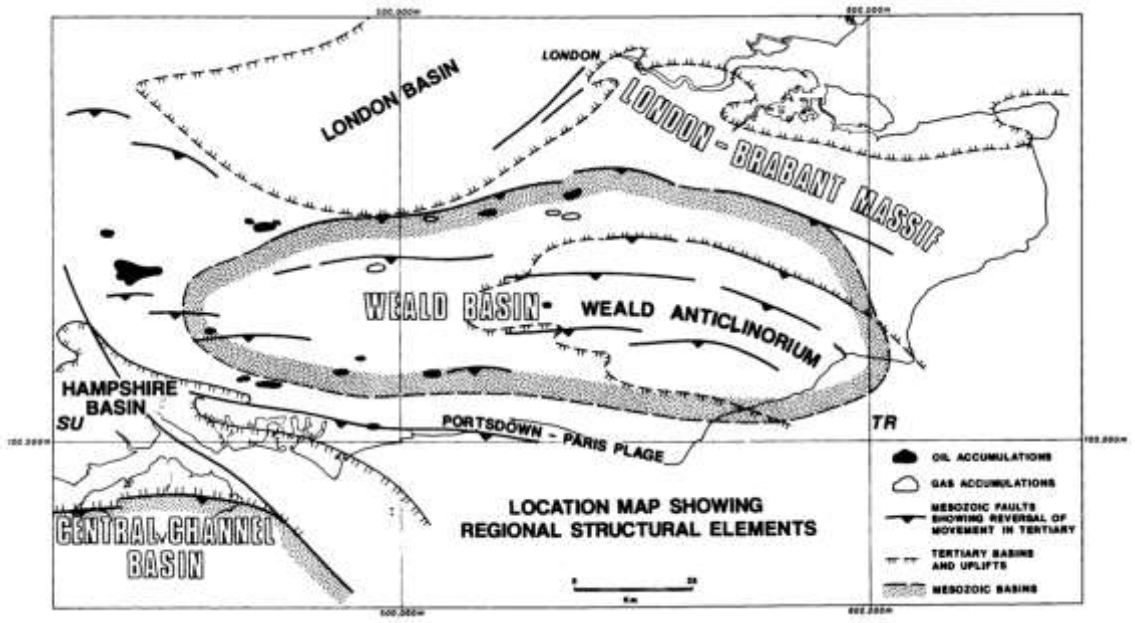

Figure 5.20 Structural element map of the Weald Basin showing present-day hydrocarbon distributions. Note the absence of significant accumulations over the central, Weald Anticlinorium (Butler & Pullan 1990).

Exhumation also has the effect of bringing previously more deeply buried conventional reservoirs such as Carboniferous sandstones to structurally shallower levels. This has resulted in reservoirs that are more greatly affected by porosity and permeability reduction through compaction and burial diagenesis than would be expected for their current burial depth. This is so pronounced in the Namurian aged gas reservoir at Kirby Misperton (Figure 5.16) that no reliable RFT measurements have been recorded across this reservoir due to supercharging, typical of a low permeability reservoir. Hydraulic fracturing of this conventional reservoir is required to achieve flow and often still only results in uneconomical flow rates (Kelt UK Ltd. 1993).

Cenozoic exhumation across the region may also have adverse implications for unconventional hydrocarbon prospectivity. The thick, regionally extensive, Mississippian aged organic-rich basinal marine shales of the Bowland Shale have been recognised as an excellent quality, thermally mature, gas-prone hydrocarbon source rock (Harvey, *et al*. 2017; Hughes, *et al*. 2017) that has provided charge to conventional oil and gas fields in the East Midlands Shelf (Figure 5.16). As a result, it is currently a prospective, if untested, unconventional hydrocarbon reservoir target across northern England, with estimated P50 total in-place gas volumes of 1,329 trillion cubic feet (tcf) for the entire play (Andrews 2013).

Exploration of the Bowland Shale is currently active within the Cleveland Basin through Third Energy's operations at the Kirby Misperton gas field (Figure 5.16). Here, Third Energy are hoping to hydraulically fracture tight sandstone units interbedded within the Bowland Shale sequence that sits structurally below the now shut in, conventional Carboniferous sandstone gas accumulation. The prospective interval is situated within the same anticlinal structural closure as the original Kirby Misperton discovery. Thus, the Kirby Misperton prospect could be considered as a conventionally trapped, tight, thin sandstone test rather than an unconventional Bowland Shale test. A P50 resource estimate in excess of 10 tcf has been reported for the Kirby Misperton structure, with considerable upside if a stratigraphic shale play, where gas is trapped in the shale matrix porosity or fracture system, can be proven beyond this structure through additional drilling (Hughes, *et al*. 2017).

Onshore US unconventional plays are often used as an analogue for prospective onshore UK unconventional plays, including the Bowland Shale (Smith, *et al*. 2010; Andrews 2013; The Department of Energy and Climate Change 2013; Harvey, *et al*. 2017; Hughes *et al*. 2017). However, an important point to note with this comparison is that successful US unconventional plays are characterised by the overpressure of shale reservoirs (including exhumed shale reservoirs such as the Marcellus (English, *et al*. 2016)). Contrary to this, onshore UK basins (and, by extension any prospective unconventional hydrocarbon plays) exhibit an absence of overpressure (Smith, *et al*. 2010; Andrews 2013; The Department of Energy and Climate Change 2013). Supporting this, Carboniferous units in Yorkshire have been encountered at hydrostatic pressure in the subsurface (Taylor Woodrow Energy Ltd. 1985). When a gas-prone source rock is exhumed, gas stored within it, as compressed free gas in the natural fracture or matrix porosity, will migrate from the source rock during exhumation, led by volumetric expansion of the hydrocarbon phase as the pore pressure within the source rock re-equilibrates to the ambient post-exhumation hydrostatic pressures (English, *et al*. 2016). Due to the present day hydrostatic pressure regime for the Carboniferous in and around the Cleveland Basin, it is proposed that any free hydrocarbons contained within potential Carboniferous shale units will have been lost during Cenozoic exhumation, limiting any remaining potential to be accessed through hydraulic fracturing. In contrast, successful, over-pressured US unconventional plays have remained part of a closed-system and protected from re-equilibrating to hydrostatic pressures during exhumation (English, *et al*. 2016).

Other important geological factors that set apart prospective onshore unconventional plays in the UK, such as the Bowland Shale in the Cleveland Basin, from their proven US analogues are the narrower, fault bound and much smaller spatial extent of UK basins compared to large scale laterally extensive US depocentres (Harvey, *et al*. 2017). Onshore UK basins are also affected by substantial syn-and post-depositional tectonic overprinting, as documented in this thesis, compared to the generally more tectonically quiescent US basins (Harvey, *et al*. 2017). The factors described above contribute to the geological challenges that need to be considered in the evaluation of unconventional hydrocarbon plays in the Cleveland Basin and beyond, which ultimately will only be resolved by drilling valid tests of these plays.

CHAPTER 6. CONCLUSIONS

This research provides a new geological model for the evolution of the Flamborough Head Disturbance, that has utilized a comprehensive well and seismic dataset that seamlessly extends from the onshore UK into the neighbouring waters of the Southern North Sea.

The presence of the buried Caledonian granite within the Market Weighton Block has controlled the development of a W-E striking array of planar faults across Flamborough Head, the Flamborough Head Fault Zone, through crustal density contrasts. Through this fault development, the Market Weighton Block granite exerted a structural control on Carboniferous sediment distribution and possibly also upon Variscan inversion, acting as a buttress against which hanging-wall deformation in the Cleveland Basin is focussed.

The Flamborough Head Fault Zone offsets Permo-Carboniferous and older strata and constitutes an onshore extension of the Dowsing Fault Zone. This fault zone does not display any clear evidence to support formation through lateral strike-slip movement. During the Late Triassic to Lower Jurassic, differential subsidence to the north of the Market Weighton Block occurred, creating the Cleveland Basin, with the Flamborough Head Fault Zone acting as a hinge between these structural domains. This resulted in the formation of a W-E striking syn-tectonic Mesozoic graben system, the Flamborough Head Graben System, above the Flamborough Head Fault Zone, which is controlled by listric faults that display a multi-layer ramp-flat detachment system along Triassic and Permian salts and is pinned by the facies change to carbonates that occurs in the footwall by the Zechstein salt basin margin. The Flamborough Head Graben System is decoupled from the underlying basement faults of the Flamborough Head Fault Zone through the presence of thick mobile evaporites of the Permian Zechstein Group, creating a thin-skinned extensional system. Previous studies in the Southern North Sea show that the growth of analogous post-salt graben systems is balanced through pre-salt extension and shortening of the post-salt cover within the basin.

In addition to the W-E striking Flamborough Head Graben System, a NNW-SSE striking post-salt detached graben system developed, the Peak Trough, the southern extent of

which is present in the north of the study area. Field observations from the Cleveland Basin record syn-sedimentary growth across the Peak Trough during the Middle Jurassic. This is inferred to be because of fault rejuvenation due to radial expansion faulting associated with the rising Central North Sea Thermal Dome. From the results of this study, it is proposed that the Zechstein salt basin margin has played a controlling role in the distribution of the Peak Trough. It is suggested that the evaporite – carbonate facies boundary at the basin margin acts as a natural zone of weakness that has pinned the footwall and allowed fault growth into the hanging wall, that detaches onto Zechstein Group evaporites towards the basin centre.

Extensional faulting and syn-tectonic sedimentation within the Flamborough Head Graben System continued until the Late Jurassic after which the post-rift Lower Cretaceous Cromer Knoll Group sediments were deposited onto a regional hiatus in deposition. This study uniquely observes that the Cromer Knoll Group deposition at Flamborough Head is syn-halokinetic, marking marine sedimentation into a depression formed by Zechstein Group salt migration from the Zechstein margin edge in the east into the Sole Pit Basin to the west. Late Cretaceous Chalk Group deposits were deposited regionally across the study area and represent the youngest preserved strata across Flamborough Head.

Flamborough Head was subjected to two discrete basin reconfiguration episodes after Chalk Group deposition. This included regional tilting to the south-east as a result of vertical stresses attributed to the onset, during the Paleocene, of the Proto-Iceland Plume in the North Atlantic. The other episode comprised of fault reactivation and inversion of the Cleveland Basin due to lateral stresses resulting in intra-plate deformation related to far-field Alpine collision and rift push from rifting in the North Atlantic. During inversion of the Cleveland Basin, deformation was concentrated in the hanging wall of the Flamborough Head Fault Zone, with the post-salt section being buckled into a monocline.

The listric faults of the Flamborough Head Graben System have remained in extension during this deformation. This deformation style is inferred to have resulted from the presence of the Market Weighton Block granite in the footwall of the Flamborough Head Fault Zone, which has effectively acted as a buttress against compression that has therefore been taken up in the hanging wall, preferentially inverting hanging wall faults. The presence of Zechstein Group salt has inhibited basement fault reactivation in the

hanging wall from propagating into the cover, instead folded the post salt section into a monocline. The inversion of the main listric detachment fault of the Flamborough Head Graben System into the Zechstein Group salt, along with basinward movement of the post-salt cover from a pin at the Zechstein shelf edge into the basin, has resulted in and accommodated the preservation of extensional listric fault geometries within the Flamborough Head Graben System.

Buckling of the post-salt cover during inversion has resulted in the intra-formational deformation observed in Chalk Group outcrops at Flamborough Head, rather than reactivation of the Flamborough Head Graben System.

Post-Chalk Group exhumation of the Cleveland Basin has severely affected hydrocarbon prospectivity of the region, with the switching off of the Carboniferous petroleum system as well as the redistribution and loss of hydrocarbons from the inverted hanging wall of the Flamborough Head Fault Zone (i.e. the Cleveland Basin). Hydrocarbons have been preserved in small, high integrity traps sealed by Zechstein Group evaporites in the un-deformed footwall (i.e. the Market Weighton Block). Exhumation has also resulted in the de-pressurisation of gas-prone Carboniferous source rocks, adding risk to unconventional exploration. This research also suggests a tectonic controlling factor from the Flamborough Head Fault Zone on the development of the proven Rotliegend Group Leman Sandstone Formation reservoir.

This work highlights the great importance that buried granites and, at a basin specific scale, the presence of mobile evaporites have on the generation, evolution and structural inversion of Mesozoic sedimentary basins in the UK. The geological model proposed for the formation of the Flamborough Head Disturbance shares similar characteristics to structurally inverted Mesozoic basins seen elsewhere in the UK. It acts as an important contributor to the greater understanding of regional uplift and intraplate deformation that has affected the UK from the Late Cretaceous into the Cenozoic and the impact this has had on hydrocarbon prospectivity in and around inverted Mesozoic basin in the UK.

CHAPTER 7. REFERENCES

Agile Geoscience, 2016. *SubSurf Wiki: Convolution Model.* [Online]
Available at: http://subsurfwiki.org/wiki/Convolutional_model
[Accessed 11 September 2017].

Andrews, I. J., 2013. *The Carboniferous Bowland Shale gas study: geology and resource estimation.*, London: British Geological Survey for Department of Energy and Climate Change.

Argent, J. D., Stewart, S. A. & Underhill, J. R., 2000. Controls on the Lower Cretaceous Punt Sandstone Member, a massive deep-water clastic deposystem, Inner Moray Firth, UK North Sea. *Petroleum Geoscience,* 6(3), pp. 275-285.

Bachmann, G. H. et al., 2010. Triassic. In: J. C. Doorenbal & A. G. Stevenson, eds. *Petroleum Geological Atlas of the Southern Permian Basin Area.* Houten: EAGE Publications b.v., pp. 149-173.

Badley, M., 1990. *Practical Seismic Interpretation,* Lincoln: Badley, Ashton & Associates Ltd..

Badley, M. E., Price, J. D. & Backshall, L. C., 1989. Inversion, reactivated faults and related structures: seismic examples from the southern North Sea. *Geological Society, London, Special Publications,* 44(1), pp. 201-219.

Bertram, G., 2012. *Seismic and Sequence Stratigraphy for Play Prediction and Basin Analysis,* Hermitage, Berkshire: Nautilus Ltd..

Bertram, G. T. & Milton, N. J., 1996. Seismic Stratigraphy. In: D. Emery & K. J. Myers, eds. *Sequence Stratigraphy.* Oxford: Blackwell Science, pp. 45-60.

Bott, M. H. P., Robinson, J. & Kohnstamm, M. A., 1978. Granite beneath Market Weighton, east Yorkshire. *Journal of the Geological Society,* 135(5), pp. 535-543.

Butler, M., 1998. The geological history of the southern Wessex Basin - a review of new information from oil exploration. *Geological Society, London, Special Publications,* 133(1), pp. 67-86.

Butler, M. & Jamieson, R., 2013. *Preliminary interpretation of six regional seismic profiles across onshore basins of England,* s.l.: UK Onshore Geophysical Library.

Butler, M. & Pullan, C. P., 1990. Tertiary structures and hydrocarbon entrapment in the Weald Basin of southern England. *Geological Society, London, Special Publications,* Volume 55, pp. 371-391.

Cartwright, J., 2009. *Polygonal faults and diagenesis: Figure 8.* [Online]
Available at: http://www.seismicatlas.org/entity?id=49d541d2-c28d-468a-b724-c3e29652b076
[Accessed 11 September 2017].

Chamberlain, J., 2013. *Geophysics for Subsurface Professionals,* Hermitage, Berkshire: Nautilus Ltd..

Chamberlain, J. & Rock Physics Associates, 2013. *The Essentials of Rock Physics for Seismic Amplitude Interpretation,* Hermitage, Berkshire: Nautilus Ltd..

Cohen, K. M., Harper, D. A. & Gibbard, P. L., 2018. *ICS International Chronostratigraphic Chart.* [Online]
Available at: www.stratigraphy.org
[Accessed 17 07 2018].

Cooper, M. & Warren, M. J., 2010. The geometric characteristics, genesis and petroleum significance of inversion structures. *Geological Society, London, Special Publications,* 335(1), p. 827–846.

Cope, J., 1994. A latest Cretaceous hotspot and the southeasterly tilt of Britain. *Journal of the Geological Society,* Volume 151, pp. 905-908.

Davis, J. W., 1885. On the contortions in the Chalk at Flamborough Head. *Proceedings of the Yorkshire Geological Society,* 9(1), pp. 43-49.

Digital Exploration Ltd, 1993. *North Sea Blk 42/27B 1992 - 93 3D Survey Processing Report,* East Grinstead: s.n.

Dixon, A. D. G., 1990. *Evolution of the Yorkshire, sole pit and east mid land basin system, U.K,* Durham theses, Durham University: Available at Durham E-Theses Online: http://etheses.dur.ac.uk/6695/.

Donato, J. A., 1993. A buried granite batholith and the origin of the Sole Pit Basin, UK Southern North Sea. *Journal of the Geological Society,* 150(2), pp. 255-258.

Duguid, C. & Underhill, J. R., 2010. Geological controls on Upper Permian Plattendolomit Formation reservoir prospectivity, Wissey Field, UK Southern North Sea. *Petroleum Geoscience,* 16(4), pp. 331-348.

Egdon Resources (UK) Ltd., 2000. *UK Landward Areas Ninth Licence Round Application Document: Appendix B, Vale of Pickering-Flamborough Head Fault Zone Petroleum Exploration and Development Application,* s.l.: s.n.

English, J. M., English, K. L., Corcoran, D. V. & Toussaint, F., 2016. Exhumation charge: The last gasp of a petroleum source rock and implications for unconventional shale resources. *AAPG Bulletin,* 100(1), pp. 1-16.

Fossen, H., 2010. *Structural Geology.* Cambridge: Cambridge University Press.

Frakes, L. A., Francis, J. E. & Syktus, J. I., 1992. *Climate Modes of the Phanerozoic.* Cambridge: Cambridge University Press.

Fraser, A. J. & Gawthorpe, R. L., 2003. *An Atlas of Carboniferous Basin Evolution in Northern England. Geological Society, London, Memoirs, 28.* London: Geological Society, London.

Gale, A. S. & Lovell, B., 2017. (in press) The Cretaceous-Paleogene unconformity in England: Uplift and erosion related to the Iceland mantle plume.. *Proceedings of the Geologists' Association.*

Gast, R. E. et al., 2010. Rotliegend. In: J. C. Doorenbal & A. G. Stevenson, eds. *Petroleum Geological Atlas of the Southern Permian Basin Area.* Houten: EAGE Publications b.v., pp. 101-121.

Glennie, K. W. & Boegner, P. L. E., 1981. Sole Pit inversion tectonics. In: L. V. Illing & G. D. Hobson, eds. *Petroleum Geology of the Continental Shelf of North-West Europe.* London: Heyden & Son LTD, pp. 110-120.

Green, P. F., 1989. Thermal and tectonic history of the East Midlands Shelf (onshore UK.) and surrounding regions assessed by apatite fission track analysis. *Journal of the Geological Society,* 146(5), pp. 755-774.

Green, P. F., Duddy, I. R. & Japsen, P., 2017. (in press). Multiple episodes of regional exhumation and inversion identified in the UK Southern North Sea based on integration of palaeothermal and palaeoburial indicators. In: M. Bowman & B. Levell, eds. *Petroleum Geology of NW Europe: 50 Years of Learning – Proceedings of the 8th Petroleum Geology Conference.* London: The Geological Society, London.

Guariguata-Rojas, G. J. & Underhill, J. R., 2017. Implications of Early Cenozoic uplift and fault reactivation for carbon storage in the Moray Firth Basin. *Interpretation,* 5(4), pp. SS1-SS21.

Harding, T. P., 1990. Identification of wrench faults using subsurface structural data: criteria and pitfalls. *AAPG Bulletin,* 74(10), pp. 1590-1609.

Harding, T. P. & Lowell, J. D., 1979. Structural styles, their plate tectonic habitats and hydrocarbon traps in petroleum provinces.. *AAPG Bulletin,* 63(7), pp. 1016-1058.

Harvey, A. L., Andrews, I. J. & Monaghan, A. A., 2017. (in press) Shale prospectivity onshore Great Britain. In: M. Bowman & B. Levell, eds. *Petroleum Geology of NW Europe: 50 Years of Learning – Proceedings of the 8th Petroleum Geology Conference.* London: The Geological Society, London.

Harvey, M. J. & Stewart, S. A., 1998. Influence of salt on the structural evolution of the Channel Basin. *Geological Society, London, Special Publications,* 133(1), pp. 241-266.

Hillis, R. R. et al., 2008. Cenozoic exhumation of the southern British Isles. *Geology,* 36(5), pp. 371-374.

Hughes, F. et al., 2017. (in press) The unconventional Carboniferous reservoirs of the Greater Kirby Misperton gas field and their potential : North Yorkshire's sleeping giant. In: M. Bowman & B. Levell, eds. *Petroleum Geology of NW Europe: 50 Years of Learning – Proceedings of the 8th Petroleum Geology Conference.* London: The Geological Society, London.

Jones, S. M. et al., 2002. Present and past influence of the Iceland Plume on sedimentation. *Geological Society, London, Special Publications,* 196(1), pp. 13-25.

Kearey, P., Brooks, M. & Hill, I., 2002. *An Introduction to Geophysical Exploration.* Third ed. Oxford: Blackwell Science Ltd..

Kelt UK Ltd., 1991. *Caythorpe Gasfield Development. PL234B, Humberside. Development Plan* , s.l.: s.n.

Kelt UK Ltd., 1993. *Ryedale Gasfields Development Plan,* London: Kelt UK Ltd..

Kent, P. E., 1980. Subsidence and Uplift in East Yorkshire and Lincolnshire: a Double Inversion. *Proceedings of the Yorkshire Geological Society,* 42(28), pp. 505-524.

Kirby, G. A. & Swallow, P. W., 1987. Tectonism and sedimentation in the Flamborough Head region of north-east England. *Proceedings of the Yorkshire Geological Society,* 46(4), pp. 301-309.

Lamplugh, G. W., 1889. On the subdivisions of the Speeton Clay. *Quarterly Journal of the Geological Society, London,* Volume 45, pp. 575-618.

Lamplugh, G. W., 1895. Notes on the White Chalk of Yorkshire. *Proceedings of the Yorkshire Geological Society,* 13(1), pp. 65-87.

Lott, G. K., Fletcher, B. N. & Wilkinson, I. P., 1986. The stratigraphy of the Lower Cretaceous Speeton Clay Formation in a cored borehole off the coast of north-east England. *Proceedings of the Yorkshire Geological Society,* 46(1), pp. 39-56.

Lott, G. K. et al., 2010. Jurassic. In: J. C. Doorenbal & A. G. Stevenson, eds. *Petroleum Geological Atlas of the Southern Permian Basin Area.* Houten: EAGE Publications b.v., pp. 175-193.

Lundin, E. R., 1992. Thin-skinned extensional tectonics on a salt detachment, northern Kwanza Basin, Angola. *Marine and Petroleum Geology,* 9(4), pp. 405-411.

Marsden, D., 1992. Vo-K method of depth conversion. *The Leading Edge,* Issue August, pp. 53-54.

Milsom, J. & Rawson, P. F., 1989. The Peak Trough - a major control on the geology of the North Yorkshire coast. *Geological Magazine,* 126(6), pp. 699-705.

Mitchum, R. M., 1977. Seismic Startigraphy and Global Changes of Sea Level, Part 11: Glossary of Terms used in Seismic Stratigraphy. In: C. E. Payton, ed. *AAPG Memoir 26: Seismic Stratigraphy - applications to hydrocarbon exploration.* Tulsa: The American Association of Petroleum Geologist, pp. 205-212.

Offshore Technology.com, 2017a. *Tolmount Prospect, North Sea, United Kingdom.* [Online]
Available at: http://www.offshore-technology.com/projects/tolmount-prospect-north-sea
[Accessed 4 September 2017a].

Offshore Technology.com, 2017b. *Breagh Gas Field, Southern North Sea, United Kingdom.* [Online]
Available at: http://www.offshore-technology.com/projects/breagh-field/
[Accessed 4 September 2017b].

Peryt, T. M. et al., 2010. Zechstein. In: J. C. Doorenbal & A. G. Stevenson, eds. *Petroleum Geological Atlas of the Southern Permian Basin.* Houten: EAGE Publications, pp. 123-147.

Philips, J., 1835. *Illustrations of the Geology of Yorkshire; Part 1 - the Yorkshire Coast.* 2nd ed. London: pr. for J. Murray.

Powell, J. H., 2010. Jurassic sedimentation in the Cleveland Basin: a review. *Proceedings of the Yorkshire Geological Society,* 58(1), pp. 21-72.

Richard, P., 1991. Experiments on faulting in a two-layer cover sequence overlying a reactivated basement fault with oblique-slip. *Journal of Structural Geology,* 13(4), pp. 459-469.

Rigzone, 2006. *News: Roc Oil Says Willows-1 Dry.* [Online]
Available at: http://www.rigzone.com/news/oil_gas/a/32577/roc_oil_says_willows1_dry/
[Accessed 25 October 2017].

Roc Oil (UK) Ltd., 2002. *Onshore UK Cleveland Basin - PEDL030: 2001 Licence Review & Status,* s.l.: s.n.

Simm, R., 2014. *Professional Level Rock Physics for Seismic Amplitude Interpretation (AVO and Seismic Inversion),* Hermitage, Berkshire: Nautilus Ltd..

Smith, D. B. et al., 1992. Permian. In: J. C. W. Cope, J. K. Ingham & P. F. Rawson, eds. *Atlas of Palaeogeography and Lithofacies.* London: The Geological Society, London, Memoir, 13, pp. 87-96.

Smith, N., Turner, P. & Williams, G., 2010. UK data and analysis for shale gas prospectivity. In: B. A. Vining & S. C. Pickering, eds. *Petroleum Geology: From Mature Basins to New Frontiers – Proceedings of the 7th PetroleumGeology Conference.* London: The Geological Society, London, pp. 1087-1098.

Smith, T., 2009. Gas hydrates - not so unconventional. *GEO ExPro,* 6(2).

Starmer, I. C., 1995. Deformation of the Upper Cretaceous Chalk at Selwicks Bay, Flamborough Head, Yorkshire: its significance in the structural evolution of north-east England and the North Sea Basin. *Proceedings of the Yorkshire Geological Society,* 50(3), pp. 213-228.

Starmer, I. C., 2008. The concentration of folding and faulting in the Chalk at Staple Newk (Scale Nab), near Flamborough, East Yorkshire. *Proceedings of the Yorkshire Geological Society,* 57(2), pp. 95-106.

Starmer, I. C., 2013. Folding and faulting in the Chalk at Dykes End, Bridlington Bay, East Yorkshire, resulting from reactivations of the Flamborough Head Fault Zone. *Proceedings of the Yorkshire Geological Society,* 59(3), pp. 195-201.

Steele, R., 2017. *Exploration and Production in a Mature Basin: The North Sea. The Permian,* Croydon, London: The Petroleum Exploration Society of Great Britain.

Stewart, S., 2008. *North Sea Salt Tectonics - 6.* [Online]
Available at: http://www.seismicatlas.org/entity?id=5ef3ea51-c50b-4e5b-b6b8-53c5acfe86a8
[Accessed 12 September 2017].

Stewart, S. A. & Bailey, H. W., 1996. The Flamborough Tertiary outlier, UK southern North sea. *Journal of the Geological Society,* Volume 153, pp. 163-173.

Stewart, S. A. & Coward, M. P., 1995. Synthesis of salt tectonics in the southern North Sea, UK. *Marine and Petroleum Geology,* 12(5), pp. 457-475.

Stewart, S. A., Harvey, M. J., Otto, S. C. & Weston, P. J., 1996. Influence of salt on fault geometry: examples from the UK salt basins. *Geological Society, London, Special Publications,* 100(1), pp. 175-202.

Taylor Woodrow Energy Ltd., 1985. *Hatfield Gas Field Development Plan,* London: Taylor Woodrow Energy Ltd..

Taylor, J. C., 2009. Upper Permian-Zechstein. In: K. W. Glennie, ed. *Petroleum Geology of the North Sea: Basic Concepts and Recent Advances.* Fourth ed. Oxford: John Wiley & Sons, Incorporated, pp. 174-211.

The Department of Energy and Climate Change, 2013. *The unconventional hydrocarbon resources of Britain's onshore basins - shale gas,* London: British Geological Survey for Department of Energy and Climate Change.

Underhill, J. R., 2003. The tectonic and stratigraphic framework of the United Kingdom's oil and gas fields. *Geological Society, London, Memoirs,* 20(1), pp. 17-59.

Underhill, J. R. & Partington, M. A., 1993. Jurassic thermal doming and deflation in the North Sea: implications of the sequence stratigraphic evidence. In: J. R. Parker, ed. *Petroleum Geology of Northwest Europe: Proceedings of the 4th Conference.* London: The Geological Society, London, pp. 337-345.

Underhill, J. R. & Paterson, S., 1998. Genesis of tectonic inversion structures: seismic evidence for the development of key structures along the Purbeck-Isle of Wight Disturbance. *Journal of the Geological Society,* 155(6), pp. 975-992.

Underhill, J. R. & Stoneley, R., 1998. Introduction to the development, evolution and petroleum geology of the Wessex Basin. *Geological Society, London, Special Publications,* Volume 133, pp. 1-18.

van Hoorn, B., 1987. Structural evolution, timing and tectonic style of the Sole Pit inversion. *Tectonophysics,* 137(1-4), pp. 239-254, 259-268, 270-284.

Vejbaek, O. V. et al., 2010. Cretaceous. In: J. C. Doorenbal & A. G. Stevenson, eds. *Petroleum Geological Atlas of the Southern Permian Basin Area.* Houten: EAGE Publications b.v., pp. 195-209.

Warwick Energy, 2006. *Preliminary Submission of Proposals for a Gas Storage Authorisation Order for the Cayhtorpe Gas Field Under Section 4 of the Gas Act 1965,* s.l.: s.n.

White, R. & Simm, R., 2003. Tutorial: Good practice in well ties. *First Break,* 21(10), pp. 75-83.

Wikipedia, 2016. *Flat spot (reflection seismology).* [Online]
Available at: https://en.wikipedia.org/wiki/Flat_spot_(reflection_seismology)
[Accessed 11 September 2017].

Ziegler, P. A., 1988. *Evolution of the Arctic-North Atlantic and the Western Tethys: AAPG Memoir 43.* Tulsa, Oklahoma, 74101, U.S.A.: The American Association of Petroleum Geologists.

Ziegler, P. A., 1989. Geodynamic model for Alpine intra-plate compressional deformation in Western and Central Europe. *Geological Society, London, Special Publications,* 44(1), pp. 63-85.

Ziegler, P. A. & van Hoorn, B., 1989. Evolution of the North Sea Rift System. In: A. Tankard & H. Balkwill, eds. *AAPG Memoir 46: Extensional Tectonics and Stritigraphy of North Atlantic Margins.* Tulsa, Oklahoma: American Association of Petroleum Geologists & Canadian Geological Foundation, pp. 471-500.

APPENDIX A. REGIONAL TWO-WAY TRAVEL TIME STRUCTURE GRIDS

All TWTT structure grids in this section are displaying time elevation z values in milliseconds with a colour shading convention of warm colours representing structural highs and cool colours representing structural lows. Displayed time structure grids are:

Sea Bed

Base Chalk

Base Cretaceous

Corallian

Lias

Triassic

Bacton

Zechstein

Zechstein Z2

Base Permian Unconformity

Sea Bed TWT. Contour Interval = 20ms

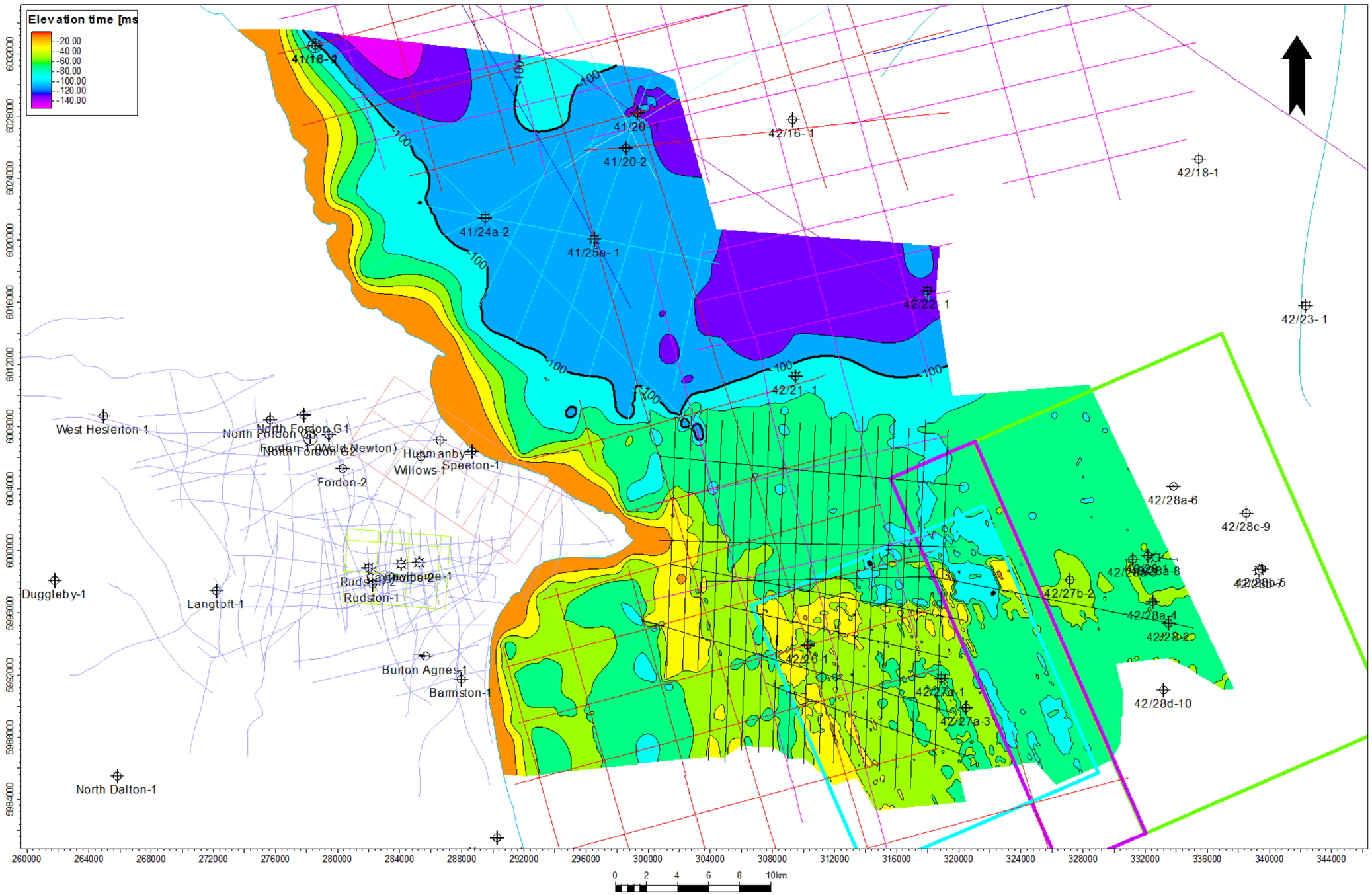

Base Chalk TWT. Contour Interval = 50ms

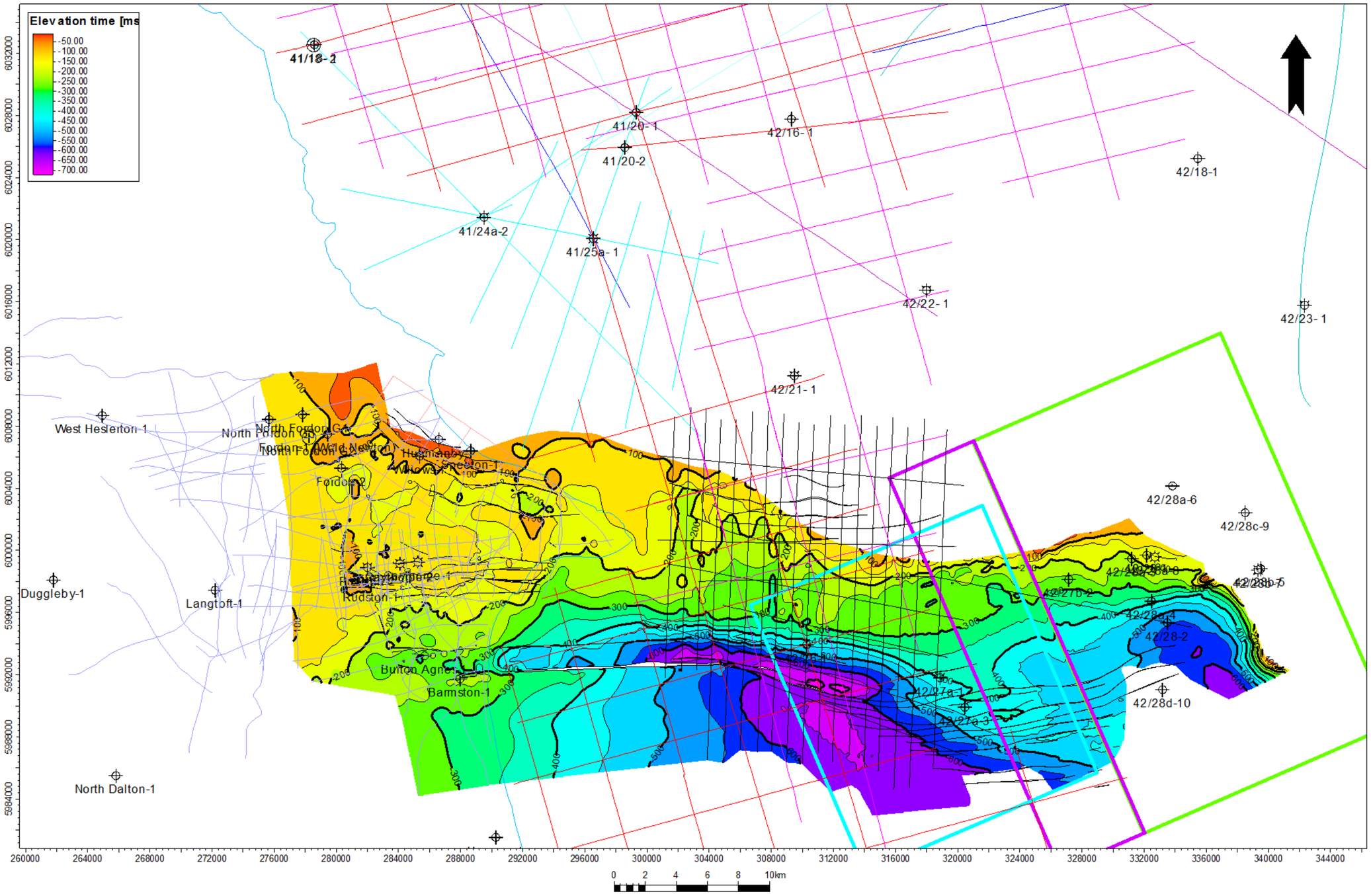

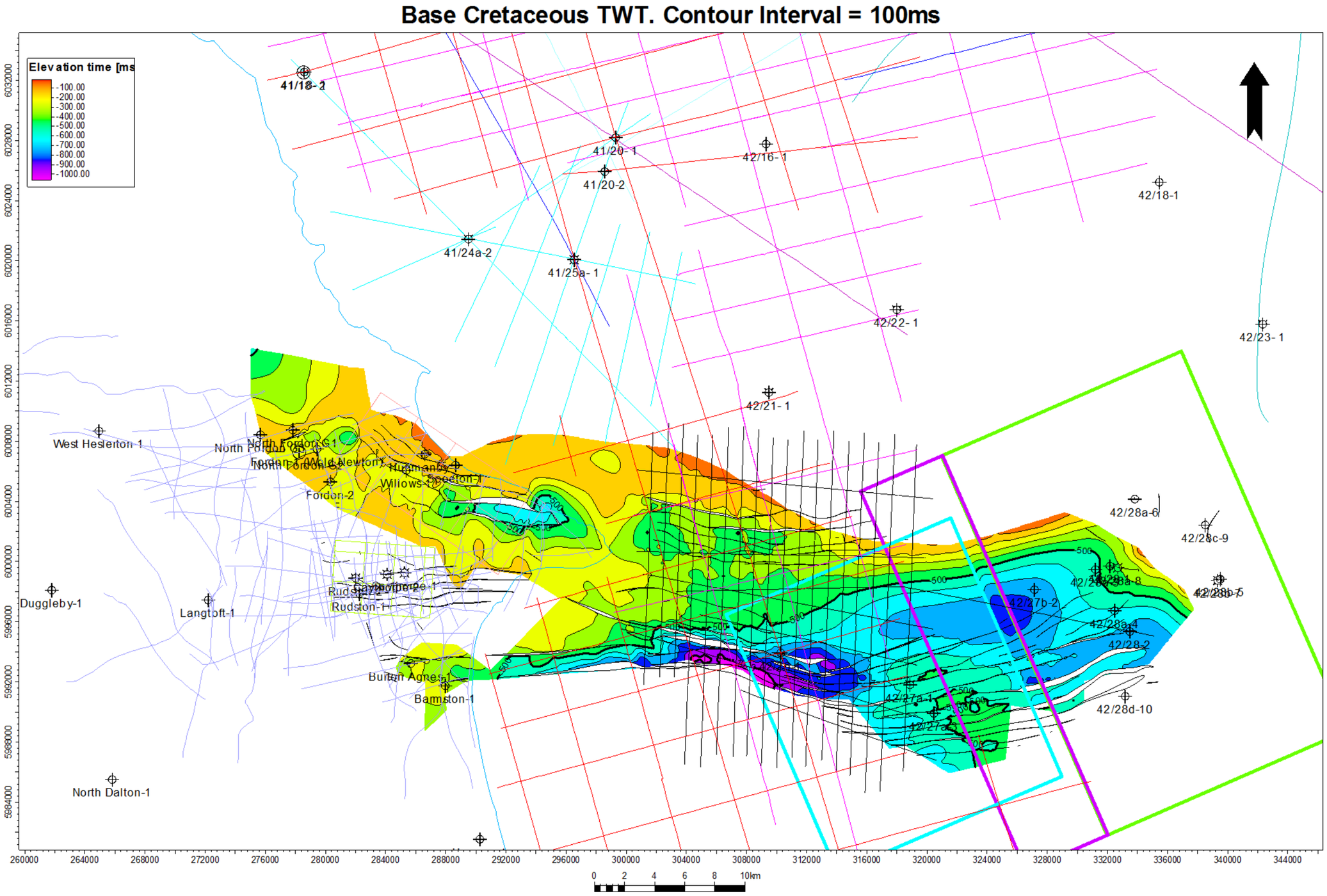
Base Cretaceous TWT. Contour Interval = 100ms
Elevation time [ms
-100.00
-200.00
-300.00
-400.00
-500.00
-600.00
-700.00
-800.00
-900.00
-1000.00
41/18-2
41/20-1
41/20-2
42/16-1
42/18-1
41/24a-2
41/25a-1
42/22-1
42/23-1
42/21-1
West Heslerton-1
North Fordon-G1
North Fordon-S1
North Fordon-S2
Fordon-2
Wold Newton-1
Humanby-1
Willows-1
Speeton-1
42/28a-6
42/28c-9
42/28a-8
42/28b-5
42/27b-2
42/28a-4
42/28-2
Duggleby-1
Langtoft-1
Rudston-2
Rudston-1
Cayton Bay-1
Burton Agnes-1
Barmston-1
42/27a-1
42/27a-2
42/28d-10
North Dalton-1
500
260000
264000
268000
272000
276000
280000
284000
288000
292000
296000
300000
304000
308000
312000
316000
320000
324000
328000
332000
336000
340000
344000
6032000
6028000
6024000
6020000
6016000
6012000
6008000
6004000
6000000
5996000
5992000
5988000
5984000
0 2 4 6 8 10km

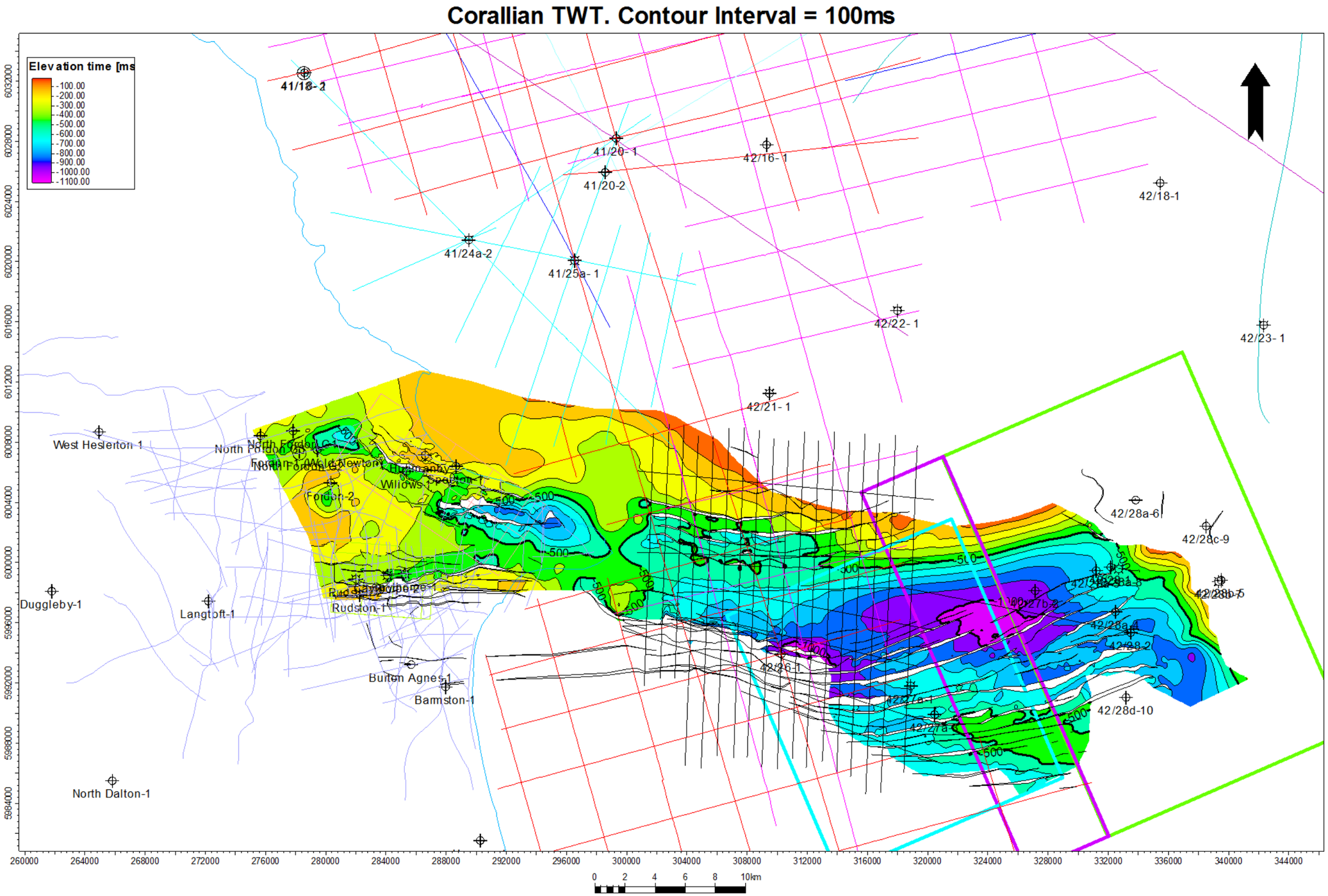
Corallian TWT. Contour Interval = 100ms
Elevation time [ms
-100.00
-200.00
-300.00
-400.00
-500.00
-600.00
-700.00
-800.00
-900.00
-1000.00
-1100.00
41/18-2
41/20-1
41/20-2
42/16-1
42/18-1
41/24a-2
41/25a-1
42/22-1
42/23-1
42/21-1
West Hesleton-1
North Foreden-1
Foreden-2
Willows-1
Duggleby-1
Langtoft-1
Rudston-1
Burton Agnes-1
Barmston-1
North Dalton-1
42/28a-6
42/28c-9
42/28b-5
42/28a-4
42/28-2
42/28d-10
42/26-1
42/27a-1
42/27a-2
42/27b-2
6032000
6028000
6024000
6020000
6016000
6012000
6008000
6004000
6000000
5996000
5992000
5988000
5984000
260000
264000
268000
272000
276000
280000
284000
288000
292000
296000
300000
304000
308000
312000
316000
320000
324000
328000
332000
336000
340000
344000
0 2 4 6 8 10km

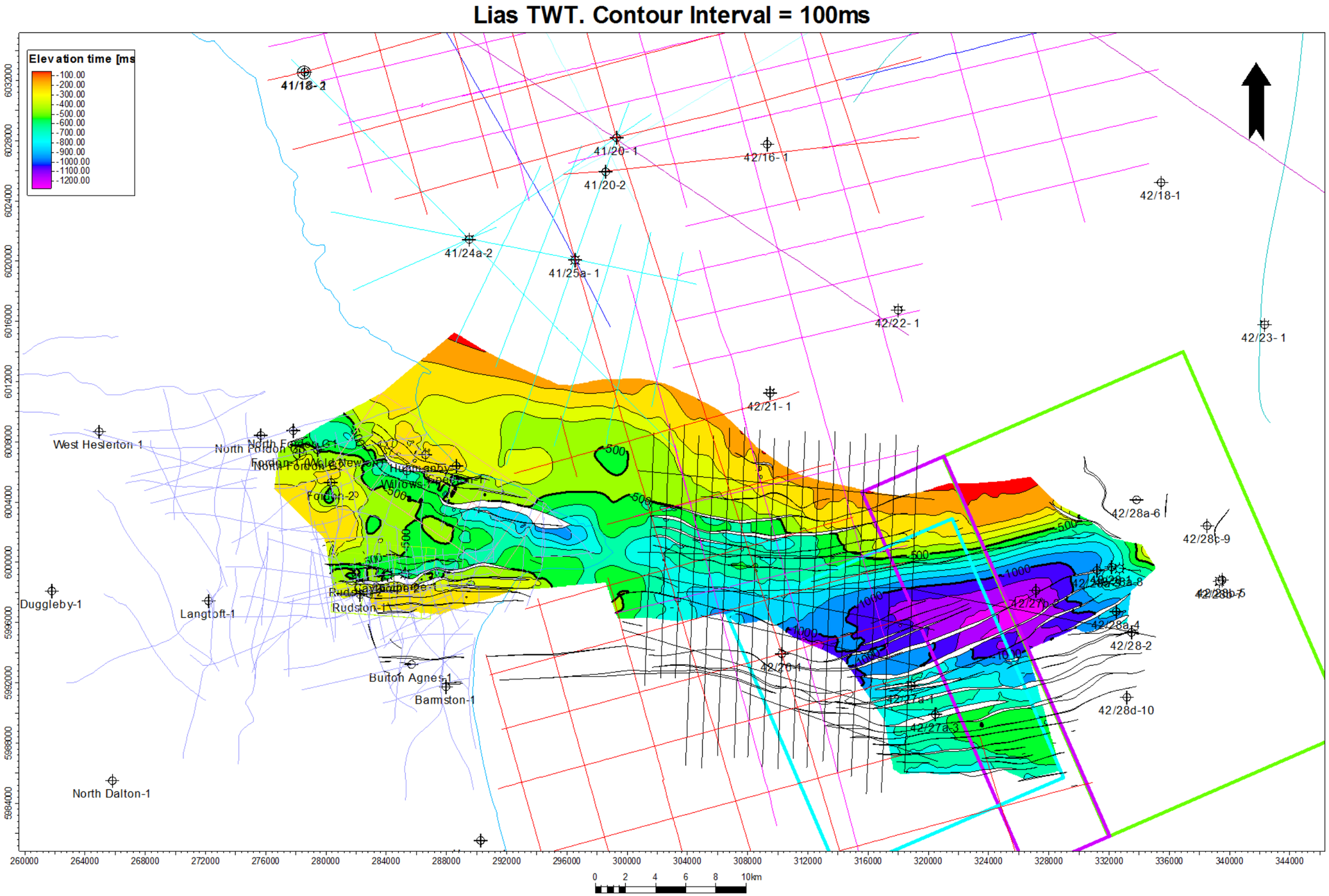
Lias TWT. Contour Interval = 100ms
Elevation time [ms
-100.00
-200.00
-300.00
-400.00
-500.00
-600.00
-700.00
-800.00
-900.00
-1000.00
-1100.00
-1200.00
41/18-2
41/20-1
41/20-2
42/16-1
42/18-1
41/24a-2
41/25a-1
42/22-1
42/23-1
42/21-1
West Heslerton-1
North Foreton-1
North Foreton-2
Foreton-2
Wold Newton-1
Huttons Ambo-1
Willows-1
Duggleby-1
Langtoft-1
Rudston-1
Burton Agnes-1
Barmston-1
North Dalton-1
42/28a-6
42/28c-9
42/28a-8
42/28b-5
42/27b-2
42/28a-4
42/28-2
42/27a-1
42/27a-3
42/28d-10
500
1000
6032000
6028000
6024000
6020000
6016000
6012000
6008000
6004000
6000000
5996000
5992000
5988000
5984000
260000
264000
268000
272000
276000
280000
284000
288000
292000
296000
300000
304000
308000
312000
316000
320000
324000
328000
332000
336000
340000
344000
0 2 4 6 8 10km

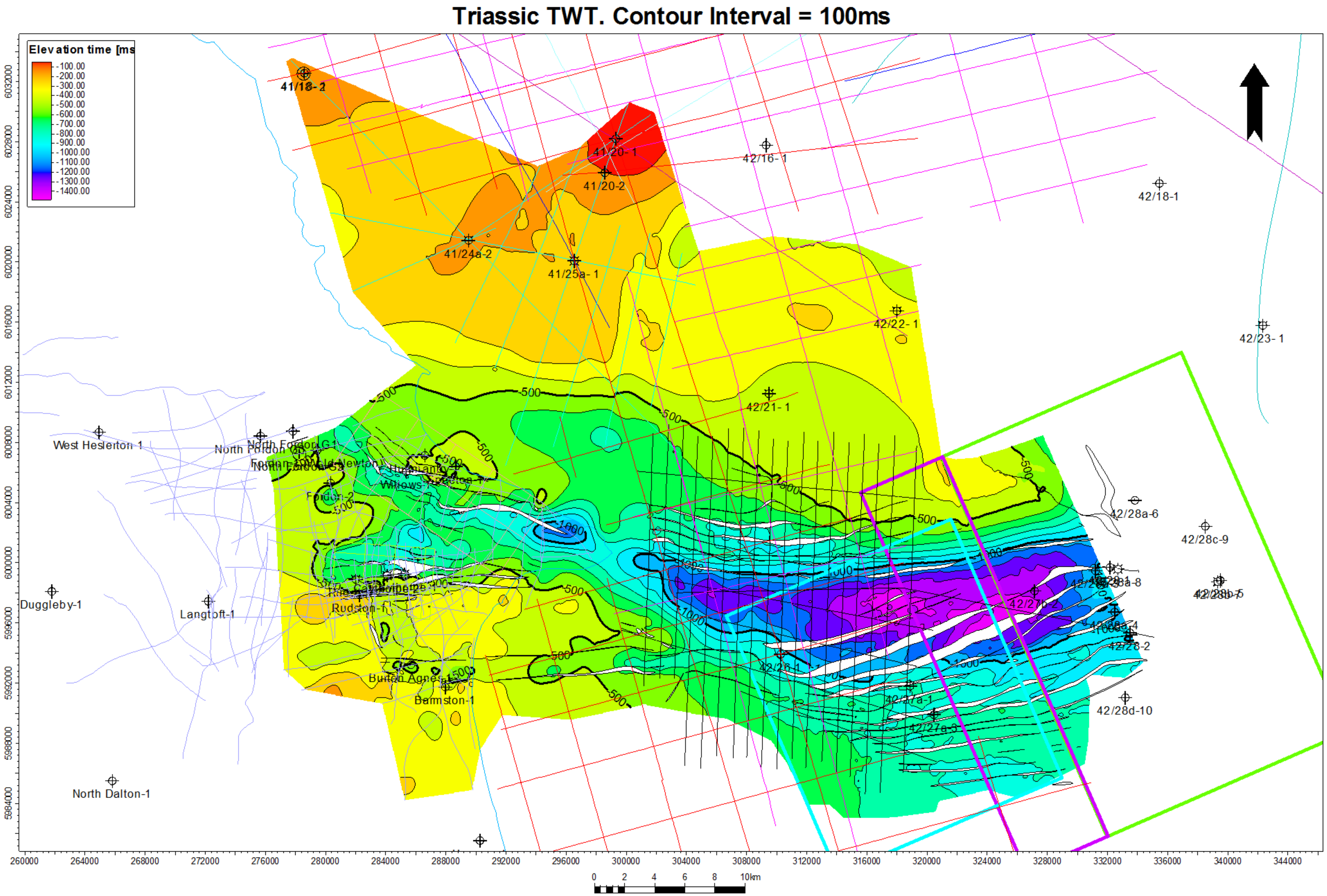
Triassic TWT. Contour Interval = 100ms
Elevation time [ms
-100.00
-200.00
-300.00
-400.00
-500.00
-600.00
-700.00
-800.00
-900.00
-1000.00
-1100.00
-1200.00
-1300.00
-1400.00
41/18-2
41/20-1
41/20-2
42/16-1
42/18-1
41/24a-2
41/25a-1
42/22-1
42/23-1
42/21-1
West Heslerton 1
North Fordon G1
North Fordon G2
Fordon-1
Fordon-2
Willows-1
Duggleby-1
Langtoft-1
Rudston-1
Burton Agnes-1
Barmston-1
North Dalton-1
42/28a-6
42/28c-9
42/28d-10
42/28-2
42/27a-1
42/27a-3
42/26-1
-500
-1000
0 2 4 6 8 10km

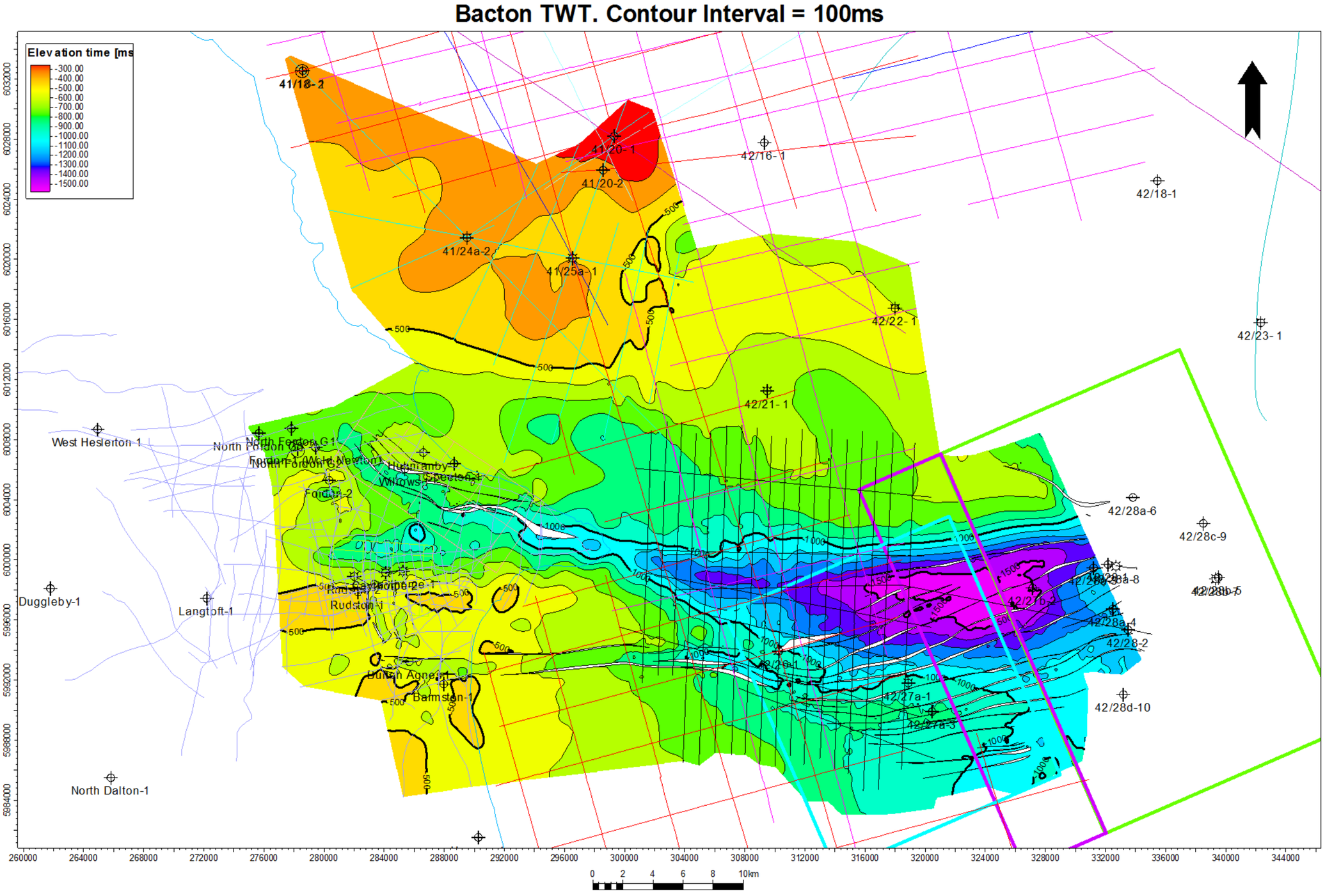
Bacton TWT. Contour Interval = 100ms
Elevation time [ms
-300.00
-400.00
-500.00
-600.00
-700.00
-800.00
-900.00
-1000.00
-1100.00
-1200.00
-1300.00
-1400.00
-1500.00
41/18-2
41/20-1
41/20-2
42/16-1
42/18-1
41/24a-2
41/25a-1
42/22-1
42/23-1
42/21-1
West Hesleton-1
North Foreton G1
North Foreton S2
Foreton-2
Whitwell Newton1
Humranby-1
Whitwell-1
Duggleby-1
Langtoft-1
Rudston-1
Burton Agnes-1
Barmston-1
North Dalton-1
42/28a-6
42/28c-9
42/28a-8
42/28b-5
42/27b-2
42/28a-4
42/28-2
42/27a-1
42/27a-3
42/28d-10
260000
264000
268000
272000
276000
280000
284000
288000
292000
296000
300000
304000
308000
312000
316000
320000
324000
328000
332000
336000
340000
344000
6032000
6028000
6024000
6020000
6016000
6012000
6008000
6004000
6000000
5996000
5992000
5988000
5984000
0 2 4 6 8 10km

Zechstein TWT. Contour Interval = 100ms

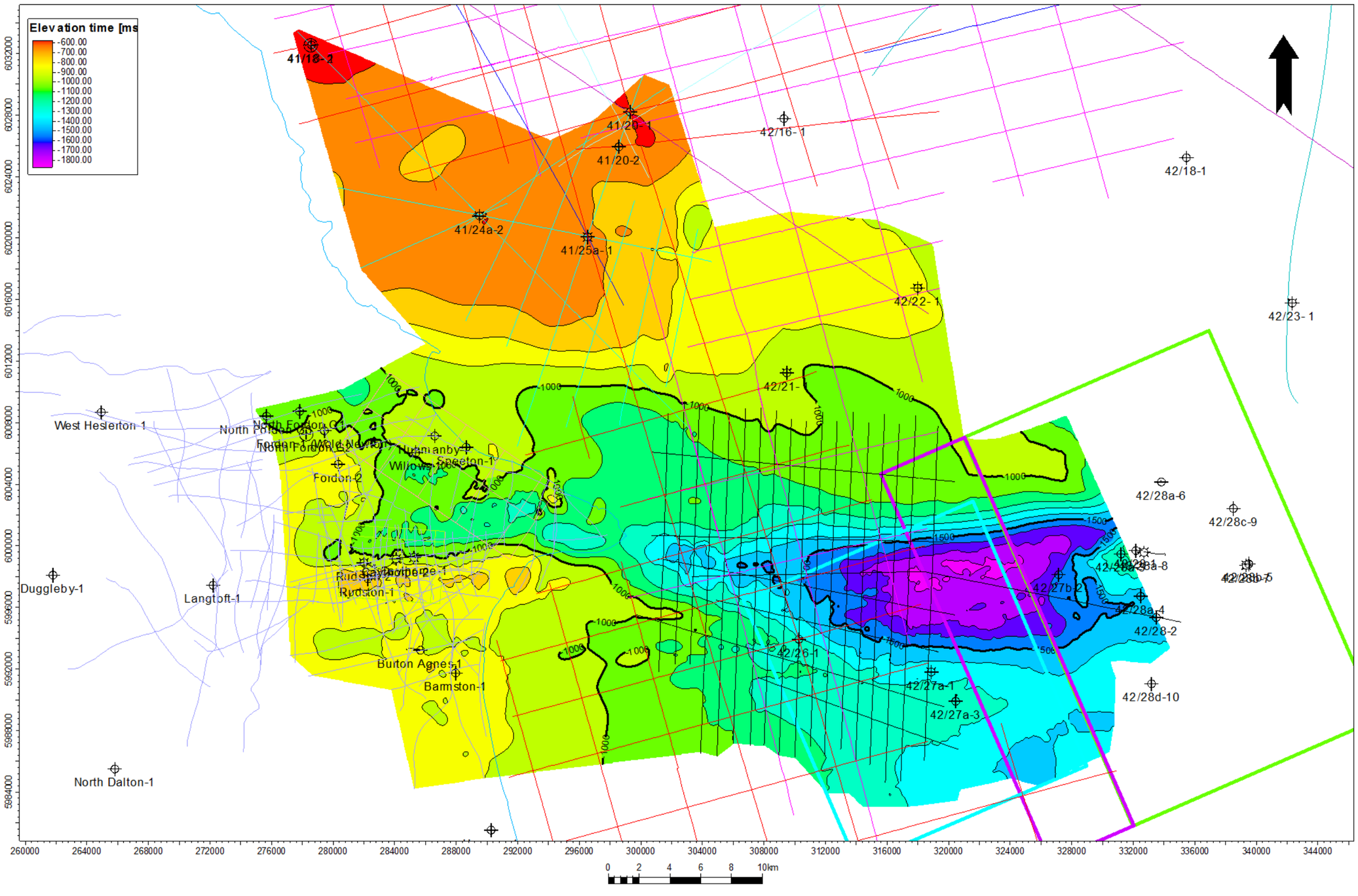

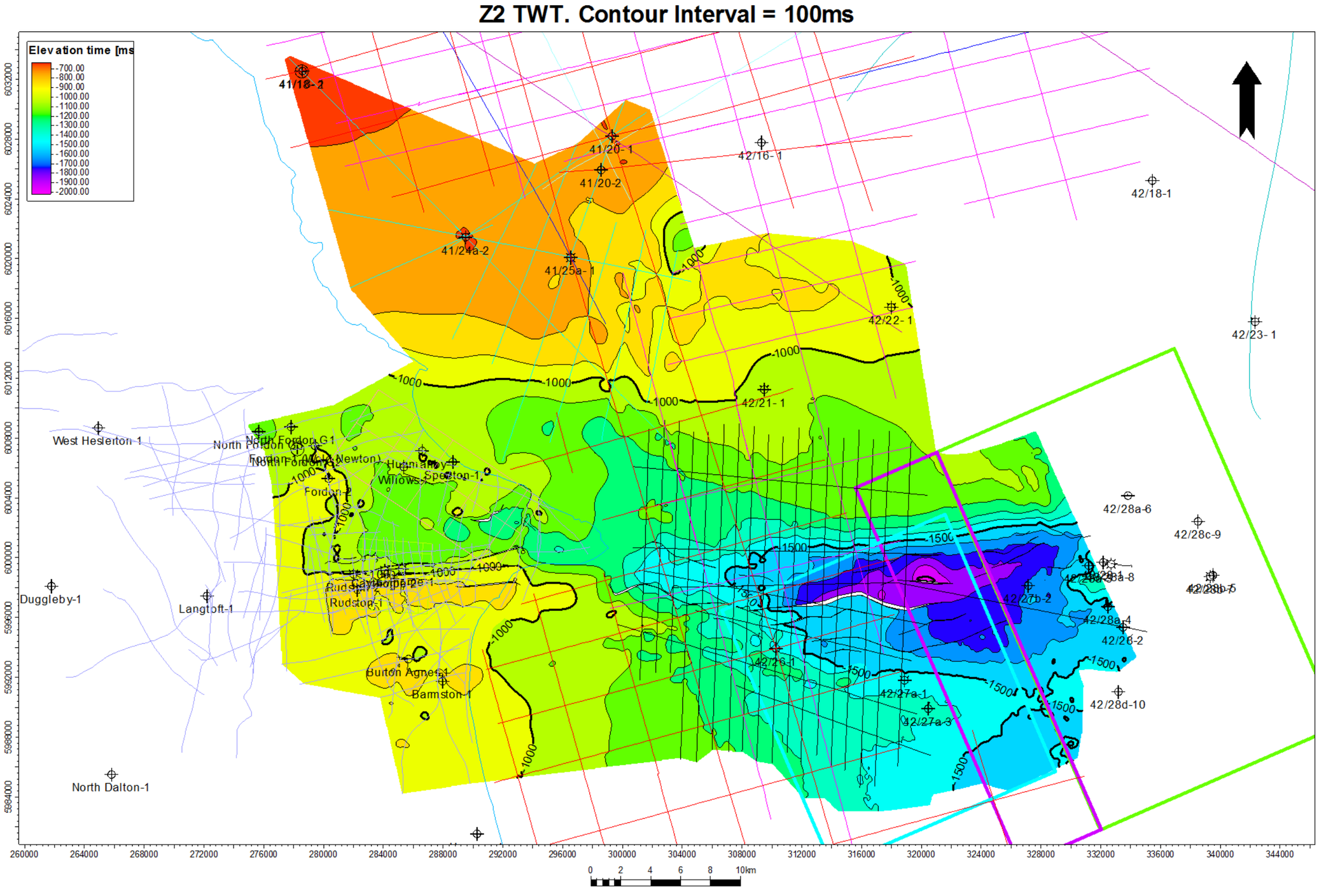
Z2 TWT. Contour Interval = 100ms
Elevation time [ms
-700.00
-800.00
-900.00
-1000.00
-1100.00
-1200.00
-1300.00
-1400.00
-1500.00
-1600.00
-1700.00
-1800.00
-1900.00
-2000.00
41/18-2
41/20-1
41/20-2
42/16-1
42/18-1
41/24a-2
41/25a-1
42/22-1
42/23-1
42/21-1
West Hesleton-1
North Fordon G1
North Fordon 2B
Fordon-1 (Well Newton)
North Fordon-2
Humanby-1
Speeton-1
Willows-1
Fordon-2
42/28a-6
42/28c-9
42/28a-8
42/27b-2
42/28a-4
42/26-2
Duggleby-1
Langtoft-1
Rudston-1
42/26-1
Burton Agnes-1
Barmston-1
42/27a-1
42/27a-3
42/28d-10
North Dalton-1
1000
1500
6032000
6028000
6024000
6020000
6016000
6012000
6008000
6004000
6000000
5996000
5992000
5988000
5984000
260000
264000
268000
272000
276000
280000
284000
288000
292000
296000
300000
304000
308000
312000
316000
320000
324000
328000
332000
336000
340000
344000
0
2
4
6
8
10km

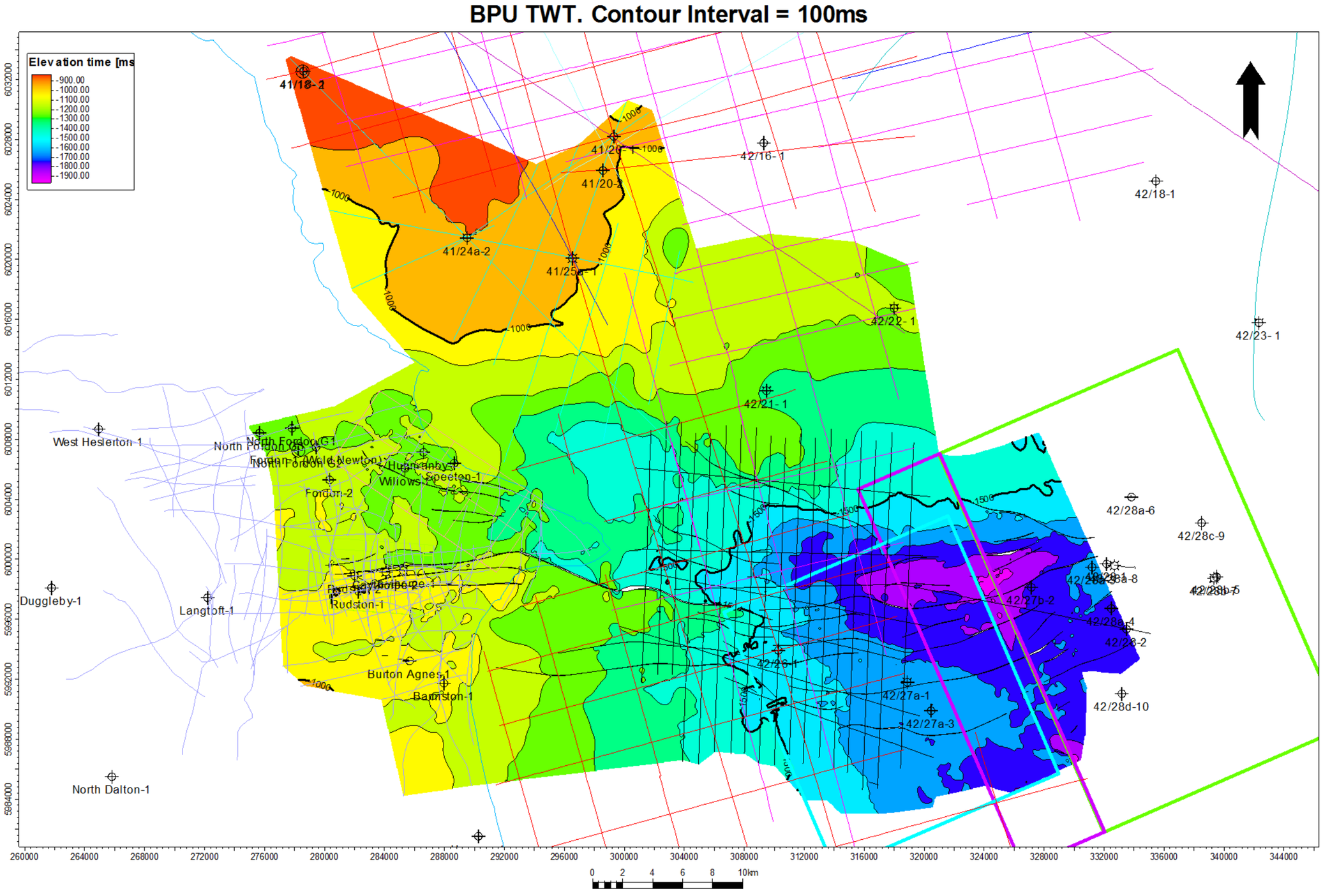
BPU TWT. Contour Interval = 100ms
Elevation time [ms
-900.00
-1000.00
-1100.00
-1200.00
-1300.00
-1400.00
-1500.00
-1600.00
-1700.00
-1800.00
-1900.00
41/18-2
41/20-1
41/20-2
42/16-1
42/18-1
41/24a-2
41/25a-1
42/22-1
42/23-1
42/21-1
West Heslerton-1
North Foreland G1
North Foreland G2
Foreland-1
Gould Newton-1
Humanby-1
Speeton-1
Willows-1
Fordon-2
42/28a-6
42/28c-9
Duggleby-1
Langtoft-1
Rudston-1
42/27b-2
42/28a-4
42/28-2
Burton Agnes-1
Bainston-1
42/27a-1
42/27a-3
42/28d-10
North Dalton-1
1000
1500
260000
264000
268000
272000
276000
280000
284000
288000
292000
296000
300000
304000
308000
312000
316000
320000
324000
328000
332000
336000
340000
344000
6032000
6028000
6024000
6020000
6016000
6012000
6008000
6004000
6000000
5996000
5992000
5988000
5984000
0 2 4 6 8 10km

APPENDIX B. REGIONAL TIME ISOCHORE MAPS

All time isochore maps in this section are displaying true vertical time thickness z values in milliseconds with a colour shading convention of warm colours representing isochore thinning and cool colours representing isochore thickening. Displayed time isochores are for the following intervals:

Chalk

Cromer Knoll

Humber Group

West Sole Group

Lias Group

Haisborough Group

Bacton Group

Zechstein Z5-Z3

Zechstein Z2 – Base Permian Unconformity

Cretaceous

Jurassic

Triassic

Permian

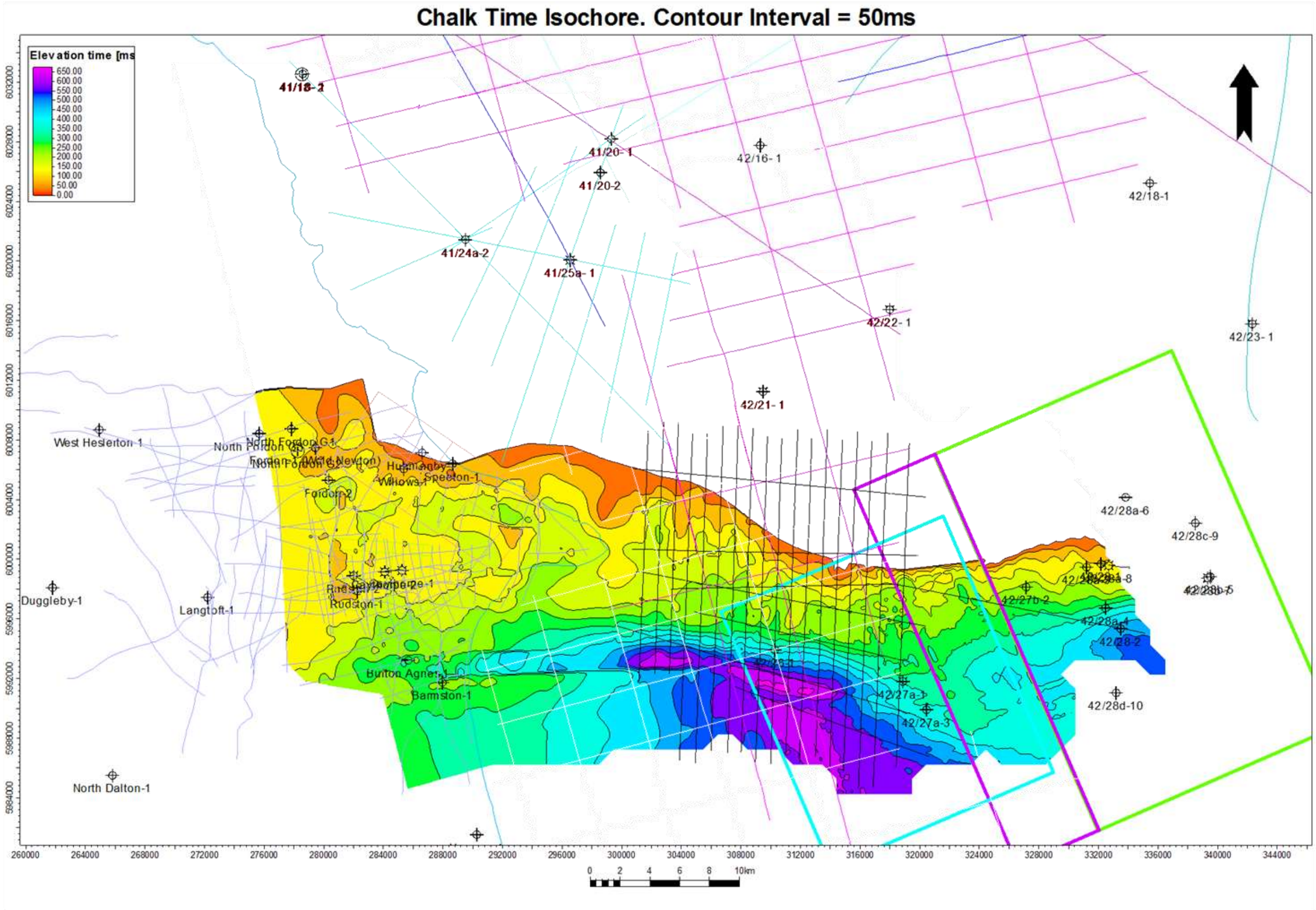
Chalk Time Isochore. Contour Interval = 50ms
Elevation time [ms
650.00
600.00
550.00
500.00
450.00
400.00
350.00
300.00
250.00
200.00
150.00
100.00
50.00
0.00
41/18-2
41/20-1
41/20-2
42/16-1
42/18-1
41/24a-2
41/25a-1
42/22-1
42/23-1
42/21-1
West Heslerton-1
North Fordon G-1
North Fordon G-2
Fordon-2
Willow-1
Preston-1
42/28a-6
42/28c-9
Duggleby-1
Langtoft-1
Rudston-1
42/27b-2
42/28a-4
42/28-2
Burton Agnes-1
Barmston-1
42/27a-1
42/27a-3
42/28d-10
North Dalton-1
6032000
6028000
6024000
6020000
6016000
6012000
6008000
6004000
6000000
5996000
5992000
5988000
5984000
260000
264000
268000
272000
276000
280000
284000
288000
292000
296000
300000
304000
308000
312000
316000
320000
324000
328000
332000
336000
340000
344000
0 2 4 6 8 10km

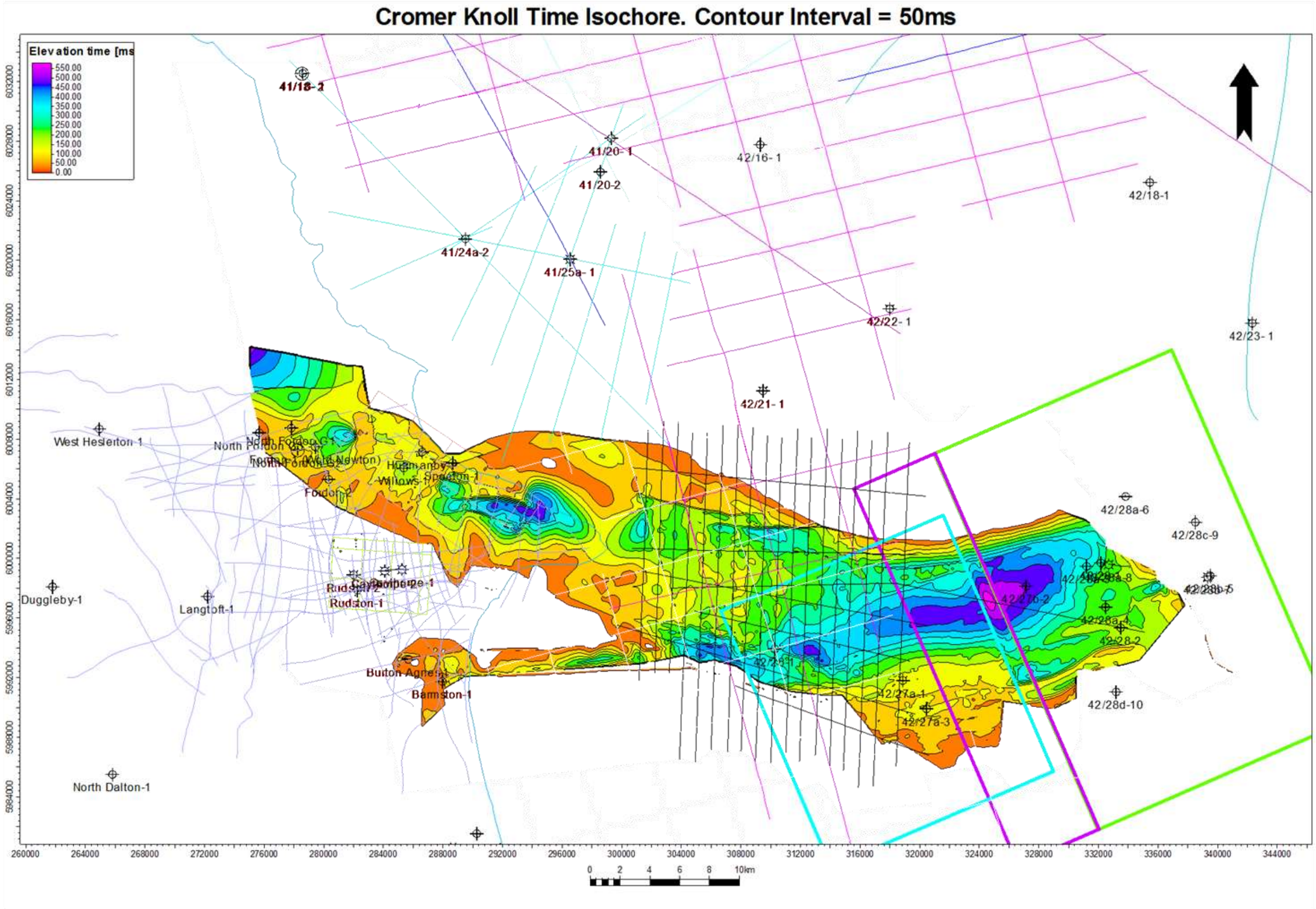
Cromer Knoll Time Isochore. Contour Interval = 50ms
Elevation time [ms
550.00
500.00
450.00
400.00
350.00
300.00
250.00
200.00
150.00
100.00
50.00
0.00
41/18-2
41/20-1
41/20-2
42/16-1
42/18-1
41/24a-2
41/25a-1
42/22-1
42/23-1
42/21-1
West Heslerton-1
North Foridon G-1
North Foridon-2
Fordon-2
Humanby-1
Willows-1
Speeton-1
42/28a-6
42/28c-9
Duggleby-1
Langtoft-1
Rudston-1
42/28a-4
42/28-2
Burton Agnes-1
Barmston-1
42/27a-1
42/27a-3
42/28d-10
North Dalton-1
6032000
6028000
6024000
6020000
6016000
6012000
6008000
6004000
6000000
5996000
5992000
5988000
5984000
260000
264000
268000
272000
276000
280000
284000
288000
292000
296000
300000
304000
308000
312000
316000
320000
324000
328000
332000
336000
340000
344000
0 2 4 6 8 10km

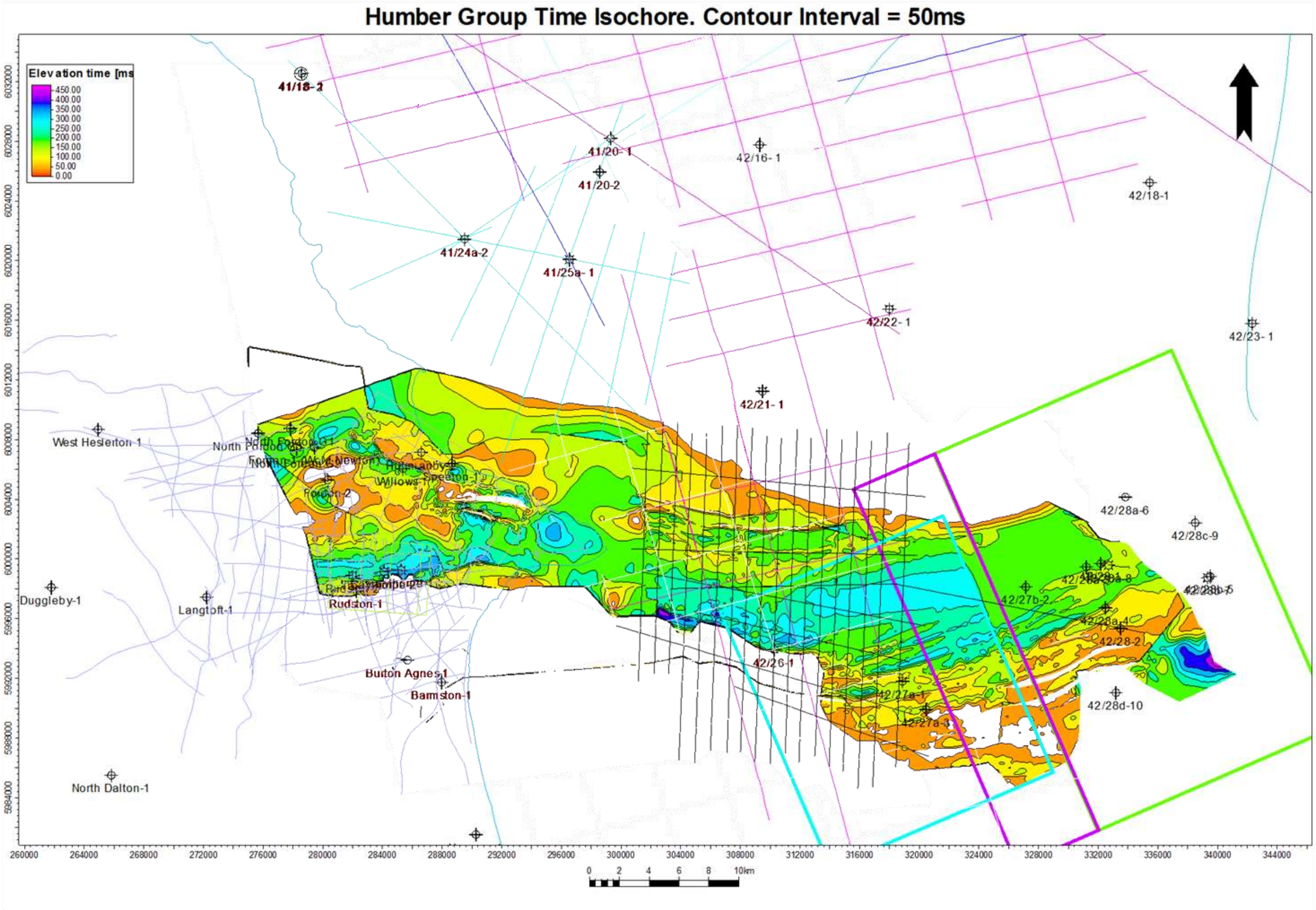
Humber Group Time Isochore. Contour Interval = 50ms
Elevation time [ms
450.00
400.00
350.00
300.00
250.00
200.00
150.00
100.00
50.00
0.00
41/18-2
41/20-1
41/20-2
42/16-1
42/18-1
41/24a-2
41/25a-1
42/22-1
42/23-1
42/21-1
West Heslerton-1
North Pickering-1
North Pickering-2
Fordon-1
Fordon-2
Willows-1
Speeton-1
42/28a-6
42/28c-9
42/28a-8
42/27b-2
42/28a-4
42/28-2
Duggleby-1
Langtoft-1
Rudston-1
42/26-1
Burton Agnes-1
Barmston-1
42/27a-1
42/27a-3
42/28d-10
North Dalton-1
260000
264000
268000
272000
276000
280000
284000
288000
292000
296000
300000
304000
308000
312000
316000
320000
324000
328000
332000
336000
340000
344000
6032000
6028000
6024000
6020000
6016000
6012000
6008000
6004000
6000000
5996000
5992000
5988000
5984000
0 2 4 6 8 10km

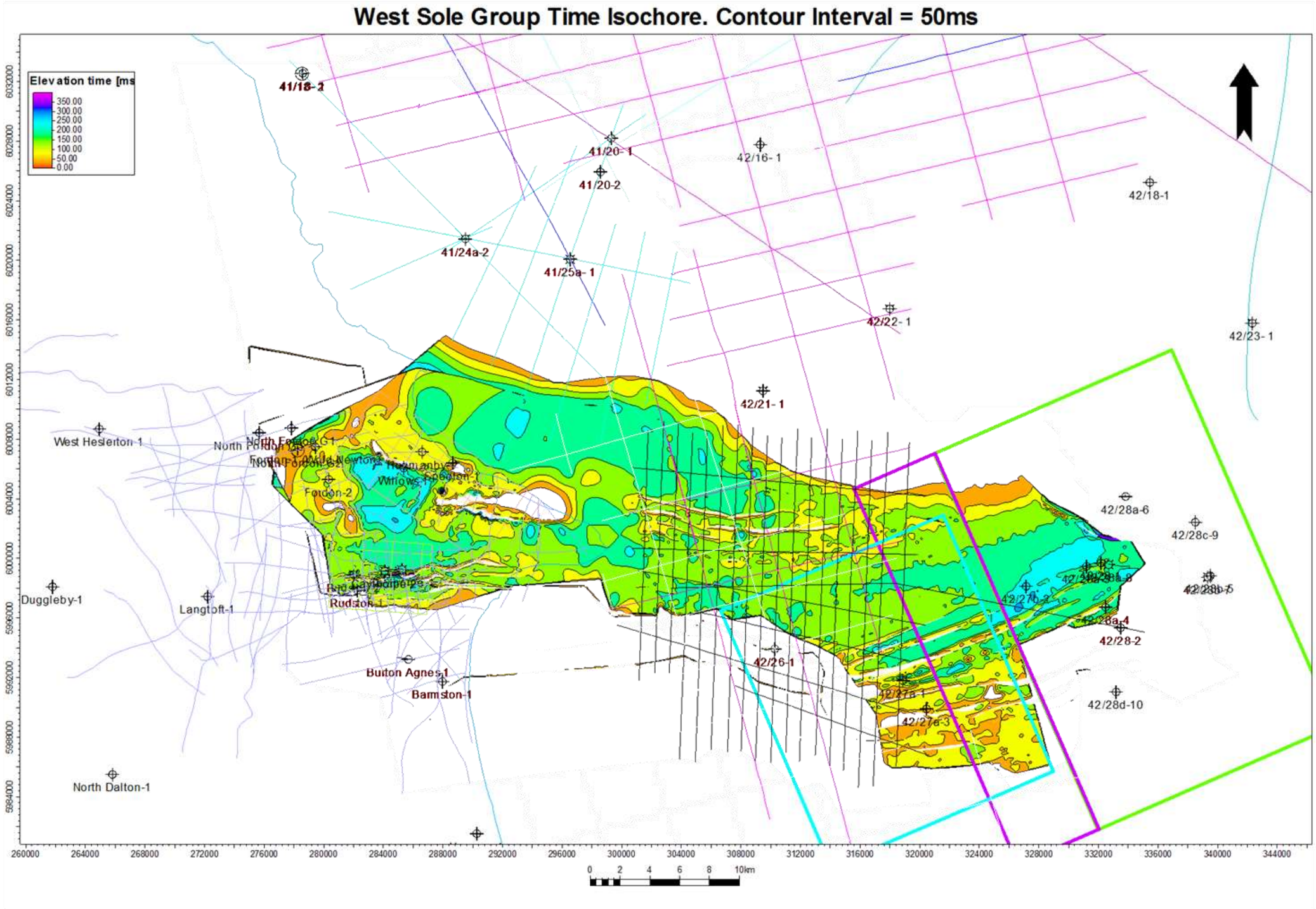
West Sole Group Time Isochore. Contour Interval = 50ms
Elevation time [ms
350.00
300.00
250.00
200.00
150.00
100.00
50.00
0.00
41/18-2
41/20-1
41/20-2
42/16-1
42/18-1
41/24a-2
41/25a-1
42/22-1
42/23-1
42/21-1
West Heslerton-1
North Foreon-G1
North Foreon-S2
Foreon-2
Willows-1
Foreon-1
42/28a-6
42/28c-9
Duggleby-1
Langtoft-1
Rudston-1
42/28a-4
42/28-2
42/26-1
Burton Agnes-1
Barmston-1
42/27a-1
42/27a-3
42/28d-10
North Dalton-1
260000
264000
268000
272000
276000
280000
284000
288000
292000
296000
300000
304000
308000
312000
316000
320000
324000
328000
332000
336000
340000
344000
6032000
6028000
6024000
6020000
6016000
6012000
6008000
6004000
6000000
5996000
5992000
5988000
5984000
0 2 4 6 8 10km

Lias Time Isochore. Contour Interval = 50ms

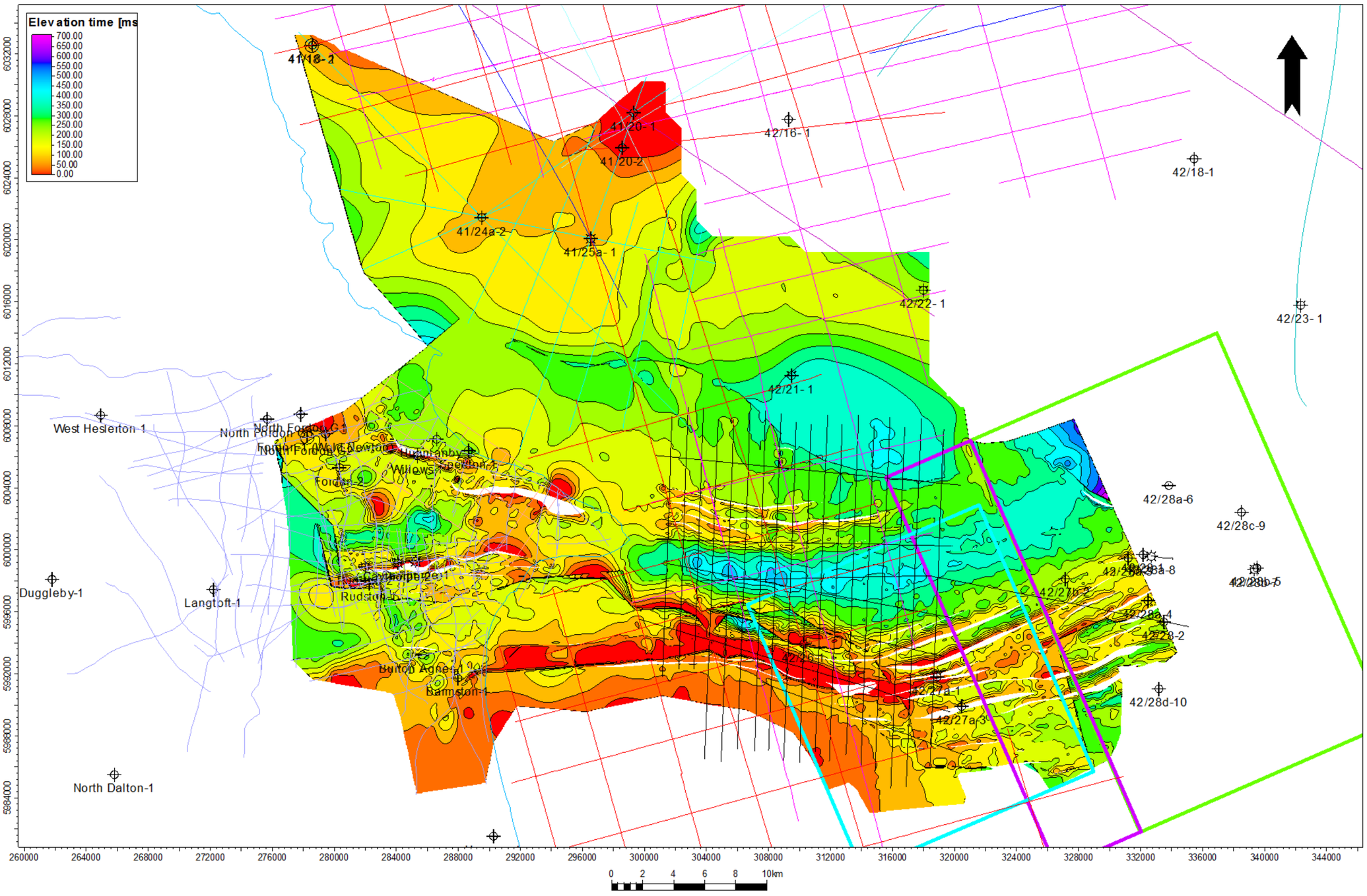

Haisborough Group Time Isochore. Contour Interval = 50ms

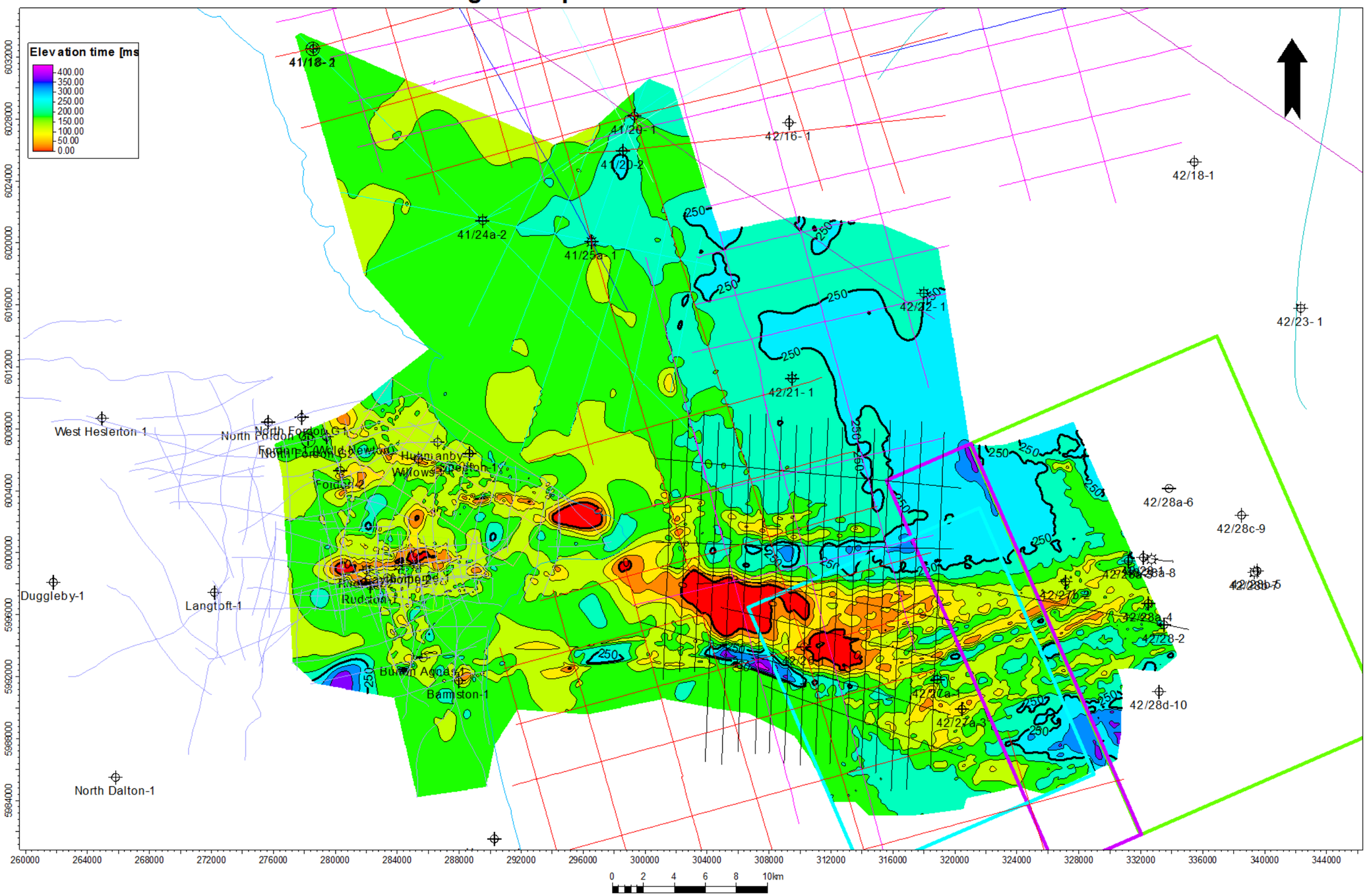

Bacton Group Time Isochore. Contour Interval = 50ms

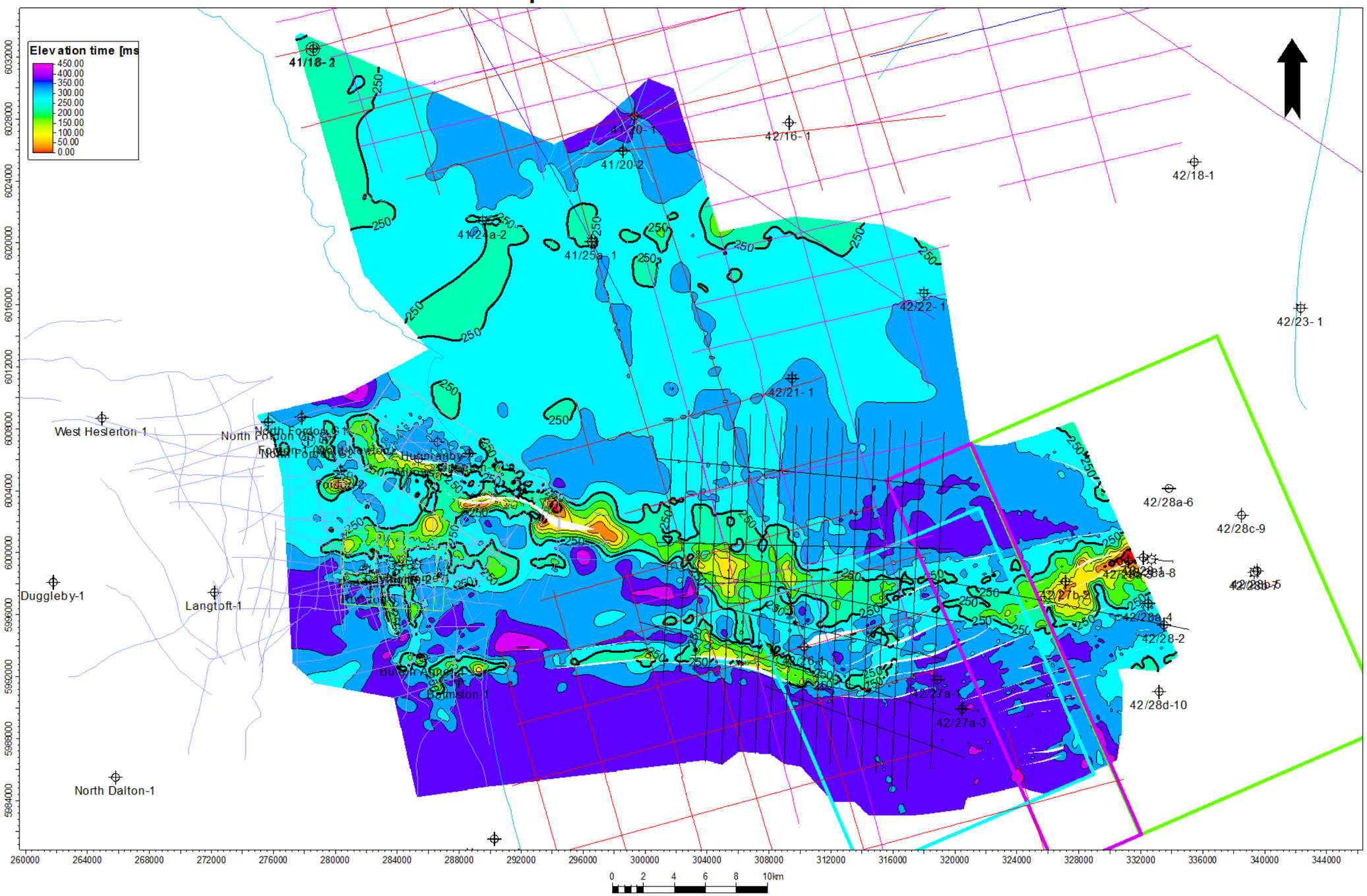

Zechstein Z5-Z3 Time Isochore. Contour Interval = 50ms

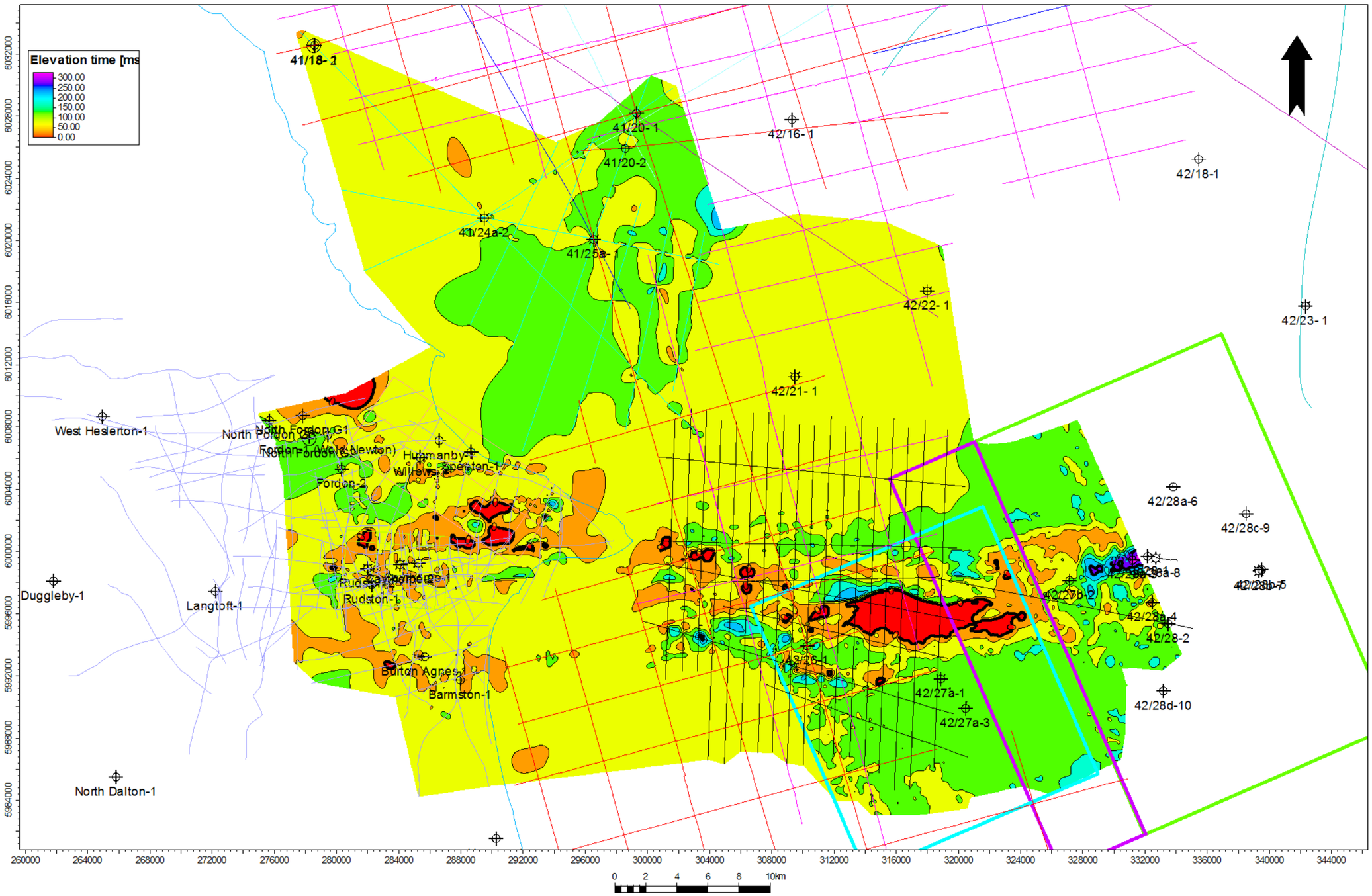

Zechstein Z2 - Base Permian Unconformity Time Isochore. Contour Interval = 50ms

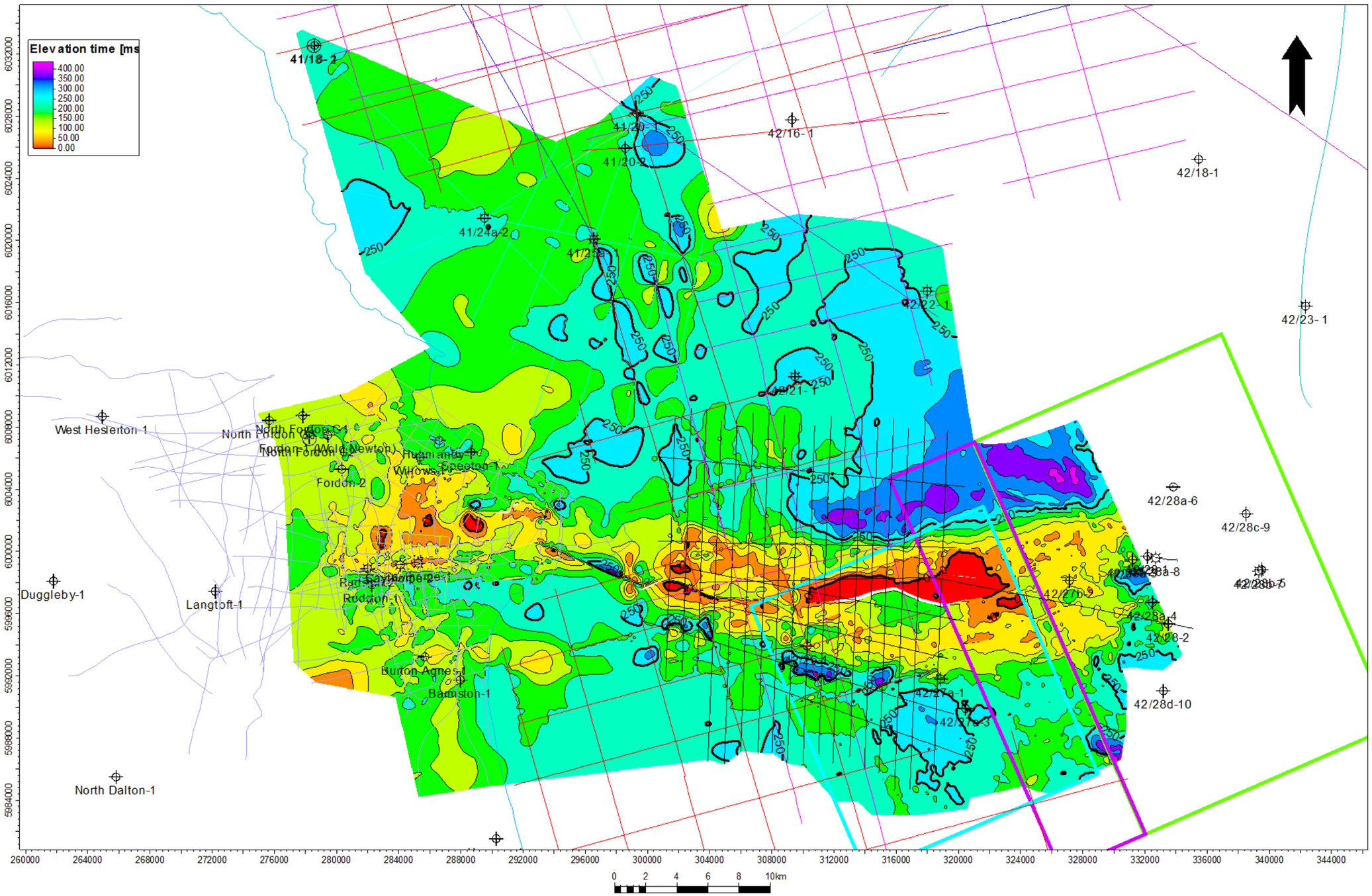

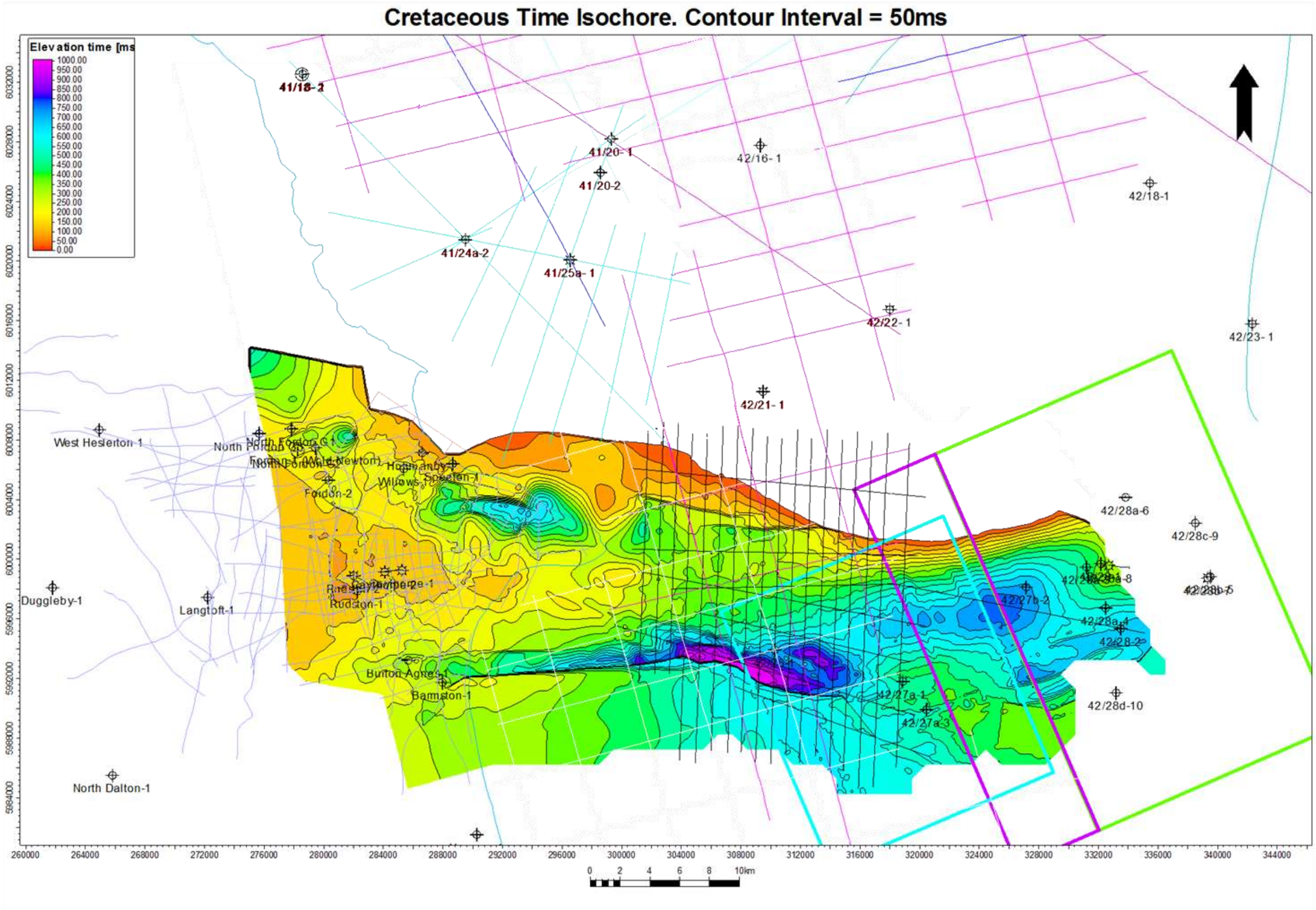
Cretaceous Time Isochore. Contour Interval = 50ms
Elevation time [ms
1000.00
950.00
900.00
850.00
800.00
750.00
700.00
650.00
600.00
550.00
500.00
450.00
400.00
350.00
300.00
250.00
200.00
150.00
100.00
50.00
0.00
41/18-2
41/20-1
41/20-2
42/16-1
42/18-1
41/24a-2
41/25a-1
42/22-1
42/23-1
42/21-1
West Heslerton-1
North Foston-1
Foston-2
Willow Newton)
Willows-1
42/28a-6
42/28c-9
Duggleby-1
Langtoft-1
Rudston-1
42/27b-2
42/28a-4
42/28-2
Burton Agnes-1
Barmston-1
42/27a-1
42/27a-3
42/28d-10
North Dalton-1
6032000
6028000
6024000
6020000
6016000
6012000
6008000
6004000
6000000
5996000
5992000
5988000
5984000
260000
264000
268000
272000
276000
280000
284000
288000
292000
296000
300000
304000
308000
312000
316000
320000
324000
328000
332000
336000
340000
344000
0 2 4 6 8 10km

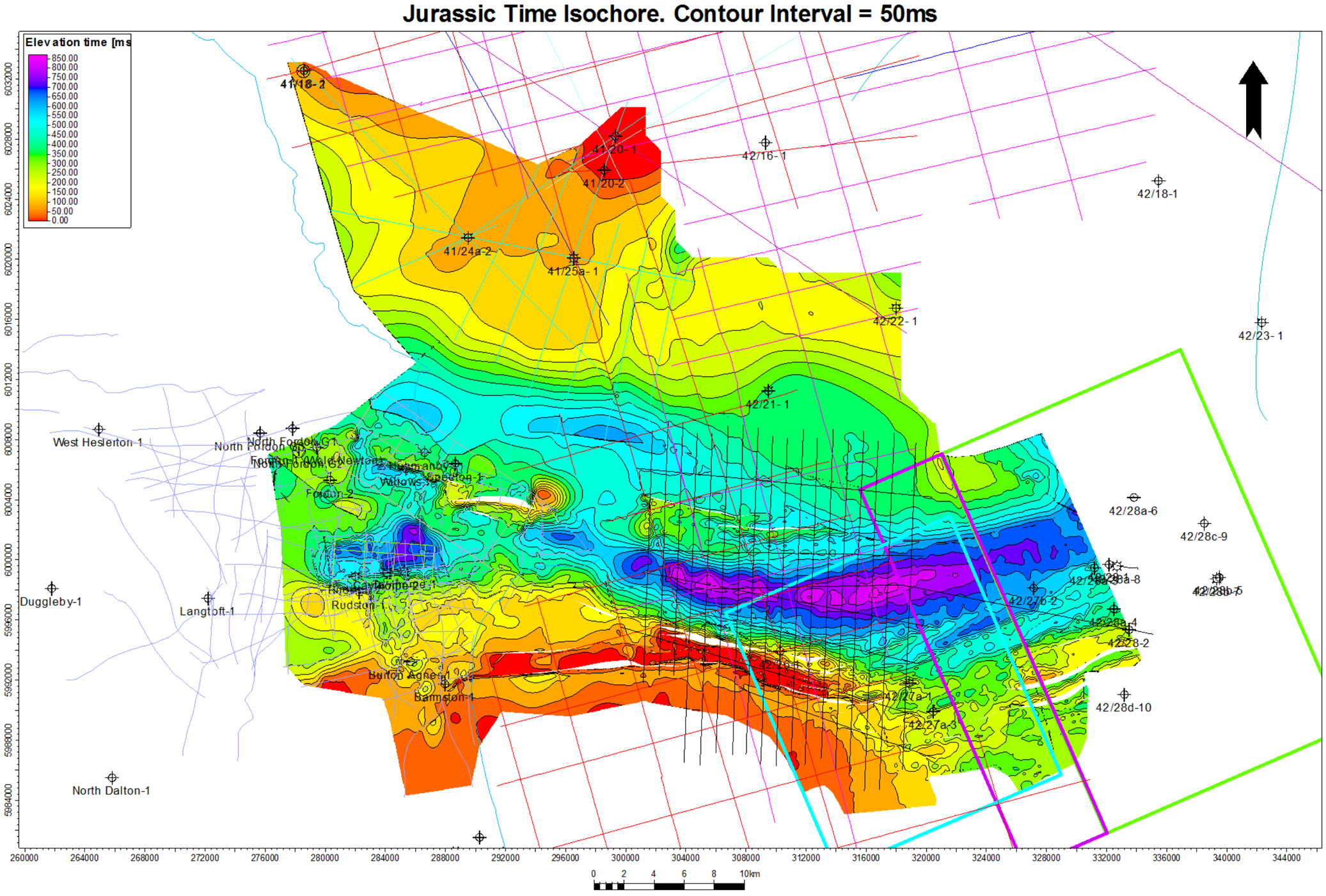
Jurassic Time Isochore. Contour Interval = 50ms
Elevation time [ms
850.00
800.00
750.00
700.00
650.00
600.00
550.00
500.00
450.00
400.00
350.00
300.00
250.00
200.00
150.00
100.00
50.00
0.00
41/18-2
41/20-1
41/20-2
42/16-1
42/18-1
41/24a-2
41/25a-1
42/22-1
42/23-1
42/21-1
West Hesleton-1
North Fordon-1
North Fordon-2
Fordon-2
Willows-1
Burnahby-1
Skipton-1
Haythorpe-1
Rudston-1
Duggleby-1
Langtoft-1
Burton Agnes-1
Barmston-1
North Dalton-1
42/28a-6
42/28c-9
42/28a-8
42/28b-5
42/27b-2
42/28a-4
42/28-2
42/27a-1
42/27a-3
42/28d-10
6032000
6028000
6024000
6020000
6016000
6012000
6008000
6004000
6000000
5996000
5992000
5988000
5984000
260000
264000
268000
272000
276000
280000
284000
288000
292000
296000
300000
304000
308000
312000
316000
320000
324000
328000
332000
336000
340000
344000
0 2 4 6 8 10km

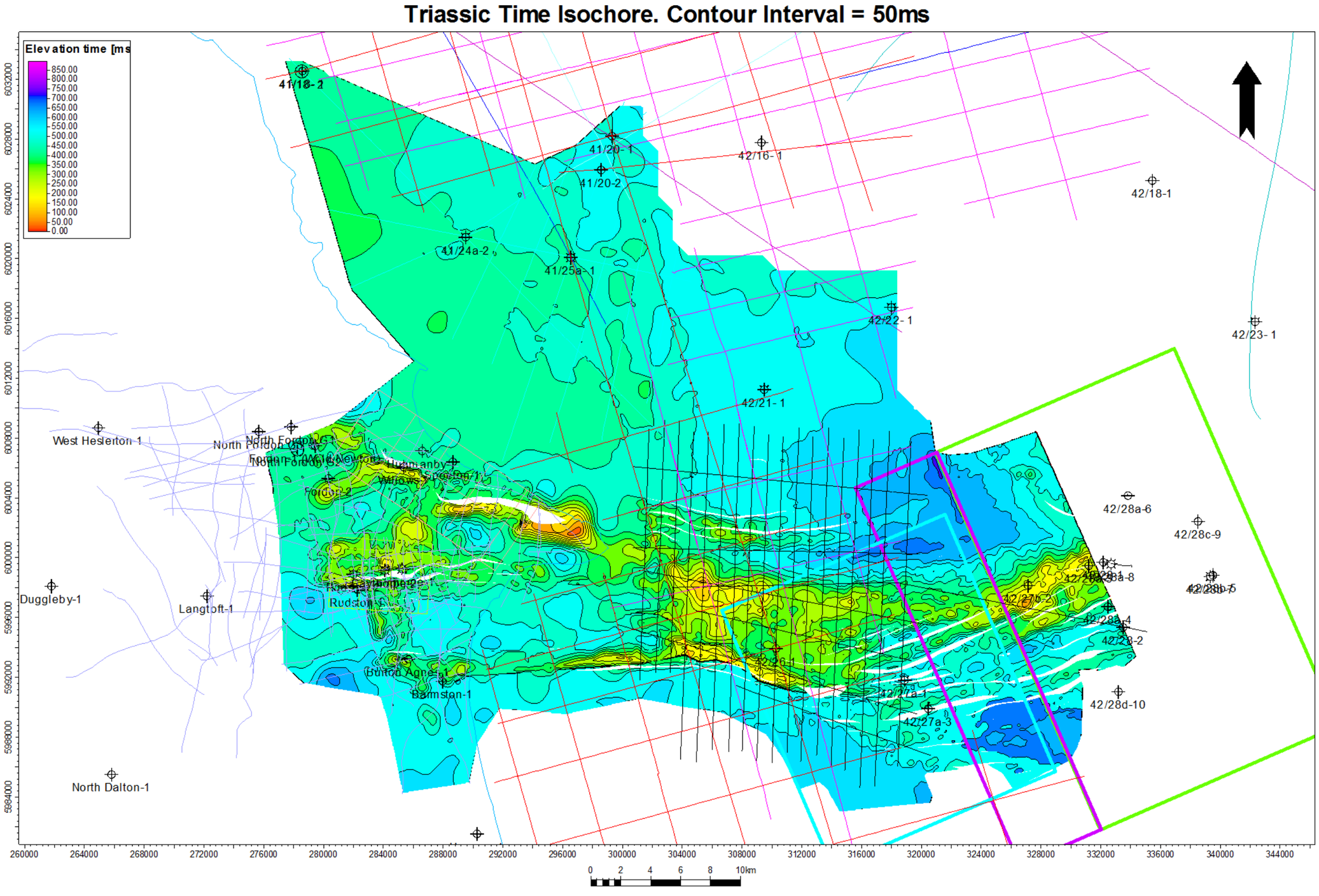
Triassic Time Isochore. Contour Interval = 50ms
Elevation time [ms
850.00
800.00
750.00
700.00
650.00
600.00
550.00
500.00
450.00
400.00
350.00
300.00
250.00
200.00
150.00
100.00
50.00
0.00
41/18-1
41/20-1
41/20-2
42/16-1
42/18-1
41/24a-2
41/25a-1
42/22-1
42/23-1
42/21-1
West Heslerton-1
North Foreton-1
North Foreton-2
Foreton-2
Willows-1
Spaldington-1
Duggleby-1
Langtoft-1
Rudston-1
Burton Agnes-1
Barmston-1
North Dalton-1
42/28a-6
42/28c-9
42/28a-8
42/27b-2
42/28-2
42/27a-1
42/27a-3
42/28d-10
6032000
6028000
6024000
6020000
6016000
6012000
6008000
6004000
6000000
5996000
5992000
5988000
5984000
260000
264000
268000
272000
276000
280000
284000
288000
292000
296000
300000
304000
308000
312000
316000
320000
324000
328000
332000
336000
340000
344000
0
2
4
6
8
10km

Permian Time Isochore. Contour Interval = 50ms

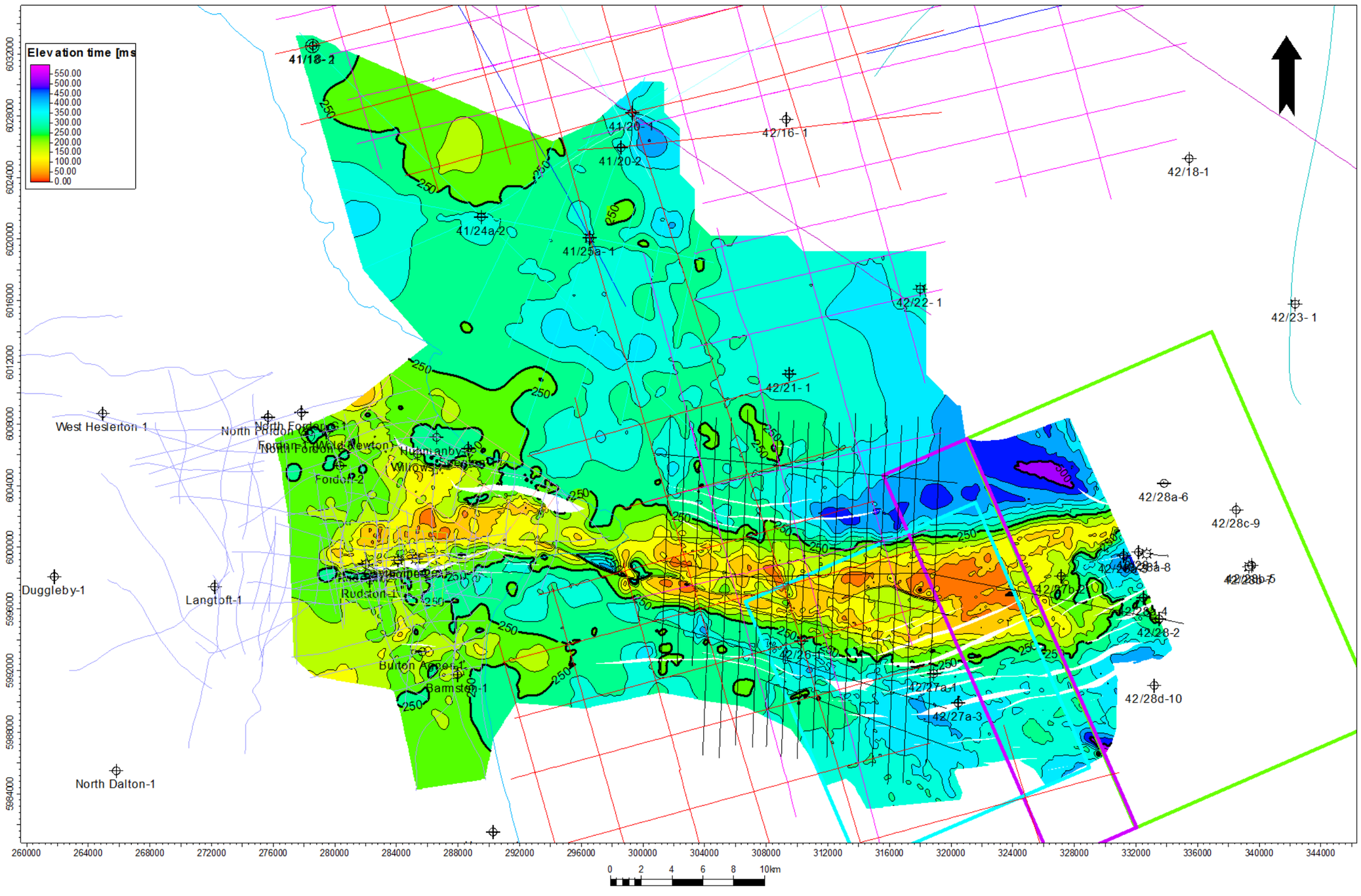

APPENDIX C. CHECKSHOT INTERVAL VELOCITY CROSS PLOTS FOR DEPTH CONVERSION

Seabed to Base Chalk (Chalk interval)

Base Chalk to Base Cretaceous (Cromer Knoll interval)

Base Cretaceous to Corallian (Humber Group interval)

Corallian to Lias (West Sole Group interval)

Lias to Triassic (Lias Group interval)

Triassic to Bacton (Haisborough Group interval)

Bacton to Zechstein (Bacton Group interval)

Zechstein to Z2 (Zechstein Z5-Z2 Interval)

Z2 to BPU (Zechstein Z2 – Base Permian Unconformity interval)

Formation: Sea Bed to Base Chalk

	Mean Vint Δz = A*ΔT/2	Graphical Vint Δz = A*ΔT	Isopach/isochron Δz = A + B*ΔT	isopach/ isochron Δz = A*ΔT + B*ΔT^2	mid-point time Δz = (A + B*Tmid)*ΔT/2	mid-point depth Δz = (ΔT/2)*(A+B*ztop)/(1-B*ΔT/4)	slotnick Δz = A*(exp(B*ΔT/2)-1)/B	Power Δz = A*ΔT^B
A (Vo) =	3633	1744.9	23.1	1874.6	3932	3914.6	3914.6	1585.1
B (k) =			1670.5	-365.38	-1854.7	-1.1586	-1.1586	0.9191
Correlation Coefficient	0.995126	0.995126	0.99512564	0.994947669	0.994527739	0.994705069	0.994753	0.99497
Standard Deviation	28.70171	23.61792	21.54274102	22.08682142	22.97607935	22.45144044	22.57294	22.20634
Mean	-12	9	0.00	1	0	-2	-6	-2
RMS Error	31.04583	24.19832	21.54274108	22.12863936	22.98126849	22.52855874	23.41074	22.29697

	Top		Base																					
Well	TVDSS (ft)	2WT (s)	TVDSS (ft)	2WT (s)	isochron	isopach	V int	ΔZ model	ΔZ error	ΔZ model	ΔZ error	ΔZ model	ΔZ error	ΔZ model	ΔZ error	T mid	ΔZ model	ΔZ error	Zmid	ΔZ model	ΔZ error	ΔZ model	ΔZ error	ΔZ model	ΔZ error
Caythorpe-1	0	0	194.79	0.12631	0.126	195	3084	229	-35	220	-26	234	-39	231	-36	0.0632	241	-46	97	239	-44	238	-44	237	42
Rudston-1	0	0	207.95	0.11823	0.118	208	3518	215	-7	206	2	221	-13	217	-9	0.0591	226	-18	104	224	-16	224	-16	223	15
Rudston-2	0	0	232.9	0.1012	0.101	233	4603	184	49	177	56	192	41	186	47	0.0506	194	39	116	192	40	192	41	193	-40
Willows-1	0	0	122.1	0.0599	0.060	122	4077	109	13	105	18	123	-1	111	11	0.0300	116	6	61	115	7	115	7	119	-3
Hunmanby-1	0	0	0	0																					
42/26-1	47.85	0.062795	669.34	0.41794	0.355	621	3500	645	-24	620	2	616	5	620	2	0.2404	619	2	369	621	0	628	-7	612	9
42/27a-1	55.17	0.072402	602.84	0.36818	0.296	548	3703	537	10	516	32	517	30	523	25	0.2203	521	27	329	525	23	532	16	517	-30
42/27a-3	54.79	0.071903	613.02	0.40241	0.331	558	3378	600	-42	577	-18	575	-17	580	-21	0.2372	577	-19	334	581	-23	589	-31	573	15
42/27b-2	54.25	0.071194	415.01	0.27253	0.201	361	3584	366	-5	351	9	359	1	363	-2	0.1719	364	-3	235	366	-6	372	-11	363	3
42/28-2	51.82	0.068005	863.78	0.54248	0.474	812	3423	862	-50	828	-16	816	-4	807	5	0.3052	799	13	458	804	8	812	0	799	-13
42/28a-4	53.34	0.07	630.68	0.40411	0.334	577	3456	607	-29	583	-6	581	-4	586	-8	0.2371	583	-6	342	587	-9	595	-17	579	1
41/24a-2	50.01	0.06563	#N/A	#N/A																					
Well A		0			#VALUE!			#VALUE!																	

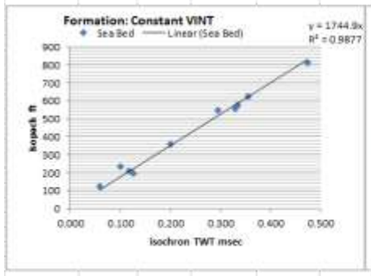

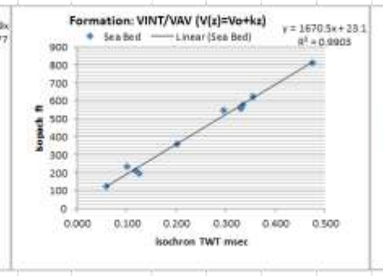

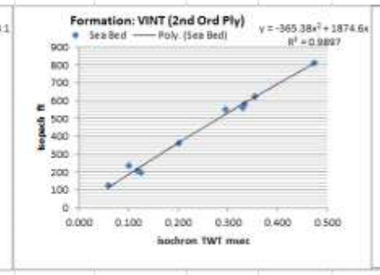

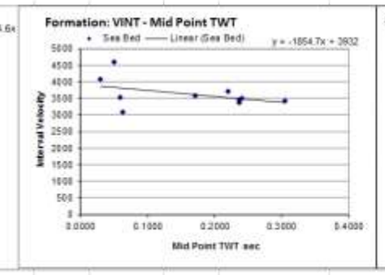

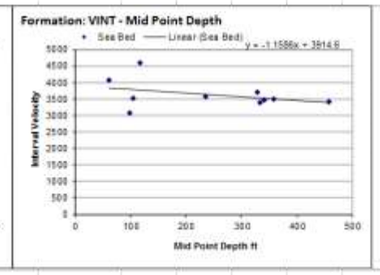

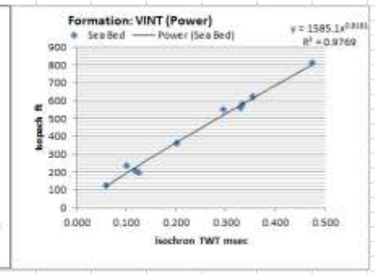

Formation: Base Chalk to Base Cretaceous

	Mean Vint Δz = A*ΔT/2	Graphical Vint Δz = A*ΔT	Isopach/isochron Δz = A + B*ΔT	isopach/ isochron Δz = A*ΔT + B*ΔT^2	mid-point time Δz = (A + B*Tmid)*ΔT/2	mid-point depth Δz = (ΔT/2)*(A+B*ztop)/(1-B*ΔT/4)	slotnick Δz = A*(exp(B*ΔT/2)-1)/B	Power Δz = A*ΔT^B
A (Vo) =	2506	1269.2	-20.656	1100.8	2335.3	2321.3	2321.3	1126.6
B (k) =			1336.4	456.99	391.97	0.2832	0.2832	0.9454
Correlation Coefficient	0.98687	0.98687	0.986869936	0.988947242	0.99137651	0.991578	0.987547	0.985035
Standard Deviation	31.86452	31.15741	29.78285011	27.36793976	25.71570655	25.6969	34.07742	40.02047
Mean	-2	-6	0.00	1	-4	-4	13	-8
RMS Error	31.92524	31.64913	29.78285034	27.37986073	26.06836722	26.04191	36.49247	40.76563

	Top		Base																					
Well	TVDSS (ft)	2WT (s)	TVDSS (ft)	2WT (s)	isochron	isopach	V int	ΔZ model	ΔZ error	ΔZ model	ΔZ error	ΔZ model	ΔZ error	ΔZ model	ΔZ error	T mid	ΔZ model	ΔZ error	Zmid	ΔZ model	ΔZ error	ΔZ model	ΔZ error	ΔZ model	ΔZ error
Caythorpe-1	194.79	0.12631	223.5	0.1453	0.019	29	3024	24	5	24	5	5	24	21	8	0.1358	23	6	209	23	6	22	7	27	-2
Rudston-1	207.95	0.11823	207.95	0.11823																					
Rudston-2	232.9	0.1012	232.9	0.1012																					
Willows-1	122.1	0.0599	332.77	0.28673	0.227	211	1858	284	-74	288	-77	282	-72	273	-62	0.1733	273	-62	227	272	-61	268	-57	277	66
Hunmanby-1	0	0	#N/A	#N/A																					
42/26-1	669.34	0.41794	1138.73	0.774	0.356	469	2637	446	23	452	17	455	14	450	20	0.5960	457	12	904	459	11	424	46	424	-45
42/27a-1	602.84	0.36818	758.55	0.51053	0.142	156	2188	178	-23	181	-25	170	-14	166	-10	0.4394	178	-23	681	179	-23	167	-11	178	23
42/27a-3	613.02	0.40241	797	0.55437	0.152	184	2421	190	-6	193	-9	182	2	178	6	0.4784	192	-8	705	192	-8	178	6	190	6
42/27b-2	415.01	0.27253	1073.14	0.77147	0.499	658	2638	625	33	633	25	646	12	663	-5	0.5220	634	24	744	631	27	600	58	584	-74
42/28-2	863.78	0.54248	1122.32	0.73038	0.188	259	2752	235	23	238	20	230	28	223	36	0.6364	243	16	993	244	14	221	38	232	-27
42/28a-4	630.68	0.40411	901.73	0.61799	0.214	271	2535	268	3	271	0	265	6	256	15	0.5111	271	0	766	271	0	252	19	262	-9
41/24a-2	#N/A	#N/A	#N/A	#N/A																					
Well A					#VALUE!			#VALUE!																	

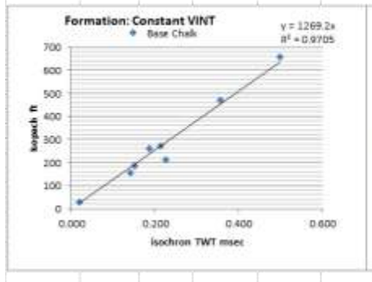

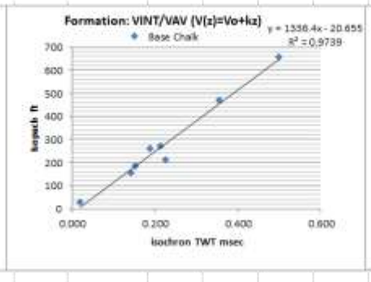

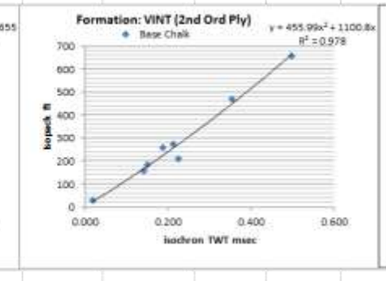

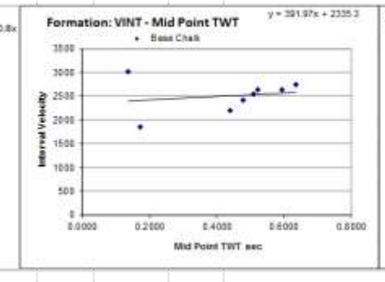

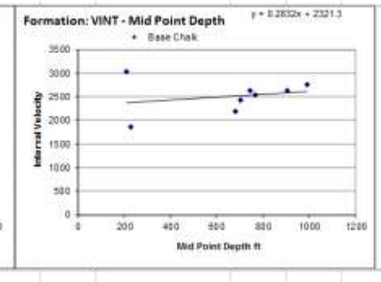

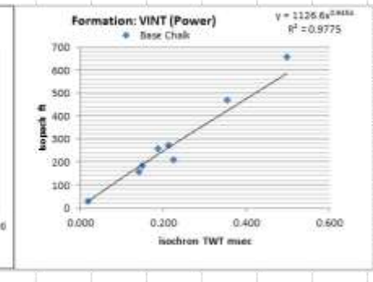

Appendix C. Checkshot Interval Velocity Cross Plots For Depth Conversion

Formation: Base Cretaceous to Corallian

	Mean Vint Δz = A*ΔT/2	Graphical Vint Δz = A*ΔT	Isopach/isochron Δz = A + B*ΔT	isopach/ isochron Δz = A*ΔT + B*ΔT^2	mid-point time Δz = (A + B*Tmid)*ΔT/2	mid-point depth Δz = (ΔT/2)*(A+B*ztop)/(1-B*ΔT/4)	slotnick Δz = A*(exp(B*ΔT/2)-1)/B	Power Δz = A*Δt^B
A (Vo) =	2559	1242.4	5.9476	1370.1	2129.4	2091.3	2091.3	1161.8
B (k) =			1205.9	-611.9	862.21	0.6377	0.6377	0.9626
Correlation Coefficient	0.985869	0.985869	0.985869032	0.987744861	0.997123876	0.996791	0.985038	0.986341
Standard Deviation	16.59625	15.8615	15.61518248	14.65568238	7.569065286	7.560529	18.01644	15.35421
Mean	-2	2	0.00	-1	-2	-2	20	-1
RMS Error	16.73417	15.97965	15.61518301	14.70085836	7.939018883	7.7698	27.27754	15.37911

Well	Top TVDSS (ft)	Top 2WT (s)	Base TVDSS (ft)	Base 2WT (s)	isochron	isopach	V int	ΔZ model	ΔZ error	ΔZ model	ΔZ error	ΔZ model	ΔZ error	ΔZ model	ΔZ error	T mid	ΔZ model	ΔZ error	Zmid	ΔZ model	ΔZ error	ΔZ model	ΔZ error	ΔZ model	ΔZ error
Caythorpe-1	223.5	0.1453	543.78	0.41941	0.274	320	2337	351	-30	341	-20	336	-16	330	-9	0.2824	325	-5	384	320	0	300	21	334	14
Rudston-1	207.95	0.11823	255.73	0.15909	0.041	48	2339	52	-5	51	-3	55	-7	55	-7	0.1387	46	2	232	46	2	43	5	54	6
Rudston-2	232.9	0.1012	314.58	0.17287	0.072	82	2279	92	-10	89	-7	92	-11	95	-13	0.1370	81	1	274	81	0	76	6	92	10
Willows-1	332.77	0.28673	#N/A	#N/A																					
Hunmanby-1	#N/A	#N/A	#N/A	#N/A																					
42/26-1	1138.73	0.774	#N/A	#N/A																					
42/27a-1	758.55	0.51053	894.46	0.63028	0.120	136	2270	153	-17	149	-13	150	-14	155	-19	0.5704	157	-21	827	157	-21	129	8	151	15
42/27a-3	797	0.55437	874.96	0.61247	0.058	78	2684	74	4	72	6	76	2	78	0	0.5834	76	1	836	76	2	61	17	75	-3
42/27b-2	1073.14	0.77147	1332.67	0.95258	0.181	260	2866	232	28	225	35	224	35	228	31	0.8620	260	-1	1203	259	1	195	65	224	-35
42/28-2	1122.32	0.73038	1180.18	0.76842	0.038	58	3042	49	9	47	11	52	6	51	7	0.7494	53	5	1151	54	4	40	18	50	-8
42/28a-4	901.73	0.61799	1026.54	0.71192	0.094	125	2658	120	5	117	8	119	6	123	2	0.6650	127	-2	964	127	-2	100	25	119	-6
41/24a-2	#N/A	#N/A	#N/A	#N/A																					
Well A					#VALUE!			#VALUE!																	

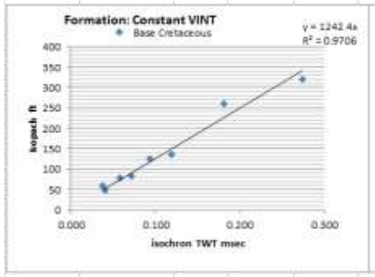

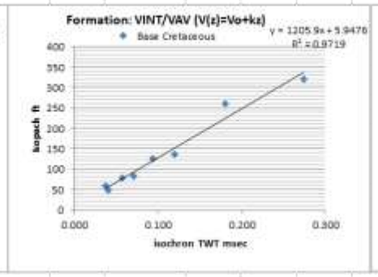

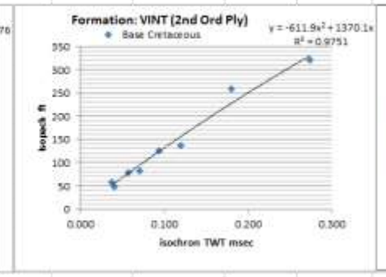

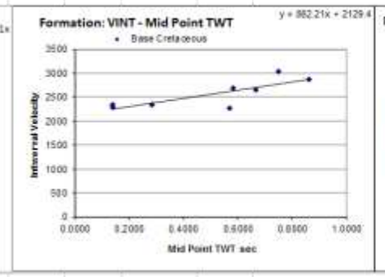

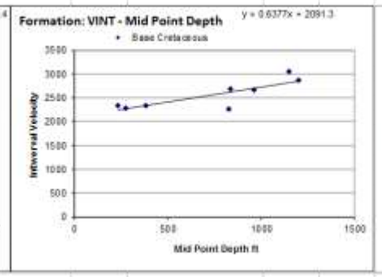

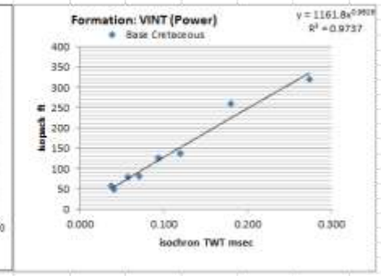

Formation: Corallian to Lias

	Mean Vint Δz = A*ΔT/2	Graphical Vint Δz = A*ΔT	Isopach/isochron Δz = A + B*ΔT	isopach/ isochron Δz = A*ΔT + B*ΔT^2	mid-point time Δz = (A + B*Tmid)*ΔT/2	mid-point depth Δz = (ΔT/2)*(A+B*ztop)/(1-B*ΔT/4)	slotnick Δz = A*(exp(B*ΔT/2)-1)/B	Power Δz = A*Δt^B
A (Vo) =	3583	1839.3	-32.309	1368.5	2712.5	2681.4	2681.4	1821.5
B (k) =			2036	2576.3	1466.9	1.0282	1.0282	1.0117
Correlation Coefficient	0.961215	0.961215	0.961214944	0.971446464	0.997688347	0.997925	0.963787	0.961636
Standard Deviation	35.83725	34.88266	33.05875937	28.84176293	10.21182777	10.29198	46.35581	35.48565
Mean	2	-4	0.00	2	-2	-2	58	-4
RMS Error	35.91219	35.16516	33.05875941	28.93351462	10.41790777	10.55019	74.16656	35.67417

Well	Top TVDSS (ft)	Top 2WT (s)	Base TVDSS (ft)	Base 2WT (s)	isochron	isopach	V int	ΔZ model	ΔZ error	ΔZ model	ΔZ error	ΔZ model	ΔZ error	ΔZ model	ΔZ error	T mid	ΔZ model	ΔZ error	Zmid	ΔZ model	ΔZ error	ΔZ model	ΔZ error	ΔZ model	ΔZ error
Caythorpe-1	543.78	0.41941	864.43	0.61111	0.192	321	3345	343	-23	353	-32	358	-37	357	-36	0.5153	332	-12	704	327	-6	270	51	342	22
Rudston-1	255.73	0.15909	459.94	0.29606	0.137	204	2982	245	-41	252	-48	247	-42	236	-32	0.2276	209	-4	358	209	-5	190	14	244	40
Rudston-2	314.58	0.17287	514.65	0.30267	0.130	200	3083	233	-32	239	-39	232	-32	221	-21	0.2378	199	1	415	202	-2	180	20	231	31
Willows-1	#N/A	#N/A	471.34	0.42483																					
Hunmanby-1	#N/A	#N/A	316.9	0.30201																					
42/26-1	#N/A	#N/A	1345.99	0.91081																					
42/27a-1	894.46	0.63028	1021.18	0.6959	0.066	127	3862	118	9	121	6	101	25	101	26	0.6631	121	6	958	120	7	89	37	116	-11
42/27a-3	874.96	0.61247	1012.37	0.68859	0.076	137	3610	136	1	140	-3	123	15	119	18	0.6505	140	-2	944	139	-2	104	33	135	-3
42/27b-2	1332.67	0.95258	1827.53	1.19207	0.239	495	4133	429	66	440	54	455	40	476	19	1.0723	513	-18	1580	517	-22	342	153	429	-66
42/28-2	1180.18	0.76842	#N/A	#N/A																					
42/28a-4	1026.54	0.71192	1335	0.86364	0.152	308	4066	272	37	279	29	277	32	267	42	0.7878	293	15	1181	296	13	212	97	270	-38
41/24a-2	#N/A	#N/A	50.01	0.0656299																					
Well A					#VALUE!			#VALUE!																	

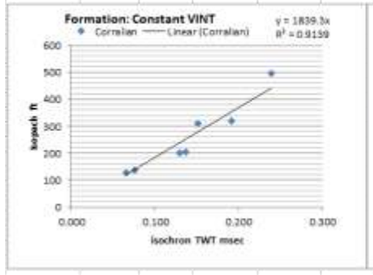

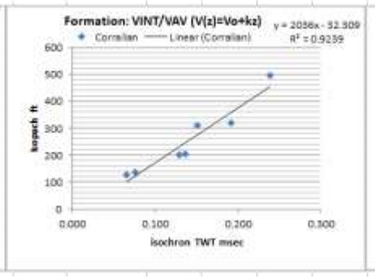

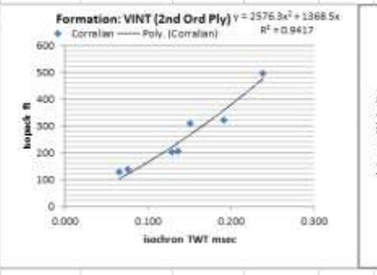

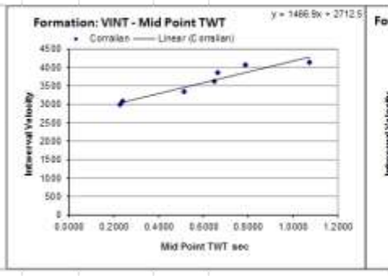

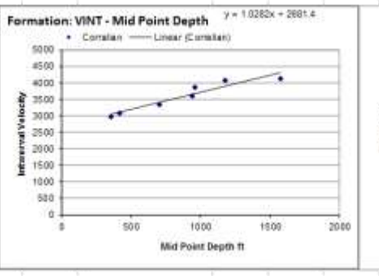

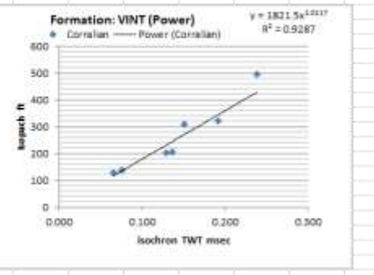

Formation: Lias to Triassic

	Mean Vint Δz = A*ΔT/2	Graphical Vint Δz = A*ΔT	Isopach/isochron Δz = A + B*ΔT	isopach/ isochron Δz = A*ΔT + B*ΔT^2	mid-point time Δz = (A + B*Tmid)*ΔT/2	mid-point depth Δz = (ΔT/2)*(A+B*ztop)/(1-B*ΔT/4)	slotnick Δz = A*(exp(B*ΔT/2)-1)/B	Power Δz = A*Δt^B
A (Vo) =	3069	1508.7	5.5866	1716.1	2515.2	2604.8	2604.8	1451
B (k) =			1469.1	-1330.2	876.56	0.5043	0.5043	0.9817
Correlation Coefficient	0.955882	0.955882	0.955881635	0.957740878	0.98107636	0.977943	0.955507	0.956103
Standard Deviation	26.86201	26.68505	26.58310263	26.0895814	18.38798072	19.77385	27.79528	26.5395
Mean	-2	1	0.00	-1	-3	-3	21	-2
RMS Error	26.9087	26.71469	26.58310273	26.10519018	18.5769505	19.9467	34.9895	26.58222

	Top		Base																					
Well	TVDSS (ft)	ZWT (s)	TVDSS (ft)	ZWT (s)	isochron	isopach	V int	ΔZ model	ΔZ error	ΔZ model	ΔZ error	ΔZ model	ΔZ error	ΔZ model	ΔZ error	T mid	ΔZ model	ΔZ error	Zmid	ΔZ model	ΔZ error	ΔZ model	ΔZ error	ΔZ model	ΔZ error
Caythorpe-1	864.43	0.61111	991.53	0.69305	0.082	127	3102	126	1	124	3	126	1	132	-5	0.6521	126	1	928	126	1	108	19	124	-3
Rudston-1	459.94	0.29606	490.12	0.31767	0.022	30	2793	33	-3	33	-2	37	-7	36	-6	0.3069	30	0	475	31	-1	28	2	34	3
Rudston-2	514.65	0.30267	755.46	0.48563	0.183	241	2632	281	-40	276	-35	274	-34	269	-29	0.3942	262	-21	635	268	-27	244	-3	274	33
Willows-1	471.34	0.42483	662.2	0.52746	0.103	191	3719	158	33	155	36	156	34	162	29	0.4761	150	40	567	148	43	135	55	155	-36
Hunmanby-1	316.9	0.30201	568.1	0.48641	0.184	251	2725	283	-32	278	-27	276	-25	271	-20	0.3942	264	-13	443	261	-10	246	5	276	25
42/26-1	1345.99	0.91081	1394.76	0.943	0.032	49	3030	49	-1	49	0	53	-4	54	-5	0.9269	54	-5	1370	53	-4	42	7	50	1
42/27a-1	1021.18	0.6959	1081.18	0.72866	0.033	60	3663	50	10	49	11	54	6	55	5	0.7123	51	9	1051	51	9	43	17	51	-9
42/27a-3	1012.37	0.68859	1260.66	0.83468	0.146	248	3399	224	24	220	28	220	28	222	26	0.7616	232	16	1137	232	16	194	54	220	-29
42/27b-2	1827.53	1.19207	2128.49	1.36234	0.170	301	3535	261	40	257	44	256	45	254	47	1.2772	309	-8	1978	307	-6	227	74	255	-46
42/28-2	#N/A	#N/A	1461.78	0.94245																					
42/28a-4	1335	0.86364	1558.12	1.01297	0.149	223	2988	229	-6	225	-2	225	-2	227	-3	0.9383	249	-26	1447	249	-26	198	25	224	1
41/24a-2	50.01	0.06563	157.51	0.16444	0.099	108	2176	152	-44	149	-42	151	-43	157	-49	0.1150	129	-22	104	132	-24	130	-23	150	42
Well A					#VALUE!			#VALUE!																	

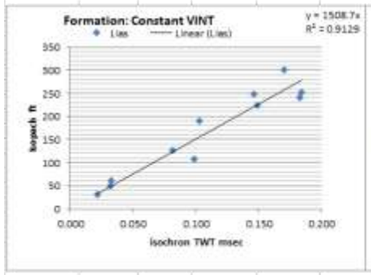

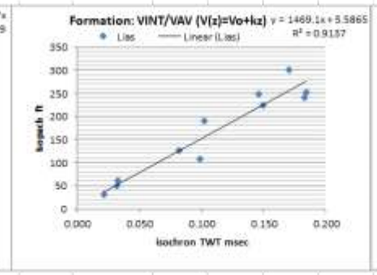

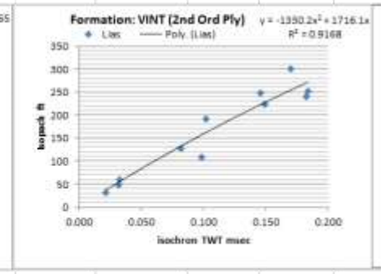

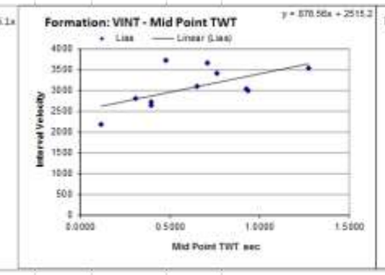

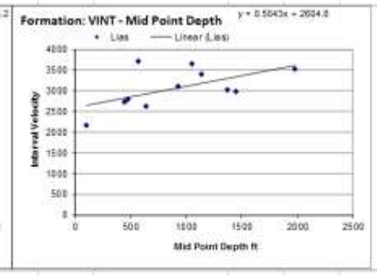

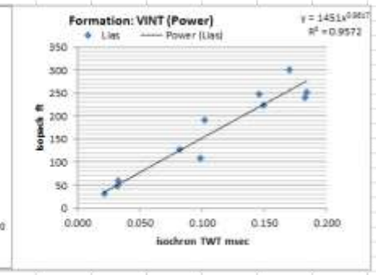

Formation: Triassic to Bacton

	Mean Vint Δz = A*ΔT/2	Graphical Vint Δz = A*ΔT	Isopach/isochron Δz = A + B*ΔT	isopach/ isochron Δz = A*ΔT + B*ΔT^2	mid-point time Δz = (A + B*Tmid)*ΔT/2	mid-point depth Δz = (ΔT/2)*(A+B*ztop)/(1-B*ΔT/4)	slotnick Δz = A*(exp(B*ΔT/2)-1)/B	Power Δz = A*Δt^B
A (Vo) =	3756	1832.8	4.9433	1788.6	3180.1	3269.8	3269.8	1692
B (k) =			1801.3	264.19	745.62	0.419	0.419	0.9573
Correlation Coefficient	0.976236	0.976236	0.976236092	0.97645686	0.988364275	0.987321	0.976403	0.975857
Standard Deviation	24.78423	24.41669	24.34125597	24.37289697	18.82466	19.59319	25.50701	24.5365
Mean	-5	1	0.00	1	-5	-6	23	0
RMS Error	25.25606	24.43377	24.34125598	24.40572444	19.60651675	20.43019	34.17889	24.54129

	Top		Base																					
Well	TVDSS (ft)	ZWT (s)	TVDSS (ft)	ZWT (s)	isochron	isopach	V int	ΔZ model	ΔZ error	ΔZ model	ΔZ error	ΔZ model	ΔZ error	ΔZ model	ΔZ error	T mid	ΔZ model	ΔZ error	Zmid	ΔZ model	ΔZ error	ΔZ model	ΔZ error	ΔZ model	ΔZ error
Caythorpe-1	991.53	0.69305	1013.48	0.70533	0.012	22	3575	23	-1	23	-1	27	-5	22	0	0.6992	23	-1	1003	23	-1	20	2	25	3
Rudston-1	490.12	0.31767	678.18	0.42883	0.111	188	3384	209	-21	204	-16	205	-17	202	-14	0.3733	192	-4	584	195	-7	184	4	207	19
Rudston-2	755.46	0.48563	1029.51	0.65993	0.174	274	3145	327	-53	319	-45	319	-45	320	-46	0.5728	314	-40	892	318	-44	290	-16	318	44
Willows-1	662.2	0.52746	902.62	0.65495	0.127	240	3772	239	1	234	7	235	6	232	8	0.5912	231	10	782	229	11	211	29	236	-5
Hunmanby-1	568.1	0.48641	833.3	0.63373	0.147	265	3600	277	-11	270	-5	270	-5	269	-4	0.5601	265	0	701	262	3	245	21	271	5
42/26-1	1394.76	0.943	1461.82	0.971	0.028	67	4790	53	14	51	16	55	12	50	17	0.9570	55	13	1428	54	13	46	21	55	-12
42/27a-1	1081.18	0.72866	1444.98	0.93337	0.205	364	3554	384	-21	375	-11	374	-10	377	-13	0.8310	389	-25	1263	389	-26	342	22	371	7
42/27a-3	1260.66	0.83468	1382.52	0.89508	0.060	122	4035	113	8	111	11	114	8	109	13	0.8649	116	6	1322	115	6	99	22	115	-7
42/27b-2	2128.49	1.36234	2528.2	1.54546	0.183	400	4366	344	56	336	64	335	65	336	63	1.4539	390	9	2328	388	11	305	95	333	-67
42/28-2	1461.78	0.94245	1812.05	1.13023	0.188	350	3731	353	-2	344	6	343	7	345	5	1.0363	371	-21	1637	372	-22	313	37	341	-9
42/28a-4	1558.12	1.01297	1797.53	1.14973	0.137	239	3501	257	-17	251	-11	251	-12	250	-10	1.0814	273	-33	1678	272	-33	227	13	252	13
41/24a-2	157.51	0.16444	450.01	0.32611	0.162	293	3618	304	-11	296	-4	296	-4	296	-4	0.2453	272	21	304	274	18	269	24	296	3
Well A					#VALUE!			#VALUE!																	

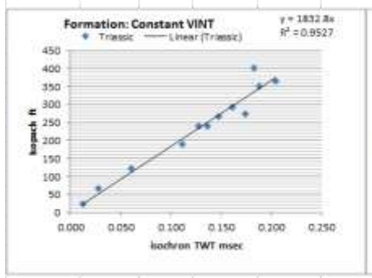

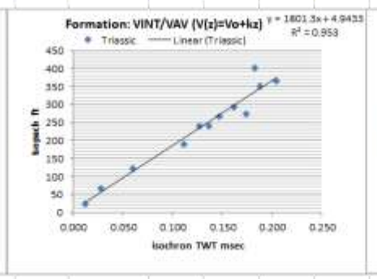

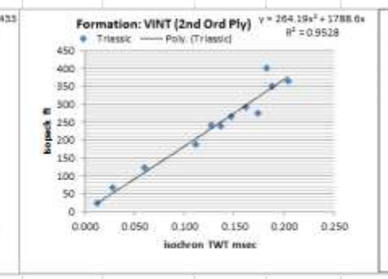

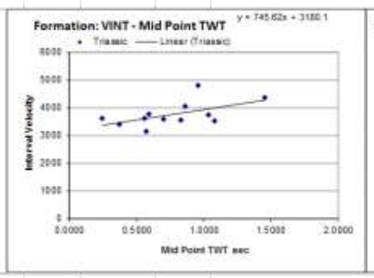

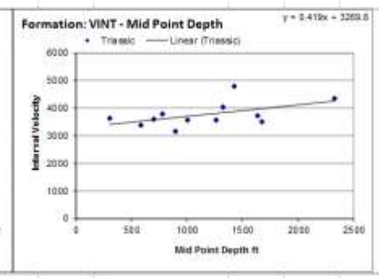

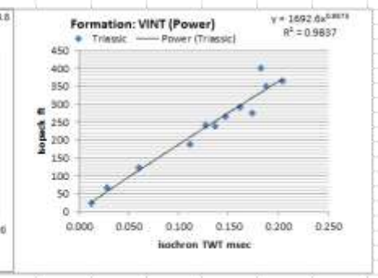

Formation: Bacton to Zechstein

	Mean Vint Δz = A*ΔT/2	Graphical Vint Δz = A*ΔT	Isopach/isochron Δz = A + B*ΔT	isopach/ isochron Δz = A*ΔT + B*ΔT^2	mid-point time Δz = (A + B*Tmid)*ΔT/2	mid-point depth Δz = (ΔT/2)*(A+B*ztop)/(1-B*ΔT/4)	slotnick Δz = A*(exp(B*ΔT/2)-1)/B	Power Δz = A*ΔT^B
A (Vo) =	3807	1978.3	-57.502	1656.4	3826.4	3828.6	3828.6	2413
B (k) =			2160.5	982.82	-20.048	-0.014	-0.014	1.1814
Correlation Coefficient	0.982013	0.982013	0.982013324	0.981635053	0.981558686	0.981533	0.982004	0.982289
Standard Deviation	44.49105	41.30998	37.83069216	38.64053141	44.89880555	44.9283	44.12238	37.60468
Mean	16	-5	0.00	-2	16	16	14	-3
RMS Error	47.35402	41.64363	37.83069227	38.68772211	47.71498401	47.7313	46.19867	37.72352

Well	Top TVDSS (ft)	Top ZWT (s)	Base TVDSS (ft)	Base ZWT (s)	isochron	isopach	V int	ΔZ model	ΔZ error	ΔZ model	ΔZ error	ΔZ model	ΔZ error	ΔZ model	ΔZ error	T mid	ΔZ model	ΔZ error	Zmid	ΔZ model	ΔZ error	ΔZ model	ΔZ error	ΔZ model	ΔZ error
Caythorpe-1	1013.48	0.70533	1591.99	0.99858	0.293	579	3946	558	20	580	-2	576	2	570	8	0.8520	559	20	1303	559	20	561	18	566	-12
Rudston-1	678.18	0.42883	1257	0.75596	0.327	579	3539	623	-44	647	-68	649	-70	647	-68	0.5924	624	-45	968	624	-45	626	-47	645	66
Rudston-2	1029.51	0.65993	1281.76	0.83759	0.178	252	2840	338	-86	351	-99	326	-74	325	-73	0.7488	339	-86	1156	339	-86	340	-88	313	61
Willows-1	902.62	0.65495	1498.42	0.95391	0.299	595	3986	569	27	591	4	588	7	583	13	0.8044	570	26	1201	570	26	572	24	579	-16
Hunmanby-1	833.3	0.63373	1431.5	0.93819	0.304	598	3930	580	19	602	-4	600	-2	595	3	0.7860	580	18	1132	580	18	582	16	592	-6
42/26-1	1461.82	0.971	2122.62	1.285	0.314	661	4209	598	63	621	40	621	40	617	44	1.1280	597	64	1792	597	64	600	60	614	-47
42/27a-1	1444.98	0.93337	2269.45	1.34126	0.408	824	4043	776	48	807	18	824	1	839	-15	1.1373	776	49	1857	776	49	780	45	836	12
42/27a-3	1382.52	0.89508	2144.63	1.27326	0.378	762	4030	720	42	748	14	760	3	767	-5	1.0842	719	43	1764	719	43	723	39	765	3
42/27b-2	2528.2	1.54546	2592.09	1.58988	0.044	64	2877	85	-21	88	-24	38	25	76	-12	1.5677	84	-20	2560	84	-20	85	-21	61	-3
42/28-3	1812.05	1.13023	2481.98	1.46933	0.339	670	3961	645	24	671	-1	675	-5	675	-5	1.2998	644	26	2147	644	26	648	22	672	3
42/28a-4	1797.53	1.14973	2419.96	1.43399	0.284	622	4379	541	81	562	60	557	66	550	72	1.2919	540	82	2109	540	82	544	79	546	-76
41/24a-2	450.01	0.32611	986.01	0.5973	0.271	536	3963	516	20	536	0	528	8	521	15	0.4617	518	18	718	518	18	519	17	516	-20
Well A					#VALUE!			#VALUE!																	

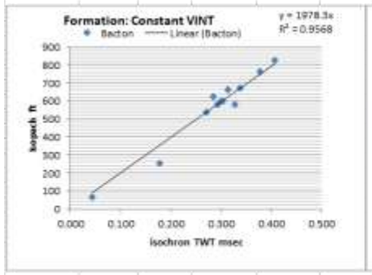

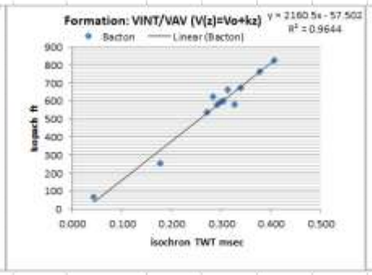

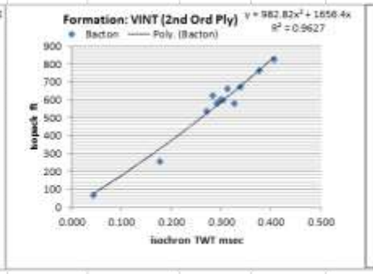

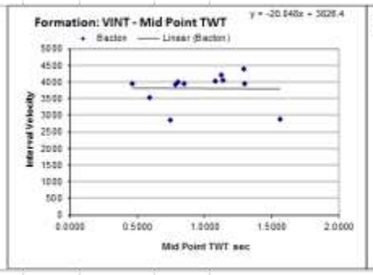

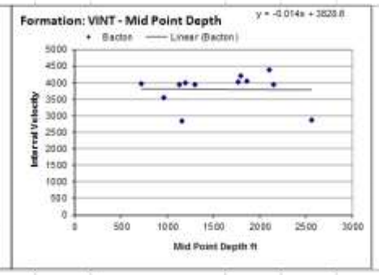

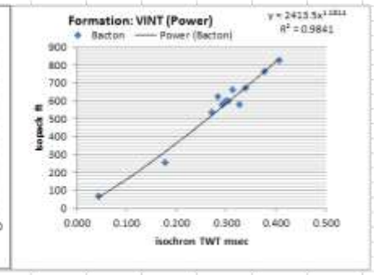

Formation: Zechstein to Z2

	Mean Vint Δz = A*ΔT/2	Graphical Vint Δz = A*ΔT	Isopach/isochron Δz = A + B*ΔT	isopach/ isochron Δz = A*ΔT + B*ΔT^2	mid-point time Δz = (A + B*Tmid)*ΔT/2	mid-point depth Δz = (ΔT/2)*(A+B*ztop)/(1-B*ΔT/4)	slotnick Δz = A*(exp(B*ΔT/2)-1)/B	Power Δz = A*ΔT^B
A (Vo) =	4743	2333.1	18.13	2410.6	4136.8	4210.6	4210.6	1736.2
B (k) =			2166.5	-655.7	517.13	0.2722	0.2722	0.8698
Correlation Coefficient	0.920655	0.920655	0.920655294	0.919331259	0.940027567	0.938542	0.920957	0.918115
Standard Deviation	28.6656	28.43302	27.97639503	28.37421396	25.58307077	25.85628	27.9405	28.71313
Mean	-2	2	0.00	1	-3	-3	23	-2
RMS Error	28.75633	28.47518	27.97639542	28.38969484	25.75941957	26.02994	35.97114	28.75684

Well	Top TVDSS (ft)	Top ZWT (s)	Base TVDSS (ft)	Base ZWT (s)	isochron	isopach	V int	ΔZ model	ΔZ error	ΔZ model	ΔZ error	ΔZ model	ΔZ error	ΔZ model	ΔZ error	T mid	ΔZ model	ΔZ error	Zmid	ΔZ model	ΔZ error	ΔZ model	ΔZ error	ΔZ model	ΔZ error
Caythorpe-1	1591.99	0.99858	1759.63	1.0638	0.065	168	5141	155	13	152	15	159	8	154	13	1.0312	152	15	1676	152	16	138	30	162	-6
Rudston-1	1257	0.75596	1421.59	0.82342	0.067	165	4880	160	5	157	7	164	0	160	5	0.7897	153	11	1339	154	10	143	22	166	2
Rudston-2	1281.76	0.83759	1547.65	0.9795	0.142	266	3747	337	-71	331	-65	326	-60	329	-63	0.9085	327	-61	1415	327	-61	302	-36	318	52
Willows-1	1498.42	0.95391	1711.38	1.04576	0.092	213	4637	218	-5	214	-1	217	-4	216	-3	0.9998	214	-1	1605	213	0	195	18	218	-5
Hunmanby-1	1431.5	0.93819	1619.98	1.00722	0.069	188	5461	164	25	161	27	168	21	163	25	0.9727	160	28	1526	160	29	146	42	170	-19
42/26-1	2122.62	1.285	2548.43	1.4496	0.165	426	5174	390	35	384	42	375	51	379	47	1.3673	399	27	2336	399	27	350	75	361	-64
42/27a-1	2269.45	1.34126	2521.42	1.45588	0.115	252	4397	272	-20	267	-15	266	-14	268	-16	1.3986	279	-27	2395	279	-27	243	9	264	12
42/27a-3	2144.63	1.27326	2404.97	1.3941	0.121	260	4309	287	-26	282	-22	280	-20	282	-21	1.3337	292	-31	2275	292	-32	257	4	276	16
42/27b-2	2592.09	1.58988	2876.06	1.69499	0.105	284	5403	249	35	245	39	246	38	246	38	1.6424	262	22	2734	260	24	223	61	245	-39
42/28-2	2481.98	1.46933	2725.22	1.56919	0.100	243	4872	237	6	233	10	234	9	234	9	1.5193	246	-3	2604	246	-2	212	32	234	-9
42/28a-4	2419.96	1.43399	2579.31	1.50199	0.068	159	4687	161	-2	159	1	165	-6	161	-2	1.4680	166	-7	2500	166	-7	144	16	168	8
41/24a-2	986.01	0.5973	1166.01	0.68277	0.085	180	4212	203	-23	199	-19	203	-23	201	-21	0.6400	191	-11	1076	193	-13	181	-1	204	24
Well A					#VALUE!			#VALUE!																	

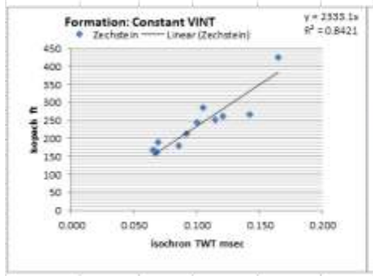

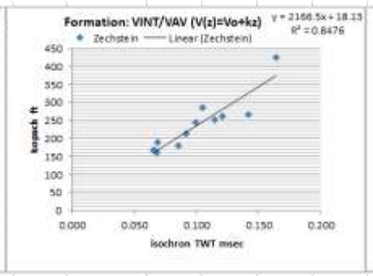

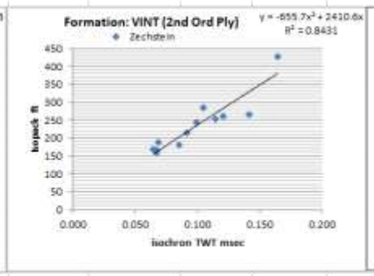

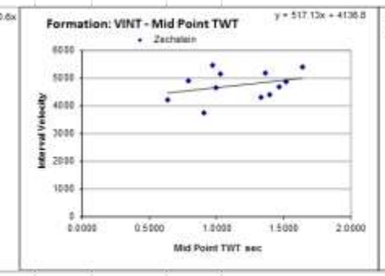

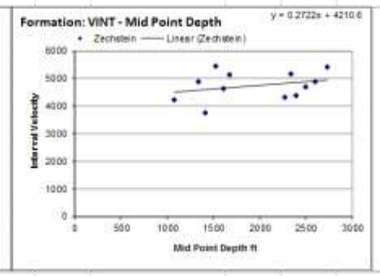

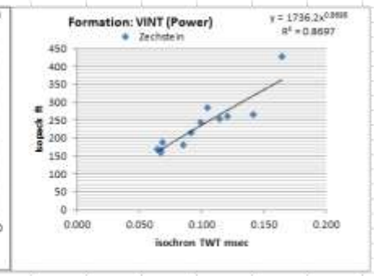

Formation: Z2 to BPU

	Mean Vint Δz = A*ΔT/2	Graphical Vint Δz = A*ΔT	Isopach/isochron Δz = A + B*ΔT	isopach/ isochron Δz = A*ΔT + B*ΔT^2	mid-point time Δz = (A + B*Tmid)*ΔT/2	mid-point depth Δz = (ΔT/2)*(A+B*ztop)/(1-B*ΔT/4)	slotnick Δz = A*(exp(B*ΔT/2)-1)/B	Power Δz = A*Δt^B
A (Vo) =	4839	2379.6	17.422	2558.8	5132.2	5135.8	5135.8	2156.7
B (k) =			2287.9	-864.61	-224.44	-0.1305	-0.1305	0.9403
Correlation Coefficient	0.993834	0.993834	0.993834477	0.994211883	0.994744979	0.994779	0.99389	0.994013
Standard Deviation	18.69769	17.65211	16.61170389	16.09909355	18.13232272	17.92182	23.35628	16.40216
Mean	-4	2	-0.01	0	-5	-5	-26	-1
RMS Error	19.16405	17.8116	16.61170511	16.09937566	18.71368622	18.47824	34.87879	16.41075

	Top		Base																				
Well	TVDSS	ZWT	TVDSS	ZWT	isochron	isopach	V int	ΔZ model	ΔZ error	ΔZ model	ΔZ error	ΔZ model	ΔZ error	ΔZ model	ΔZ error	T mid	ΔZ model	ΔZ error	Zmid	ΔZ model	ΔZ error	ΔZ model	ΔZ error	ΔZ model	ΔZ error
	(ft)	(s)	(ft)	(s)																					
Caythorpe-1	1759.63	1.0638	1891	1.1134	0.050	131	5297	120	11	118	13	131	0	125	7	1.0886	121	10	1825	121	10	127	4	128	-3
Rudston-1	1421.59	0.82342	1887.02	1.01666	0.193	465	4817	468	-2	460	6	460	6	462	3	0.9200	476	-10	1654	475	-10	493	-28	460	-6
Rudston-2	1547.65	0.9795	1875.18	1.11456	0.135	328	4850	327	1	321	6	326	1	330	-2	1.0470	331	-3	1711	332	-4	345	-18	328	1
Willows-1	1711.38	1.04576	2140.78	1.21608	0.170	429	5042	412	17	405	24	407	22	411	19	1.1309	415	14	1926	416	13	435	-6	408	-21
Hunmanby-1	1619.98	1.00722	2113.3	1.21798	0.211	493	4681	510	-17	502	-8	500	-6	501	-8	1.1126	515	-21	1867	515	-22	538	-44	499	6
42/26-1	2548.43	1.4496	2745.64	1.527	0.077	197	5096	187	10	184	13	195	3	193	4	1.4883	186	12	2647	185	12	198	-1	194	-3
42/27a-1	2521.42	1.45588	2928.22	1.63581	0.180	407	4522	435	-29	428	-21	429	-22	432	-26	1.5458	431	-24	2725	430	-23	459	-53	430	23
42/27a-3	2404.97	1.3941	3010.65	1.66404	0.270	606	4488	653	-48	642	-37	635	-29	628	-22	1.5291	646	-41	2708	645	-39	687	-81	630	24
42/27b-2	2876.06	1.69499	3110.35	1.79491	0.100	234	4690	242	-7	238	-3	246	-12	247	-13	1.7450	237	-3	2993	237	-3	256	-21	247	13
42/28-3	2725.22	1.56919	3016.61	1.69257	0.123	291	4723	299	-7	294	-2	300	-8	303	-11	1.6309	294	-3	2871	294	-2	316	-24	301	10
42/28a-4	2579.31	1.50199	3112.03	1.7137	0.212	533	5033	512	20	504	29	502	31	503	30	1.6078	505	28	2846	505	28	540	-7	501	-32
41/24a-2	1166.01	0.68277	1762.01	0.92932	0.247	596	4835	597	-1	587	9	582	14	578	18	0.8060	610	-14	1464	609	-13	628	-32	578	-18
Well A					#VALUE!			#VALUE!																	

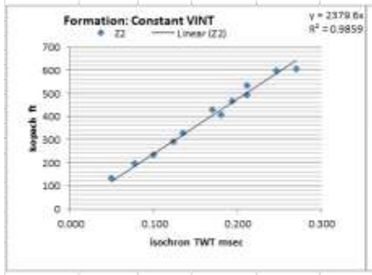

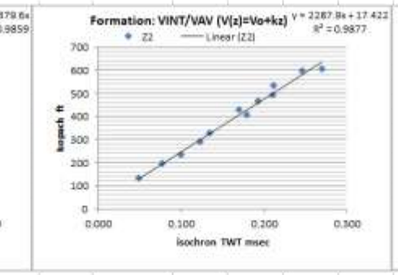

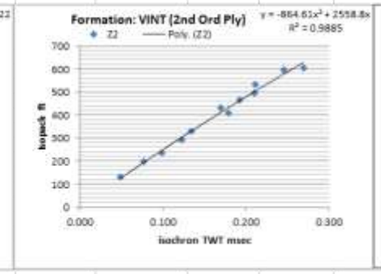

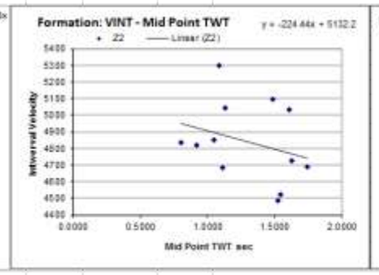

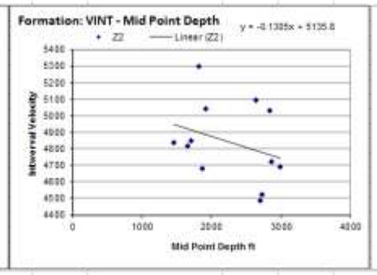

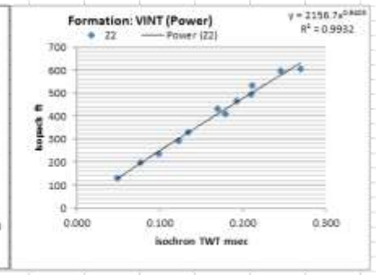

APPENDIX D. DEPTH SURFACE WELL TIE ERROR AND CORRECTION

Tabulated absolute depth error in metres and correction used to tie each depth structure surface.

Base_UK_Chalk_TVDSS_TIED_m

Well	Md	X-value	Y-value	Z-value	Horizon before	Diff before	Horizon after	Diff after
Willrex-1	2357	2854549.5	6006236.2	-122.1	-100.52	-21.58	-122.1	0
Rudrose-3	2611.49	2822063.1	5997896.3	-207.95	-201.24	-6.7	-207.95	0
Castlespec-1	2211.39	2852452.3	5999289.3	-194.79	-231.73	36.94	-194.78	0
42/27a-3	6501.99	3209569.5	5999310.5	-613.02	-657.37	44.35	-613.02	0
42/27a-1	6361.42	3188754.9	5999193.25	-602.84	-620.73	17.89	-602.84	0
42/27a-2	6888.85	3110271.3	5999368.7	-669.34	-687.56	18.22	-669.34	0
42/27b-2	4954.15	3270888.6	5998020	-415.01	-441.13	26.12	-415.01	0
42/28-2	8396.7	3339492.3	5995386.1	-865.78	-878.68	14.9	-865.78	0
42/28a-4	6669.04	3324542.3	5996691.2	-630.68	-624.08	-6.6	-630.68	0

Top_Cromarty_TVDSS_TIED_m

Well	Md	X-value	Y-value	Z-value	Horizon before	Diff before	Horizon after	Diff after
Hassmilly-1	2329	2866601.2	6007176.7	-152.1	-161.93	9.83	-152.1	0
Rudrose-2	3661.67	2830769.9	5998289.2	-314.58	-295.44	-19.13	-314.58	0
Rudrose-3	3093.37	2822063.1	5997896.3	-255.73	-281.9	26.17	-255.73	0
Castlespec-1	4702.28	2852452.3	5999289.3	-543.78	-557.66	13.88	-543.78	0
42/28a-4	6864.28	3324542.3	5996704.9	-1026.54	-1036.91	10.37	-1026.54	0
42/28-2	7413.3	3339492.3	5995386.1	-1180.18	-1200.18	19.97	-1180.18	0
42/27a-3	9113	3209567.5	5999315.5	-874.96	-854.38	-20.58	-874.96	0
42/27a-1	9281.12	3188754.9	5999193.4	-894.46	-895.8	1.34	-894.46	0
42/27b-2	8372.21	3270981.8	5998994.7	-1332.67	-1331.42	-1.25	-1332.67	0

Top_Eriswell_TVDSS_TIED_m

Well	Md	X-value	Y-value	Z-value	Horizon before	Diff before	Horizon after	Diff after
Hassmilly-1	648.9	2866601.2	6007176.7	-568.1	-608.08	39.98	-568.1	0
Willrex-1	778.1	2854549.5	6006240	-662.2	-676.42	14.22	-662.2	0
Rudrose-2	834.34	2829980.8	5998370.2	-755.46	-777.89	22.42	-755.46	0
Rudrose-3	543.76	2822063.1	5997896.3	-490.12	-529.84	39.72	-490.12	0
Castlespec-1	1018.03	2852452.3	5999289.3	-991.53	-966.98	-24.55	-991.53	0
41/24b-2	192.5	2849408.1	6021477	-157.51	-153.65	-3.86	-157.51	0
42/28a-4	1597.76	3324509.5	5996725	-1558.12	-1533.23	-24.89	-1558.12	0
42/28-2	1694.7	3339492.3	5995386.1	-1461.78	Outside		Outside	
42/27a-3	1299	3209549	5999315.5	-1260.66	-1265.37	4.71	-1260.66	0
42/27a-1	1134.96	3188769.6	5999196.9	-1081.18	-1002.44	-78.74	-1081.19	0
42/26-1	1414.27	3102711.3	5999368.7	-1394.76	-1241.58	-153.19	-1394.76	0
42/22-1	487.5	3182221	6016684.3	-419.84	-340.54	-79.3	-419.84	0
42/27b-2	2169.57	3270992.9	5998988.7	-2128.49	-2163.87	35.39	-2128.49	0

Top_Forbisher_TVDSS_TIED_m

Well	Md	X-value	Y-value	Z-value	Horizon before	Diff before	Horizon after	Diff after
Hassmilly-1	1512.3	2866601.2	6007176.7	-1431.5	-1435.96	4.46	-1431.5	0
Willrex-1	1628.8	2854549.5	6006220.4	-1498.42	-1524.3	26.88	-1498.42	0
Rudrose-2	1672.7	2829399.4	5998369.4	-1281.76	-1456.76	175	-1281.76	0
Rudrose-3	1310.64	2822063.1	5997896.3	-1247	-1346.39	89.3	-1247	0
Castlespec-1	1618.49	2852452.3	5999289.3	-1591.99	-1566.77	-25.22	-1591.99	0
41/24b-2	1021	2849408.1	6021477	-986.01	-945.47	-39.54	-986.01	0
42/28a-4	2460.95	3324485	5996746.7	-2419.96	-2364.87	-55.09	-2419.96	0
42/28-2	2514.9	3339492.3	5995386.1	-2461.78	Outside		Outside	
42/27a-3	2183.5	3209529	5999315.5	-2144.63	-2110.87	-33.76	-2144.63	0
42/27a-1	2104.29	3188769.6	5999196.9	-2269.45	-2236.63	-32.81	-2269.45	0
42/26-1	2142.13	3102711.3	5999368.7	-2122.62	-2126.08	3.46	-2122.62	0
42/22-1	1661.16	3181501.5	6016703	-1620.91	-1892.36	271.45	-1620.91	0
42/27b-2	2855.91	3271183.3	5998132.1	-2592.09	-2661.93	69.82	-2592.09	0

BPC_TVDSS_TIED_m

Well	Md	X-value	Y-value	Z-value	Horizon before	Diff before	Horizon after	Diff after
Hassmilly-1	2194.1	2866601.2	6007176.7	-2113.3	-2098.29	-15.01	-2113.3	0
Willrex-1	2292.1	2854581.5	6006197.7	-2140.78	-2104.37	-36.41	-2140.78	0
Rudrose-2	2412.3	2829829.4	5998922.5	-1875.18	-1847.49	-27.69	-1875.18	0
Rudrose-3	1940.66	2822063.1	5997896.3	-1887.02	-1840.32	-46.7	-1887.02	0
Castlespec-1	1917.8	2852452.3	5999289.3	-1893	-1864.07	-28.92	-1893	0
41/24b-2	1797	2849408.1	6021477	-1762.01	-1715.86	-46.15	-1762.01	0
42/28-2	2765.15	3102711.3	5999368.7	-2745.64	-2860.87	115.23	-2745.64	0
42/27b-2	3649.52	3339492.3	5995386.1	-3016.61	Outside		Outside	
42/27a-2	3156.51	3271486.4	5998166.7	-3110.35	-3076.22	-34.12	-3110.35	0
42/27a-3	3151	3209462.5	5999382.2	-3010.65	-3029.07	18.42	-3010.65	0
42/27a-1	2964.48	3188754.5	5998966.1	-2928.22	-2909.03	-19.19	-2928.22	0
42/22-1	2430.42	3180318	6016703.4	-2364.88	-2408.97	44.09	-2364.88	0
42/26a-4	3192.85	3324471.7	5998761.5	-3112.03	-3128.41	16.37	-3112.03	0

Seabed_TVDSS_TIED_m

Well	Md	X-value	Y-value	Z-value	Horizon before	Diff before	Horizon after	Diff after
41/24b-2	85	2849408.1	6021477	-50.01	-81.16	31.15	-50.01	0
42/27a-3	92.69	3209553.5	5999303.8	-54.79	-43.36	-11.43	-54.79	0
42/26-1	67.36	3102711.3	5999368.7	-47.85	-47.24	-0.62	-47.85	0
42/22-1	93.14	3182240.4	6016683.6	-53.62	-94.29	40.67	-53.62	0
42/26a-4	91.44	3324543.3	5996676.9	-53.34	-49.03	-4.31	-53.34	0
42/28-2	84.73	3339492.3	5995386.1	-51.82	-45.96	-5.85	-51.82	0
42/28-1	54.45	3342199.4	5996688.8	-24.1	-51.18	27.08	-24.1	0
42/27b-2	83.27	3270981.7	5998013.7	-54.25	-40.04	-14.21	-54.25	0
42/27b-1	88.7	3188758.9	5999193.3	-54.17	-49.9	-4.27	-54.17	0

Base_Cretaceous_TVDSS_TIED_m

Well	Md	X-value	Y-value	Z-value	Horizon before	Diff before	Horizon after	Diff after
Hassmilly-1	3362	2866601.2	6007176.7	-554	-348.93	-205.07	-554	0
Willrex-1	3488.4	2854549.5	6006240.5	-532.77	-344.09	-188.68	-532.77	0
Rudrose-2	3264.99	2830769.9	5998291.4	-312.9	-272.31	-40.59	-312.9	0
Rudrose-3	2951.59	2822063.1	5997896.3	-207.95	-207.34	-0.6	-207.95	0
Castlespec-1	3250	2852452.3	5999289.3	-323.5	-297.39	-26.11	-323.5	0
42/28-2	3359.24	3339492.3	5995386.1	-1122.52	-1087.6	-34.91	-1122.52	0
42/27a-1	3292.18	3188758.9	5999196	-758.55	-777.22	18.67	-758.55	0
42/26-1	3358.24	3102711.3	5999368.7	-1138.73	-1078.01	-60.72	-1138.73	0
42/27b-2	3313.42	3270981.6	5998035.6	-1071.14	-1024.96	-47.19	-1071.14	0
42/26a-4	3440.31	3324586.6	5996700.4	-901.73	-906.25	4.52	-901.73	0

Top_Lias_TVDSS_TIED_m

Well	Md	X-value	Y-value	Z-value	Horizon before	Diff before	Horizon after	Diff after
Hassmilly-1	397.7	2866601.2	6007176.7	-316.9	-297.26	-19.64	-316.9	0
Willrex-1	487	2854547.5	6006241.6	-471.34	-597.24	125.9	-471.34	0
Rudrose-2	567.84	2830664.8	5998288.5	-514.65	-527.1	12.45	-514.65	0
Rudrose-3	415.59	2822063.1	5997896.3	-459.04	-438.47	-21.47	-459.04	0
Castlespec-1	890.93	2852452.3	5999289.3	-864.43	-871.1	6.67	-864.43	0
41/24b-2	85	2849408.1	6021477	-50.01	52.78	-102.79	-50.01	0
42/28a-4	1335	3324529.8	5996713.2	-1395.96	-1355.85	-59.89	-1395.96	0
42/27b-3	1050.69	3209549.5	5999319.5	-1012.37	-1013.73	1.36	-1012.37	0
42/27a-1	1054.91	3188772	5999192.4	-1021.18	-1146.63	125.45	-1021.18	0
42/22-1	93.14	3182240.4	6016683.6	-53.62	-91.78	38.15	-53.62	0
42/27b-2	1867.51	3270985.4	5998064.7	-1827.53	-1795.73	-55.82	-1827.55	0

Top_Rutrix_TVDSS_TIED_m

Well	Md	X-value	Y-value	Z-value	Horizon before	Diff before	Horizon after	Diff after
42/26-1	1483.33	3102711.3	5999368.7	-1462.82	-1412.27	-49.56	-1462.82	0
Hassmilly-1	934.1	2866601.2	6007176.7	-833.3	-799.69	-33.61	-833.3	0
Willrex-1	1019.7	2854660.6	6006271.5	-902.62	-875.03	-27.6	-902.62	0
Rudrose-2	1198.47	2827764.7	5998503.4	-1029.51	-1001.8	-27.71	-1029.51	0
Rudrose-3	751.82	2822063.1	5997896.3	-678.18	-601.67	-76.51	-678.18	0
Castlespec-1	1039.98	2852452.3	5999289.3	-1013.48	-1038.54	25.07	-1013.48	0
41/24b-2	485	2849408.1	6021477	-450.01	-420.62	-29.39	-450.01	0
42/28a-4	1837.64	3324499.3	5996758.6	-1797.52	-1824.01	26.48	-1797.52	0
42/28-2	1844.97	3339492.3	5995386.1	-1812.05	Outside		Outside	
42/27b-3	1421	3209578	5999334	-1382.52	-1387.64	-4.87	-1382.52	0
42/27a-1	1478.89	3188767.4	5999194.2	-1444.98	-1407.48	-37.5	-1444.98	0
42/22-1	964.34	3182304	6016688.9	-926.38	-857.61	-68.77	-926.38	0
42/27b-2	2571.6	3271116.2	5998198	-2528.2	-2482.57	-102.63	-2528.2	0

Top_ZZ_TVDSS_TIED_m

Well	Md	X-value	Y-value	Z-value	Horizon before	Diff before	Horizon after	Diff after
Hassmilly-1	1700.78	2866601.2	6007176.7	-1619.98	-1586.82	-33.17	-1619.98	0
Rudrose-2	1967.48	2832288	5998778.4	-1747.65	-1452.71	-294.95	-1747.65	0
Rudrose-3	1475.23	2822063.1	5997896.3	-1423.59	-1412.64	-8.95	-1423.59	0
Willrex-1	1851.5	2854453.5	6006175	-1733.38	-1683.44	-27.94	-1733.38	0
Castlespec-1	1786.13	2852452.3	5999289.3	-1759.63	-1759.47	-20.16	-1759.63	0
41/24b-2	1201	2849408.1	6021477	-1166.01	-1171.69	5.68	-1166.01	0
42/28a-4	2619.76	3324881.3	5996749	-2579.31	-2533.86	-45.45	-2579.31	0
42/28-2	2758.14	3339492.3	5995386.1	-2725.22	Outside		Outside	
42/27b-3	2445.99	3209527.1	5999327.1	-2404.97	-2404.97	22.79	-2404.97	0
42/27a-1	2556.66	3188771.9	5999189.4	-2521.42	-2551.98	30.57	-2521.42	0
42/26-1	2567.94	3102711.3	5999368.7	-2548.43	-2438.09	-110.34	-2548.43	0
42/22-1	2039.02	3181119.2	6016714.2	-1876.87	-1821.77	-54.8	-1876.87	0
42/27b-2	2921.81	3271134.6	5998169.7	-2876.06	-2863.69	-12.37	-2876.06	0

APPENDIX E. REGIONAL TIED DEPTH STRUCTURE MAPS

All depth structure grids in this section are displaying true vertical depth sub-sea (TVDSS) elevation z values in metres with a colour shading convention of warm colours representing structural highs and cool colours representing structural lows. Displayed depth structure grids are:

Sea Bed

Base Chalk

Base Cretaceous

Corallian

Lias

Triassic

Bacton

Zechstein

Zechstein Z2

Base Permian Unconformity

Sea Bed TVDSSm. Contour Interval = 10m

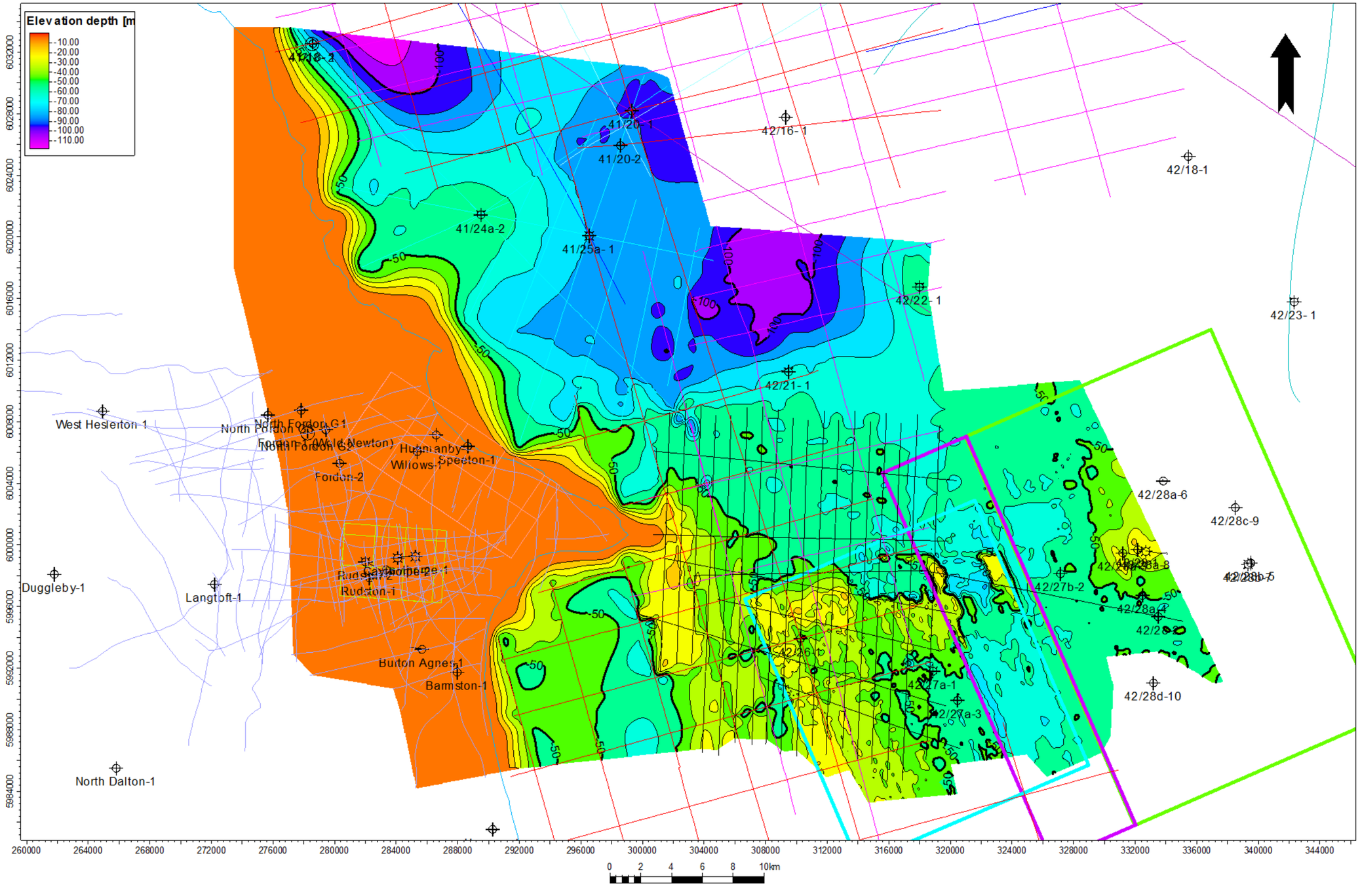

Base Chalk TVDSSm. Contour Interval = 50m

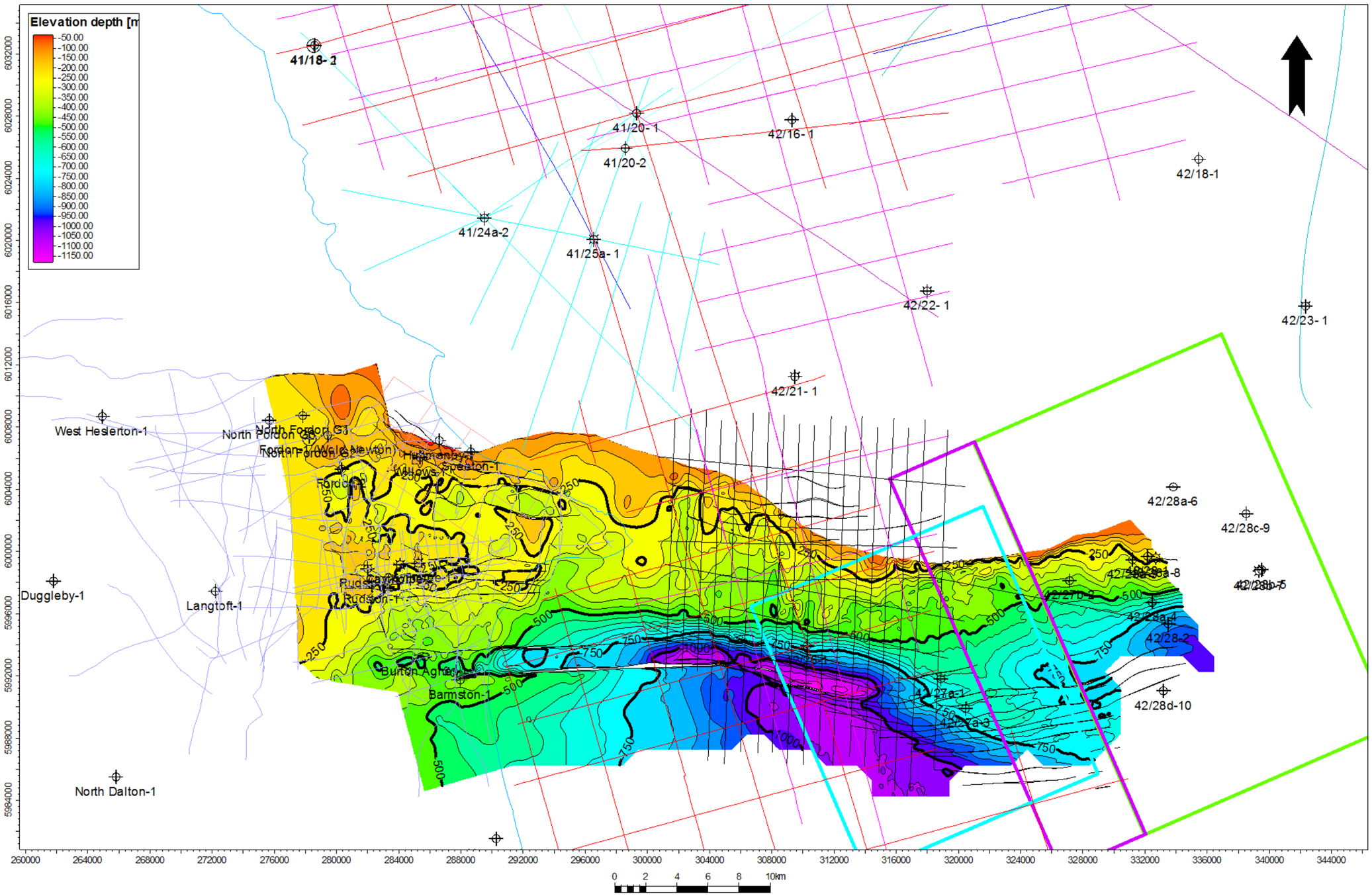

Base Cretaceous TVDSS. Contour Interval = 50m

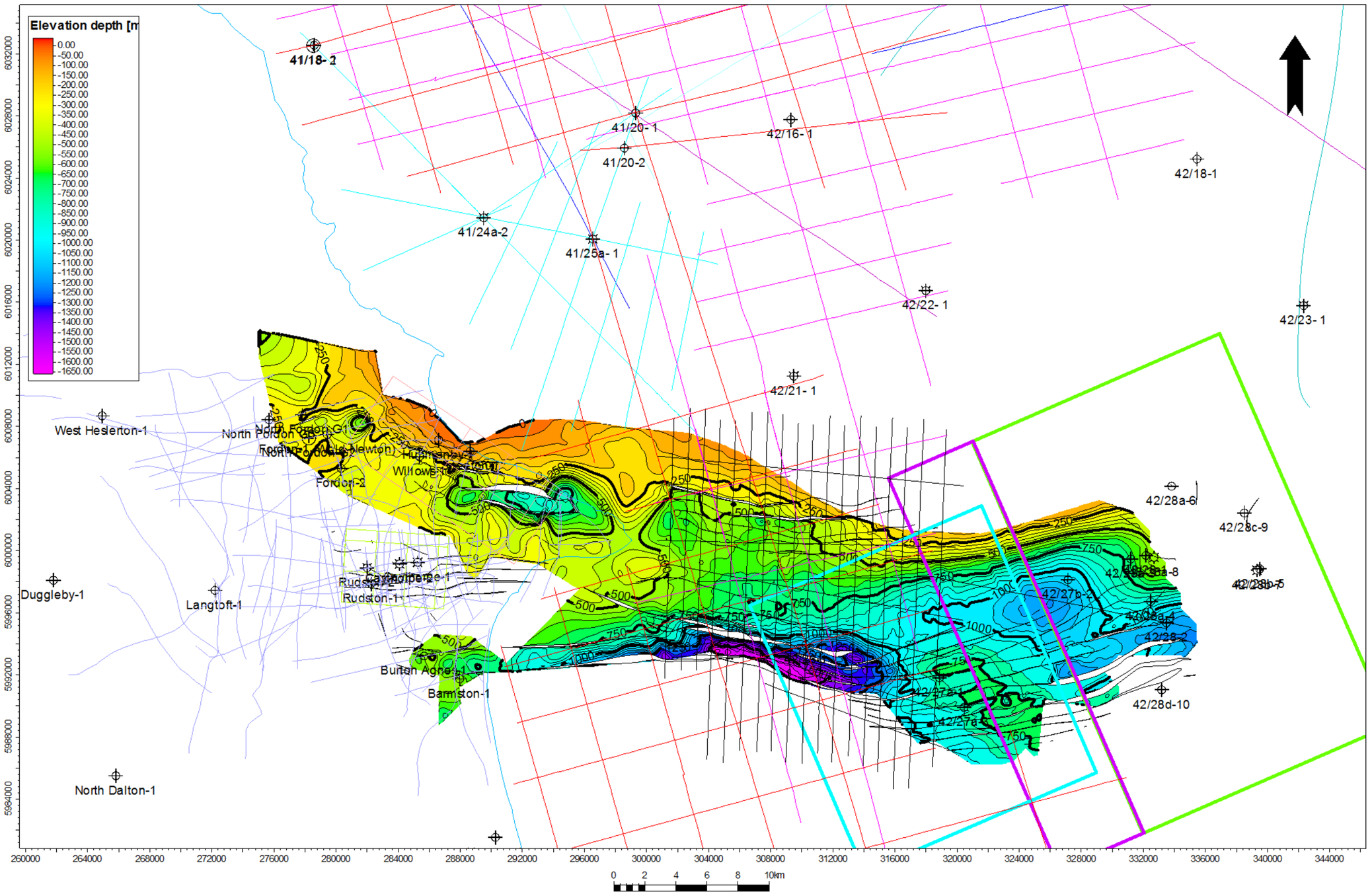

Corallian TVDSSm. Contour Interval = 50m

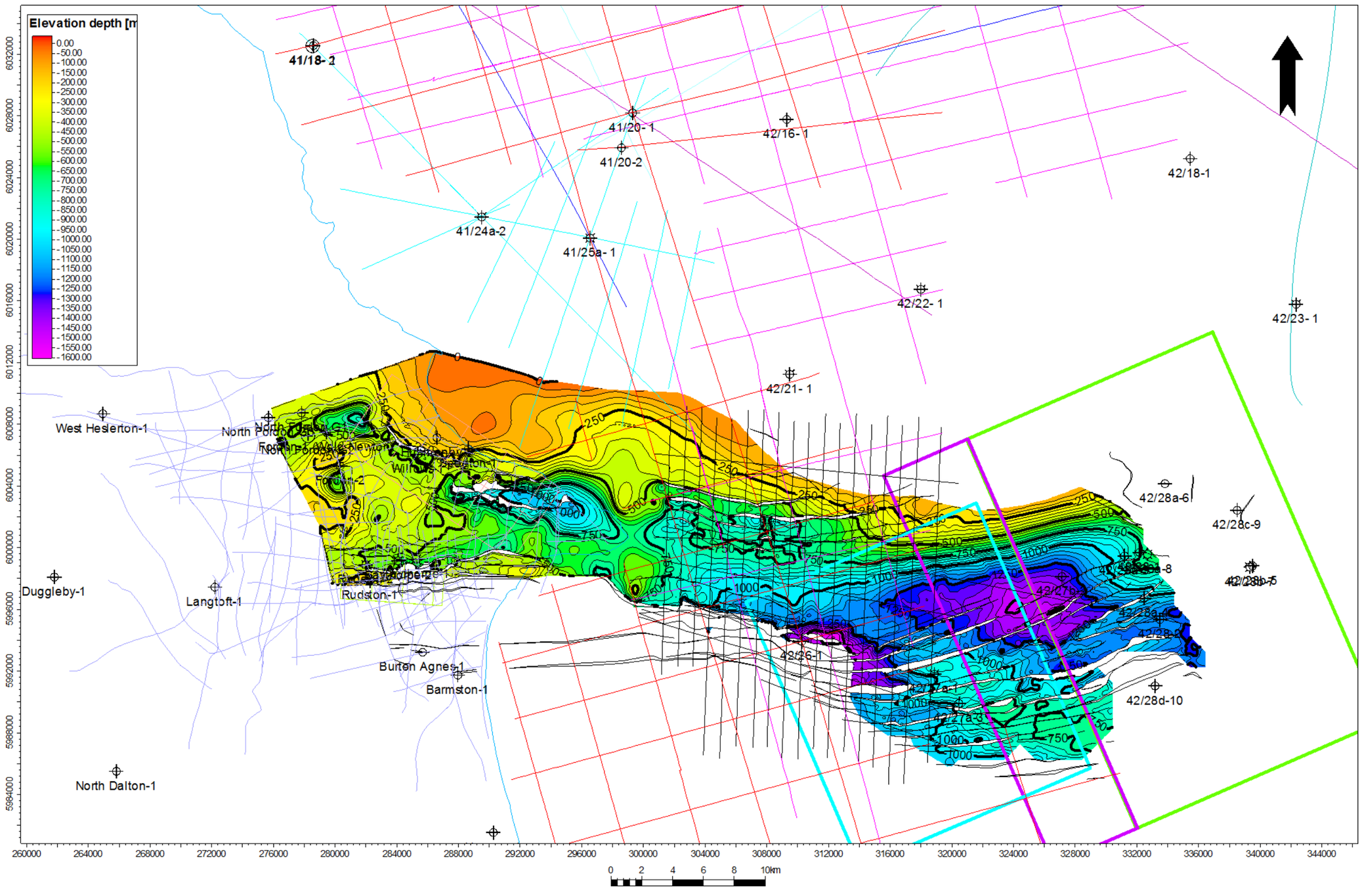

Lias TVDSS. Contour Interval = 100m

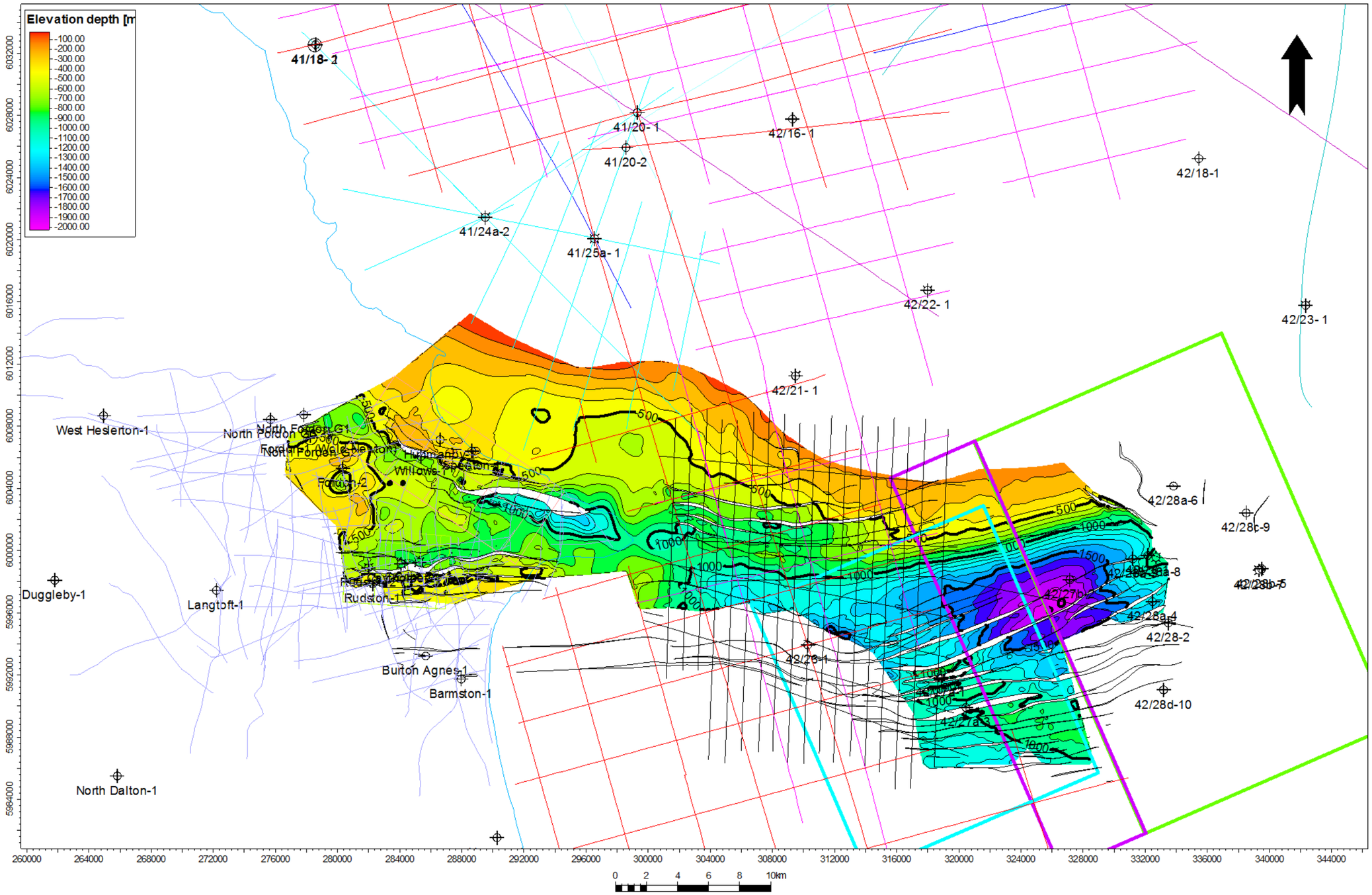

Triassic TVDSS. Contour Interval = 100m

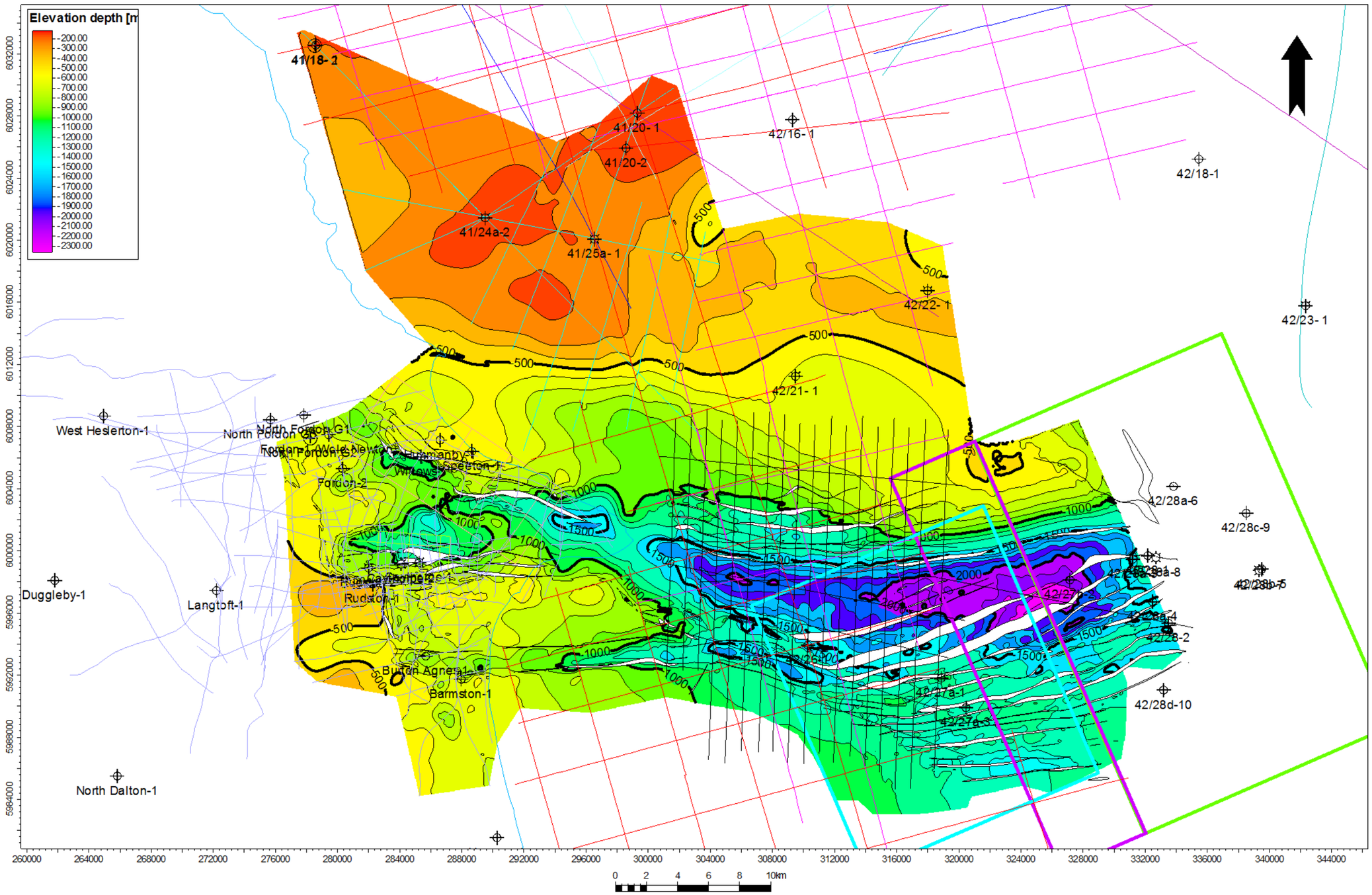

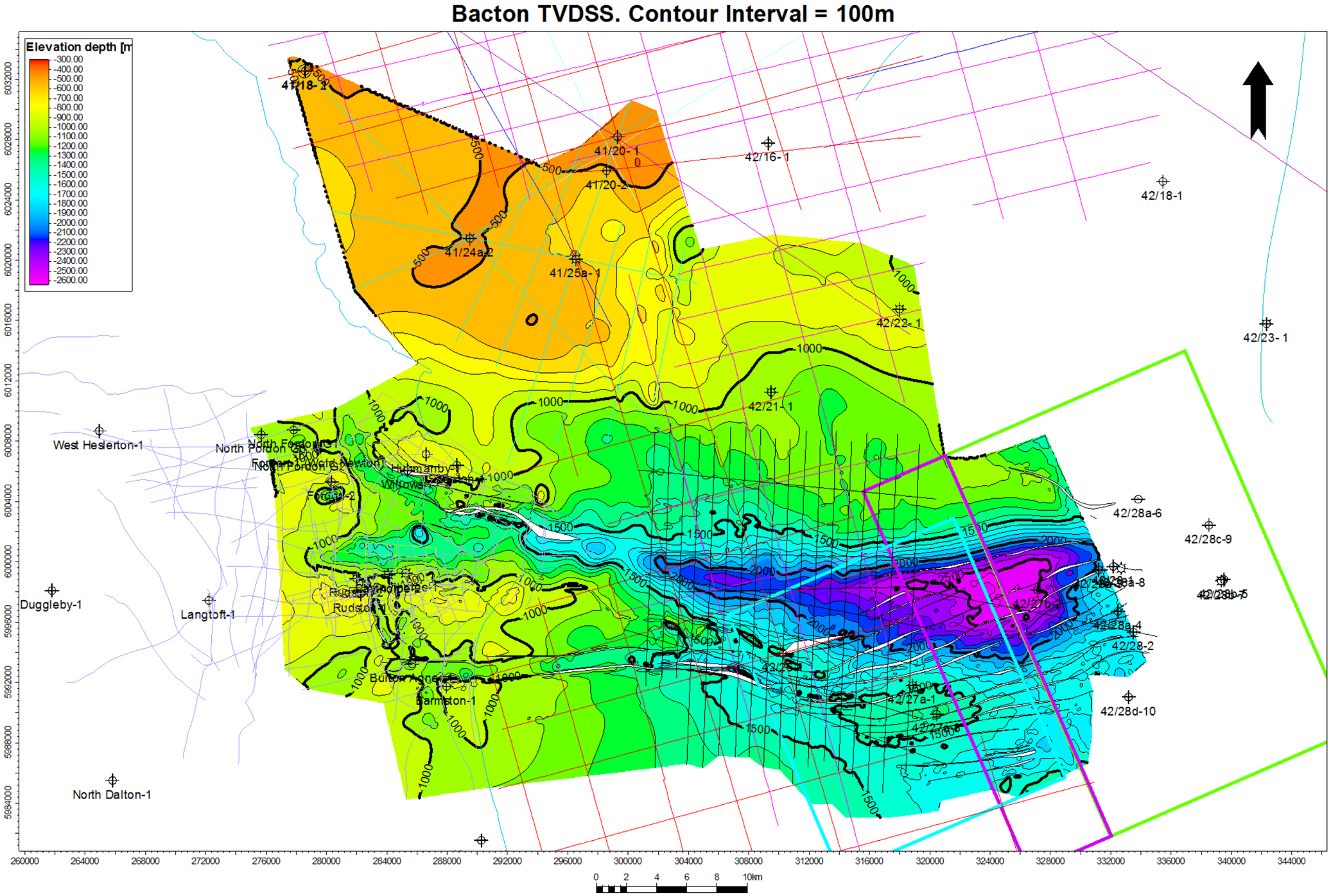
Bacton TVDSS. Contour Interval = 100m
Elevation depth [m
-300.00
-400.00
-500.00
-600.00
-700.00
-800.00
-900.00
-1000.00
-1100.00
-1200.00
-1300.00
-1400.00
-1500.00
-1600.00
-1700.00
-1800.00
-1900.00
-2000.00
-2100.00
-2200.00
-2300.00
-2400.00
-2500.00
-2600.00
41/18-2
41/20-1
41/20-2
41/24a-2
41/25a-1
42/16-1
42/18-1
42/22-1
42/23-1
42/21-1
42/28a-6
42/28c-9
42/28a-8
42/28a-4
42/28-2
42/28d-10
42/27a-1
West Heslerton-1
North Pickering-1
Foston-1
Hutmanby-1
Willows-1
Rudston-1
Burton Agnes-1
Barmston-1
Duggleby-1
Langtoft-1
North Dalton-1
6032000
6028000
6024000
6020000
6016000
6012000
6008000
6004000
6000000
5996000
5992000
5988000
5984000
260000
264000
268000
272000
276000
280000
284000
288000
292000
296000
300000
304000
308000
312000
316000
320000
324000
328000
332000
336000
340000
344000
0 2 4 6 8 10km

Zechstein TVDSS. Contour Interval = 100m

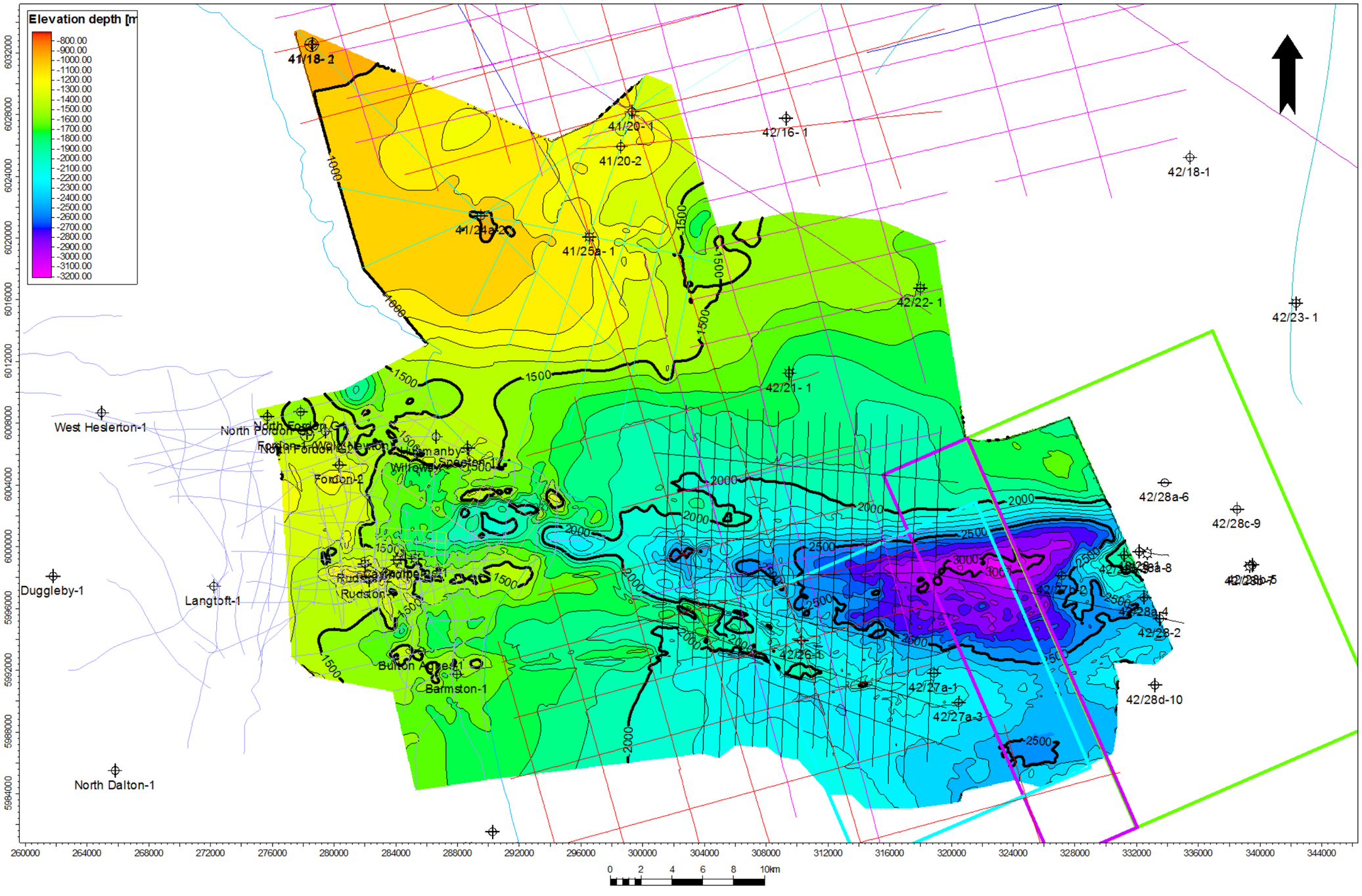

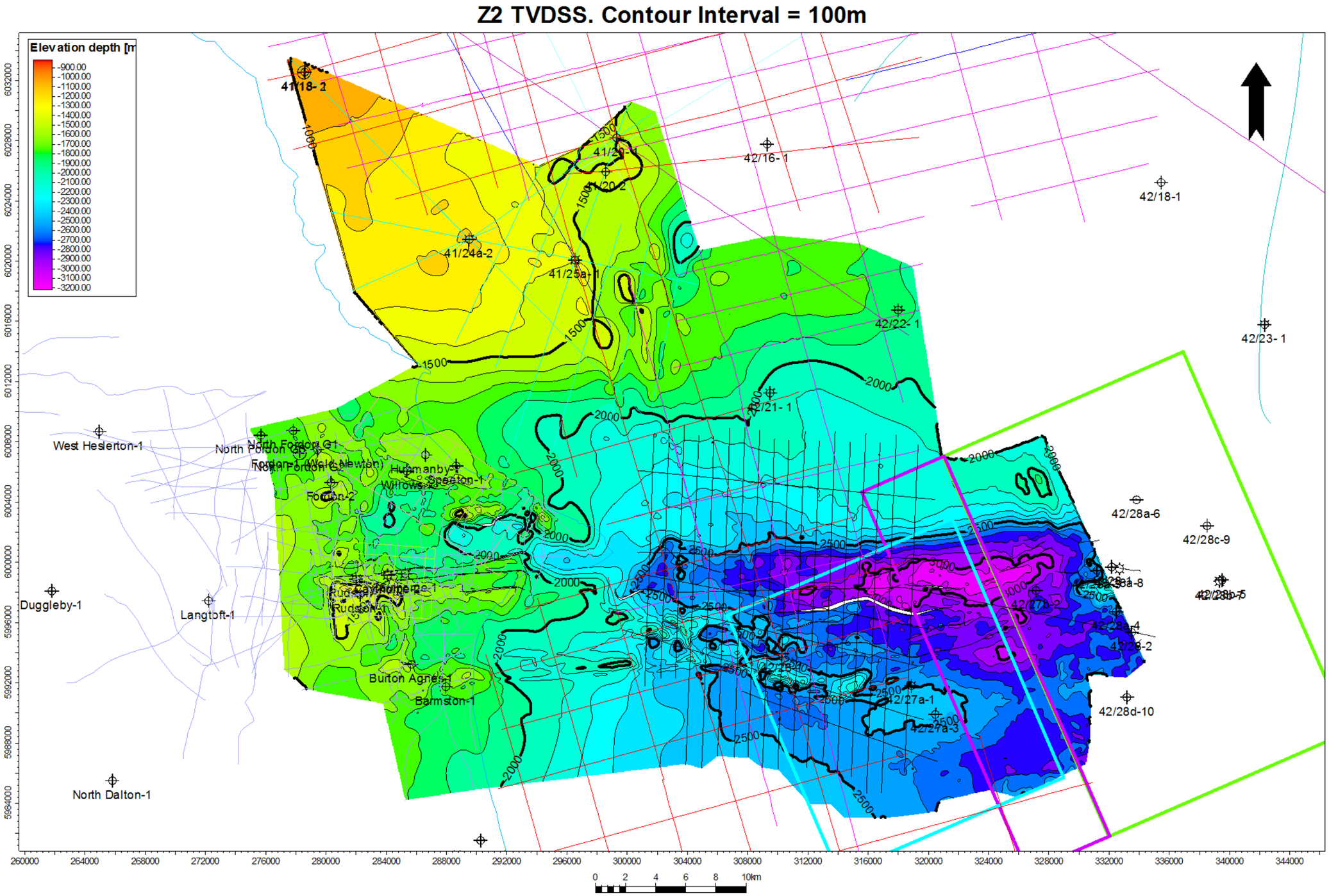
Z2 TVDSS. Contour Interval = 100m
Elevation depth [m
-900.00
-1000.00
-1100.00
-1200.00
-1300.00
-1400.00
-1500.00
-1600.00
-1700.00
-1800.00
-1900.00
-2000.00
-2100.00
-2200.00
-2300.00
-2400.00
-2500.00
-2600.00
-2700.00
-2800.00
-2900.00
-3000.00
-3100.00
-3200.00
41/18-2
41/20-1
42/16-1
41/20-2
42/18-1
41/24a-2
41/25a-1
42/22-1
42/23-1
42/21-1
West Heslerton-1
North Foston G1
North Foston G5
Foston-2
Hutmanby-1
Speeton-1
Willows-2
Duggleby-1
Langtoft-1
Burton Agnes-1
Barmston-1
North Dalton-1
42/28a-6
42/28c-9
42/28a-8
42/27a-2
42/28a-4
42/28-2
42/28d-10
42/27a-1
42/27a-3
1500
2000
2500
3000
6032000
6028000
6024000
6020000
6016000
6012000
6008000
6004000
6000000
5996000
5992000
5988000
5984000
260000
264000
268000
272000
276000
280000
284000
288000
292000
296000
300000
304000
308000
312000
316000
320000
324000
328000
332000
336000
340000
344000
0 2 4 6 8 10km

BPU TVDSS. Contour Interval = 100m